INFORMATION TO USERS

This manuscript has been reproduced from the microfilm master. UMI films the text directly from the original or copy submitted. Thus, some thesis and dissertation copies are in typewriter face, while others may be from any type of computer printer.

The quality of this reproduction is dependent upon the quality of the copy submitted. Broken or indistinct print, colored or poor quality illustrations and photographs, print bleedthrough, substandard margins, and improper alignment can adversely affect reproduction.

In the unlikely event that the author did not send UMI a complete manuscript and there are missing pages, these will be noted. Also, if unauthorized copyright material had to be removed, a note will indicate the deletion.

Oversize materials (e.g., maps, drawings, charts) are reproduced by sectioning the original, beginning at the upper left-hand corner and continuing from left to right in equal sections with small overlaps.

Photographs included in the original manuscript have been reproduced xerographically in this copy. Higher quality 6" x 9" black and white photographic prints are available for any photographs or illustrations appearing in this copy for an additional charge. Contact UMI directly to order.

ProQuest Information and Learning
300 North Zeeb Road, Ann Arbor, MI 48106-1346 USA
800-521-0600

UMI®

DISSERTATION

TRANSIENT GRATING SPECTROSCOPY AND THE CALORIMETRY OF PHOTOSYNTHESIS IN *RHODOBACTER SPHAEROIDES*

Submitted by

Micah John McCauley

Department of Physics

In partial fulfillment of the requirements

for the degree of Doctor of Philosophy

Colorado State University

Fort Collins, Colorado

Fall 2001

COLORADO STATE UNIVERSITY

April 10, 2001

WE HEREBY RECOMMEND THE DISSERTATION PREPARED UNDER OUR SUPERVISION BY MICAH MCCAULEY ENTITLED: TRANSIENT GRATING SPECTROSCOPY AND THE CALROIMETRY OF PHOTOSYNTHESIS IN *RHODOBACTER SPHAEROIDES*, BE ACCEPTED AS FULFILLING IN PART REQUIREMENTS FOR THE DEGREE OF DOCTOR OF PHILOSOPHY.

Committee on Graduate Work

Co-Advisor

Co-Advisor

Advisor

Department Head

ABSTRACT OF DISSERTATION

TRANSIENT GRATING SPECTROSCOPY AND THE CALORIMETRY OF PHOTOSYNTHESIS IN *RHODOBACTER SPHAEROIDES*

Enormous numbers and varieties of experiments have been performed to elucidate the mechanisms of photosynthesis. Within the last twenty years, a host of new studies were enabled by the techniques of ultrafast laser spectroscopy. This work continues to explore the exchange of energy on the picosecond and even the femtosecond regime. Yet in even the relatively simple and determined structure of the photosynthetic centers in the bacteria *Rhodobacter sphaeroides*, the mechanisms and energetics are unclear. The early events in photosynthesis allow energy trapping through resonance energy transfer and charge separation, in what appears to be a mixture of classical and quantum mechanical motion with strong interactions with the surrounding environment.

The technique of transient thermal grating spectroscopy offers unique insight into the mechanisms of energy relaxation in photosynthesis. A pair of laser pulse are tuned to the excitation wavelength and crossed inside the sample. The resulting pattern of interference drives excitation and the subsequent relaxation forms a density grating which diffracts a time-delayed third beam. Thus the energies and the rates of motion may be discerned.

The peripheral light harvesting antenna (LH2) is composed of polypeptides that coordinate rings of bacteriochlorophyll. Upon excitation, energy migrates around the ring until intra-ring transfer may take place. Samples of LH2 were purified and studied.

While characteristic times of energy release were determined, a volume change due to solvent interaction was found as well.

In the membrane spanning protein known as the reaction center, the energy of the light harvesting rings is ultimately transferred to a pair of chlorophyll. From here, the energy is localized onto an electron, which rapidly (picoseconds) transfers to other active pigments. Samples of wild-type and the mutated (M)214H reaction centers were purified and examined. By studying the temperature dependence of the signals, the free energy was determined as a function of time. Additionally, volume changes due to solvent-protein interaction were determined.

Micah McCauley
Physics Department
Colorado State University
Fort Collins, CO 80523
Fall 2001

ACKNOWLEDGMENTS

I would like to thank my committee for their patience, direction, and helpful criticism during the course of my studies.

I would also like to thank Ray and Sue Krueger, who grew and purified may of the samples studied in this project while showing a 'pysics nerd' how to do the rest.

While at Colorado State University, I was supported by a CIRB fellowship, a physics first year fellowship, and by NIH and USDA grants to C. C. Schenck.

DEDICATION

To my family – without whose support, guidance and faith I could never have persisted.

To Gail – for her patience.

TABLE OF CONTENTS

" The summer's flower is to the summer sweet,

though to itself it only live and die."

Shakespeare *Sonnet 94, 7*

I. ENERGY TRANSFER IN PHOTOBIOLOGICAL SYSTEMS

Though as well studied as it is fundamental, many questions linger over the early events in photosynthesis. It is known that the energy of a photon localizes upon an electron and its subsequent motion drives a change in the local electric field. This, in turn, catalyzes the chemical reactions of photosynthesis. Furthermore, the active structures in bacterial photosynthesis, termed light harvesting centers and reaction centers, are well known to consist of subassemblies of chlorophyll molecules. Finally, the conditions for in vitro experiments, which allow concentrated samples of proteins to be studied, are well outlined. Though much is known about various energy pathways from the light harvesting centers to the reaction centers, the interactions between energy and motion are poorly understood. The relationship between structure and function are similarly unclear.

I.A. Photosynthesis

I.A.1. *Introduction and Significance:* Photosynthesis, the conversion of sunlight into chemical energy, plays a role in life that is difficult to overstate. Phototrophs, organisms that rely directly on photosynthesis for their energy, are clearly dependent on sunlight. However, chemotrophs, which utilize chemical forms of energy, also ultimately trace that energy back down the food chain to phototrophs. Thus photosynthesis provides the basis for most life on the planet, including nearly all of the food and most of the fuel humans consume (thermal sources provide the rest) (Hall and Rao 1999).

As the subject of considerable study, a reasonably clear picture of the chemical nature of photosynthesis has been uncovered. In the overall metabolic scheme, the goal is to convert sunlight (or thermal energy) into a chemical form. Incredibly, there are

relatively few variations in this process. Usually, the energy is stored in some chemical bond, typically in ATP (adenosine triphosphate), although there are some variations on this molecule. Figure I-1 illustrates a typical metabolic map, showing most of the intermediate paths from raw nutrients to the finished products (Lehninger, Nelson et al. 1993) (Stryer 1995) (Garret and Geisham 1995). Though apparently complicated, the main paths (darkened) are more straightforward. The heavy vertical line represents glycolysis, the conversion of the energy of glucose into ATP, while the circle represents the citric acid cycle. The role of photosynthesis is highlighted in blue.

I.A.2. *Blue-Green Photosynthesis:* Despite a fairly complete metabolic understanding, the exact picture of photosynthesis is not clear, especially on the earliest time scales. What is known is shown schematically in Figure I-2 (Stryer 1995) (Lehninger, Nelson et al. 1993) (White 2000). The Z-scheme illustrated there applies to both blue-green algae and plants. Photosynthesis in eukaryotic plant cells takes place in a chloroplast, a subcellular organelle. In the choroplast are two centers, known as Photosystem I (PSI) and Photosystem II (PSII). Central to these systems are the plant forms of chlorophyll (a and b), which strongly absorb red and blue light. However, other molecules may absorb different frequencies, and pass the energy along to the chlorophyll (though chlorophyll's absorption generally determines a plant's color). Ultimately, a photon enters PSII and excites chlorophyll. This energy may be transferred to a free electron which migrates out of the complex and into PSI. Another photon excites chlorophyll here, allowing energy to be trapped in the chemical bond of NADPH. The motion of the electron (coupled with the motion of protons in response) has now set up a

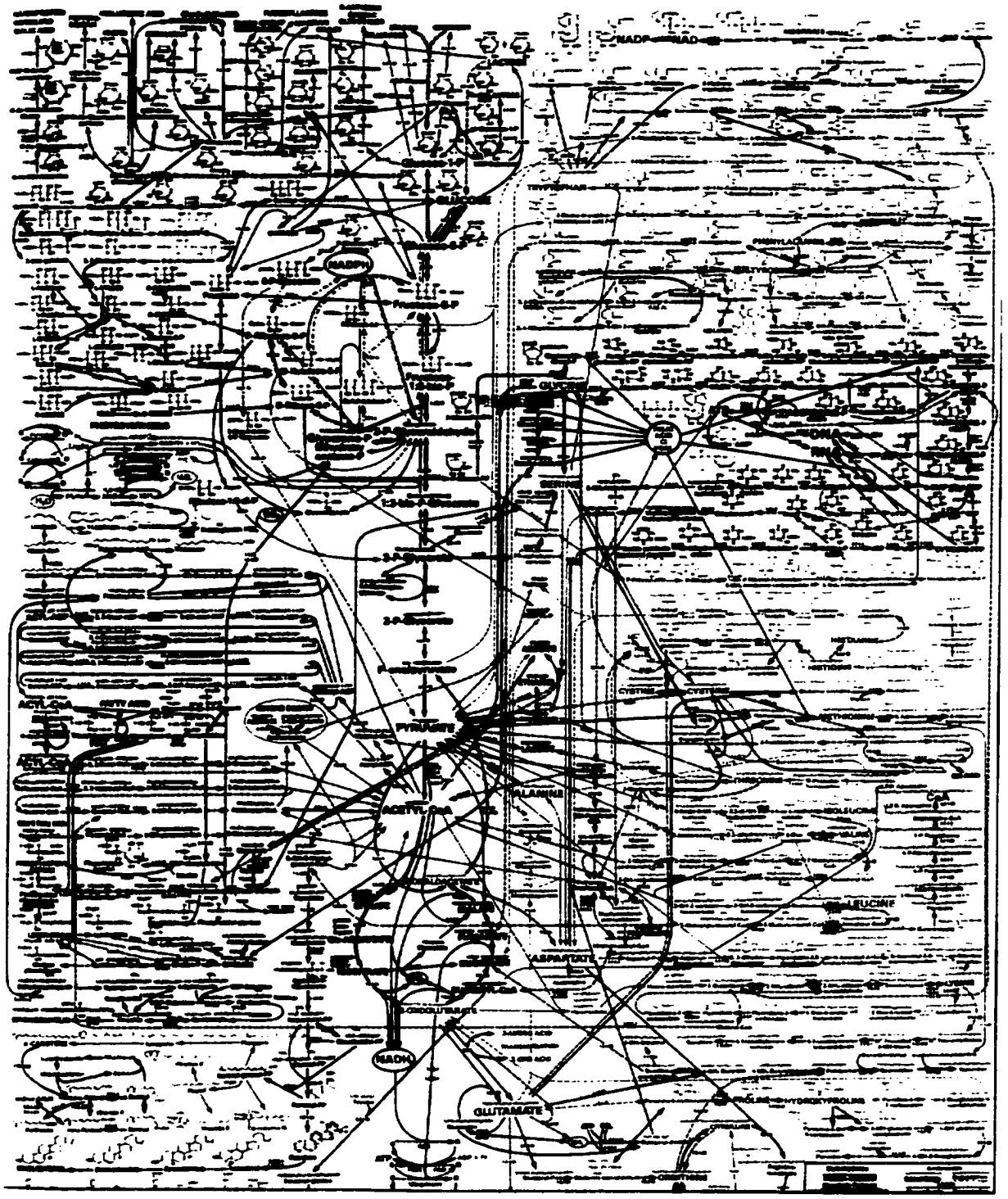

Figure I-1: Metabolic map illustrating the pathways involved in the conversion of nutrients into energy. The heavier lines indicate glycolysis and the citric acid cycle; the storage of energy in ATP and its equivalents. The role of photosynthesis is highlighted in blue (from Garrett and Grisham 1995).

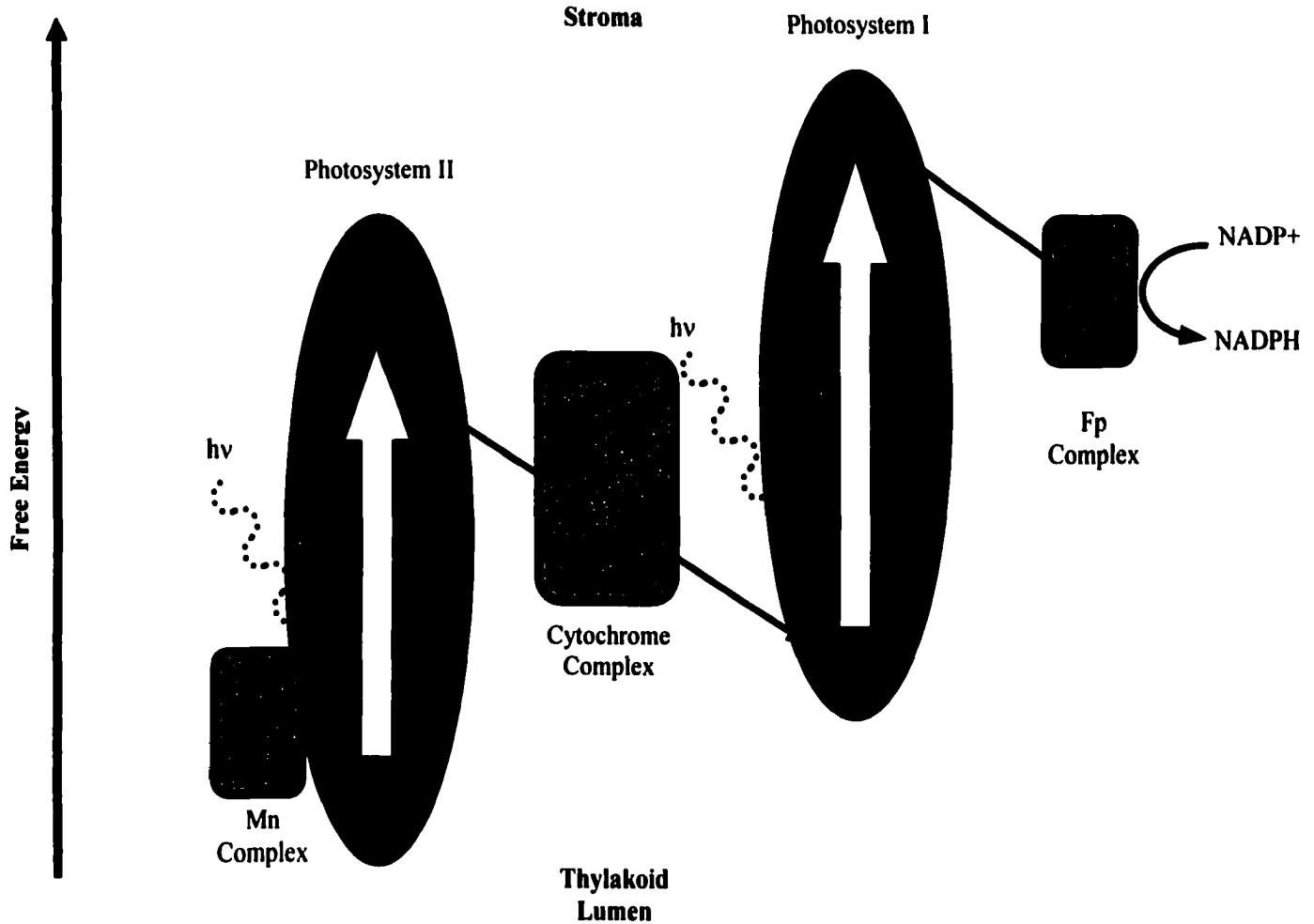

Figure I-2: Simplified Z-scheme for blue-green photosynthesis inside the chloroplast. Light is absorbed by the inner membrane spanning Photosystem I (PSI) and Photosystem II (PS II). P680 and P700 refer to the approximate wavelength (nm) of absorption for the chlorophyll. The Mn complex separates water, liberating an electron that is passed through PS II and reduces the cytochrome complex. Ultimately, charge separation in PS I allows energy storage in NADPH.

proton gradient that powers the synthesis of ATP (from ADP and P) in a nearby protein known aptly as the synthase.

In this process, the energetics of the electron, or the relationship between the electron's free energy and its trajectory is uncertain. Even the charge's exact path is unclear, as the structure is not completely understood, and is further complicated by the number of sites involved. Though electron transfer is simple in principle, factors that control the rates and specificity of these reactions are poorly understood.

I.A.3. *Bacterial Photosynthesis and Rhodobacter sphaeroides:* Not all phototrophs utilize the non-cyclical Z-scheme. *Rhodobacter sphaeroides* (Figure I-3) belongs to a class of purple bacteria that are able to store the energy of thermal or photosynthetic reactions, depending upon growth conditions. The photosynthetic pathway here, however, is markedly simpler that the Z-scheme. In these bacteria, there is only one reaction center and electron transfer is (typically) cyclical. Otherwise, the basic element, of electron transfer establishing a proton gradient, is the same. Thus *Rhodobacter* affords a chance to study a simpler scheme.

High-resolution 3-dimensional structures have been determined by x-ray crystallography for reaction centers from *Rhodopseudomonas viridis* and *Rhodobacter sphaeroides* (Deisenhofer, Epp et al. 1985; Allen, Feher et al. 1988; Chang, Elkabbani et al. 1991; Ermler, Fritzsch et al. 1994). The Nobel Prize winning work (1988) grants a clearer picture of the charge's possible pathways. This also affords the opportunity to examine the relationship between structure and function for many key components (chlorophyll chief among them).

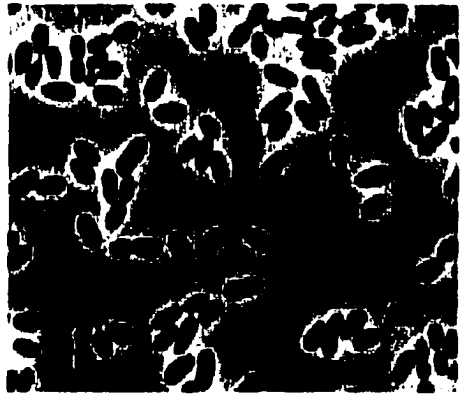

Figure I-3: *Rhodobacter sphaeroides.* Above figure shows collection of bacteria, while to the right is a close up of a single cell. Lines point to folds in the cell wall that increase the surface area of the bacteria. The line in the picture to the right represents one micron.

Finally, considerable expertise has been acquired with the preparation of Rhodobacter. In particular, detailed protocols allow the various components (including the reaction center) to be separated from the inner membrane and purified (Sistrom 1960) (Griffiths and Stanier 1956) (Krueger-Koplin 1998). The techniques of site directed mutagenesis may also be utilized to alter the structure of the photosynthetic apparatus. Thus the reaction center may be harvested, concentrated and tested.

I.A.4. *Overview and Purpose:* Biological electron transfer is a fundamentally important process in biological energy transduction in all living organisms and in various human disease states. Thousands of papers on biological electron transfer, both experimental and theoretical, have been published in the last quarter century on a host of systems (both prokaryotic and eukaryotic), and reaction type (both light-activated and thermally-activated). The photosynthetic reaction center protein is an attractive system for studying electron transfer due to the ability to activate the system with light and to follow the evolution of the excited state into products with very high time resolution. Fundamental questions regarding the basic nature of the light-induced charge separation mechanism remain unanswered. The shapes of the relevant potential energy surfaces and the coupling between them, and the trajectory of the reactants along these surfaces as they evolve into products are all controversial and of intense interest.

While Chapter I will describe bacterial photosynthesis as currently understood, Chapter II will explore the relationship between the reaction rate and the free energy change. This coupling is understood to obey the Marcus equation, which will be discussed, and the relevant experiments related. Continuing into Chapters III & IV will reveal the theory and experiment behind the transient grating technique. This laser

spectroscopy method allows the rate and the energy of the transfer to be measured simultaneously. These results are presented and discussed in the final three chapters.

I.B. Chlorophyll and the Inner Membrane of *Rhodobacter sphaeroides*

I.B.1. *Bacteriochlorophyll and Bacteriopheophytin:* Photosynthesis hinges upon the photosensitivity of chlorophyll. The surprisingly planar structure of bacteriochlorophyll is portrayed in Figure I-4. A cyclic tetrapyrrole (each is numbered) coordinates an Mg^{2+} ion. All four of the bonds are roughly equivalent (as the pyrrole is only roughly symmetrical). The groups that bind to the outside of the ring change not only its ability to stabilize in different environments but affect its overall ability to absorb light as well. Chlorophyll a ($C_{56}H_{72}MgN_4O_5$) and b ($C_{55}H_{77}MgN_4O_6$) differ primarily in these groups. Interestingly, replacing the Mg^{2+} with an Fe^{2+} (and a few appropriate changes in the groups that bind to the pyrrole ring) yields a heme, the active center in hemoglobin and myoglobin. Finally, eliminating the ions altogether, and satisfying the bonds with a pair of hydrogen atoms yields a pigment known as (bacterio)pheophytin.

The delocalized π bonds above and below the pyrrole rings are said to make chlorophyll highly aromatic. The spacing between electronic energy levels matches the wavelengths of visible light (generally in the red and blue ends of the spectrum). Upon photoexcitation, a valence electron jumps to an orbital of higher energy, which is said to be vibronic, or a combination of electronic and vibrational energy levels. Though the excited state is spread over the ring, a significant dipole develops (Figure I-4), which determines the pigment interaction (van Brederode 1999) (Beekman 1997; Van Amerongen, Valkunas et al. 2000). From here a combination of several things may happen. The chlorophyll may *fluoresce*, though only a few percent of chlorophyll in vivo

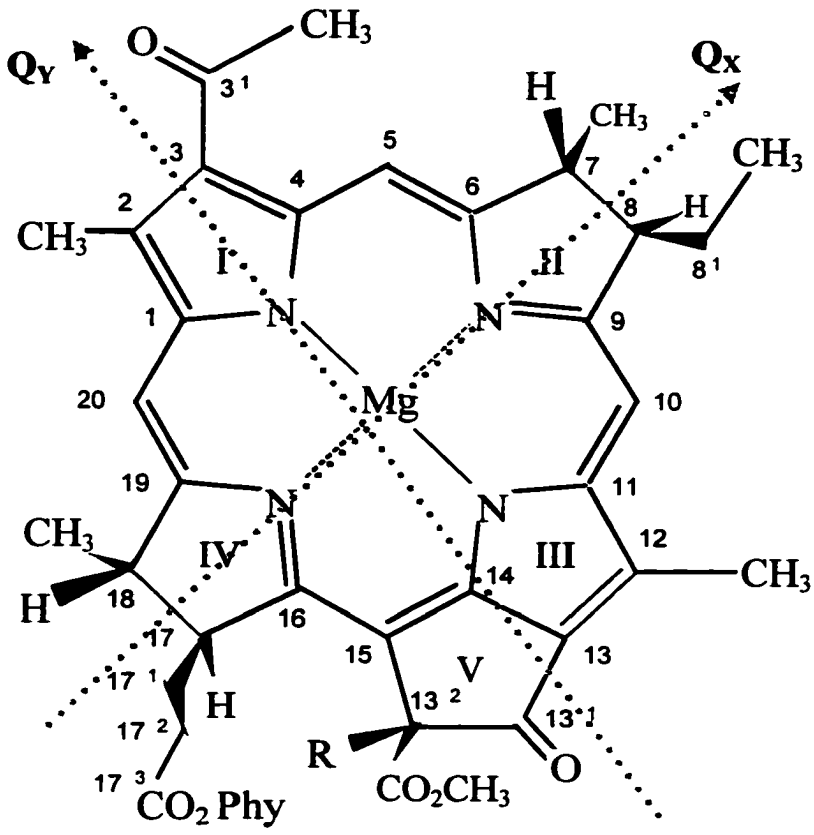

Figure I-4: In bacteriochlorophyll *a* (BChl) the prosthetic group is a magnesium porphyrin ring. In bacteriopheophytin (BPhe) the magnesium is replaced by hydrogen atoms on the nitrogen of groups I and III. Phy is phytyl ($C_{20}H_{39}$) and typically R is –H, though -OH may be substituted at position R. Grey lines show the approximate direction of the dipoles of the excited states. Of the two moments, Q_Y is stronger than Q_X by a factor of about 5.

do (though purified chlorophyll does fluoresce fairly strongly) (Voet and Voet 1990). There may also occur a *resonant energy transfer* (or exciton transfer) between electronically coupled chlorophyll. Next, the energy may allow the liberation of the electron from the chlorophyll entirely, *photooxidizing* the chlorophyll. Finally, the energy may also be *dissipated vibrationally*, or internally. Some electron energy is inevitably lost this way even if one of the other three processes occurs.

Not surprisingly then, chlorophyll possesses the ability to absorb photons of higher energy and to redistribute the excess energy via internal conversion. The remaining energy is then utilized for photooxidation. Internal conversion also allows photons of lesser energy to be 'boosted' and absorbed. Also present are other accessory pigments (including caroteniods) that are coupled to and absorb outside of the range of chlorophyll. This allows plants and bacteria to effectively utilize much of the energy of the visible spectrum.

I.B.2. *The Inner Membrane:* The arrangement of these chlorophyll inside the bacteria's inner membrane is highlighted in Figure I-5. Separating the cytoplasm and the periplasm (which is in turn, encased by the outer membrane), this plasma membrane is a bilayer formed of amphipathic lipids (see Section I.E.). This bilayer allows interaction between polar and non-polar (membrane bound) groups. All of the reactions of photosynthesis occur across the membrane spanning proteins (including ATP synthesis) that are bound by the non-polar 'tails' of the lipids.

The specific structures of these photosynthetic components are discussed below. There are three main subgroups; the reaction center, the proximal light harvesting center (LH1) that surrounds the reaction center and the peripheral light harvesting center (LH2).

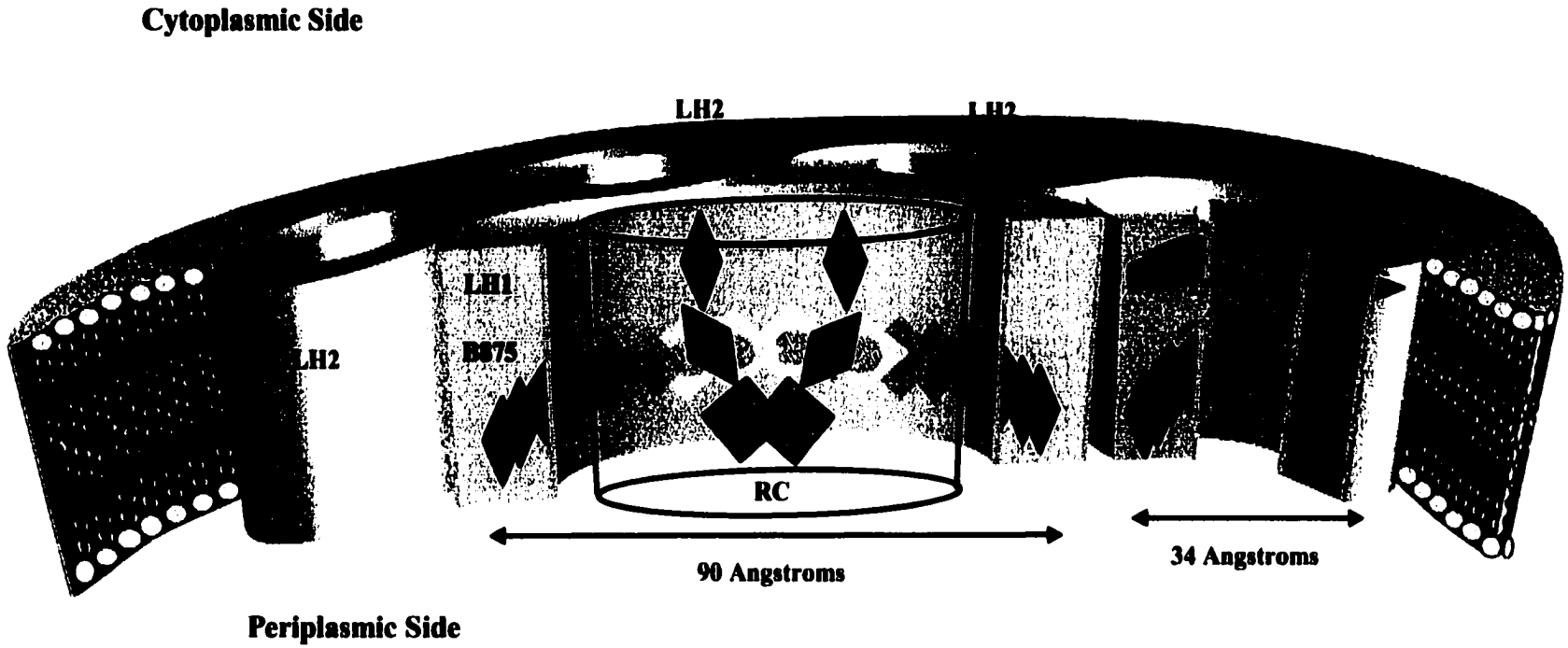

Figure I-5: The photosystem of *Rhodobacter sphaeroides* as seen from the side. The inner membrane is shown in blue, and the proteins that coordinate the active components are boxed in grey. Chlorphylls are rectangles enclosing circles, while pheophytins are squares only. The peripheral light harvesting antennae, LH2, serve to conduct photons to the proximal light harvesting complexes, LH1. Photons are subsequently conducted to the reaction center (RC), where they initiate charge transfer. The chlorophyll rings are labelled with their absorption maximum. The distances indicated are approximate (adapted from Krueger 1998).

Each consists of an arrangement of chlorophyll coordinated (usually) by polypeptide protein chains. Curiously, most of the chlorophyll in bacteria are not located inside the reaction center, but are found in the light harvesting centers.

I.B.3. *Energy Transfer Though the Membrane:* The arrangement of the chlorophyll within the peptides and near each other alters their absorption maximum. Each arrangement alters the maximum of peak absorption, and so each arrangement is often referred to by that wavelength. These are noted on Figure I-5 as well as Figure I-6. The actual ratio of LH2 to LH1/RC is quite high, close to 50 to 1. The rate-limiting step in photosynthesis is exciton transfer, which takes place at a rate 50 times slower than charge transfer. Thus the excess of LH2 serves to increase the overall ratio of stored energy to incident light (Krueger-Koplin 1998). Furthermore, the LH2 complex has a greater density of chlorophyll than the RC, and thus a greater absorption cross-section.

The side-on view of Figure I-6 also relates how a photon may be 'captured' and relayed to the reaction center (Krueger-Koplin 1998) (Sundstrom, Pullerits et al. 1999) (Scholes and Fleming 2000) (Nagarajan and Parson 1997). Photons absorbed by the B800 chlorophylls may be transferred to another B800, or to a B850 chlorophyll, though with some vibrational energy loss (the other processes mentioned above are also posssible). The face to face geometry (see below) of the B850 chlorophyll means that there is strong electronic coupling and thus strong probability for energy transfer. The proximity of one ring to another allows the energy to cross, and ultimately to move along the membrane (in a pseudo-random walk). The LH1 ring itself has a strong coupling with the reaction center, and so the energy is funneled into the components responsible

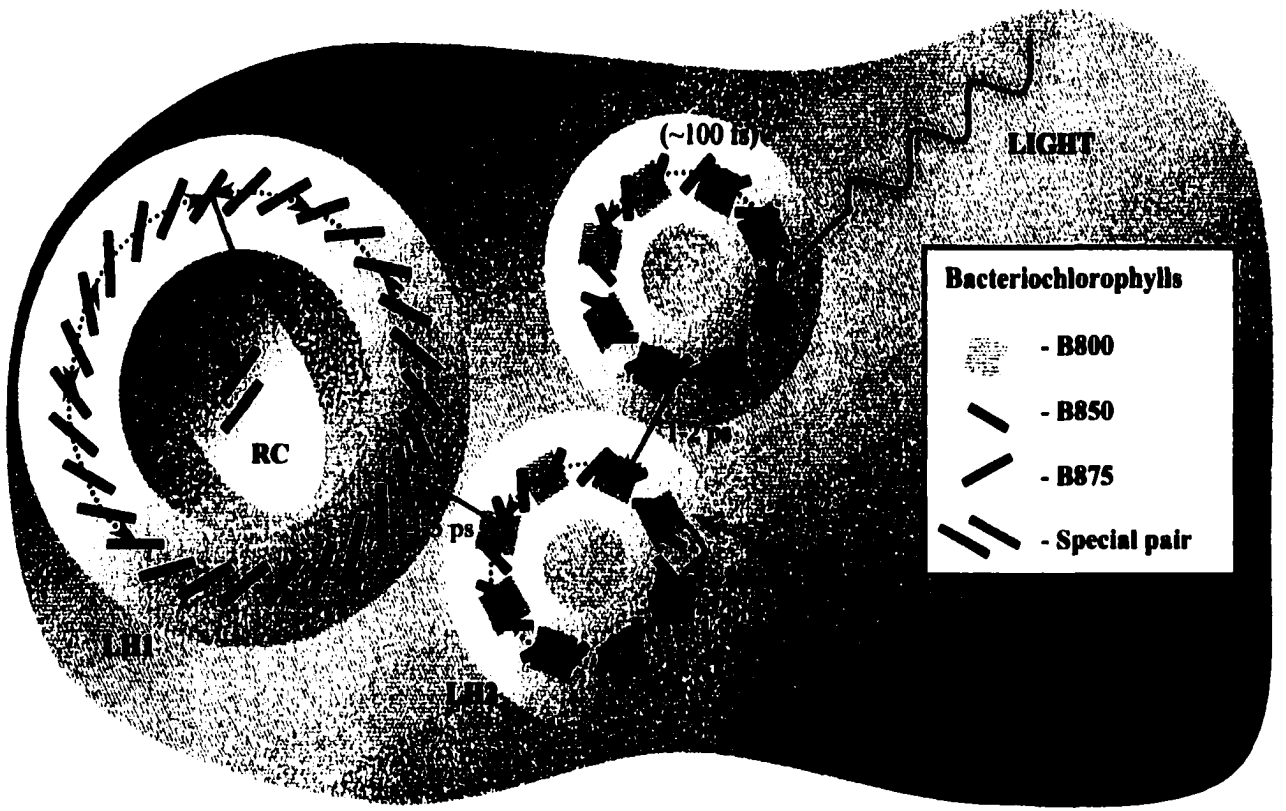

Figure I-6: Energy transfer seen from the periplasmic side. The inner membrane is in blue, the coordinating proteins are gray. Chlorophylls are color-coded according their absorption maximum. The red arrows represent possible paths of electronic excitation. LH2 conducts the energy (with some loss) to LH_1, then to the reaction center. The dotted arrows signify energy delocalization over several chlorophyll pigments (adapted from Krueger 1998 with rates from Sundstrom et al. 1999).

for electron transfer. As in blue-green photosynthesis, this charge separation ultimately leads to ATP synthesis, though the synthase is not shown in either figure.

I.C. The Peripheral Light Harvesting Center and Energy Transfer

I.C.1. *Protein Structure:* The structure of LH2 *Rhodopseudomonas acidophila 10050* (McDermott, Prince et al. 1995) and in Rhodopspirillum molischianum (Koepke, Hu et al. 1996) has been solved from X-Ray diffraction studies. Figure I-7 illustrates one half of the LH2 ring for *Rhodopseudomonas acidophila*, which is believed to be similar to the structure for *Rhodobacter sphaeroides*. The α and β peptides form an inner and outer ring, and serve to coordinate the chlorophyll. The residues on these peptides significantly impact the absorption maximum and the electronic overlap between adjacent molecules (Scholes and Fleming 2000). The overall diameter of the ring is believed to be about 34 Angstroms (Å) (McDermott, Prince et al. 1995).

I.C.2. *Chlorophyll Arrangement and Absorption:* The pigments are arranged in two rings inside the proteins, vertically displaced. One set of rings consists of a flat arrangement of pigments. Adjacent chlorophyll show some edge-to-edge electronic orbital contact, and the time of transfer between pigments is fairly rapid (500fs) (Sundstrom, Pullerits et al. 1999). The absorption that excites these pigments is centered around 800nm. This is shown in the absorption spectrum of Figure I-8. The second ring consists of pairs of chlorophyll in a somewhat displaced face-to-face contact. This second ring has a fairly poor contact with the first, as they are separated by ~18Å (Scholes and Fleming 2000). The time of transfer is judged to be slower as a result (a few ps) (Sundstrom, Pullerits et al. 1999) (Beekman 1997).

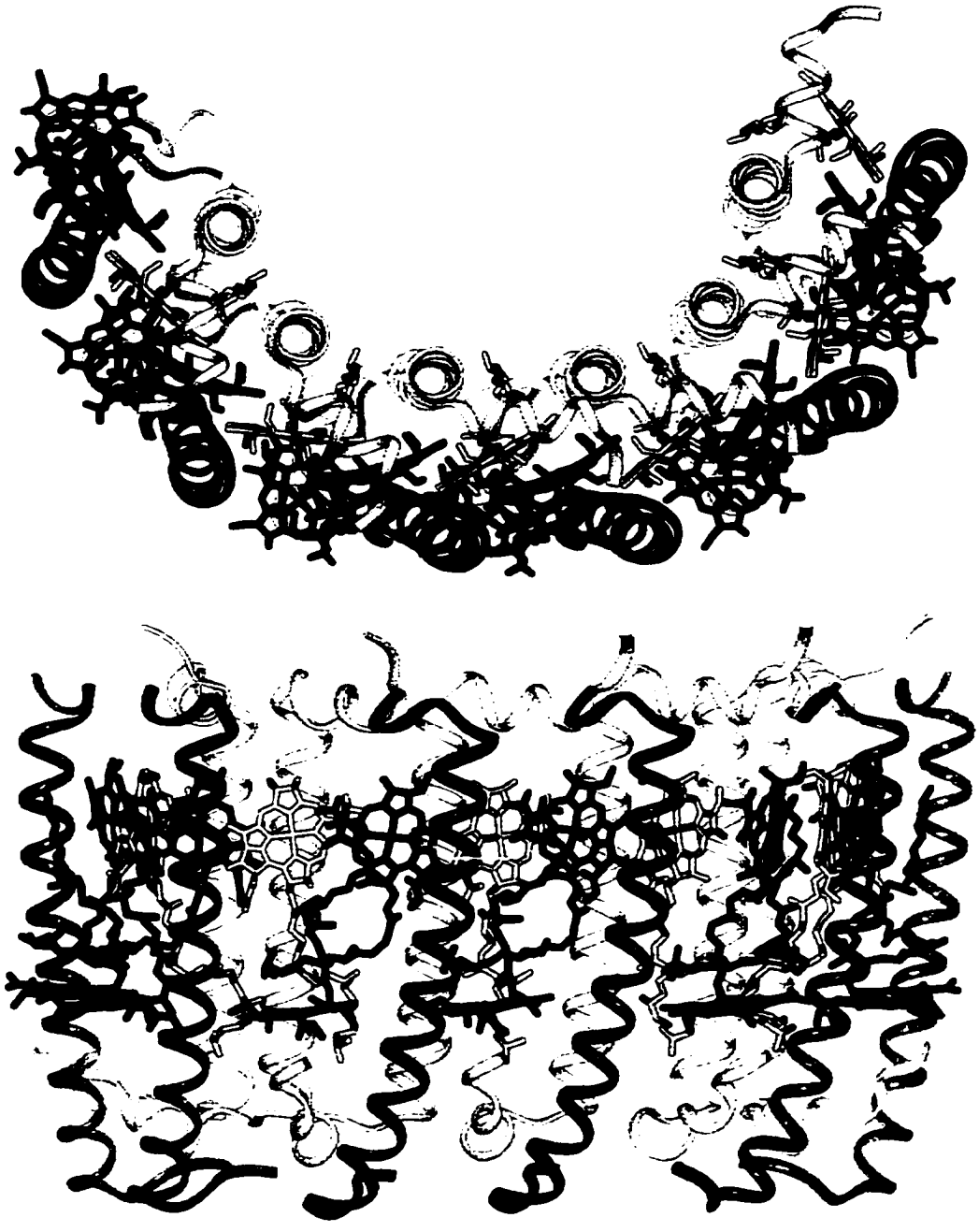

Figure I-7: Half of the ring from the peripheral light harvesting center of *R. acidophila* (the top view is from the periplasmic side). The α peptides are shown in yellow, and the β peptides are in yellow. The red chlorophyll form a ring that may be excited at 800nm, while the yellow and green chlorophyll pair together in a ring reached at 850nm. The figure was generated using InsightII software and the coordinates for the 2.6 Å resolution structure deposited at Brookhaven national labs [McDermott, et al. 1995].

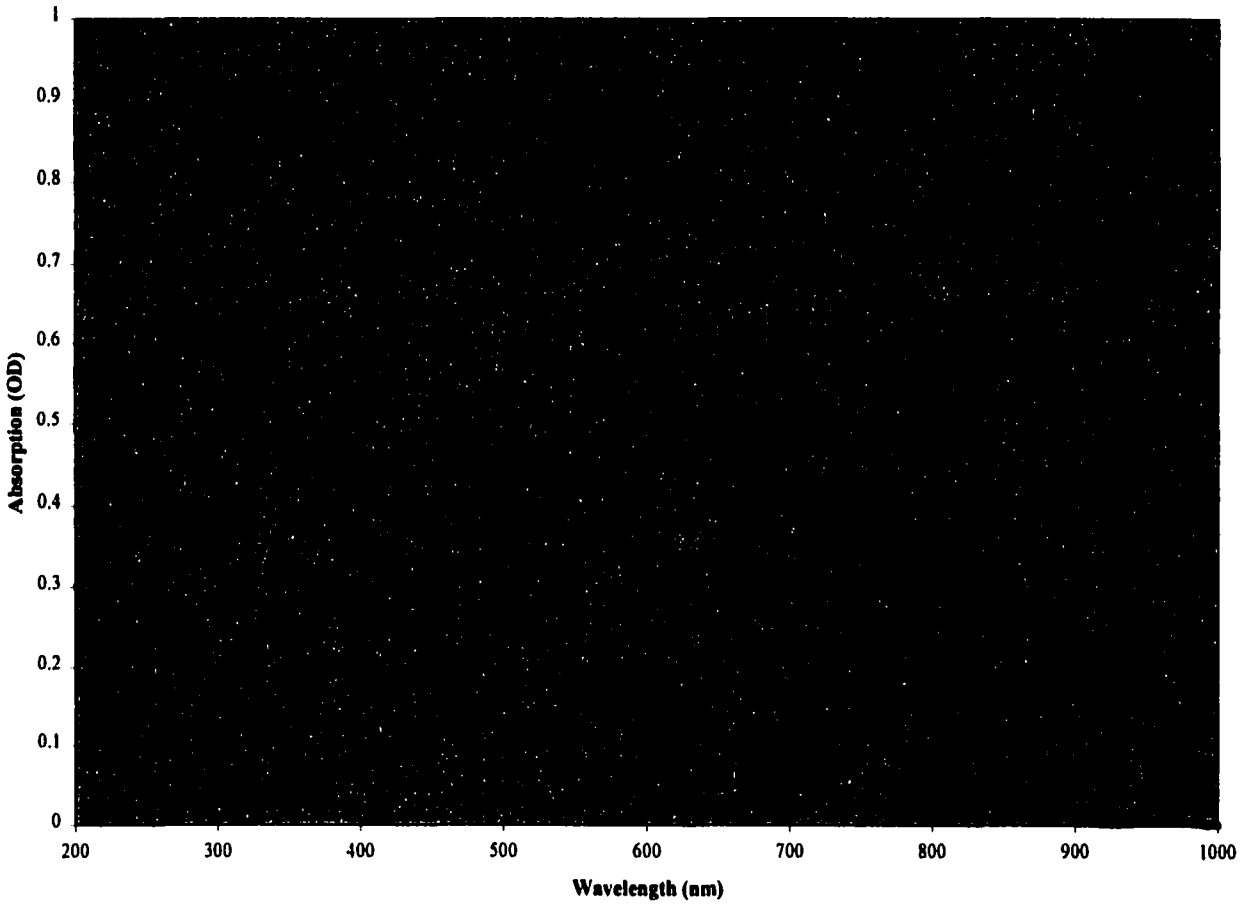

Figure I-8: Spectrum of the peripheral light harvesting complex of *Rhodobacter sphaeroides*, in standard units of optical density (per cm). Absorption peaks at 800nm and 850nm correspond to the two chlorophyll rings of Figure I-7. The 280nm peak is generally an indicator of several amino acid groups, and thus allows a general assessment of general sample contamination. Note the low absorption above 900nm.

I.C.3. *Resonance Energy Transfer:* Not surprisingly, the chlorophyll in the face-to-face ring have a much stronger overlap, and energy levels are more strongly mixed. Thus the absorption maximum to excite these pigments is centered about 850nm. So strong is the level mixing that the entire ring is said to constitute a delocalized orbital. Excitation is spread over several pigments, localizing near the junction of two rings, just before transfer. This mechanism is still not well understood and will be discussed further in the next chapter.

I.D. The Reaction Center and Charge Separation

I.D.1. *Protein Scaffolding:* The X-ray crystallographic structure of Figure 1-9 represented a major breakthrough in protein structure (Deisenhofer, Epp et al. 1985). The reaction center structures from both organisms reveal two homologous polypeptide chains, the L and M subunits, that lace back and forth across the membrane five times each as transmembranous alpha-helices. All of the prosthetic groups are found to interact with these two proteins. A third protein, the H subunit, spans the membrane once and has a large extrinsic domain.

I.D.2. *The Active Components:* The reaction center contains 4 molecules of bacteriochlorophyll (BChl), 2 molecules of bacteriopheophytin (BPh), 2 quinones (Q_A and Q_B) and a nonheme ferrous iron atom, as illustrated in Figure I-10 (the quinones are not shown). Two of the BChls interact strongly to form the so-called primary electron donor, P (also called the special pair). The two BChls of the special pair are arranged parallel to each other and they are separated by about 3.4Å at the ring I pyrroles. The accessory monomer BChls (B_L and B_M), the BPhs (H_L and H_M) and the quinones (Q_A and Q_B) are all placed with approximate C_2 symmetry about an axis that transects P and

Figure I-9: Photosynthetic reaction center from *R. sphaeroides*. The ribbons are polypeptides that coordinate the active components of the reaction center (which are in purple). These proteins are grouped into three subunits; the L subunit is on the left in light blue, while the M subunit is in dark blue on the right. The large H subunit spans the bottom and the backside of the reaction center in medium blue. Insight II software generated this figure with the structure from Brookhaven national labs [Ermler, et al. 1992].

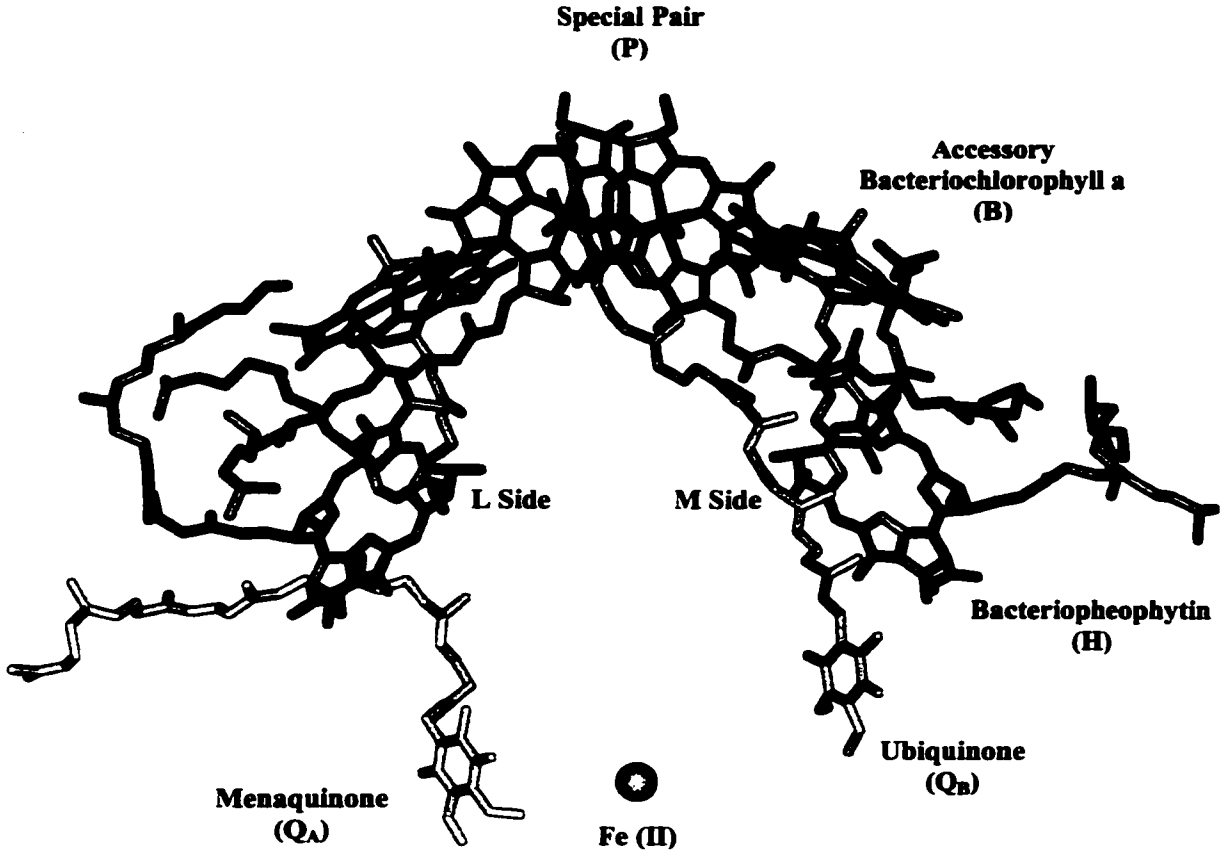

Figure I-10: The active components of the reaction renter are color coded, while the protein scaffolding is stripped away. The special pair is in dark blue, the accessory chlorophyll in purple, and the pheophytin are in green. The mena and ubiquinones are in yellow and orange, respectively. Despite the strong symmetry evident in this figure, electron transfer proceeds only along the left-hand side, or the L side, and not the M side. A common mutation (known as M214H) changes the active (L) pheophytin to chlorophyll.

the iron atom. The polypeptide chains of the L and M protein subunits also obey the approximate symmetry relation. However, the primary structures of L and M are not identical. In spite of the symmetry in the structure, it is well known from functional studies that electron transfer is decidedly asymmetric (Kirmaier and Holten 1987). Electrons are transferred exclusively down the L side of the reaction center (possibly due to stronger dipole overlap).

I.D.3. *Charge Separation and Energetics:* Upon absorption of a photon, the excitation energy quickly localizes on P to form the electronically excited singlet state, P* (Figure I-11 and Figure I-12). P* transfers an electron to one of the two BPhs (H_L) in about 3.5 ps at 295 K (Woodbury, Becker et al. 1985) (Martin, Antonetti et al. 1986) (Paschenko, Chamorovsky et al. 1985; Breton, Fleming et al. 1988) (Wasielewski and Tiede 1986) (Kirmaier and Holten 1988) (Kirmaier and Holten 1990) (Kirmaier and Holten 1991) (Holzapfel, Finkele et al. 1990). The reduced BPh, H_L^-, donates an electron to Q_A in about 200 ps (Rockley, Windsor et al. 1975) (Kaufmann, Dutton et al. 1975) (Kirmaier and Holten 1987), and the electron moves from Q_A to Q_B in about 200 μs. If the photo-oxidized P^+ is reduced by a secondary electron donor such as cytochrome c_2, a second photoelectron can be transferred, ultimately to form doubly reduced (and protonated) Q_BH_2. Q_BH_2 serves as a substrate for the cytochrome b/c_1 complex. The two electron oxidation of Q_BH_2 is coupled to the formation of a proton motive force and ATP synthesis.

Though the general outline of charge transfer is understood, much of the specific details are not well understood. For reasons not totally clear, these reactions occur with quantum yields of essentially 1.0 (Wraight and Clayton 1974). Another characteristic is

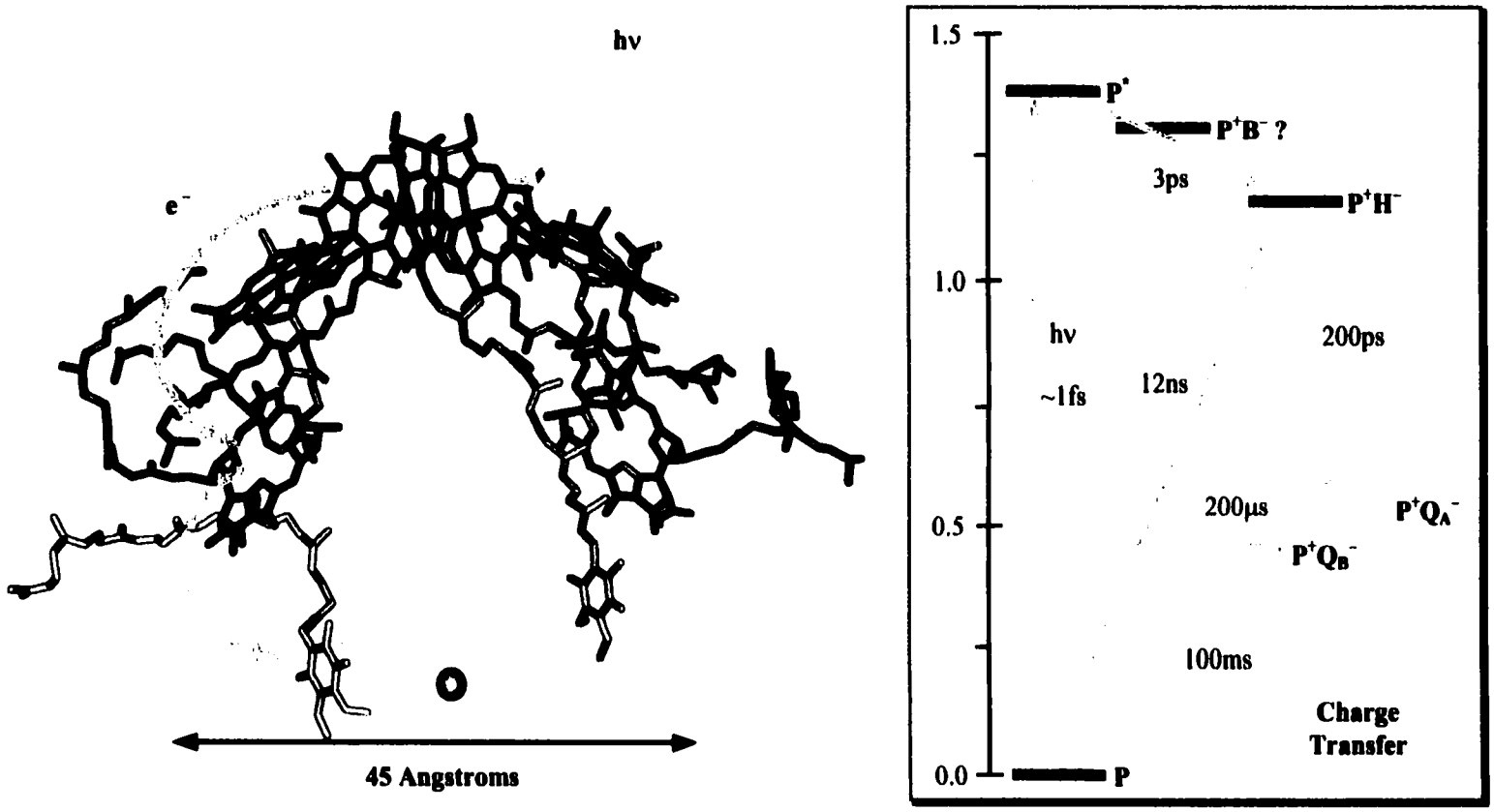

Figure I-11: Charge separation and the possible energetics of the photosynthetic reaction center. Excitation of the special pair initiates the release of a free electron, which localizes upon the pheophytin after only 3ps. The electron transfers to the ubiquinone after 200μs. If the quinone is chemically pre-reduced, the electron returns to the special pair (or is replaced) after only 12ns (the solid line on the energy diagram). The role of the accessory chlorophyll is unclear. Approximate free energies are in electronvolts.

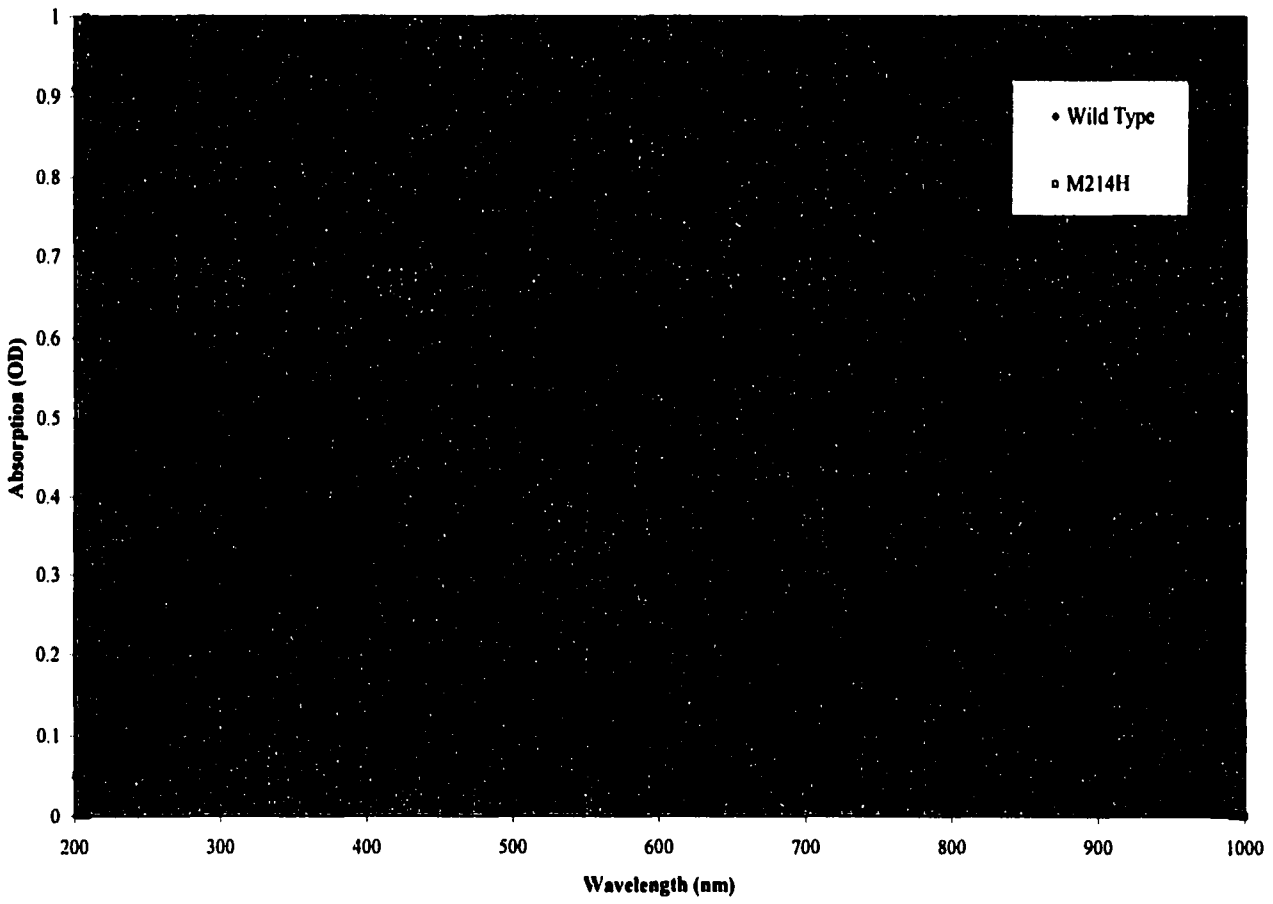

Figure I-12: Spectrum of the reaction center for Wild-type and the mutant M214H (scaled) for *Rhodobacter sphaeroides*. The absorption peak at 875nm corresponds to the excitation of the special pair, while the 800nm peak corresponds to exciting the accessory chlorophyll directly. The 760nm peak excites the pheophytin directly, and is diminished in the mutant, where a chlorophyll has replaced the pheophytin. The height of the 280nm peak illustrates typical sample purities, and reveals the greater difficulty involved with purifying the mutant reaction centers.

their unusual temperature dependence, as they actually speed up with decreasing temperature, down to 4 K (Vos, Jones et al. 1996) (Kaufmann, Dutton et al. 1975) (Kirmaier and Holten 1987) (Fleming, Breton et al. 1988). The study of the initial reaction is particularly important and controversial. Although B_L lies between P and H_L in the reaction center structure, it is not clear that the radical-pair state $P^+B_L^-$ participates in the electron transfer as an authentic electron transfer intermediate (Holzapfel, Finkele et al. 1990). Alternatives to the two-step mechanism have been discussed in the literature (Woodbury, Becker et al. 1985) (Marcus 1988) (Michelbeyerle, Michel et al. 1988). Though the free energy of the P^+Q^- states (on Figure I-11) is fairly well understood (though not all of the data agrees here) (Puchenkov, Kopf et al. 1995) (Arata and Parson 1981) (Edens, Gunner et al. 2000), the free energy of P^+H^- is not clear (Woodbury, Peloquin et al. 1994) (Ogrodnik, Keupp et al. 1994) (Bixon, Jortner et al. 1989) (Skourtis and Mukamel 1995).

I.E. In Vitro Experiments

I.E.1. *Detergent and Micelle Environments:* Most laboratory experiments are not performed in vivo. Instead, the bacteria are lysed and the photosynthetic apparatus are harvested and purified. The hydrophobic peptides that support the pigments will aggregate in water, altering their spectroscopic properties. Figure I-13 shows the amphipathic detergents that support the peptides. The detergents form micelles, as the non-polar 'tails' bind to the protein, while the polar 'heads' will bond to water. Thus the individual components of photosynthesis may be studied separately and in the high concentrations necessary for laser experiments.

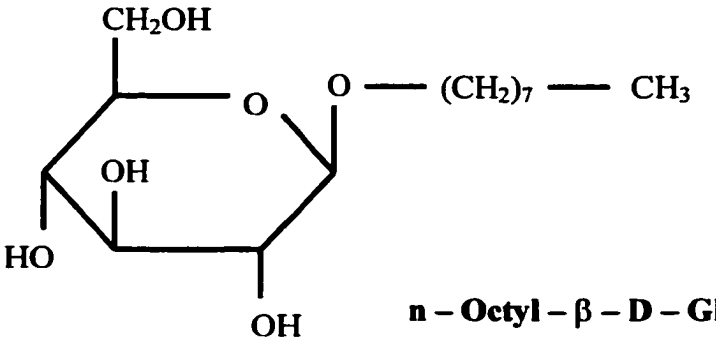

n – Octyl – β – D – Glucoside (βOG)

$C_{14}H_{28}O_6$

M.W. = 292.4

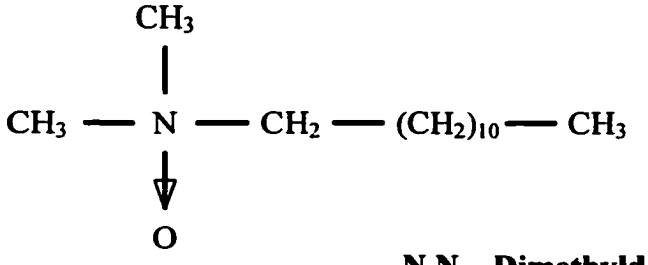

N,N – Dimethyldodecylamine (LDAO)

$C_{14}H_{31}NO$

M.W. = 229.4

Figure I-13: The detergents that support the components of photosynthesis outside the bacterial membrane. The long carbon chains, or tails, on the left side are hydrophobic, while the right sides, known as the heads, are hydrophilic. LDAO is the preferred solvent for protein purification due to its cost. βOG, a milder detergent, provides a more stable protein environment.

I.E.2. *Stabilization:* Keeping the components in detergent is not the only concern for lab work, as the proteins require a variety of protections to prevent degredation. Experiments must ensure that these light sensitive proteins are kept in the dark and that they are stored at around 4 degrees C (Krueger-Koplin 1998). Exposure to light and heat causes rapid protein degradation (and are revealed in the spectra). Finally, purification separates a complex known as a cytochrome (containing four hemes) from the perplasmic side of the reaction center. This protein's chief function is to prevent free oxygen from reaching the reaction center. This strong free radical quickly breaks down the protein. Ultimately, it is difficult to prevent this destructive process, though bubbling the purified proteins with nitrogen delays it considerably. These proteins are relatively stable over a time scale of several weeks under these conditions.

I.E.3. *Quinone Reduction:* Even the simplest model for electron transfer involves a four state vibronic system. As mentioned above, the quinones may be pre-reduced chemically, preventing electron transfer. The electron typically returns directly to the ground state of the special pair. Though this obviously effects the rate of recombination, the charge separation should be unaffected (Figure I-11 relates the energetics of a pre-reduced reaction center).

I.F. Literature Cited

Allen, J. P., G. Feher, et al. (1988). "Structure of the reaction center from *Rhodobacter sphaeroides* R 26 protein cofactor (quinones and Fe 2+) interactions 5." **85**: 8487-8491.

Arata, H. and W. Parson (1981). "Delayed Fluorescence from *Rhodopseudomonas sphaeroides* reaction centers: Enthalpy and free energy changes accompanying electron transfer from P-870 to quinones." Biochimical et Biophysica Acta **638**: 201-209.

Beekman, L. M. P. (1997). A Structural and Functional Characterization Study of the Bacterial Photosynthetic Apparatus: Mutants, Charge Separation and Electric Field Effects., Vrije Universitiet te Amsterdam.

Bixon, M., J. Jortner, et al. (1989). "A superexchange mechanism for the primary charge separation in photosynthetic reaction centers." Biochimica et Biophysica Acta **977**: 273-286.

Breton, J., G. R. Fleming, et al. (1988). "Low Temperature Femtosecond Spectroscopy of the Initial Step of Electron Transfer in Reaction Centers from Photosynthetic Purple Bacteria." Biochemistry **27**: 8276-8284.

Chang, C. H., O. Elkabbani, et al. (1991). "Structure of the Membrane Bound Protein Photosynthetic Reaction Center from *Rhodobacter sphaeroides*." Biochemistry **30**: 5352-5360.

Deisenhofer, J., O. Epp, et al. (1985). "Structure of the Protein Subunits in the Photosynthetic Reaction Center of *Rhodopseudomonas viridis* at 3A Resolution." Nature **318**: 618-624.

Edens, G. J., M. R. Gunner, et al. (2000). "The enthalpy and entropy of reaction for formation of P+QA- from excited reaction centers of *Rhodobacter sphaeroides*." Journal of the American Chemical Society **122**(7): 1479-1485.

Ermler, U., G. Fritzsch, et al. (1994). "Structure of the Photosynthetic Reaction Center from Rhodobacter Sphaeroides at 2.65 Angstrom Resolution Cofactors and Protein Cofactor Interactions." Structure **2**: 925-936.

Fleming, G. R., J. Breton, et al. (1988). "Rates of Primary Electron Transfer in Photosynthetic Reaction Centers and Their Mechanistic Implications." Nature **333**: 190-192.

Garret, R. H. and C. M. Geisham (1995). Biochemistry. Fort Worth, Saungers College Publishing.

Griffiths, M. and R. Y. Stanier (1956). "Some Mutational Changes in the Photosynthetic Pigment System of *Rhodopseudomonas spheroides*." Journal of General Microbiology **14**: 698-715.

Hall, D. O. and K. K. Rao (1999). Photosynthesis. Cambridge, Cambridge University Press.

Holzapfel, W., U. Finkele, et al. (1990). "Initial Electron Transfer in the Reaction Center from *Rhodobacter sphaeroides*." **87**: 5168-5172.

Kaufmann, K., P. L. Dutton, et al. (1975). "Picosecond Kinetics of Events Leading to Reaction Center Bacteriochlorophyll Oxidation." Science **188**: 1301.

Kirmaier, C. and D. Holten (1987). "Primary Photochemistry of Reaction Centers from the Photosynthetic Purple Bacteria." Photosynthesis Research **13**: 225-260.

Kirmaier, C. and D. Holten (1988). "Subpicosecond Spectroscopy of Charge-Separation in *Rhodobacter capsulatus* Reaction Centers." **28**: 79-85.

Kirmaier, C. and D. Holten (1990). "Evidence That a Distribution of Bacterial Reaction Centers Underlies the Temperature and Detection Wavelength Dependence of the Rates of the Primary Electron Transfer Reactions." **87**: 3552-3556.

Kirmaier, C. and D. Holten (1991). "An Assessment of the Mechanism of Initial Electron Transfer in Bacterial Reaction Centers." Biochemistry **30**: 609-613.

Koepke, J., X. C. Hu, et al. (1996). "The crystal structure of the light-harvesting complex II (B800- 850) from *Rhodospirillum molischianum*." Structure **4**(5): 581-597.

Krueger-Koplin, R. D. (1998). Structural Constraints and Assembly of Subunits from the Proximal Light-Harvesting Antenna of *Rhodobacter sphaeroides*. Department of Biochemistry and Molecular Biology. Fort Collins, Colorado State University: 198.

Krueger-Koplin, S. (1998). .

Lehninger, A. L., D. L. Nelson, et al. (1993). Principles of Biochemistry. New York, Worth Publishers.

Marcus, R. A. (1988). "Mechanisms of the Early Steps in Bacterial Photosynthesis and their Implications for Experiment." **28**: 205.

Martin, J. L., A. Antonetti, et al. (1986). "Femtosecond Spectroscopy of Electron Transfer in the Reaction Center of the Photosynthetic Bacterium *Rhodopseudomonas sphaeroides* R 26 Direct Electron Transfer from the Dimeric Bacteriochlorophyll Primary Donor to the Bacteriopheophytin Acceptor with a Time Constant 2.8 +/ 0.2 Psec." **83**: 957-961.

McDermott, G., S. M. Prince, et al. (1995). "Crystal structure of an integral membrane light-harvesting complex from photosynthetic bacteria." Nature **374**(6522): 517-521.

Michelbeyerle, M. E., H. Michel, et al. (1988). "Unidirectionality of Charge Separation in Reaction Centers of Photosynthetic Bacteria." Biochimica et Biophysica Acta **932**: 52-70.

Nagarajan, V. and W. W. Parson (1997). "Excitation energy transfer between the B850 and B875 antenna complexes of *Rhodobacter sphaeroides*." Biochemistry **36**: 2300-2306.

Ogrodnik, A., W. Keupp, et al. (1994). "Inhomogeneity of radical pair energies in photosynthetic reaction centers revealed by differences in recombination dynamics of

P+HA- when detected in delayed emission and in absorption." Journal of Physical Chemistry **98**(13): 3432-3439.

Paschenko, V. Z., S. K. Chamorovsky, et al. (1985). "Estimation of the Rate of Photochemical Charge Separation in *Rhodopseudomonas sphaeroides* Reaction Centers by Fluorescence and Absorption Picosecond Spectroscopy." FEBS Letters **191**: 245-248.

Puchenkov, O. V., Z. Kopf, et al. (1995). "Photoacoustic diagnostics of laser-induced processes in reaction centers of *Rhodobacter sphaeroides*." Biochimica et Biophysica Acta: Bio-Energetics **1231**(2): 197-212.

Rockley, M. G., M. Windsor, et al. (1975). "Picosecond Detection of an Intermediate in the Photochemical Reaction of Bacterial Photosynthesis." **72**: 2251.

Scholes, G. D. and G. R. Fleming (2000). "On the mechanism of light harvesting in phtotsynthetic prurple bacteria: B800 to B850 energy transfer." Journal of Physical Chemistry **104**: 1854-1868.

Sistrom, W. R. (1960). "A Requirement for Sodium in the Growth of *Rhodopseudomonas spheroides*." Journal of General Microbiology **22**: 778-785.

Skourtis, S. S. and S. Mukamel (1995). "Superexchange versus sequential long range electron transfer; density matrix pathways in Liouville space." Chemical Physics **197**: 367-388.

Stryer, L. (1995). Biochemistry. New York, W. H. Freeman.

Sundstrom, V., T. Pullerits, et al. (1999). "Photosynthetic light harvesting: Reconciling dynamics and structure of purple bacterial LH2 reveals function of photosynthetic unit." Journal of Physical Chemistry B **103**(13): 2327-2346.

Van Amerongen, H., L. Valkunas, et al. (2000). Photosynthetic Excitons. Singapore, World Scientific.

van Brederode, M. E. (1999). New Pathways for Ultrafast Electron Transfer in Photosynthetic Reaction Centers of *Rhodobacter sphaeroides*, Vrije Universiteit te Amsterdam.

Voet, D. and J. G. Voet (1990). Biochemistry. New York, John Wiley & Sons.

Vos, M. H., M. R. Jones, et al. (1996). "Vibrational dephasing of long- and short-lived primary donor excited states in mutant reaction centers of *Rhodobacter sphaeroides*." Biochemistry **35**(8): 2687-2692.

Wasielewski, M. R. and D. M. Tiede (1986). "Subpicosecond Measurements of Primary Electron Transfer in Rhodopseudomonas Viridis Reaction Centers Using Near Infrared Excitation." FEBS Letters **204**: 368-372.

White, D. (2000). The Physiology and Biochemistry of Prokaryotes. New York, Oxford University Press.

Woodbury, N., M. Becker, et al. (1985). "Picosecond kinetics of the initial photochemical electron- transfer reaction in bacterial photosynthetic reaction centers." Biochemistry **24**(26): 7516-7521.

Woodbury, N. W., J. M. Peloquin, et al. (1994). "Relationship between thermodynamics and mechanism during photoinduced charge separation in reaction centers from *Rhodobacter sphaeroides*." Biochemistry **33**(26): 8101-8112.

Wraight, C. A. and R. K. Clayton (1974). "The absolute quantum efficiency of bacteriochlorophyll photooxidation in reaction centers." Biochimica et Biophysica Acta **333**: 246-260.

II. ENERGY TRANSFER: THEORIES & EXPERIMENTS

Though much is known about the early events in photosynthesis, many issues remain in doubt. In particular, theory and experiment seek to understand the relationship between the rate of the steps of photosynthesis and the energies involved. The energy pathway of the inner membrane appears to exhibit both classical and quantum mechanical behavior. In the light harvesting center, energy is in the form of photons and the pathway lies through resonance energy transfer. In the reaction center, though the energy is known to localize upon an electron, the exact energies are not clear. Even the electron's exact path is not fully known. Though a wealth of information has been determined from a variety of experiments, some of it is contradictory, and there is little agreement over the appropriate models of energy transfer.

II.A. Introduction

II.A.1. *Probability Amplitudes and Physical Processes:* The time evolution of any physical process may be described quantum mechanically using the formalism of probability amplitudes. A system is initially in an arbitrary state, described by the wavefunction ψ_i. We may subject it to some change, denoted by $U(t_f,t_i)$, known as the evolution operator (t_f and t_i refer to some final and initial times, respectively). The probability that the system may be found in some new state (ψ_f) is given by Equation II-1. The bra and ket notation of this equation signifies an integral of the product of ψ_i

$$P_{if} = \left|\langle \psi_f | \, U(t_f, t_i) | \psi_i \rangle\right|^2 \qquad \textbf{(II - 1)}$$

(after operation by U) and the complex conjugate of ψ_f. From this result, probabilities and rates of the process may be found, using Equation II-2, known as 'Fermi's golden

$$k = \frac{2\pi}{\hbar}\left|\langle \psi_f | H'(t_f, t_i) | \psi_i \rangle\right|^2 \rho \qquad \textbf{(II - 2)}$$

rule.' Here ρ is the density of states per unit energy, while H' is the perturbing part of the Hamiltonian (sometimes denoted by H_{RP}) (Cohen-Tannoudji, Dupont-Roc et al. 1992) (Bransden and Joachain 1990) (Oppenheimer 1928).

Determining the form of the evolution operator requires knowing the Hamiltonian of the system, while describing the wavefunctions requires relating the key variables of the system to those that may be observed (via the quantum Liouville equation). Obtaining all of this information is often extremely difficult, and some approximations must be invoked. Many body problems pose especially serious issues. Simply knowing which variables are crucial is as tough as knowing which upon approximations to rely. Examining the interactions between photons, phonons and electrons in large molecules becomes a daunting task. These cases present difficult challenges for those who wish to reconcile theory and experiment.

II.A.2. *Energy Transfer:* When an atom within molecule is excited, the energy may be localized upon a single electron (or, more typically, the valence electron is the only particle directly affected). Often the orbitals of the atom are so strongly mixed with those of adjacent atoms that it is appropriate to discuss the wavefunction of the entire molecule (found approximately by superposing the individual atomic wavefunctions). The excited state exists over the entire molecule, as it does in bacteriochlorophyll.

When neighboring molecules are fairly distant, their wavefunctions are said to be diabatic and the energy levels do not overlap. Energy transfer between these molecules must involve a photon (or phonon) or an energetic particle that will carry the energy

between the molecules. As the wavefunctions overlap more strongly in the adiabatic case, some mixing of the molecular orbitals occurs, and the rate of transfer is generally faster. In the case of very strong overlap, an excited electronic state may exist between the two and the energy is described as delocalized over the adjacent molecules.

II.A.3. *Classical Rate Kinetics:* Even without the exact eigenfunctions of the system, it seems reasonable that knowledge of the energies involved should lead to a reasonable prediction concerning the speed of the reaction. The Arrhenius model (sometimes known as the collision model) is defined in Figure II-1, while the rate at which reactants convert into products, as they move along the reaction, or nuclear coordinate is shown in Equation II-3. The rate is k, E_a is the activation energy, T the

$$k = zpe^{-E_a/k_BT} \qquad \textbf{(II - 3)}$$

temperature, z is the collision frequency and p is the probability of correct orientation. This rate decreases with increasing activation energy, which is the energy required to reach the transition state. The rate increases with increasing reaction temperature, as the number of collisions is assumed to increase.

II.A.4. *Quantum Mechanical Tunneling:* As a classical model, Equation II-3 does not explain the reactions that occur when there is either little overlap between the initial and final states or a physical barrier prevents the reaction classically. Figure II-2 details such a barrier problem, including the quantum mechanically allowed transmission (or reaction) probability, P , in Equation II-4 (De Vault 1984) (Park 1974). E is the

$$P = \frac{16EV}{(E+V)^2} e^{-2b\sqrt{2mV}/\hbar} \qquad \textbf{(II - 4)}$$

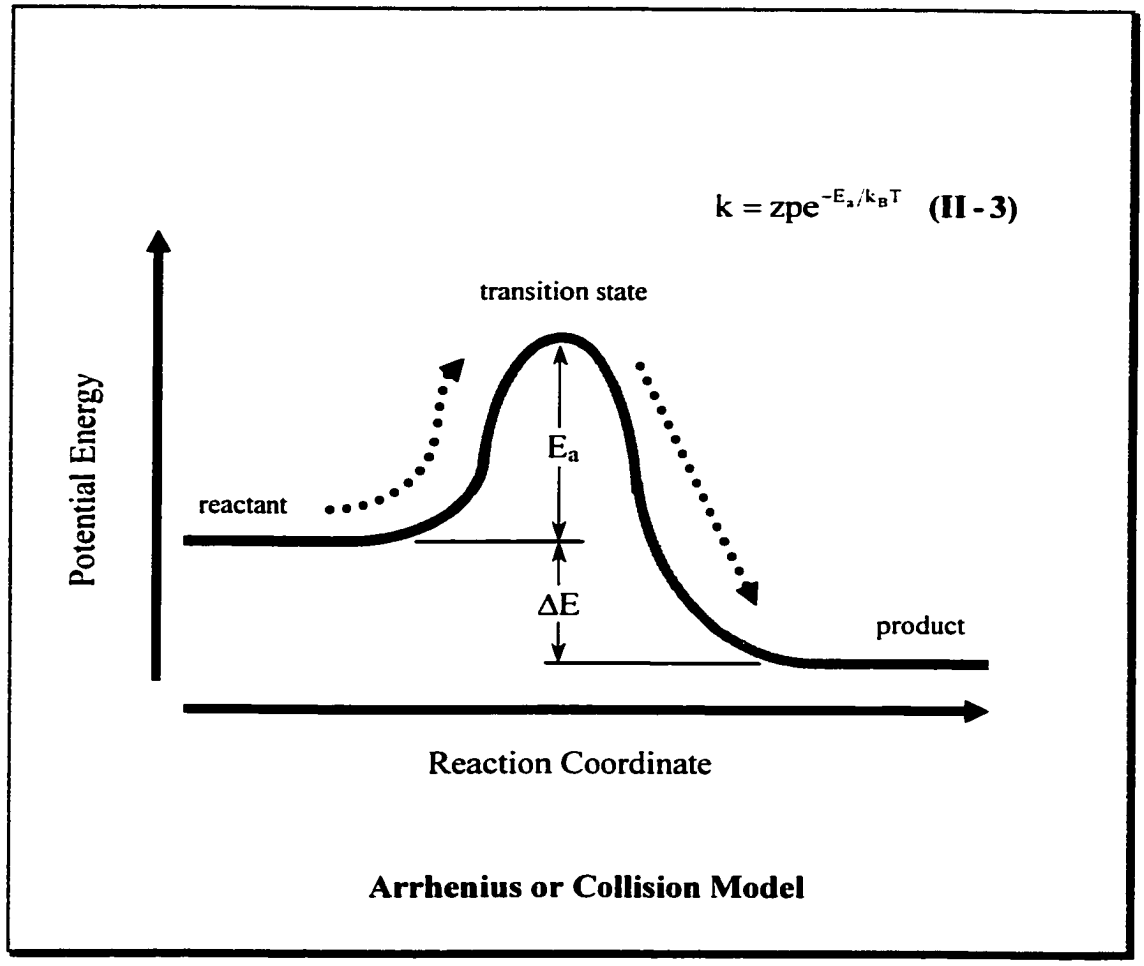

Figure II-1: Collision model for reactions. A system starts off in a state known as the reactant. As the system converts into the product, energy ΔE is given off to the surroundings, though an activation energy E_a must be acquired by the system before the reaction may complete. The activation energy is obtained randomly through collisions with the surroundings, which occur with a frequency z. Equation II-2 relates the activation energy to the reaction rate k. p represents the fraction of collisions with the correct orientation.

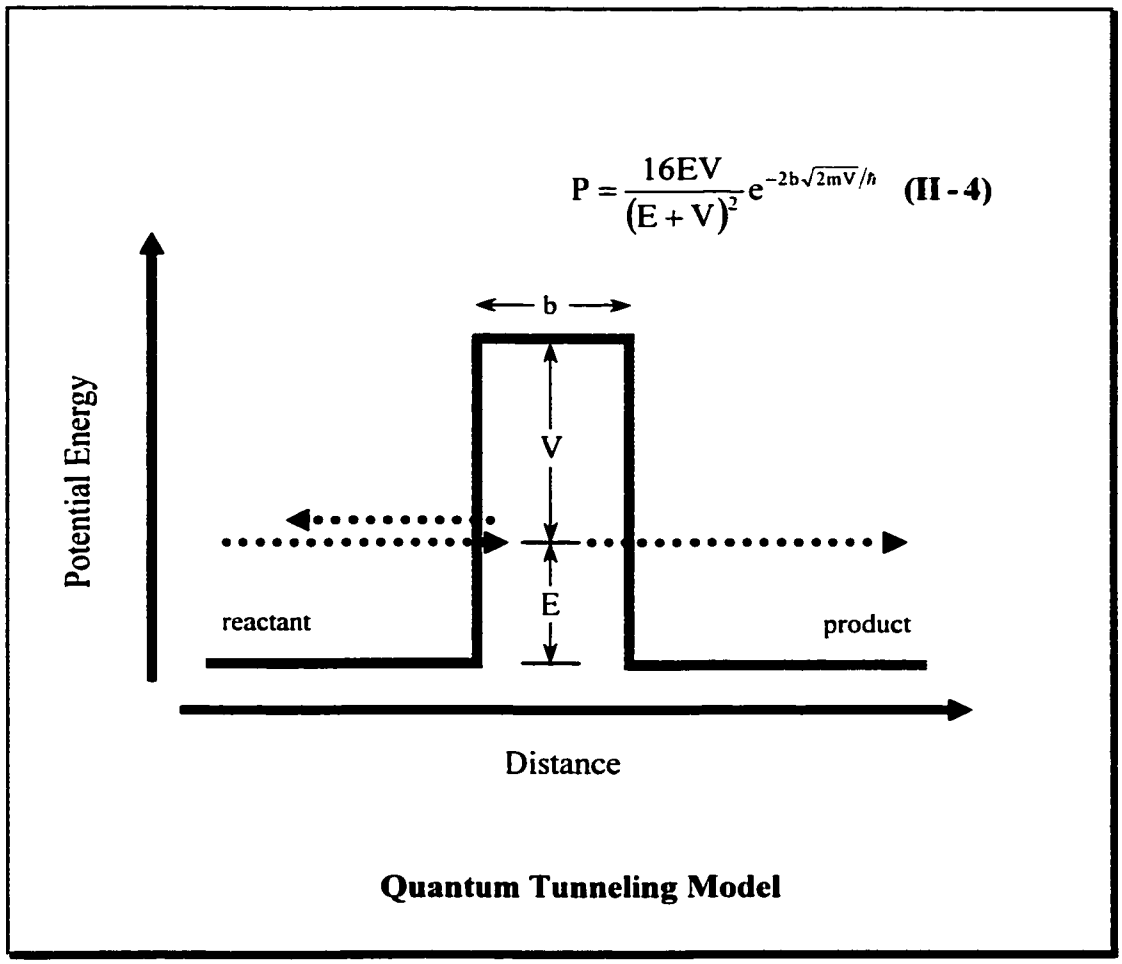

Figure II-2: Tunneling model for reactions. With energy E, a particle approaches a barrier of width b. Classically, the particle may never pass though a barrier of greater energy than the particle. The probability of transmission, though small, is given by Equation II-4 (from which the rate may be found). Here the transition state is virtual, while the reactant and product are interpreted as before. In this special case, the reactant and product states are isoenergetic.

particle energy, m is the particle's mass, ħ is Planck's constant and V and b are the barrier height and width, respectively. Variations on this problem allow the initial energy to differ from the final energy or to enclose the left and right hand side in a potential box, or well. Again, the rate of reaction increases with increasing energy and temperature.

II.B. The Light Harvesting Center and Resonance Energy Transfer

II.B.1. *Exciton or Förster Energy Transfer:* The interaction of matter and electromagnetic energy is not accurately described by either of the above models. Instead, most of the theory relies upon developing Equation II-1 directly to calculate the appropriate rates, though the electromagnetic field is typically treated semi-classically. The Einstein A and B coefficients describe the probabilities of absorption and emission of radiation by atoms and molecules. Thus the transfer of electromagnetic energy from one molecule to another is usually described in terms of emission from what is termed a 'donor' molecule followed by absorption by the 'acceptor.' However, energy may also be directly transferred to an adjacent molecule.

Shown schematically in Figure II-3, the theory of resonance energy transfer was first suggested by Frenkel (Frenkel 1931) and applied to biological molecules by Förster (Forster 1948) (Forster 1959) (Stryer 1978). The rate that results is shown in Equation II-5, while Equation II-6 reveals the dependence of the transfer efficiency (ε) upon distance

$$k_T = \frac{J\kappa^2 k_F}{n^4 r^6}(8.71\times10^{23}s^{-1}) \qquad \textbf{(II - 5)}$$

$$\varepsilon = \frac{R_o^{\,6}}{R_o^{\,6} + r^6} \qquad \textbf{(II - 6)}$$

(r). The distance at which the efficiency is 50% is R_o. This distance, like the rate (k_T) depends upon the orientation factor κ, the fluorescence rate of the donor k_F, the index of

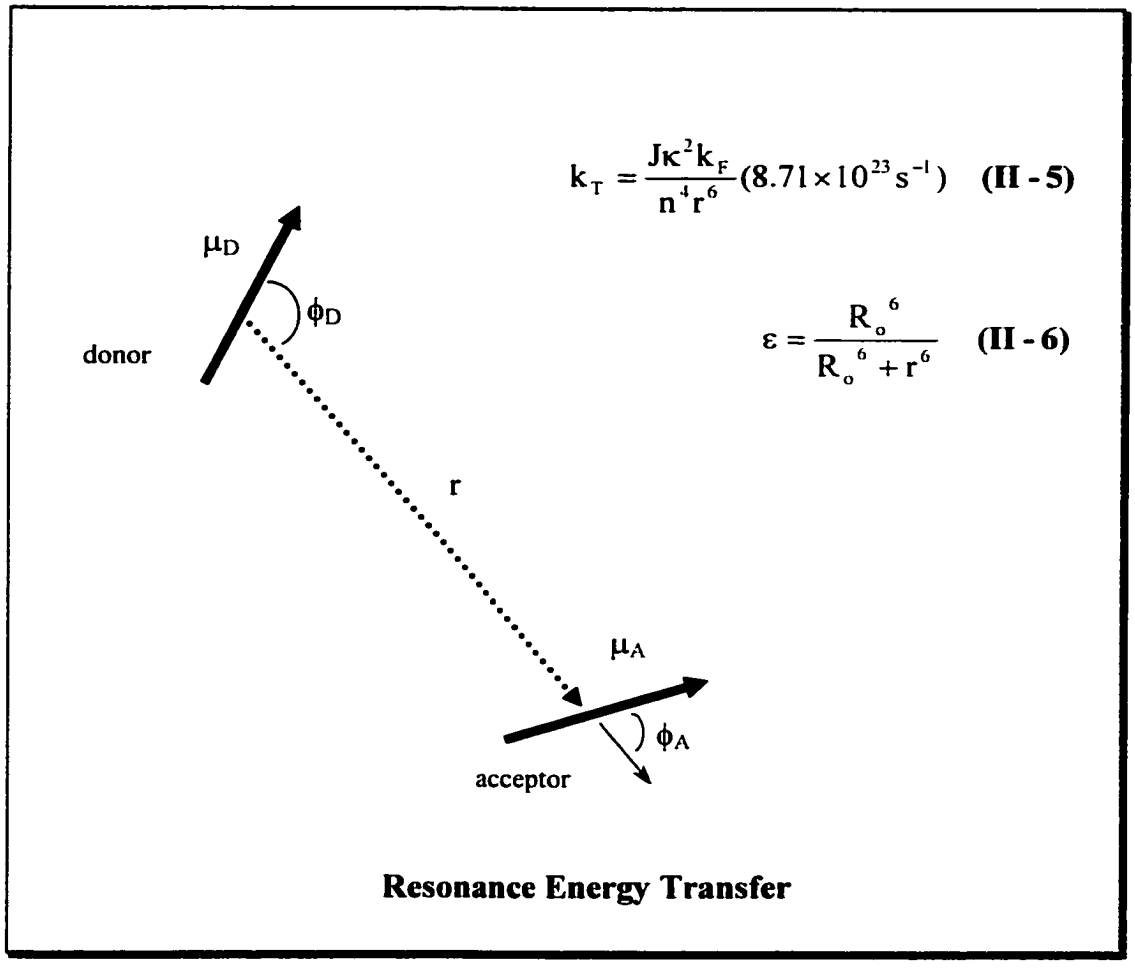

Figure II-3: Resonance energy transfer. Förster's theory relates the overlap between two dipoles and the rate of direct energy transfer k_r, in equation II-5. κ is an orientation factor, determined by the angles in the figure, k_F is the fluorescence rate for the donor, n is the index of refraction. Finally, J is an integral of the overlap between the donor's emission spectrum and the acceptor's absorption spectrum. Equation II-6 reveals the dependence of the efficiency upon the distance between the two dipoles. R_o is the distance where the efficiency is 50% (which is dependent upon the same variables above).

refraction n and an integral of the overlap between the donor's emission spectrum and the acceptor's absorption spectrum. The exciton of the model is defined as a superposition of molecular excitations. Appropriate for distances from 10 Å and as far as 70 Å (and contingent upon the terms defined in the figure), this mechanism has been developed to explain the strong and fast energy transfer seen in many systems. Fluorescence and absorption models do not account for the yields and rates of these processes. There are still discrepancies in the evaluation of the terms in II-5. Even its derivation is approximate, as it treats the molecules as dipoles, ignores the electronic environment, dismisses possible structural inhomogeneities and ignores transitions to forbidden states (Van Amerongen, Valkunas et al. 2000) (Van Der Meer, Coker et al. 1994) (Sumi 2000). However, the outline of the theory is accepted.

II.B.2. *The Peripheral Light Harvesting Center:* As mentioned in Chapter I, the peripheral light harvesting centers consist of rings of bacteriochlorophyll coordinated by peptides. The higher energy ring, known as B800, consists of bacteriochlorophyll that show some electronic overlap, with an intermolecular distance of about 20Å. Energy 'hops' from one chlorophyll to another, requiring roughly 500fs (recall Figure I-6). Traversing the larger gap between the B800 ring and the B850 ring requires a few picoseconds (Sundstrom, Pullerits et al. 1999). This coupling appears to be due to the orientation of the dipole of the donating chlorophyll (recall Figure I-4) (Van Amerongen, Valkunas et al. 2000), as well as surprisingly strong electron-phonon interactions (Scholes and Fleming 2000). The chlorophylls of the B850 ring, however, are close (only several Angstroms) and face-on. Thus the pi orbitals mix strongly and the energy levels are delocalized over the entire ring. Similar delocalization is believed to exist for

the proximal light harvesting center, as well as between the rings themselves (and even onto the RC) (Van Amerongen, Valkunas et al. 2000).

II.B.3. *Observations:* Many different types of ultrafast laser experiments have been performed on LH2, both isolated and in membranes. Femtosecond pump-probe spectroscopy upon membrane-bound LH2 appears to support a coherent excitation of inhomogeneous antennae (Nagarajan, Johnson et al. 1999). Membrane bound LH2 seem to transfer energy between each other with a characteristic rate of a few picoseconds (Timpmann, Woodbury et al. 2000). Room temperature fluorescence decay experiments also suggest that the exciton is delocalized over about 3 to 4 pigments (the excitation is also referred to as a coherence over the appropriate length) (Pullerits, Chachisvilis et al. 1996) (Monshouwer, Abrahamsson et al. 1997). The time for energy to spread from one chlorophyll to another is typically 100fs (Van Amerongen, Valkunas et al. 2000). Low temperature fluorescence and transient absorption data on isolated LH2 seem to indicate fairly short (~ 500fs) relaxation times for the excited energy, while room temperature transient grating experiments appear to show a similar fast decay (~ 800fs) (Joo, Jia et al. 1996). The decay is due to the eventual localization of energy and its release into the solvent or as fluorescence. As mentioned in the previous chapter, energy transfer appears to have evolved to favor the eventual capture of as many photons as possible, not the rapid conversion of any single photon.

II.C. Electron Transfer

II.C.1. *Introduction:* Though the transfer of photons and excitons are important mechanisms in biological systems, most of the major metabolic processes involve charge separation and transfer. For this problem it becomes necessary to treat not just the

electronic moment, but the electronic and vibrational energy levels of the molecules involved (though more correct treatments of exciton transfer involve that as well). Though the simple energy level diagrams of Chapter I only portray the electronic structure of the reaction center, the vibrational structure is generally understood to be important (and often too complicated to draw). These levels are usually modeled as simple harmonic oscillators, though more exact approaches for larger nuclear vibrations utilize the Morse oscillator model (Bransden and Joachain 1990). Whatever the model used, there are also generally more than one independent variables, though again, for clarity's sake, only one is typically shown.

Such a complicated problem necessarily leads to approximations in the Hamiltonian. In addition to the harmonic oscillator model approximation, the nuclear and electronic wavefunctions may be treated separately in the Born-Oppenheimer approximation (Born and Oppenheimer 1927). This is allowed due to the significantly heavier mass of the nuclei, allowing them to be treated as stationary with respect to the more mobile electrons. The Condon approximation similarly treats the electronic wavefunction separately from the nuclear wavefunction (De Vault 1984). Furthermore, the overlap between the nuclear wavefunctions is assumed to be fairly weak (diabatic), so that Fermi's Golden Rule may be applied (Kuznetsov and Ulstrop 1999). Finally, the treatment of the surrounding environment is perhaps the trickiest aspect. A common approach is to treat the environment as a simple dielectric medium, though there is no one agreed upon model. Additionally, perturbation theory is often applied to the developed equations for electron transfer.

II.C.2. *Marcus Theory of Electron Transfer:* Surprisingly, the key to understanding electron transfer lies in the *nuclear* motions of the molecules involved. Figure II-4 lays out the important aspects of quantum electron transfer. The heavy gray surfaces represent the allowed nuclear energy surfaces (one-dimensional and harmonic). Two different configurations are shown by the two different curves. When an electron tunnels or is transferred either inter or intra-molecularly, the molecule moves from one surface to the other as the nuclear equilibrium polarization changes. Conservation of energy insists that a molecule may only make the jump along a horizontal line, while the Franck-Condon principle demands that the nuclear configuration remain the same immediately after the transfer and limits the jump to a vertical line. Thus the reactant state may only convert into the product state at the crossing point marked 'transition.'

In this low overlap (diabatic) picture, Fermi's Golden Rule (Eqn. II-2) is useful. The matrix element H_{RP} is also known as the electronic overlap, describing the overlap between the wavefuctions of the reactant and product. The appropriate density of states is heavily determined by the Franck-Condon principle and is known as the Franck-Condon weighted density of states, or FCWD. Marcus first developed a full statistical mechanical treatment of the density of states by considering nuclear motions classically (Marcus 1956) (Marcus and Sutin 1985). The simple, one-dimensional picture of the figure yields the same result, and the rate of transfer is shown in Equation II-7. While

$$k = \frac{2\pi}{\hbar}|H_{RP}|^2 \frac{1}{\sqrt{4\pi\lambda k_B T}} \exp\left(-\frac{(\lambda + \Delta G)^2}{4\lambda k_B T}\right) \qquad \textbf{(II - 7)}$$

ΔG is the Gibbs free energy of the reaction, λ is the reorganization energy required to conform the nucleus from the reactant into the product. Finally, T is the temperature, k_B

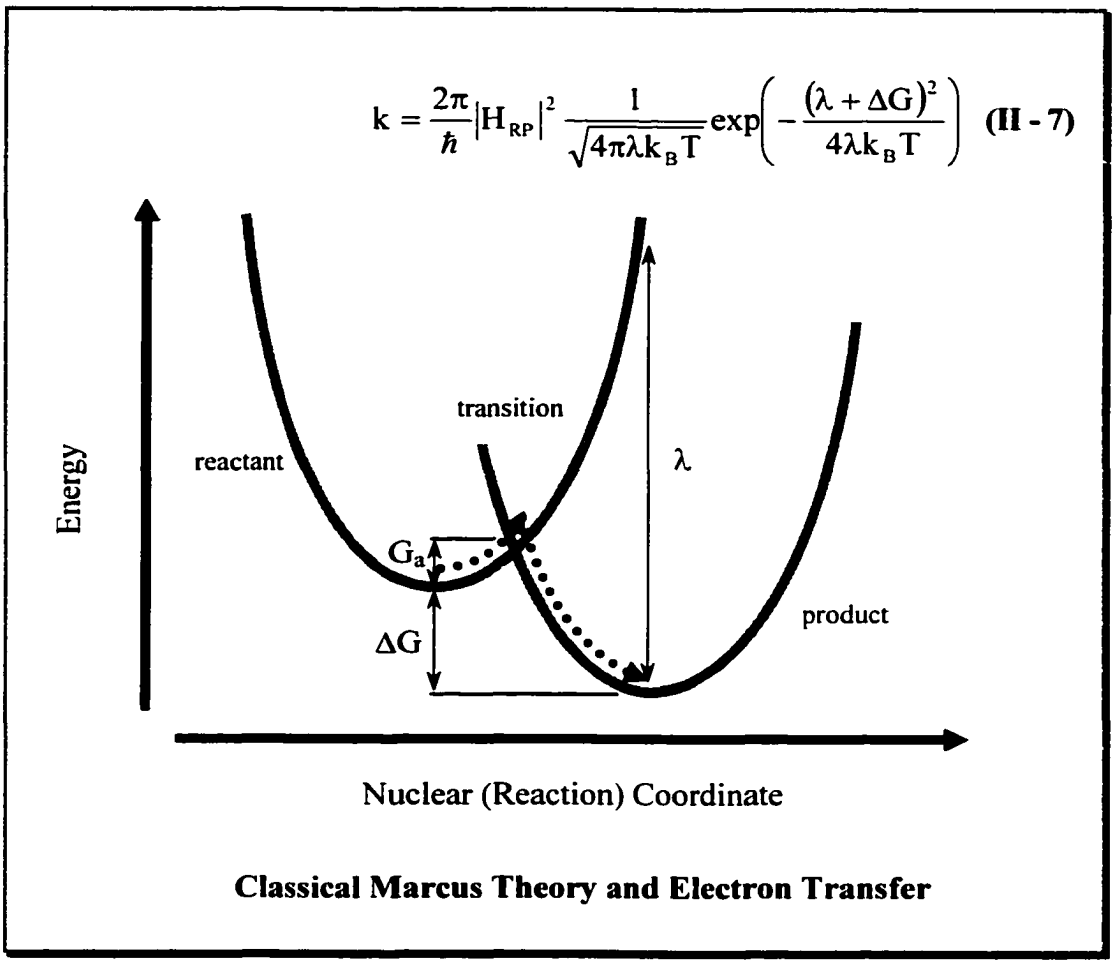

Figure II-4: Marcus theory of electron transfer in the diabatic (low overlap) and classical (high temperature) limits. The solid curves are the potential energy wells for the nuclear motion of the product and reactant. Here ΔG is the Gibbs free energy of the reaction, G_a is the activation energy, and λ is the reorganization energy required to conform the nucleus from the reactant into the product. Equation II-7 gives the result of Fermi's Golden Rule (II-2) for the model above.

is the Boltzmann constant and ħ is again Planck's constant. It is possible to treat nuclear motions in a semi and fully quantum mechanical way as well, though all models converge in the high temperature limit.

II.C.3. *Adiabaticity:* Though the picture above was derived for weakly overlapping orbitals, it is possible examine the consequences of adiabatic overlap. In this case, the free energy surfaces of the reactant and the product are not distinct, but mix strongly. As shown in Figure II-5, this picture now resembles the classical transition theory. Now the free energy, ΔG, may be transformed into the energy of the reaction using Equation II-8 (the energy, ΔU, and enthalpy, ΔH, differ only by $k_B T$). Equation II-

$$\Delta G = \Delta H - T\Delta S \qquad \textbf{(II - 8)}$$

3 is recovered, with the entropy term assigned to the collision frequency term (and is also fairly small) (De Vault 1984).

II.C.4. *The Activation, Gibbs Free and Reorganization Energy:* While the activation and Gibbs free energy have the same meaning in classical theory, the appearance of the reorganization energy has no classical analogue. This energy is needed to change the nuclear conformation from the initial to the final state without the electron's transfer. Classically, the reaction rate increases with increasing free energy. In the quantum theory, however, the rate increases until it reaches the activationless region, then decreases, as shown in Figure II-6.

II.D. The Reaction Center and Experimental Data

II.D.1. *Initial Observations:* In reaction centers, the fluorescence decay experiments upon P* have shown complicated decay rates. Original experiments showed that when the quinone was pre-reduced, the electron localized upon a pheophytin. There

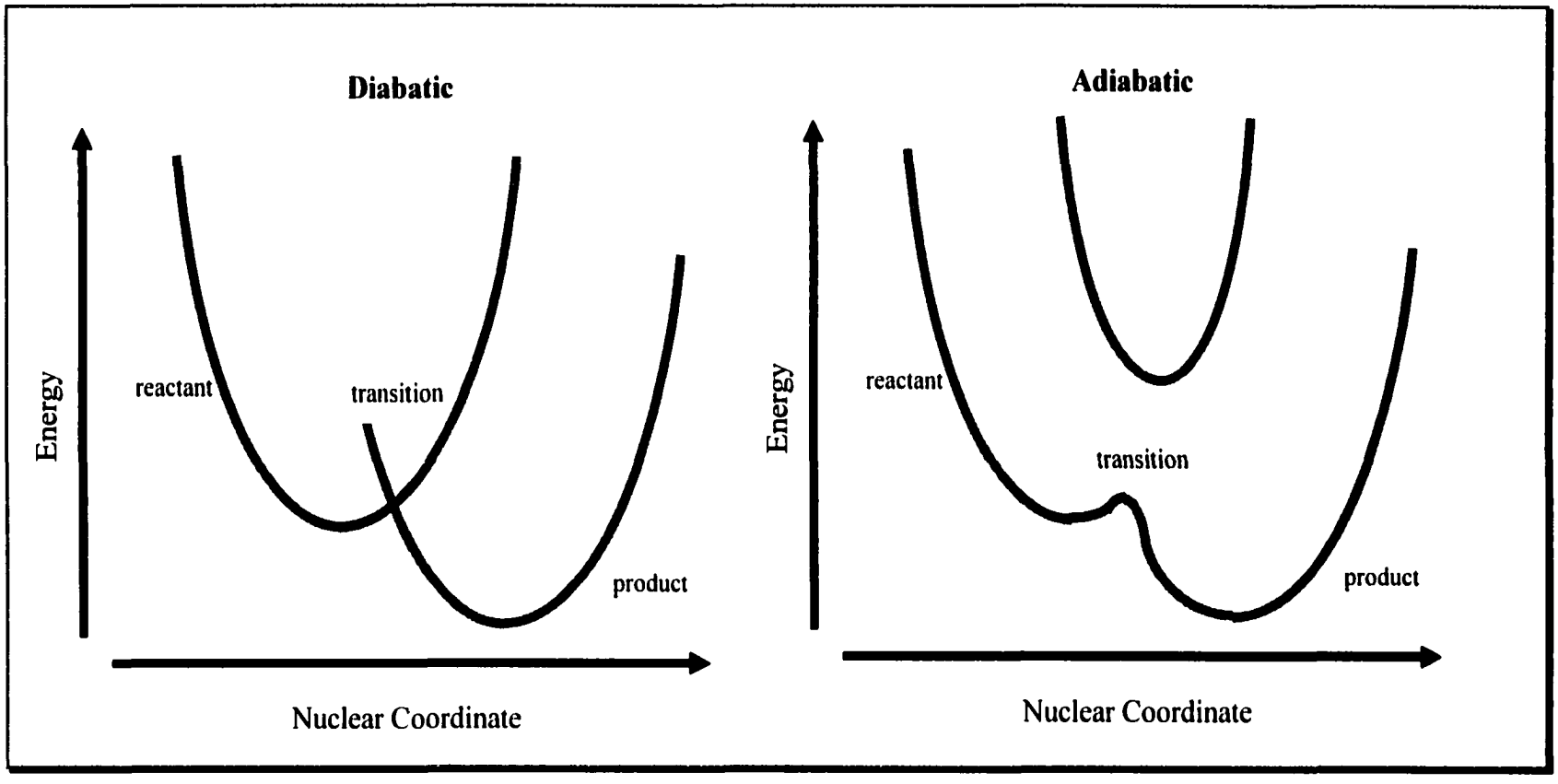

Figure II-5: Adiabatic and diabatic transfer. On the left, there is poor overlap between wavefunctions, and the electron must tunnel through some barrier (or over a distance). The probability of reverse tunneling may be quite high, and the electron may spend some time moving back and forth through the crossing area. On the right, the wavefunctions strongly overlap, the middle region splits onto two curves, and the lower one is a smooth transition state. No tunneling occurs here, and the picture is now similar to that of Figure II-1.

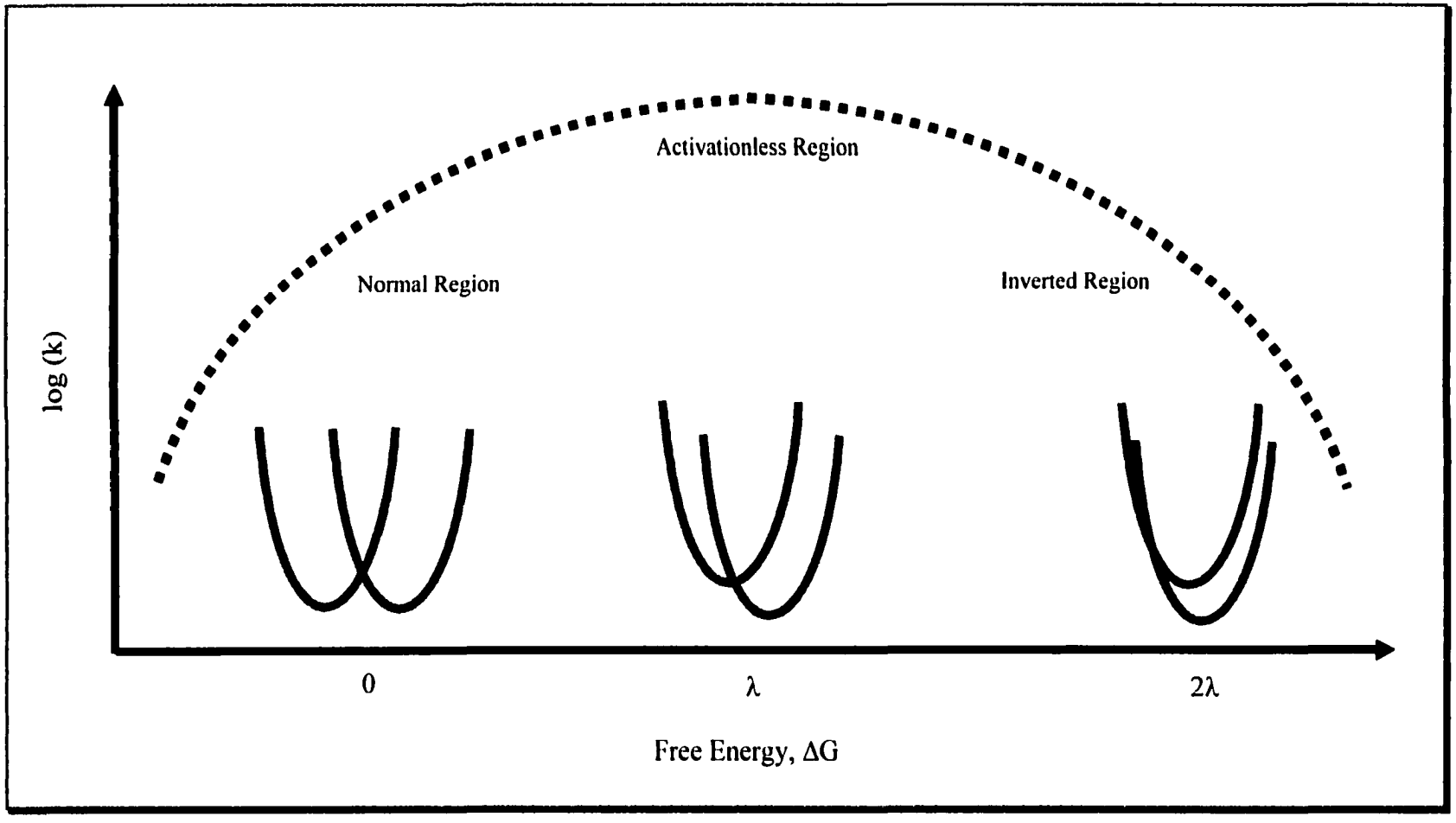

Figure II-6: Dependence of the reaction rate upon free energy is given by the heavy dotted line. In the normal region, as the free energy is increased, the reaction rate increases as well. In the activationless region, the rate is still higher (but not infinite). As the free energy increases further, the activation energy reappears, and the rate of electron transfer decreases (from Marcus 1960).

is some fluorescence from both states, however (typically only a few percent). The charge separated state, P^+H^-, is a metastable state, forming in 3ps and decaying in 12ns (Rockley, Windsor et al. 1975). Figure II-7 shows these results. The fluorescence lifetime of P* (energetically distinct from P^+H^-) revealed a component with the lifetime of 12ns as well (Schenck, Blankenship et al. 1982) (Woodbury and Parson 1984). This delayed fluorescence was believed to be due the repopulating of P* (see above). With the knowledge of the fluorescence rates, the forward and reverse rates may be deduced, and ultimately, the free energy of the charge separated state (using a modified form of equation II-3).

As the experiments were refined, other components in the fluorescence decay were noticed, with a variety of lifetimes (Peloquin, Williams et al. 1994). Interpreting these results was complicated by the data from time-resolved absorption spectroscopy (Schenck, Blankenship et al. 1982). In particular, the kinetic rates did not appear to match up to the known states involved. The focus of much of these studies became the initial transfer from P* to P^+H^-. The speed and efficiency of the transfer appeared to pose a unique opportunity to test and refine the theory. A particular concern was whether the intermediate chlorophyll, B, served as a barrier to or facilitated the transfer by serving as an intermediate state in a system where the electronic overlap is much stronger (Marcus 1987) (Skourtis, Regan et al. 1994) (Parson, Chu et al. 1990) (Kirmaier, Holten et al. 1985).

II.D.2. *Subsequent Results & Adiabaticity:* Assigning these 'extra' rates to a transition has been a central difficulty in biological electron transfer. The key goal is to determine the parameters in the Marcus rate equation (II-7). Determining the electronic

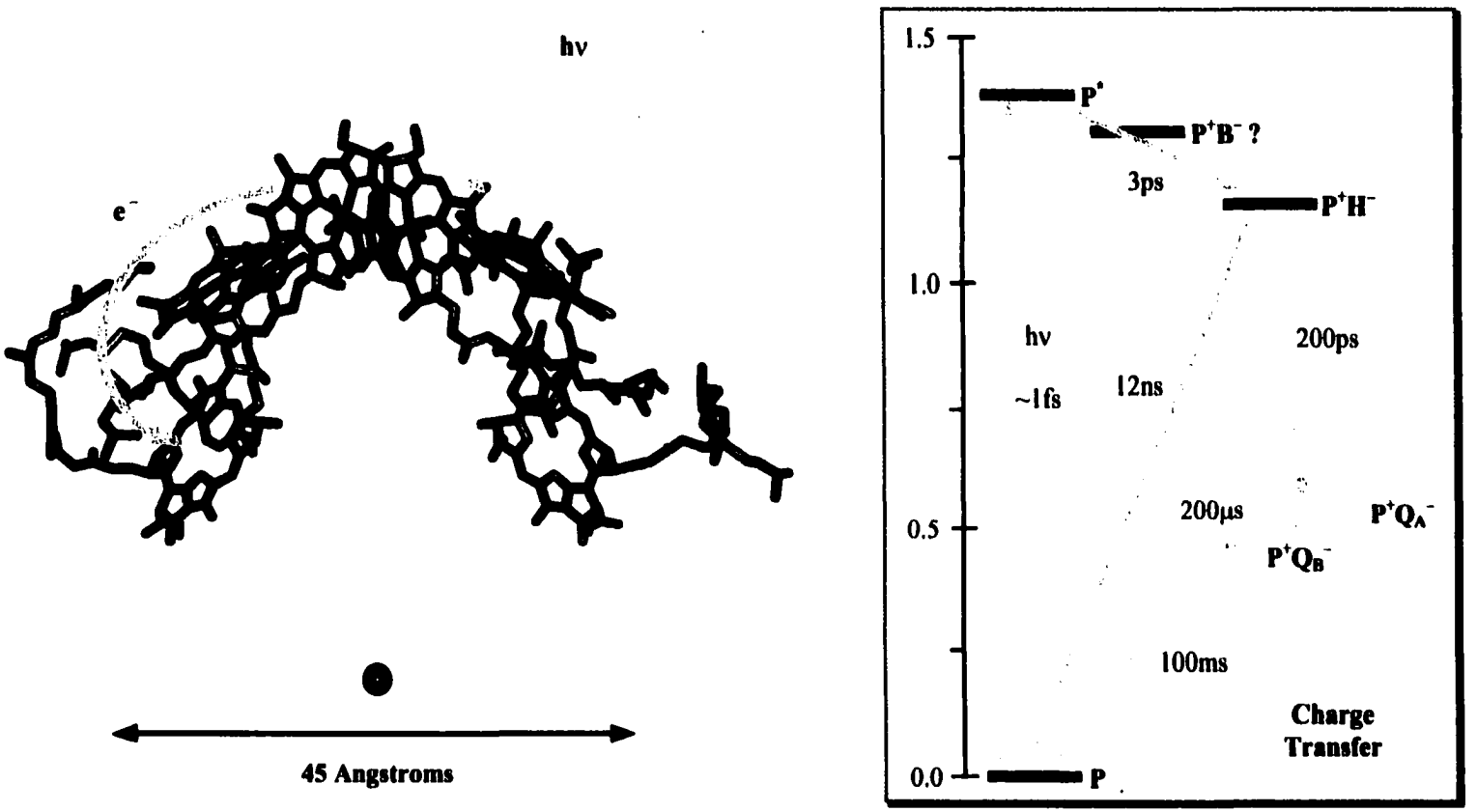

Figure II-7: Charge separation and the possible energetics of the photosynthetic reaction center. Excitation of the special pair initiates the release of a free electron, which localizes upon the pheophytin after only 3ps. For chemically pre-reduced reaction centers, the electron returns to the special pair after only 12ns (the solid line on the energy diagram). The role of the accessory chlorophyll (B) is unclear, as it may serve as a kinetic intermediate for or a barrier to charge transfer. The kinetic intermediates are not shown here. Approximate free energies are in electronvolts.

coupling, free energy and the reorganization energy will allow the validity of electron transfer theory to be tested.

Over the last twenty-five years, much progress has been made. The relatively large differences between the pigments have prompted most to pursue Marcus' non-adiabatic model of electron transfer. The bulk of the work holds to this assumption, estimating H_{RP} (often written as V_{RP} in the literature) to be between 10 cm^{-1} to 500 cm^{-1} (fairly weak coupling) and λ to be 1000 cm^{-1} (a fairly weak, non-polar environment) (Marchi, Gehlen et al. 1993) (Warshel and Parson 1991) (Parson and Warshel 1987) (Parson, Chu et al. 1998) (Jortner and Bixon 1999). The exponential dependence of the rate of transfer upon the distance has been observed. Other experiments have noted an inverted region in the rate of electron transfer. Compelling evidence has emerged to support the diabatic picture developed by Marcus, who earned the Nobel Prize in chemistry in 1990 for his formulation of this theory.

However, the question of the 'extra' kinetics remains, while many groups have questioned several assumptions of the diabatic theory. In particular, a key unresolved issue is the nonadiabatic assumption of the initial charge transfer. Studying the fluorescence and absorption data has led some to agree with the Marcus picture of the role of nuclear motions in the charge transfer (Peloquin, Williams et al. 1994) (Woodbury, Peloquin et al. 1994). Others feel that there must be a considerably stronger coupling between P* and P^+B^- (Small 1995) (Parson, Chu et al. 1990). Still others have noted that energy transfer from B* to P and the population of P* is too fast to be explained by a dipolar Förster mechanism, implying significant orbital overlap between the pigments (Jia, Jonas et al. 1995) (Scholes, Jordanides et al. 2001) (Jordanides,

Scholes et al. 2001). Another popular theory of strong overlap is known as 'superexchange.' Here, the intermediate chlorophyll, B, is not an intermediate, but serves to modulate the effective electronic coupling between P* and $P^{+}H_{L}^{-}$ (Bixon, Jortner et al. 1989) (Skourtis and Mukamel 1995).

II.D.3. *The Protein Environment:* Another problem is the protein environment of the chlorophylls. The protein scaffolding of both the RC and LH2 contain polar residues that must somehow influence the electron's transfer. As explained above, treating all of these electronic interactions in the Hamiltonian is quite difficult. Instead, several theories have arisen that deal with the ensemble of charges. Generally, short-range interactions may be dealt with by considering individual atomic interactions, while the more numerous long-range interactions may be dealt with using the dielectric model. The long-range interactions are often the only ones considered due to their larger number, and for simplicity's sake. If the electron moves slowly enough to remain in thermal equilibrium, then dielectric relaxation affects the free energy, enthalpy and entropy. However, the electron transfer is rapid, then it may not remain in thermal equilibrium, and the free energies, as well as the kinetics rates may be time dependent. A quantum statistical mechanical treatment is often necessary to explain experimental results, though (Marcus' theory utilized a statistical treatment of nuclear motion) (Marcus 1956) (Chandler 1987).

Dynamic solvation in simpler chemical systems has been extensively examined. In these experiments, it is understood that the fluorescence spectrum is time dependent. Even a simple two level transition will show a multi-exponential decay, as the dielectric relaxes to the new configuration of a charge or a dipole. A strong body of experiments

has been completed (Stratt and Maroncelli 1996) (Simon and Su 1988) (Vanderzwan and Hynes 1985) (Rossky and Simon 1994) (Barbara and Jarzeba 1988) (Horng, Gardecki et al. 1995) (Reynolds, Gardecki et al. 1996).

Solvation in complex proteins has proven more difficult to study. Some have suggested a simple single exponential (Debye-like) relaxation (Bashkin, McLendon et al. 1990). Yet others have suggested a broad range of solvation times modulate the fluorescence spectrum (Pierce and Boxer 1992). Interpreting these results in terms of Marcus' theory has proven even more difficult.

II.D.4. *Solvation & Time Dependent Free Energies:* A useful way to examine the energy of the charge separation is to apply a magnetic field on the triplet (^3P) decay (^3P forms in low quantum yield by charge recombination from the state $^3P^+H^-$) (Ogrodnik, Michelbeyerle et al. 1988) (Goldstein, Takiff et al. 1988). Since the free energy of ^3P is known from phosphorescence studies, determining the activation free energy to form P^+H^- from ^3P allows the free energy of P^+H^- to be obtained. Thus, the free energy of P^+H^- is believed to be 0.26 eV below P* (see Figure II-7). Unfortunately, the free energy obtained from delayed fluorescence does not agree with this result. Furthermore, the stimulated emission spectrum of P* is time-independent, implying that the free energy of this vibronic state is constant. The delayed fluorescence was then ascribed to the free energy change in the charge-separated state, P^+H^-. This change, referred to "dynamic solvation," was believed to account for the range of kinetic rates (Woodbury, Peloquin et al. 1994). In this view, illustrated in Figure II-8, the initial charge separation occurs with very small initial negative free energy gap (<50-150 meV) at room temperature, and an even smaller negative free energy gap (<10 meV) at 20 K (Peloquin, Williams et al.

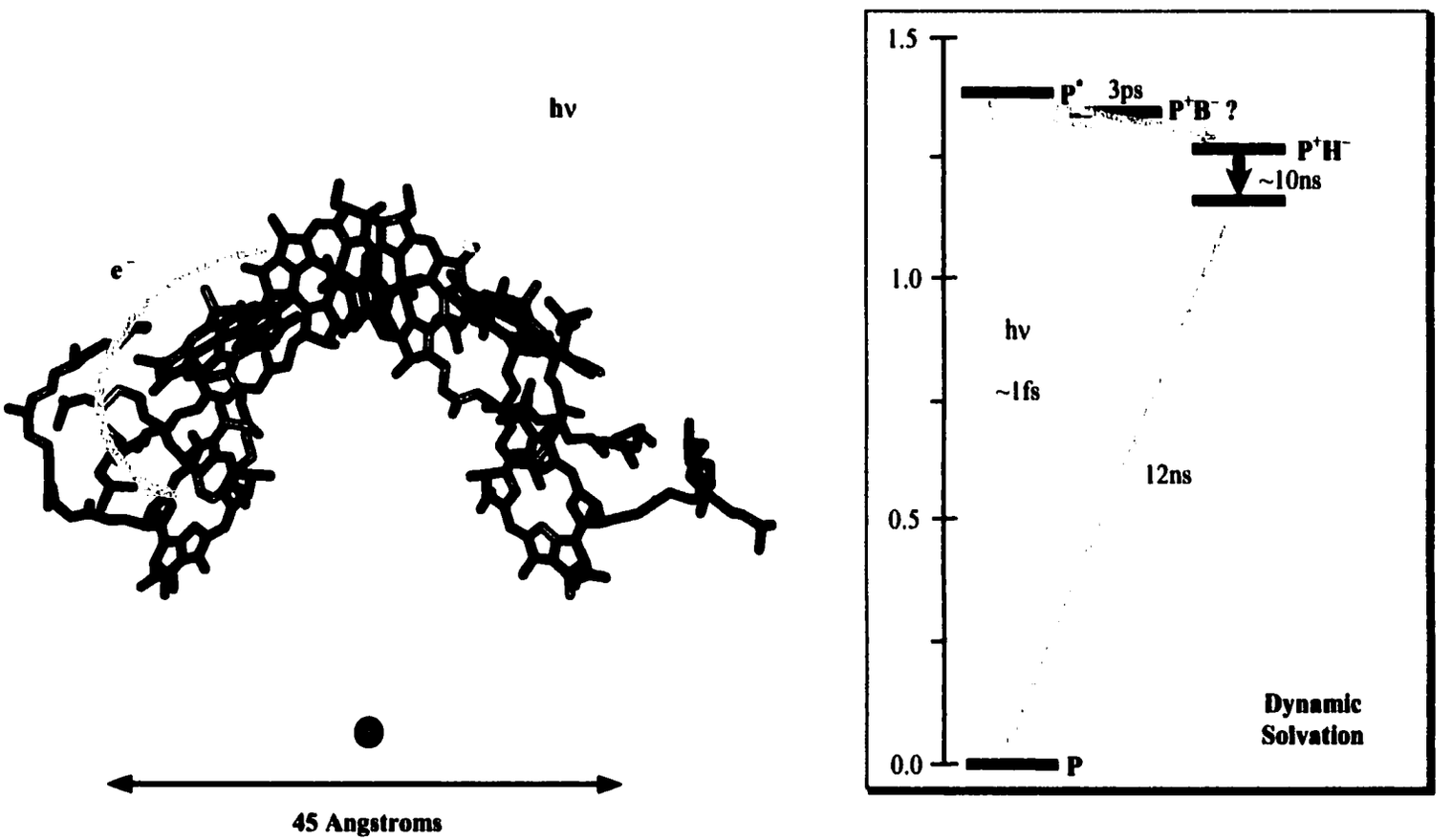

Figure II-8: The dynamic solvation picture of charge transfer. Excitation of the special pair initiates the release of a free electron, which localizes upon a nearly isoenergetic pheophytin after a few picoseconds. The free energy of this state decreases with time, due to solvent adjustment to the new location of the electron. Initially, the probability of reverse transfer is quite high, but this rate decreases significantly at the free energy of the charge separated state decreases. Approximate free energies are in electronvolts.

1994). This gap is time-dependent and relaxes to a value > 0.2 eV within 12 ns, due to reorganization of the solvent. The forward reactions occur with high rate at all times and they are only weakly-dependent on ΔG (or, the forward reactions are essentially activationless). This also implies that the reorganization energy λ must be extraordinarily small (Jia, DiMagno et al. 1993) (Parson, Chu et al. 1998).

II.D.5. *Heterogeneity:* Another interpretation of the delayed fluorescence experiment has been proposed under the name 'static heterogeneity' (Ogrodnik, Keupp et al. 1994) (Bixon, Jortner et al. 1995). In this view, there is a static distribution, or ensemble, of reaction centers, due to subtle differences in structure and specific solvent environment. As a result, the energy levels and the rate coefficients for charge transfer are not discrete, but exist as a distribution. Such a mechanism has also been suggested for the transfer to the quinones (Goushcha, Kapoustina et al. 1997). The model for initial charge separation is shown in Figure II-9. The charge-separated state is populated, then begins to decay. Those that have the highest free energy relative to the ground state decay the fastest (presumably with a lifetime near 3ps), while the lower states decay more slowly over a range extending to 12ns.

II.D.6. *Time Dependent Reorganization Energy:* In yet another picture, the time dependence of the delayed fluorescence is ascribed to the reorganization energy λ. Here the shapes of the potential energy surfaces become narrower with time. The activation energy for reverse electron transfer becomes greater with increasing time, resulting in decreasing probability for crossing the barrier to re-form P^*. This model is attractive because it may help explain the very small values for λ in the initial reaction at early times (Jia, DiMagno et al. 1993) and the much larger values for λ deduced from slower

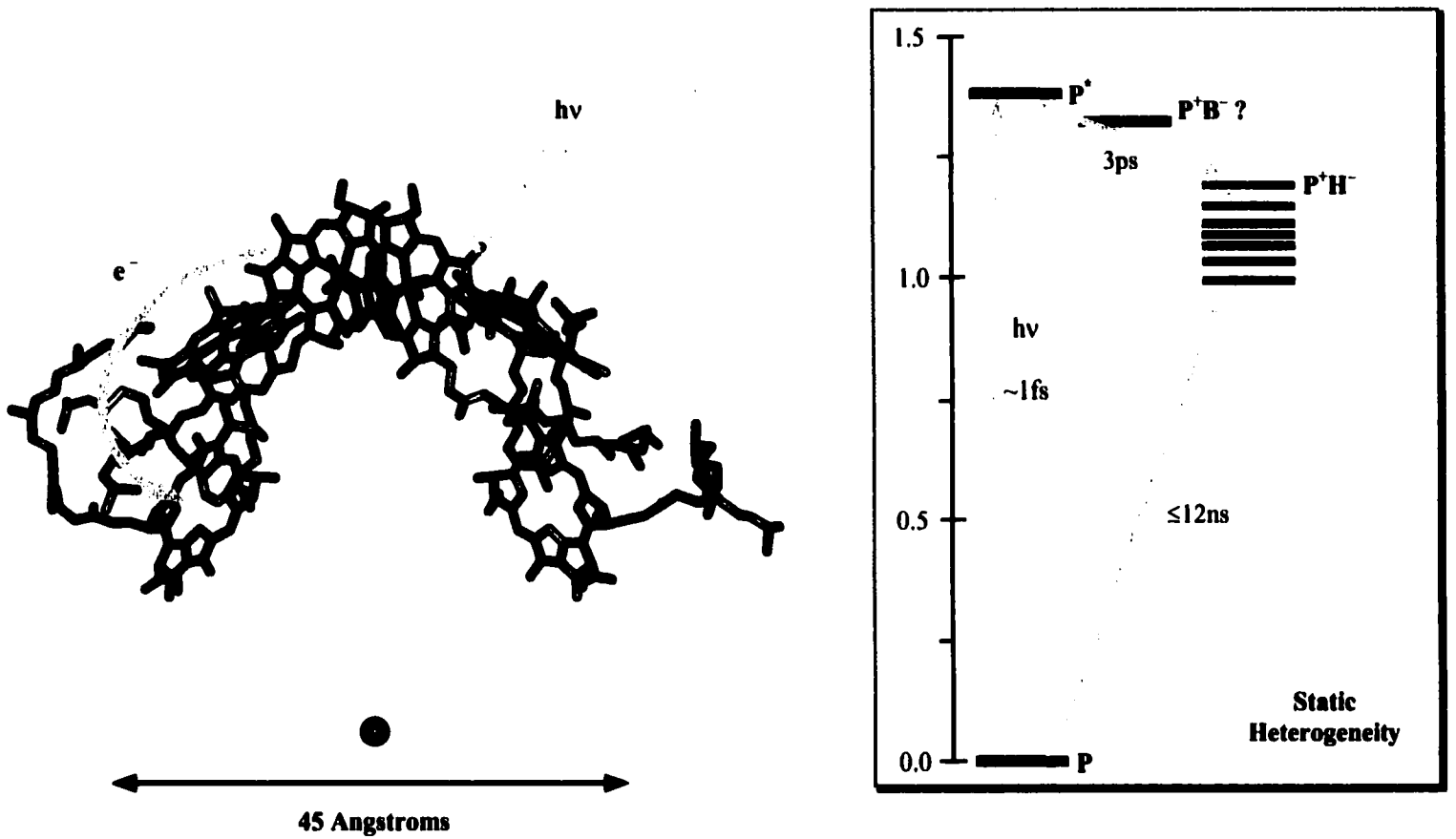

Figure II-9: Static heterogeneity and electron transfer. Excitation of the special pair initiates the release of a free electron, which localizes upon the pheophytin after a few picoseconds. The energy of the charge-separated state varies from protein to protein. An ensemble of proteins has the distribution of free energies shown in the figure. The rate of recombination is fastest for the states with the highest energy, and the rate ranges out to 12ns. Approximate free energies are in electronvolts.

electron transfer steps (Gunner, Robertson et al. 1986) (Gunner and Dutton 1989) (Kirmaier, Laporte et al. 1995) and from molecular dynamics simulations (Warshel, Parson et al. 1989) (Creighton, Norris et al. 1988) (Marchi, Gehlen et al. 1993). Newer calculations have suggested that both the reorganization and the free energy may be time dependent, especially for the intermediate $P+B^-$ (Parson, Chu et al. 1998).

II.D.7. *Calorimetry:* Time-dependent (nanosecond) calorimetry is a well-established technique (Bratslavsky and Heibel 1992) (Peters and Snyder 1988). Generally, an experiment detects a volume change (ΔV) associated with some reaction. Time-dependent volume changes typically stem from two processes, ΔV_{rx} and ΔV_{th}. ΔV_{rx} measures the change in volume of the system as reactants are converted into products, including changes due to electrostriction and solvation. ΔV_{th} accounts for expansion or contraction of the system through the coefficient of thermal expansion as heat is released to the solvent, due to enthalpy changes in the system. The method has been applied to reaction centers and other photo-biological systems on the nanosecond to millisecond time-scale (Arata and Parson 1981) (Mauzerall, Gunner et al. 1995) (Malkin, Churio et al. 1994) (Edens, Gunner et al. 2000) (Puchenkov, Kopf et al. 1995). Though acoustic calorimetry experiments are limited to microsecond resolution, the laser induced calorimetry experiments discussed in the work may be used down to the picosecond scale.

II.D.8. *Site Directed Mutagenesis:* This extremely powerful technique allows the amino acids in various places of the reaction center protein to be replaced. Thus the electronic structure of the pigments and their surrounding scaffolding may be altered. Mutations allow the rate, yield and free energy to be manipulated. Much of the work

above has been supplemented by studies on appropriate mutations in the reaction center (Beekman 1997) (Lin, Xiao et al. 1996) (Kirmaier, Laporte et al. 1995) (Kirmaier, Laporte et al. 1995). Of particular interest are efforts to generate a mutant that slows charge transfer significantly, and to ascertain the presence of time-delayed fluorescence, as well as the intermediate P^+B^-. An interesting example involves the replacement of the M subunit Leu^{214} by His, which results in the replacement of the photoactive pheophytin by chlorophyll. Electron transfer is delayed and the yield reduced, possibly due to increased recombination with the excited dimer (Kirmaier, Gaul et al. 1991) (Czarnecki, Schenck et al. 1997).

II.E. Literature Cited

Arata, H. and W. Parson (1981). "Enthalpy and volume changes accompanying electron transfer from P-870 to quinones in *Rhodopseudomonas sphaeroides* reaction centers." Biochimica et Biophysica Acta **636**: 70-81.

Barbara, P. F. and W. Jarzeba (1988). "Dynamic Solvent Effects on Polar and Nonpolar Isomerizations." Accounts of Chemical Research **21**: 195-199.

Bashkin, J. S., G. McLendon, et al. (1990). "Influence of Medium Dynamics on Solvation and Charge Separation Reactions Comparison of a Simple Alcohol and a Protein Solvent." Journal of Physical Chemistry **94**: 4757-4761.

Beekman, L. M. P. (1997). A Structural and Functional Characterization Study of the Bacterial Photosynthetic Apparatus: Mutants, Charge Separation and Electric Field Effects., Vrije Universitiet te Amsterdam.

Bixon, M., J. Jortner, et al. (1995). "A Kinetic Analysis of the Primary Charge Separation in Bacterial Photosynthesis Energy Gaps and Static Heterogeneity." Chemical Physics **197**: 389-404.

Bixon, M., J. Jortner, et al. (1989). "A superexchange mechanism for the primary charge separation in photosynthetic reaction centers." Biochimica et Biophysica Acta **977**: 273-286.

Born, M. and J. R. Oppenheimer (1927). "Zur quantentheorie der molekeln." Annalen der Physik **84**: 457-484.

Bransden, B. H. and C. J. Joachain (1990). Physics of Atoms and Molecules. New York, Longman Scientific and Technical.

Bratslavsky, S. E. and G. E. Heibel (1992). "Time resolved photothermal and photoacoustic methods applied to photoinduced processes in solution." Chemical Reviews **92**: 1381-1410.

Chandler, D. (1987). Introduction to Modern Statistical Mechanics. New York, Oxford University Press.

Cohen-Tannoudji, C., J. Dupont-Roc, et al. (1992). Atom-Photon Interactions: Basic Processes and Applications. New York, John Wiley & Sons, Inc.

Creighton, S., J. Norris, et al. (1988). "Simulating the Dynamics of the Primary Charge Separation Process in Bacterial Photosynthesis." Biochemistry **27**: 774-781.

Czarnecki, K., C. C. Schenck, et al. (1997). "Resonance Raman characterization of reaction centers in which bacteriochlorophyll replaces the photoactive bacteriopheophytin." Biochemistry **36**(48): 14697-14704.

De Vault, D. (1984). Quantum Mechanical Tunneling in Biological Systems. New York, Cambridge University.

Edens, G. J., M. R. Gunner, et al. (2000). "The enthalpy and entropy of reaction for formation of P+QA- from excited reaction centers of *Rhodobacter sphaeroides*." Journal of the American Chemical Society **122**(7): 1479-1485.

Forster, T. (1948). "Zwischenmolekulare energiewanderung und fluoreszenz." Annalen der Physik **6**(2): 55-75.

Forster, T. (1959). "Tranfer mechanisms of the electronic excitation." Discussions of the Faraday Society **27**: 7-17.

Frenkel, Y. I. (1931). Physical Review **37**: 17.

Goldstein, R. A., L. Takiff, et al. (1988). "Energetics of Initial Charge Separation in Bacterial Photosynthesis The Triplet Decay Rate in Very High Magnetic Fields." Biochimica et Biophysica Acta **934**: 253-263.

Goushcha, A. O., M. T. Kapoustina, et al. (1997). "Nonlinear dynamic processes in an ensemble of photosynthetic reaction centers. Theory and experiment." Journal of Physical Chemistry B **101**(38): 7612-7619.

Gunner, M. R. and P. L. Dutton (1989). "Temperature and Delta G Degrees Dependence of the Electron Transfer from Bph. to Qa in Reaction Center Protein from *Rhodobacter*

sphaeroides with Different Quinones As Qa." Journal of the American Chemical Society **111**: 3400-3412.

Gunner, M. R., D. E. Robertson, et al. (1986). "Kinetic studies on the reaction center protein from Rhodopseudomonas sphaeroides: the temperature and free energy dependence of electron transfer between various quinones in the QA site and the oxidized bacteriochlorophyll dimer." Journal of Physical Chemistry **90**: 3783-3795.

Horng, M. L., J. A. Gardecki, et al. (1995). "Subpicosecond measurements of polar solvation dynamics: Coumarin 153 revisited." Journal of Physical Chemistry **99**: 17311-17337.

Jia, Y., T. J. DiMagno, et al. (1993). "Primary charge separation in mutant reaction centers of *Rhodobacter capsulatus*." Journal of Physical Chemistry **97**(50): 13180-13191.

Jia, Y., D. M. Jonas, et al. (1995). "Observation of ultrafast energy transfer from the accessory bacteriochlorophylls to the special pair in photosynthetic reaction centers." Journal of Physical Chemistry **99**(17): 6263-6266.

Joo, T. H., Y. W. Jia, et al. (1996). "Dynamics in isolated bacterial light harvesting antenna (LH2) of *Rhodobacter sphaeroides* at room temperature." Journal of Physical Chemistry **100**(6): 2399-2409.

Jordanides, X. J., G. D. Scholes, et al. (2001). "The mechanism of energy transfer in the bacterial photosynthetic reaction center." Journal of Physical Chemistry B **105**(8): 1652-1669.

Jortner, J. and M. Bixon (1999). Electron transfer - from isolated molecules to biomolecules. Electron Transfer - From Isolated Molecules to Biomolecules. Part One. New York, John Wiley & Sons. **106**.

Kirmaier, C., D. Gaul, et al. (1991). "Charge Separation in a Reaction Center Incorporating Bacteriochlorophyll for Photoactive Bacteriopheophytin." Science **251**: 922-927.

Kirmaier, C., D. Holten, et al. (1985). "The question of the intermediate state P+BChl- in bacterial photosynthesis." FEBS **185**(1): 76-82.

Kirmaier, C., L. Laporte, et al. (1995). "The nature and dynamics of the charge-separated intermediate in reaction centers in which bacteriochlorophyll replaces the photoactive bacteriopheophytin. 1. Spectral characterization of the transient state." Journal of Physical Chemistry **99**: 8903-8909.

Kirmaier, C., L. Laporte, et al. (1995). "The nature and dynamics of the charge-separated intermediate in reaction centers in which bacteriochlorophyll replaces the photoactive

bacteriopheophytin. 2. The rates and yields of charge separation and recombination." Journal of Physical Chemistry **99**: 8910-8917.

Kuznetsov, A. M. and J. Ulstrop (1999). Electron Transfer in Chemistry and Biology. Chichester, John Wiley & Sons.

Lin, S., W. Z. Xiao, et al. (1996). "Low-temperature femtosecond-resolution transient absorption spectroscopy of large-scale symmetry mutants of bacterial reaction centers." Biochemistry **35**(10): 3187-3196.

Malkin, S., M. S. Churio, et al. (1994). "Photochemical energy storage and volume changes in the microsecond time range in bacterial photosynthesis--a laser induced optoacoustic study." **23**: 79-85.

Marchi, M., J. N. Gehlen, et al. (1993). "Diabatic surfaces and the pathway for primary electron transfer in a photosynthetic reaction center." Journal of the American Chemical Society **115**(10): 4178-4190.

Marcus, R. A. (1956). "On the theory of oxidation-reduction reactions involving electron transfer: I." Journal of Chemical Physics **24**(5): 966-978.

Marcus, R. A. (1987). "Superexchange Versus an Intermediate Bchl Mechanism in Reaction Centers of Photosynthetic Bacteria." Chemical Physics Letters **133**: 471-477.

Marcus, R. A. and N. Sutin (1985). "Electron Transfers in Chemistry and Biology." Biochimica et Biophysica Acta **811**: 265-322.

Mauzerall, D. C., M. R. Gunner, et al. (1995). "Volume contraction on photoexcitation of the reaction center from *Rhodobacter sphaeroides* R-26: Internal probe of dielectrics." Biophysical Journal **68**(1): 275-280.

Monshouwer, R., M. Abrahamsson, et al. (1997). "Superradiance and exciton delocalization in bacterial photosynthetic light-harvesting systems." Journal of Physical Chemistry B **101**(37): 7241-7248.

Nagarajan, V., E. T. Johnson, et al. (1999). "Femtosecond pump-probe spectroscopy of the B850 antenna complex of *Rhodobacter sphaeroides* at room temperature." Journal of Physical Chemistry B **103**: 2297-2309.

Ogrodnik, A., W. Keupp, et al. (1994). "Inhomogeneity of radical pair energies in photosynthetic reaction centers revealed by differences in recombination dynamics of P+HA- when detected in delayed emission and in absorption." Journal of Physical Chemistry **98**(13): 3432-3439.

Ogrodnik, A., M. E. Michelbeyerle, et al. (1988). "Determination of Free Energies in Reaction Centers of *Rhodobacter sphaeroides*." Biochimica et Biophysica Acta **936**: 361-371.

Oppenheimer, J. R. (1928). "Three notes on the quantum theory of aperiodic effects." Physics Review **13**: 66-81.

Park, D. A. (1974). Introduction to the Quantum Theory. New York, McGraw-Hill.

Parson, W. W., Z. T. Chu, et al. (1990). "Electrostatic control of charge separation in bacterial photosynthesis." Biochimica et Biophysica Acta **1017**: 251-272.

Parson, W. W., Z. T. Chu, et al. (1998). "Reorganization energy of the initial electron-transfer step in photsynthetic reaction centers." Biophysical Journal **74**: 182-191.

Parson, W. W. and A. Warshel (1987). "Spectroscopic Properties of Photosynthetic Reaction Centers .2. Application of the Theory to *Rhodopseudomonas viridis*." Journal of the American Chemical Society **109**: 6152-6163.

Peloquin, J. M., J. C. Williams, et al. (1994). "Time-dependent thermodynamics during early electron transfer in reaction centers from *Rhodobacter sphaeroides*." Biochemistry **33**(26): 8089-8100.

Peters, K. S. and G. J. Snyder (1988). "Time-Resolved Photoacoustic Calorimetry: Probing the Energetics and Dymanics of Fast Chemical and Biochemical Reactions." Science **241**: 1053-1057.

Pierce, D. W. and S. G. Boxer (1992). "Dielectric relaxation in a protein matrix." Journal of Physical Chemistry **96**(13): 5560-5566.

Puchenkov, O. V., Z. Kopf, et al. (1995). "Photoacoustic diagnostics of laser-induced processes in reaction centers of *Rhodobacter sphaeroides*." Biochimica et Biophysica Acta: Bio-Energetics **1231**(2): 197-212.

Pullerits, T., M. Chachisvilis, et al. (1996). "Exciton delocalization length in the B850 antenna of *Rhodobacter sphaeroides*." Journal of Physical Chemistry **100**(25): 10787-10792.

Reynolds, L., J. A. Gardecki, et al. (1996). "Dipole solvation in nondipolar solvents: experimental studies of reorganization energies and solvation dynamics." Journal of Physical Chemistry **100**: 10337.

Rockley, M. G., M. Windsor, et al. (1975). "Picosecond Detection of an Intermediate in the Photochemical Reaction of Bacterial Photosynthesis." **72**: 2251.

Rossky, P. J. and J. D. Simon (1994). "Dynamics of Chemical Processes in Polar Solvents." Nature **370**: 263-269.

Schenck, C. C., R. E. Blankenship, et al. (1982). "Radical-pair decay kinetics, triplet yield and delayed fluorescence from bacterial reaction centers." Biochimica et Biophysica Acta **680**: 44-59.

Scholes, G. D. and G. R. Fleming (2000). "On the mechanism of light harvesting in phtotsynthetic prurple bacteria: B800 to B850 energy transfer." Journal of Physical Chemistry **104**: 1854-1868.

Scholes, G. D., X. J. Jordanides, et al. (2001). "Adapting the Forster theory of energy transfer for modeling dynamics in aggregated molecular assemblies." Journal of Physical Chemistry B **105**(8): 1640-1651.

Simon, J. D. and S. G. Su (1988). "Dynamic Solvent Effects on Intramolecular Electron Transfer Reactions Fluctuation Time Scales and Population Decays." Journal of Physical Chemistry **92**: 2395-2397.

Skourtis, S. S. and S. Mukamel (1995). "Superexchange versus sequential long range electron transfer; density matrix pathways in Liouville space." Chemical Physics **197**: 367-388.

Skourtis, S. S., J. J. Regan, et al. (1994). "Electron transfer in proteins: A novel approach for the description of donor-acceptor coupling." Journal of Physical Chemistry **98**(13): 3379-3388.

Small, G. J. (1995). "On the Validity of the Standard Model for Primary Charge Separation in the Bacterial Reaction Center." Journal of Chemical Physics **197**: 239-257.

Stratt, R. M. and M. Maroncelli (1996). "Nonreactive dynamics in solution: The emerging molecular view of solvation dynamics and vibrational relaxation." Journal of Physical Chemistry **100**(31): 12981-12996.

Stryer, L. (1978). "Fluorescence energy transfer as a spectroscopic ruler." Annual Reviews of Biochemistry **47**: 819-846.

Sumi, H. (2000). "Structural strategies in the antenna system of photosynthesis on the basis of quantum-mechanical coherence among pigments." Journal of Luminescence **87-89**: 71-76.

Sundstrom, V., T. Pullerits, et al. (1999). "Photosynthetic light harvesting: Reconciling dynamics and structure of purple bacterial LH2 reveals function of photosynthetic unit." Journal of Physical Chemistry B **103**(13): 2327-2346.

Timpmann, K., N. W. Woodbury, et al. (2000). "Unraveling exciton relaxation and energy transfer in LH2 photosynthetic antennas." Journal of Physical Chemistry B **104**(42): 9769-9771.

Van Amerongen, H., L. Valkunas, et al. (2000). Photosynthetic Excitons. Singapore, World Scientific.

Van Der Meer, B. W., G. Coker, et al. (1994). Resonance Energy Transfer: Theory & Data. New York, VCH Publishers.

Vanderzwan, G. and J. T. Hynes (1985). "Time Dependent Fluorescence Solvent Shifts, Dielectric Friction, and Nonequilibrium Solvation in Polar Solvents." Journal of Physical Chemistry **89**: 4181-4188.

Warshel, A. and W. W. Parson (1991). "Computer Simulations of Electron Transfer Reactions in Solution and in Photosynthetic Reaction Centers." Aunnual Review of Physical Chemistry **42**: 279-309.

Warshel, A., W. W. Parson, et al. (1989). "Dispersed Polaron Simulations of Electron Transfer in Photosynthetic Reaction Centers." Science **246**: 112-116.

Woodbury, N. and W. Parson (1984). "Nanosecond fluorescence from isolated photosynthetic reaction centers of *Rhodopseudomonas sphaeroides*." **767**(2): 345-361.

Woodbury, N. W., J. M. Peloquin, et al. (1994). "Relationship between thermodynamics and mechanism during photoinduced charge separation in reaction centers from *Rhodobacter sphaeroides*." Biochemistry **33**(26): 8101-8112.

III. TRANSIENT GRATING SPECTROSCOPY

The goal of the work in this dissertation is to obtain free energies of charge separation and to directly associate them with kinetic rates. The theoretical formalism of transient gratings creates the equations that may be fit to the data (and yield the parameters of best fit). As diffraction from a transient grating is the cause of the signal, each of the causes that drive grating formation must be detailed. Density gratings due to volume changes and heat releases in the sample may be derived, with the specific addition of acoustic attenuation. These equations may be applied to simple two and three level kinetic systems. More complicated schemes include the presence of triplet states and dynamic solvation of the intermediate level. Finally, simulations and numeric solutions add flexibility to data analysis.

III.A. Transient Gratings

III.A.1. *Introduction:* Previous spectroscopy experiments have typically relied upon kinetic experiments to deduce free energies of reaction, while calorimetric experiments have found enthalpies of reaction directly. Unfortunately, charge separation occurs too rapidly for the calorimetric experiments to resolve (with the exception of the quinone energy, though there have been some discrepancies there as well) (Arata and Parson 1981) (Mauzerall, Gunner et al. 1995) (Mauzerall, Feitelson et al. 1995) (Edens, Gunner et al. 2000). Furthermore, the number of kinetic components makes it difficult to determine the free energies correctly (Woodbury, Peloquin et al. 1994) (Ogrodnik, Keupp et al. 1994). Transient thermal phase grating spectroscopy (also previously known as laser induced phonons) is a time-resolved technique that determines the free enthalpy directly, allowing many assumptions of charge transfer to be directly tested. In the

picosecond time-resolved optical calorimetry experiment, transient thermal phase grating spectroscopy is used to measure time-dependent changes in refractive index which can be correlated with changes in density of the system, and ultimately the heat which evolves from a reaction (Eichler, Gunter et al. 1986).

III.A.2. *Physical Explanation:* The technique of transient grating spectroscopy relies upon the diffraction of a delayed probe pulse at a transient diffraction grating formed by two intersecting coherent pump pulses (Kogelnik 1969). This pump-probe experiment is shown schematically on the next page (Figure III-1). Two pulses of roughly equal power (Kogelnik 1969) converge upon the sample at an angle, θ. These coherent pulses alternately interfere constructively and destructively. The space between adjacent maxima is known as the grating wavelength, or Λ, and is determined by Equation III-1, where λ_{ex} is the photon wavelength and θ is the angle between the pump

$$\Lambda = \frac{\lambda_{ex}}{2\sin\theta/2} \qquad \textbf{(III-1)}$$

wavevectors.

The pump pulse energies are tuned to an excitation energy of the sample, which relaxes to the ground state along varying pathways. In many proteins, the sheer size of the structures leads to a complicated set of coupled vibrational and electronic energy levels. While some of the pump energy will be fluoresced, much is converted into intermolecular vibrational energy, and ultimately into intramolecular energy. The photon that excites the sample is converted into several quanta of infrared energy that is ultimately transferred into the solvent. While these energy transfers affect the electronic properties of the sample, the bulk properties of the solvent change as well. These

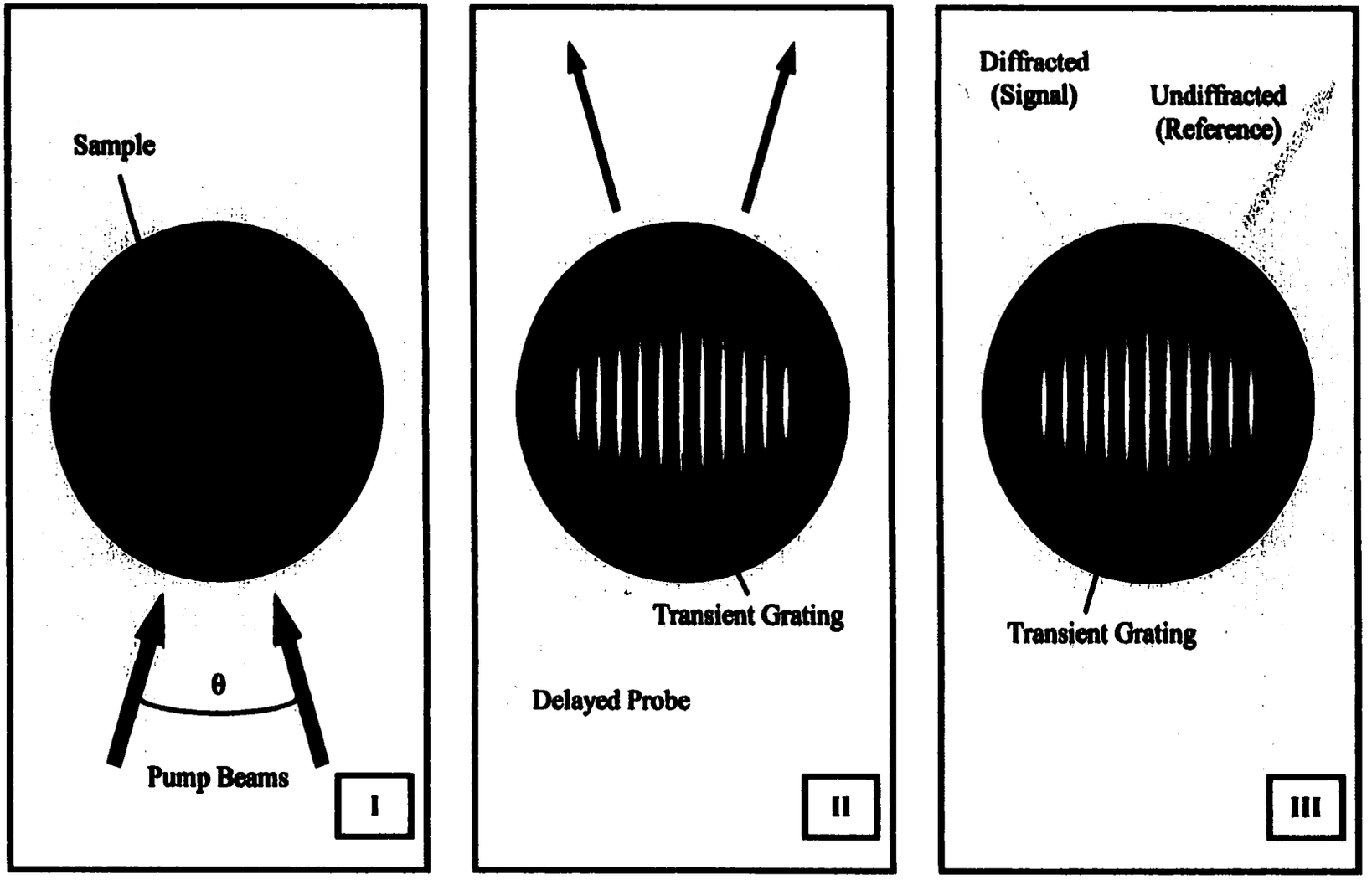

Figure III-1: This transient grating schematic reads from left to right. In the first panel, the pump beams converge with frequencies matched to the excitation energy of the sample. The sample has absorbed energy in the second frame, and until it fully relaxes, the complex index of refraction is altered. The variably delayed probe beam has been diffracted in the final picture.

variations, shown schematically in the second panel of Figure III-1, are collectively known as the transient grating. This grating may consist of varying proportions of excited state differences, temperature changes and density fluctuations (of the solvent and the sample).

As mentioned above, energy transferred into the solvent may induce density changes. These variations also prompt fluctuations in pressure, with a wavelength that matches the grating wavelength, Λ. These coherent pressure and displacement fluctuations will propagate longitudinally in opposite directions, perpendicular to the pump bisector, as a sound wave. The result will be a standing wave with the wavelength of Λ and a frequency of $f = v_o/\Lambda$, where v_o is the speed of sound. Such a grating will disappear (destructively interfere) at times equal to n/f and maximize every (2n-1)/f, where n is an integer. For this reason, transient thermal grating spectroscopy is said to holographically write an acoustic wave into the sample (Fayer 1986) (Nelson, Miller et al. 1981).

Finally, a time delayed probe beam is directed into the sample. The grating (Figure III-1) diffracts a small portion of this beam, typically less than .1%, at the Bragg angle, where λ_p is the probe wavelength (Equation III-2). The Bragg angle insures that

$$\theta_p = \sin^{-1}\left(\frac{\lambda_p}{2\Lambda}\right) \qquad \textbf{(III - 2)}$$

the maximum diffraction efficiency (η_o) is obtained. As the time delay of the probe may be varied, this data may be collected as a function of time after the arrival of the pump beams. The relative size of the signal and any changes with time may be used to extract the energetics of the system. Unlike traditional calorimetric and spectroscopic methods,

the heat release and the rate coefficients may be discerned independently. Furthermore, in principle, the diffracted probe is detected against zero background, providing excellent signal to noise.

III.A.3. *The Diffraction Efficiency for Absorptive and Dispersive Gratings:* For relatively thick gratings with low diffraction efficiency, η_o is well known and may be expressed as Equation III-3 (Kogelnik 1969) (Eichler, Gunter et al. 1986) (Genberg, Bao et al. 1989) (Deak, Richard et al. 1994). This approximate relation is particularly appropriate for the lower efficiencies observed in a typical experiment ($\eta < .001$).

$$\eta_o = \exp\left(\frac{-2.3D}{\cos\theta_p}\right)\left(\frac{\pi d}{\lambda_p \cos\theta_p}\right)^2 \times \left[\left(\Delta k_{ex} + \Delta k_\rho + \Delta k_T\right)^2 + \left(\Delta n_{ex} + \Delta n_\rho + \Delta n_T\right)^2\right] \qquad \textbf{(III - 3)}$$

Defined within are D, the average optical density, θ_p, the angle that the probe makes with the bisector of the pump pulses (and determined by the Bragg diffraction condition), and d, the thickness of the grating. The remaining terms describe changes in absorption (k) and dispersion (n – sometimes also referred to as the phase term) due to changes in excited state populations, sample density, and temperature.

III.A.4. *Excited State and Density Gratings:* Though the number of terms affecting the material absorption and dispersion may complicate the data analysis, they also afford the opportunity to study a range of properties of the system. Furthermore, it is often possible to select experimental conditions that favor desired terms at the expense of others. Here information will be obtained primarily through changes in density that lead to changes in the index of refraction, as predicted by Equation III-4. The absorption may also change due to density modulations, but this effect is small with respect to the

$$\Delta n_\rho = \frac{\partial n}{\partial \rho}\Big)_p \Delta\rho \qquad \textbf{(III - 4)}$$

refractive index change, so it may be ignored (Nelson, Casalengo et al. 1982). Other changes in the density due to solvation or electrostriction may be determined (Morais and Zimmt 1995) (Miller, Casalengo et al. 1982) (Miller 1994); such effects are to be dealt with below.

In addition, the changes in k and n due to changes in temperature (at constant density) are often a factor of ten less than those due to density modulations (Desai, Levenson et al. 1983). Finally, if the probe beam is set to a wavelength well separated from any resonance in the sample (e.g., 1200nm for this system), the excited-state contribution to the grating may be ignored. What remains is a grating efficiency that depends primarily on variations in the material index of refraction due to changes in density.

However, in many systems several broad absorption peaks overlap in the excited state spectrum (this is especially true in large proteins). For these experiments, the excited state grating terms must be retained in the analysis to accurately remove these components from the thermal contribution to the signal. It is important to consider the effect of the excited state upon the amplitude and the phase (dispersive) gratings as a function of the wavelength (Morais and Zimmt 1995) (Nelson, Casalengo et al. 1982) (Deak, Richard et al. 1994). Expressions for these effects have been derived before, and may assume the form of Equations III-5, III-6 and III-7. These equations are found by assuming a damped harmonic oscillator model for excited state dispersion. The resonance is centered about the frequency ω_0, N_1 is the number density of excited

$$\Delta n_{ex} = -\frac{N_1}{N_o}\frac{2(\omega_o - \omega)}{\gamma_o}k_o(\omega) \qquad \textbf{(III - 5)}$$

$$\Delta k_{ex} = -\frac{N_1}{N_o}k_o(\omega) \qquad \textbf{(III - 6)}$$

$$k_o(\omega) = \frac{N_o f_o \gamma_o}{2n_o\omega_o}\frac{1}{4(\omega_o - \omega)^2 + \gamma_o^2} \qquad \textbf{(III - 7)}$$

molecules and N_0 and n_0 are the unperturbed density and index of refraction, respectively. Finally, γ_0 is FWHM transition linewidth and f_0 is the absorption strength (the absorption cross section summed over the various oscillators) (Nelson, Casalengo et al. 1982). The time dependent portions of these terms may be exponential (following N_1), with a characteristic rate determined by the decay rate of the excited state. These excited state terms simply fit into the expression for the diffraction efficiency, Equation III-3. Note that the absorption change maximizes at resonance while the dispersion change maximizes on either side (recall that the efficiency follows the change squared in III-3). Furthermore, the change in the absorption may generate an acoustic wave, though the amplitude appears small relative to the exponential decay, especially near resonance (Fayer 1986).

III.A.5. *Solvation and Thermodynamics:* As mentioned in Chapter II, all calorimetric experiments measure changes in density, or volume. Time-dependent volume changes are attributable to two terms, ΔV_{rx} and ΔV_{th}. ΔV_{rx} measures the change in volume of the system as reactants are converted into products, including changes due to electrostriction and solvation. ΔV_{th} accounts for expansion or contraction of the system through the coefficient of thermal expansion as heat is released to the solvent due to enthalpy changes in the sample. Though the primary aim of these experiments is to

seek information through the heat release from photo-excited samples, solvation effects do occur, and may provide useful insights.

In simple continuum dielectric electrostatic theory, the free energy of solvation may be expanded. The partial derivative with respect to pressure yields the electrostatic volume change, which is shown to first order in Equation III-8. Though this equation

$$\Delta V = \frac{\partial \Delta G}{\partial p} = \frac{N_A z^2 e^2}{2a_o}\left[\frac{\partial \varepsilon_o^{-1}}{\partial p} + \left(1 - \frac{1}{\varepsilon_o}\right)\frac{\partial \ln a_o}{\partial p}\right] \qquad \textbf{(III - 8)}$$

only describes a point charge for clarity, it may be expanded to include effects upon a point dipole and point quadrupole. Here ε is the dielectric constant of the medium (ε_o is at zero field strength), the charge ze sits at the center of a cavity of radius a_o (when ε_o = 1) (Whalley 1963) (Kirkwood 1934). In this equation, the first term is due to the change in volume of the dielectric, known as electrostriction. The second term is a change in volume of the cavity due to the dielectric.

The detailed analysis of these data provides insights into the relative contributions of thermal heating, conformational volume change and electrostrictive volume change to the grating signal. In particular, performing experiments at the zero-expansion point of water should eliminate the thermal contribution to the signal, laying the solvation contribution bare. Furthermore, the electrostrictive volume change reveals information on the outer-sphere (solvational) reorganization energy and its time evolution. Transient grating experiments allow study of these changes on the picoseconds time scale, while more traditional calorimetric experiments are limited to the microsecond scale (Arata and Parson 1981) (Mauzerall, Gunner et al. 1995) (Malkin, Churio et al. 1994).

III.A.6. *Stimulated Brillouin Gratings:* Typically gratings are formed through photon absorption and the subsequent alteration of the index of refraction. Yet even optically transparent materials may see the generation of an acoustic wave. In this instance, the mechanism isn't thermal relaxation (for there is no absorption), but stimulated Brillouin scattering (Nelson, Lutz et al. 1981; Nelson, Miller et al. 1981; Fayer 1982; Nelson 1982; Robinson, Yan et al. 1984; Shen 1984). The natural spectral width of the pump pulses is the key to this effect. A photon, with a high frequency relative to the absorption maximum, from one of the pump beams is converted into a low frequency photon of the *other* pulse. Conservation of energy and momentum demand that phonons of the difference frequency and momentum be created. As this happens in both directions, two counter-propagating acoustic waves are generated.

These waves form a standing acoustic wave that drives grating formation, even though no excitation has taken place. Expressions for these gratings have been found and are simplified and repeated as Equations III-9 and III-10 (Fayer 1982) (Nelson, Casalengo et al. 1982), with the additional inclusion of acoustic attenuation, α (this term is more thoroughly explained below) (Shen 1984) (Bass, Stryland et al. 1995). Other

$$\Delta\rho = Fe^{-\alpha t}\sin(\omega t)\cos Kx \qquad \textbf{(III - 9)}$$

$$F = \frac{KI}{2cv_o}\rho_o\left.\frac{\partial n}{\partial \rho}\right)_p \qquad \textbf{(III - 10)}$$

terms are as defined above, with the addition of c as the speed of light and I as the energy intensity (J/cm^2) of light in the sample (at the grating peaks). These equations describe the formation of the stimulated Brillouin grating, though they don't explain its persistence after the beams have left the sample (Nelson 1982) (Nelson, Lutz et al. 1981).

Others have explored the mechanism that couples Brillouin scattering directly to the acoustic wave, but for reflected acoustic waves and not transmitted ones (Shen 1984).

This result fits into the diffraction efficiency (III-3) through Equation III-4. Note that this is actually an *additional* source term, not explicitly covered in III-3, which only covers gratings that follow energy absorption. Finally, this grating signal will have no offset, so acoustic wave will swing above and below the equilibrium density. The thermal and volume gratings, by contrast, will oscillate from zero to some maximum, due to the temperature and volume driven expansions explained above and treated below. The stimulated Brillouin grating thus shows a distinctive oscillation with a frequency of 2f, where f is the grating frequency predicted by $f = v_o/\Lambda$. When the two mechanisms appear together, the relative strengths of each determine the character of the signal. For the case where the mechanisms produce roughly equal signals, the outcome is shown in Figure III-2. The addition of the stimulated Brillouin term shifts the dominant peaks forward in time and gives rise to a secondary set of smaller, intermediate peaks. When the coefficient is negative, the peaks are shifted backward in time (Fayer 1986).

III.B. Theory of Transient Thermal and Volume Gratings

III.B.1. *Introduction:* Laser excitation of the sample leads to spatial and temporal alterations in the material density. The first schemes to describe this change utilized a simple one-dimensional approach to the diffusion of energy in an elastic medium (Genberg, Bao et al. 1989). The model below will begin instead with the equations of motion for a fluid. The temperature dependence equation reduces to the previous result for simple systems. However, internal volume changes and more general systems may now be included, and the displacement equation now includes acoustic attenuation.

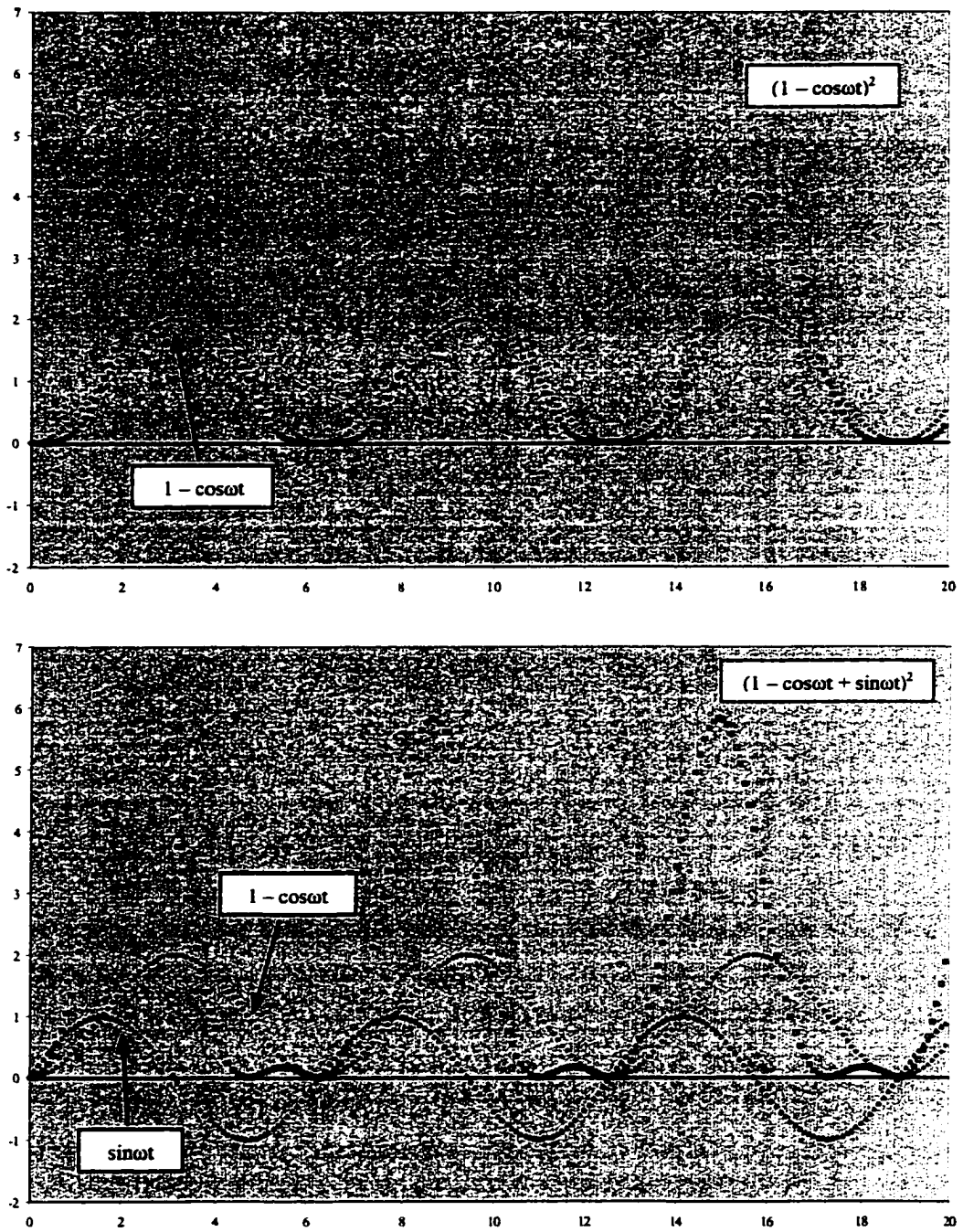

Figure III-2: Thermal and Brillouin components to a transient grating. For the thermal case, the density change develops approximately as (1 - cosωt), where ω is the acoustic frequency, in the top figure. The efficiency is proportional to the density change squared. The Brillouin component, by contrast, appears as (sinωt). They interfere in the lower figure, shifting the grating maxima to shorter times and producing small intermediate peaks. When the sign of the Brillouin component is reversed, the peaks shift toward longer times.

Others have formed more sophisticated, three-dimensional solutions (Sun, Morais et al. 1992), that were appropriate for diffusion studies (Cao, Chen et al. 1997). That approach is not considered here, though the simpler, one-dimensional model may yield somewhat incorrect results for the diffusion constant. This will not affect the volume and enthalpies measured, however. Furthermore, since the laser pulsewidth is quite short (~750fs for the pump and several picoseconds for the probe), compared to the resolution of the experiment, they will be treated as delta functions, though it is possible to include pulse width effects (Miller 1989).

III.B.2. *Linearized Fluid Motion:* Any fluid requires five equations to full describe its motion. The equation of continuity and conservation of entropy yield two, while the Euler equation yields the remaining three. Fluids that are mixtures require additional continuity equations for each additional fluid component. For viscous fluids, the Euler equation is approximated by the Navier-Stokes equation. These equations are generally complicated, nonlinear and strongly coupled. A great simplification is made by assuming that the variables will show small variations about an equilibrium value. Keeping only the linear terms in the variations, the equations of motion reduce to the linear equations III-11, III-12 and III-13. In the linear continuity equation (III-11) ρ_o is

$$\frac{\partial \rho}{\partial t} - \rho_o \bar{\nabla} \cdot \bar{v} = 0 \qquad \textbf{(III - 11)}$$

$$\rho_o \frac{\partial \bar{v}}{\partial t} = -\bar{\nabla} p + \left(\zeta + \frac{4}{3} \eta \right) \bar{\nabla} \left(\bar{\nabla} \cdot \bar{v} \right) - \eta \bar{\nabla} \times \left(\bar{\nabla} \times \bar{v} \right) \qquad \textbf{(III - 12)}$$

$$\rho_o T_o \frac{\partial s}{\partial t} = \bar{\nabla} \cdot \left(k_{th} \bar{\nabla} T \right) \qquad \textbf{(III - 13)}$$

the average density, while ρ is the variation in density and the vector v is the fluid

velocity. The Navier-Stokes equation (III-12) also contains the pressure, p, the viscosity, η, and the second viscosity is ζ. Lastly, in the entropy conservation equation (III-13), k_{th}, T and s are the thermal conductivity, the temperature and the entropy of the sample, respectively.

III.B.3. *Heat Conduction (Energy Conservation):* For small variations in pressure, the entropic conservation equation (III-13) reduces to Equation III-14, the

$$\rho_o C_p \frac{\partial T}{\partial t} - k_{th} \frac{\partial^2 T}{\partial x^2} = \dot{Q}(1 + \cos Kx) \qquad \textbf{(III - 14)}$$

equation for thermal diffusion. The right-hand side of the equation represents an external driving force upon the system, due to heat release in the areas of constructive grating interference. The left-hand side is the material response, reflecting temperature changes and the eventual flow of energy away from the sample. Recall that K is the wavevector of the grating ($K = 2\pi/\Lambda$). Finally, Q dot is the rate *change* of heat release of a non-radiative transition (per volume) in the sample. This heat release drives the sinusoidal temperature gradient. The sinusoidal variation in the grating should be modulated by a term that describes the falling off of the maxima at the edges of the beams. However, if the probe diameter is smaller than the pump laser diameter, this effect will be small, and approximately only affects the overall efficiency by some constant factor.

III.B.4. *Displacement (Material Conservation):* The linearized continuity and Navier-Stokes equations (III-11 and III-12) may be combined to eliminate the change in density as a variable. Assuming the Stokes condition ($\zeta = 0$) and that the fluid is irrotational (all cross products are zero) yields the simplified equation for displacement, III-15 (Kinsler, Frey et al. 1982) (Fetter and Walecka 1980) (Landau and Lifshitz 1997).

$$\left(1+\frac{2\alpha v_o}{\omega^2}\frac{\partial}{\partial t}\right)\frac{\partial^2\xi}{\partial x^2}-\frac{1}{v_o^2}\frac{\partial^2\xi}{\partial t^2}=\frac{B}{\rho_o v_o^2}\left(\beta\frac{\partial T}{\partial x}-\frac{1}{V_o}\frac{\partial V}{\partial x}\right) \qquad \textbf{(III - 15)}$$

The right-hand side allows added density changes in the liquid, due to thermal expansion or a volume change ($\partial V/\partial x$) from some external source. The left-hand side of this equation determines the system's response, explicitly including damping. Here ξ is the component of the material displacement in the x direction. α is the acoustic attenuation (its presence is explained below), ω is the acoustic frequency, the constant v_o is the speed of sound in the sample and β and B are the coefficient of volume expansion and the bulk modulus for the solvent. Finally, V_o is the equilibrium volume of the system.

III.B.5. *Acoustic Attenuation:* If the driving terms in the displacement equation are set to zero, the result is clearly a wave equation with a damping term. The geometry of the fluid expansion means that acoustic waves are generated holographically in an experiment, as described above. As these waves propagate in a viscous medium, the losses they suffer are characterized by α. Acoustic attenuation is generally treated phenomenologically, as full descriptions of the factors underlying it are complex. However, it is believed that the dominant contributions are due to viscous and thermal conduction losses (Fetter and Walecka 1980) (Kinsler, Frey et al. 1982) (Kleppe 1989). The viscous term shown in the Navier-Stokes equation (III-12) has been related to the

$$\alpha=\frac{2}{3}\frac{\omega^2}{\rho_o v_o^3}\eta+\sum_i\alpha_i \qquad \textbf{(III - 16)}$$

attenuation in the classical approximation of Equation III-16. Additional absorption effects are simply assumed to add to this term, and are represented by α_i (Gray 1972) (Kinsler, Frey et al. 1982). Though other absorption mechanisms do serve to increase

attenuation, they do not change the form of Equation III-16, or more importantly, Equation III-15.

III.C. Density gratings for Two and Three Level Systems

III.C.1. *Linear Dynamics and Enthalpy of Two Level Systems:* Typical reviews on transient gratings assume a simple two-level model for the heat release (Genberg, Bao et al. 1989) (Vauthey and Henseler 1995) (Morais and Zimmt 1995). Furthermore, the system is assumed to obey first-order rate laws. Though for most systems, this model is only approximate, it may be easily solved. The terms are defined in Figure III-3. Equation III-17 gives the ground state population. The rate change of heat release that accompanies the relaxation of the excited state may be given by Equation III-18. N_0

$$N_0 = N\left(1 - e^{-k_0 t}\right) \qquad \textbf{(III - 17)}$$

$$\dot{Q} = Qk_0 e^{-k_0 t} \qquad \textbf{(III - 18)}$$

represents the ground state population while N is the total population of the system. The thermal energy released by the state is Q (which represents a flow of heat) and the rate coefficient is k_0. Q may only represent a fraction of the energy released by the sample as it relaxes as energy may also be released through non-thermal channels. Q dot is the time derivative of the heat flow, as mentioned above.

III.C.2. *Exact Solution for Two Level Thermal Grating:* Using Equation III-18 to define the driving term for a two level system, Equation III-14 is complete. Assuming separation of variables, it may be solved by standard inhomogeneous differential equation techniques. The boundary conditions are found by assuming the temperature to be independent of position at zero time, while the fluid is not allowed to leave the ends of

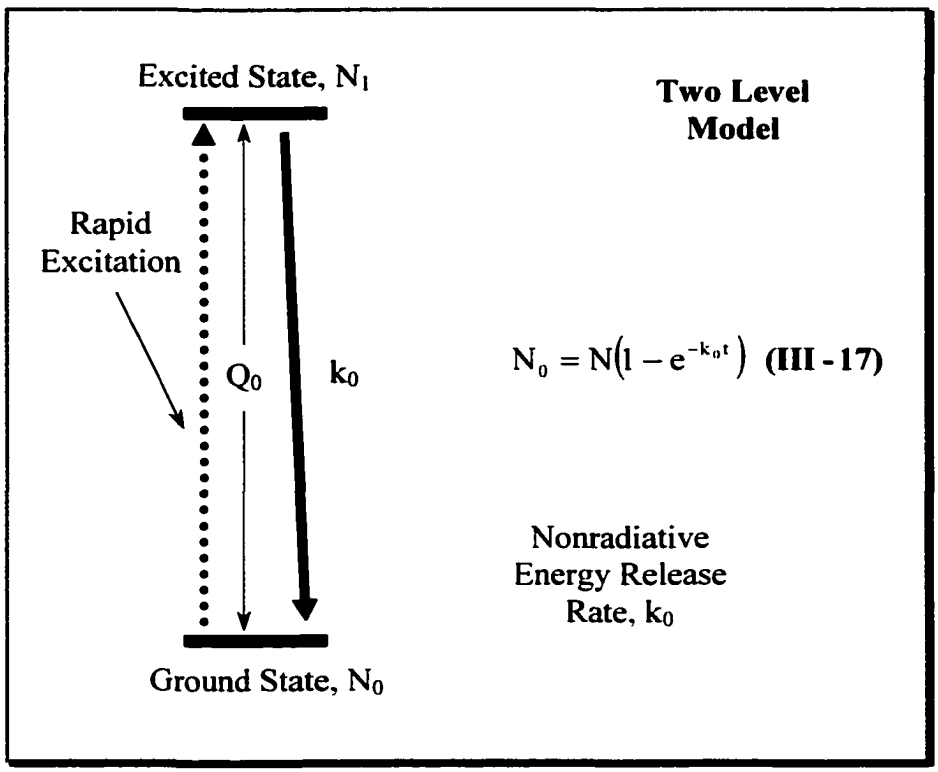

Figure III-3: The two level model utilizes a rapid excitation, followed by a relatively slow decay to the ground state. The energy of the excitation photon is broken up into several quanta of energy that appear as vibrational modes in the solvent and the solute. The population of the ground state (proportional to the energy given off) is given by Equation III–17.

the grating over the short time scale of the experiment. The gradient of this temperature solution is calculated and used as the driving term in Equation III-15. For this case, the volume change that is not temperature driven is ignored. Separation of the time and position variables now allows the displacement equation to be solved. The displacement, ξ, and its time rate of change are assumed to be zero at zero time, while the fluid is again not allowed to leave the ends of the grating. Finally, the solution for ξ allows approximation of the material strain and the change in density according to Equation III-19.

$$\Delta\rho = \rho_o \frac{\partial \xi}{\partial x} \qquad \textbf{(III - 19)}$$

At last, substitution into (III-4) gives Δn_ρ (Equation III-20), where A and b are constants defined in turn by Equations III-21 and III-22. This solution differs from

$$\Delta n_\rho = \frac{AQ_0}{(1-b/k_0)}\left[\frac{1}{\omega^2+b^2-2\alpha_o b}\left[e^{-bt}+e^{-\alpha_o t}\left(\frac{b-\alpha_o}{\omega}\sin(\omega t)-\cos(\omega t)\right)\right]\right.$$
$$\left. - \frac{1}{\omega^2+k_o^2-2\alpha_o k_0}\left[e^{-tk_0}+e^{-\alpha_o t}\left(\frac{k_0-\alpha_o}{\omega}\sin(\omega t)-\cos(\omega t)\right)\right]\right] \qquad \textbf{(III - 20)}$$

$$A = \frac{NK^2B\beta}{C_p}\frac{\partial n}{\partial \rho}\Big)_p \qquad \textbf{(III - 21)}$$

$$b = \frac{\lambda_w K^2}{\rho_o C_v} \qquad \textbf{(III - 22)}$$

previous work by the direct inclusion of the acoustic attenuation. However, the acoustic frequency, ω, has been assumed to be large compared to the acoustic attenuation, α so that $(\omega^2-\alpha^2)^{1/2}$ has been replaced by ω in III-20). The change in the index of refraction

must be inserted into Equation III-3 for the full solution to the diffraction efficiency. α_o is shorthand for αv_o, or is the attenuation per meter.

III.C.3. *Three Level Decay and Thermal Gratings:* Systems with three level decays may also be treated. In particular, a sample may relax to a stable, intermediate state before the remainder of its excitation energy escapes. Such a situation is shown in Figure III-4, and III-23 and III-24 give the populations. The intermediate state

$$N_1 = \frac{Nk_1}{k_1 - k_0}\left(e^{-k_0 t} - e^{-k_1 t}\right) \qquad \textbf{(III - 23)}$$

$$N_0 = N\left(1 + \frac{k_0 e^{-k_1 t} - k_1 e^{-k_0 t}}{k_1 - k_0}\right) \qquad \textbf{(III - 24)}$$

population is given by N_1, the rate by k_1, while the other terms are as before. The total heat release is now approximated according to Equation III-25, where Q_1 is the heat

$$Q(t) = Q_1 N_1(t) + Q_0 N_0(t) \qquad \textbf{(III - 25)}$$

release as the sample relaxes from the excited state to the intermediate state (see Figure III-4). Next, Equation III-25 is then differentiated to get the rate change of heat release, noting that only the populations are time dependent. The result is again set into the driving term of Equation III-14, and in turn into Equation III-15. The final result is shown on the next page (Equation III-26). Of course this model may be extended further to include more levels.

III.C.4. *Volume Gratings in Three Level Systems:* The sample density may change not only with temperature, but with conformational volume changes (discussed above, due to electrostriction and solvation). This volume change should be approximately constant with temperature, and is represented in Equation III-15. If we

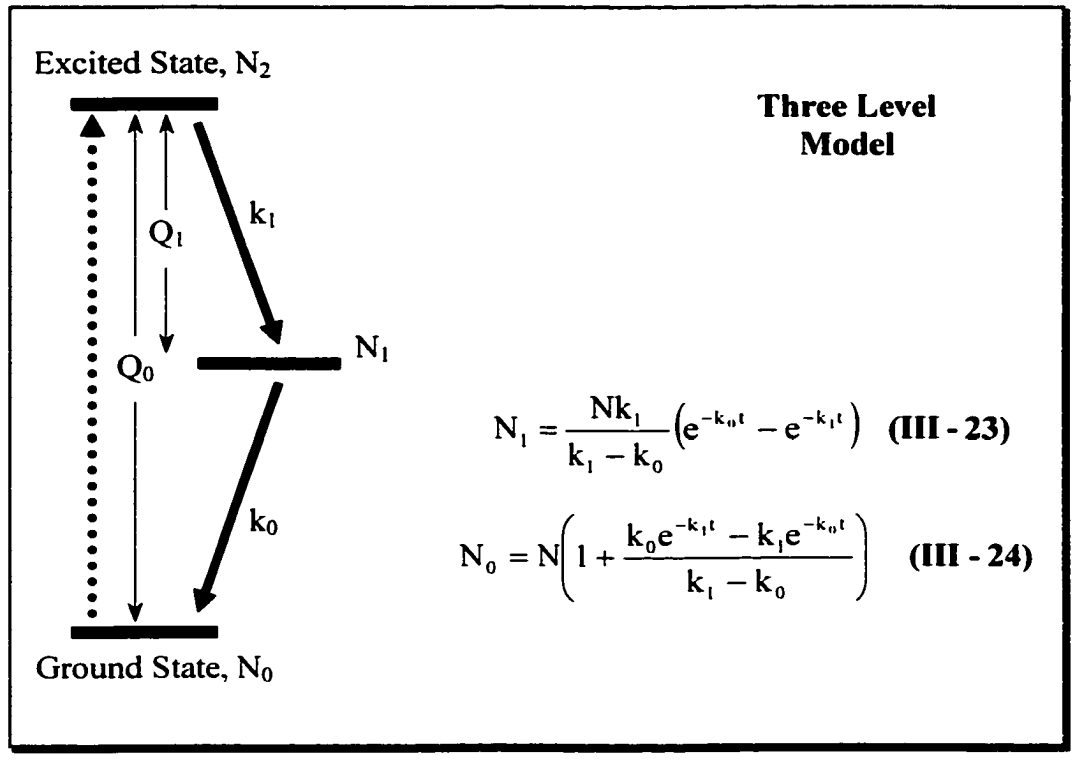

Figure III-4: After a fast initial excitation, the sample relaxes through an intermediate level, N_1. The solution to the first order rate equations for this system is shown to the right, as Equations III–23 and III–24. In this simple picture no reverse reactions are included, under the assumption that these effects are relatively small.

$$\Delta n_\rho = A\frac{(Q_0 - Q_1)k_0k_1}{(k_1 - k_0)(1 - b/k_0)}\left[\frac{1}{(\alpha - b)^2 + \omega^2}\left[e^{-bt} + e^{-\alpha t}\left(\frac{b-\alpha}{\omega}\sin(\omega t) - \cos(\omega t)\right)\right]\right.$$
$$\left. - \frac{1}{(\alpha - k_0)^2 + \omega^2}\left[e^{-tk_0} + e^{-\alpha t}\left(\frac{k_0 - \alpha}{\omega}\sin(\omega t) - \cos(\omega t)\right)\right]\right]$$
$$+ A\frac{(Q_1k_1 - Q_0k_0)k_1}{(k_1 - k_0)(1 - b/k_1)}\left[\frac{1}{(\alpha - b)^2 + \omega^2}\left[e^{-bt} + e^{-\alpha t}\left(\frac{b-\alpha}{\omega}\sin(\omega t) - \cos(\omega t)\right)\right]\right.$$
$$\left. - \frac{1}{(\alpha - k_1)^2 + \omega^2}\left[e^{-tk_1} + e^{-\alpha t}\left(\frac{k_1 - \alpha}{\omega}\sin(\omega t) - \cos(\omega t)\right)\right]\right] \quad \textbf{(III - 26)}$$

Figure III-5: Equation III-26 is the modulation of the index of refraction, for a three level model of the heat release. As before, the strain yields the change in the index of refraction, as determined by Equations III-14, III-15 & III-25. The symbols are defined in the text for the two-level model (III-21 and III-22).

consider a situation where there is no heat release, or no thermal expansion (at the zero expansion point, perhaps), then we may deal with this term separately. Situations that call for both thermal expansion and conformational changes may be treated by simply summing the two solutions (a direct result of summing them in the driving term of III-15).

Modeling the volume change may be done straightforwardly by using the rate equations for the three level model. The intermediate state represents some state involving solvation or a conformational change. The ground state may represent the relaxation from that state, but not necessarily the electronic or vibrational ground state. This time dependent volume change may be written as Equation III-27. Here V_o is the

$$V(t) = V_o + \Delta V N_1(t) \qquad \textbf{(III - 27)}$$

equilibrium volume, ΔV is the volume change, and the rate constants are as explained above (and in Figure III-4). Now the gradient of this expression looks much like the gradient for the temperature change, so it is not surprising that the solution should resemble the thermal grating. This solution follows as Equations III-28 and III-29.

$$\Delta n_\rho = \frac{A\Delta V}{(1 - k_0/k_1)}\left[\frac{1}{\omega^2 + k_0^2 - 2\alpha_o k_0}\left[e^{-k_0 t} + e^{-\alpha_o t}\left(\frac{k_0 - \alpha_o}{\omega}\sin(\omega t) - \cos(\omega t)\right)\right]\right.$$
$$\left. - \frac{1}{\omega^2 + k_1^2 - 2\alpha_o k_1}\left[e^{-tk_1} + e^{-\alpha_o t}\left(\frac{k_1 - \alpha_o}{\omega}\sin(\omega t) - \cos(\omega t)\right)\right]\right] \qquad \textbf{(III - 28)}$$

$$A = \frac{NK^2B}{V_o}\left.\frac{\partial n}{\partial \rho}\right)_p \qquad \textbf{(III - 29)}$$

Recall that the attenuation may be expressed as α_o, where this is equal to the product of the true attenuation and the speed of sound, or αv_o.

III.C.5. *Holographic Acoustic Wave and Resolution:* As mentioned above, the displacement equation (III-15) obviously allows counter propagating waves. Physically, this is a standing acoustic wave that may be observed as a sinusoidal modulation on the rise and decay of the thermal grating, or as a damped sine wave that completely determines the response for a delta function energy relaxation. To minimize the contribution of the acoustic mode to the signal, the angle between the pump beams may be increased. As the angle increases, the grating wavelength and the period of the resultant acoustic wave decreases. As the period of the acoustic wave becomes smaller than the time constant for thermal relaxation, the thermal component to the signal will dominate (see Figure III-6). The maximum temporal resolution is realized when the pump pulses approach a counter propagating geometry, though the overall strength of the signal attenuates (Miller 1989). For liquids (water, in particular) the limit is in the tens of picoseconds, though exploiting other terms in Equation III-3 could push this limit further (Miller 1989) (Eichler, Gunter et al. 1986). A compromise between appropriate time resolution and signal height must be accepted.

Finally, it is important to remember that thermal and volume gratings involve spatially dependent density changes. These modulations drive the generation of acoustic waves. Excited state gratings, by contrast, show no density changes, and no acoustic wave. Though an acoustic wave may be generated through changes in the dispersion, these effects should be relatively small.

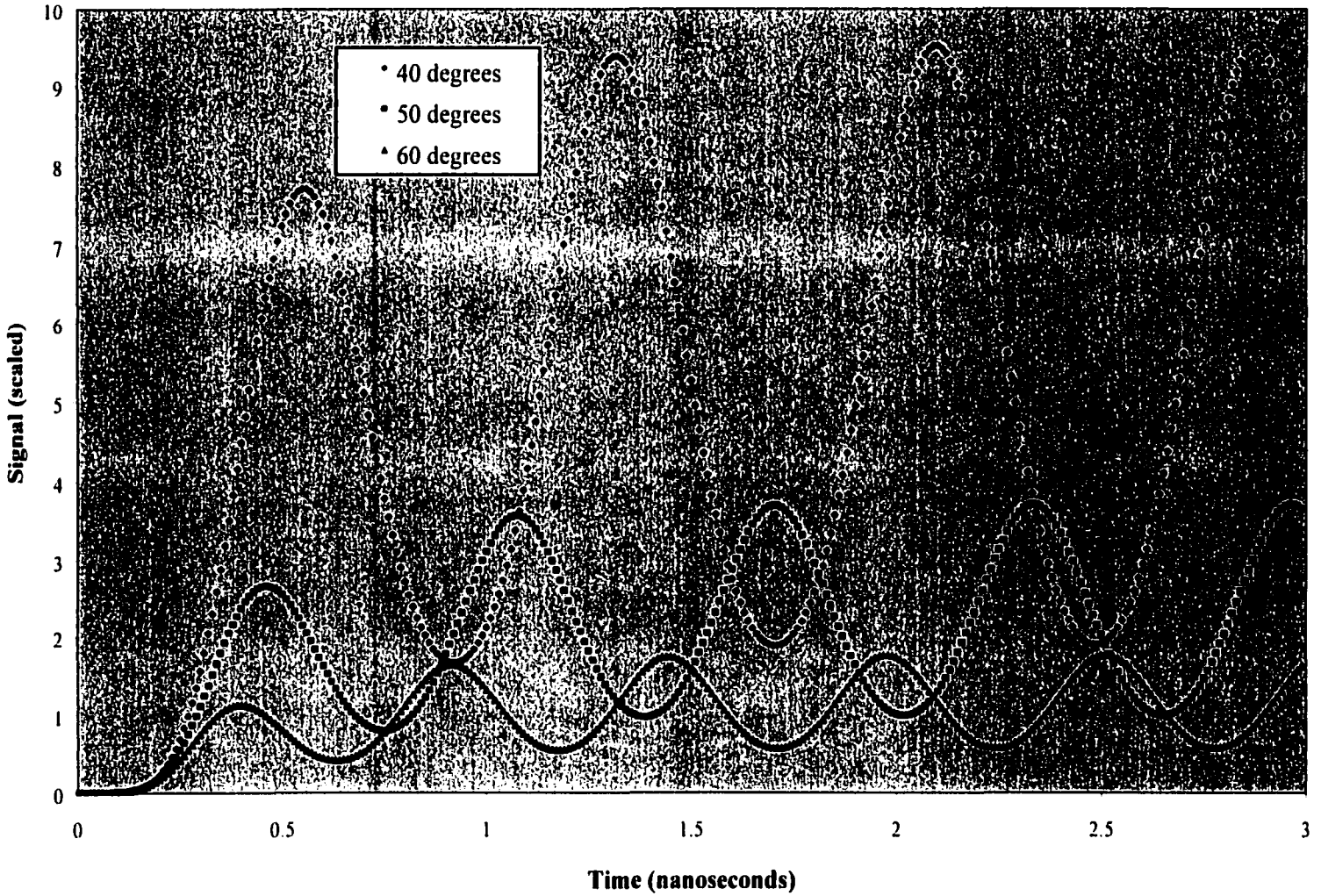

Figure III-6: Changing the incident angle of the pump beams through 40, 50 and 60° alters the acoustic period to 780, 630 and 530ps, respectively. In this instance the time constant for thermal relaxation is 300ps. Consequently, though the overall signal decreases, the time constant becomes easier to resolve as the thermal relaxation becomes larger relative to the acoustic signal.

III.D. Linear Dynamics for Complex Systems

III.D.1. *Triplet States:* A simple elaboration upon the three level model incorporates another (fourth) state. This level is not in sequence with the intermediate, but lies in parallel to it. Such a description is particularly useful for systems with significant triplet yield. Figure III-7 depicts a system that initially decays to the intermediate state. Subsequent relaxation may occur directly to the ground state, or through another intermediate. Typically this intermediate is a relatively stable spin triplet state and the fraction of molecules that take this path is the triplet yield. The stability of this state allows the recombination rate to be ignored (as the lifetime is typically longer than the time scale of the experiment). The rate equations established by Figure III-7 are relatively easy (if tedious) to solve. They yield the new intermediate population of Equation III-30 ($k_{0t} = k_t + k_0$), while the expressions for the other levels are only slightly

$$N_t = \frac{Nk_1k_t}{k_1 - k_{0t}}\left(\frac{e^{k_1 t} - 1}{k_t} - \frac{e^{k_{0t} t} - 1}{k_{0t}}\right) \qquad \textbf{(III - 30)}$$

altered under the conditions $k_t < k_0$ and $N_t << N$. The heat that evolves away from the system may be expressed by Equation III-31, where Q_t is the triplet energy difference

$$Q(t) = Q_0N_0(t) + Q_1N_1(t) + Q_tN_t(t) \qquad \textbf{(III - 31)}$$

below the excited state and k_t is the rate of triplet formation.

When the triplet yield is small, the simplest approach to such a model is simply to fit it to a three level model, and numerically correct the heat release for the amount lost in the triplet state. For systems where the population of N_0 is more strongly affected, the rate equations must be solved. Using these solutions, the change in the index of

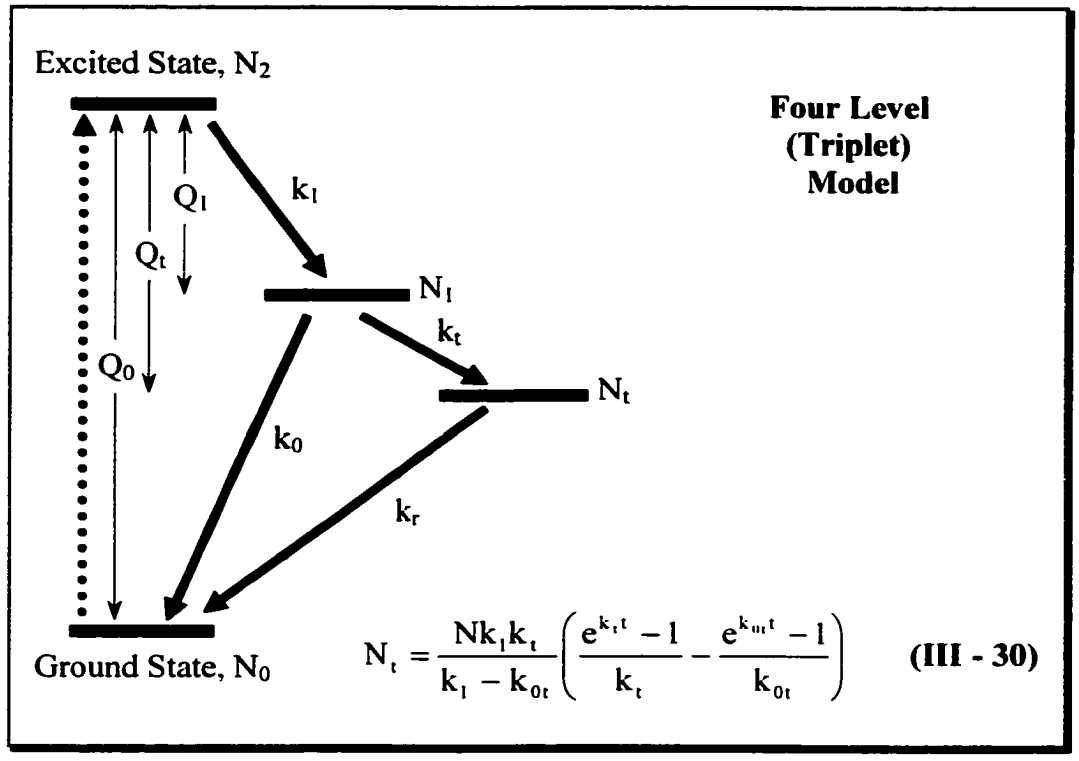

Figure III-7: After a fast initial excitation, the sample relaxes to an intermediate level, N_1. From here, the system may relax directly to the ground state, or through another level. This additional state, N_t, may be associated with a (spin) triplet state. Its population is shown in Equation III-30, where $k_{0t} = k_t + k_0$. In most systems, the recombination rate k_r is relatively small (and may be ignored).

$$\Delta n_\rho = A\frac{(Q_0k_0 - Q_1k_{0t} - Q_tk_t)k_1}{(k_1 - k_{0t})(k_{0t} - b)}\left[\frac{1}{(\alpha - b)^2 + \omega^2}\left[e^{-bt} + e^{-\alpha t}\left(\frac{b-\alpha}{\omega}\sin(\omega t) - \cos(\omega t)\right)\right]\right.$$
$$\left. - \frac{1}{(\alpha - k_{0t})^2 + \omega^2}\left[e^{-tk_{0t}} + e^{-\alpha t}\left(\frac{k_{0t} - \alpha}{\omega}\sin(\omega t) - \cos(\omega t)\right)\right]\right]$$
$$+ A\frac{(Q_1k_1 - Q_0k_0 - Q_tk_t)k_1}{(k_1 - k_{0t})(k_1 - b)}\left[\frac{1}{(\alpha - b)^2 + \omega^2}\left[e^{-bt} + e^{-\alpha t}\left(\frac{b-\alpha}{\omega}\sin(\omega t) - \cos(\omega t)\right)\right]\right.$$
$$\left. - \frac{1}{(\alpha - k_1)^2 + \omega^2}\left[e^{-tk_1} + e^{-\alpha t}\left(\frac{k_1 - \alpha}{\omega}\sin(\omega t) - \cos(\omega t)\right)\right]\right] \quad \textbf{(III - 32)}$$

Figure III-8: Equation III-32 is the modulation of the index of refraction, for a three level model of the heat release. As before, the strain yields the change in the index of refraction, as determined by Equations III-14, III-15 & III-31. The symbols are defined in the text and $k_{0t} = k_0 + k_t$.

refraction may be found as before, and is shown in Equation III-32 (Figure III-8). Though a complicated expression, III-32 is easily simplified as k_t is typically much less than k_0.

III.D.2. *Dynamic Solvation:* Another consideration is for an energy level that is not static, but that changes over the time scale of the experiment. Figure III-9 illustrates such a potential model, similar to the dynamic solvation model of Chapter II. The energy level decays exponentially, yet the leaving the rate equations approximately unaffected (which is acceptable under certain conditions detailed in the figure). The solutions to the level populations thus remain the same as for the three level system. Now the heat release assumes the form of Equation III-33. Q_s is the heat released by the changing

$$Q(t) = \left(Q_1 - Q_S(t)\right) \times N_1(t) + Q_0 N_0(t) \qquad \textbf{(III - 33)}$$

level, and k_s is the rate for this process. Note that Q_0 and Q_1 are still independent of time. Solving for the change in the index of refraction yields Equation III-34 (Figure III-10). The constants $k_{0S} = k_0 + k_S$ and $k_{1S} = k_1 + k_S$ have been defined. These combinations of the rate constants would not appear in a four level model, distinguishing this scheme from a four exponential decay.

III.D.3. *Heterogeneity:* Yet another scheme allows the intermediate state to exist as a distribution of levels, shown in Figure III-11. Each is weighted by some probability, P_i, which may by distributed evenly for the two states shown, or in any distribution for larger number of states (this probability must sum to one, of course). If level crossing, coherence and reverse reactions are ignored, then Equations III-35 and III-36 describe the populations, and may be used to redevelop the grating solution. Though this scheme is impossibly difficult for even a moderate number of levels (much less a continuum of

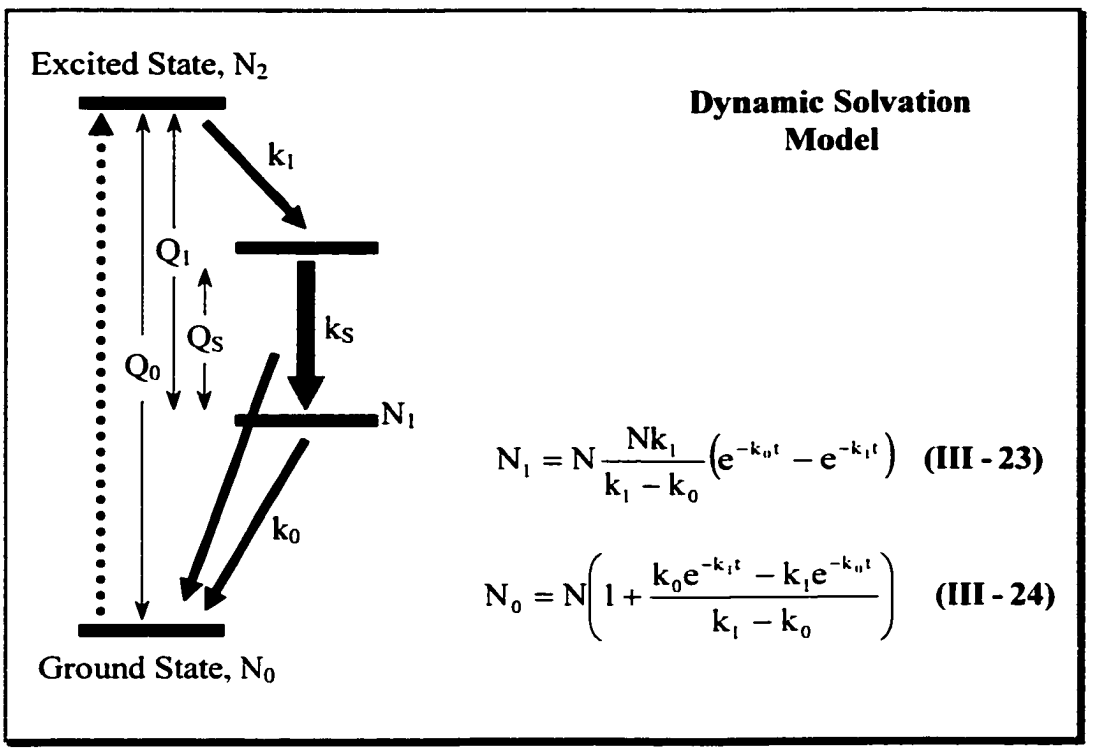

Figure III-9: The three level model is expanded to allow the decay of the intermediate energy level. The rate equations remain the same as before, but the time dependence of the heat release has changed. This model is most appropriate when the initial rate (k_1) is fast, and when the recombination energy ($Q_0 - Q_1$) is relatively large. These conditions minimize the possible time dependence of the reaction rates k_0 and k_1.

$$\Delta n_\rho = A\frac{(Q_0-Q_1)k_0k_1}{(k_1-k_0)(1-b/k_0)}\left[\frac{1}{(\alpha-b)^2+\omega^2}\left[e^{-bt}+e^{-\alpha t}\left(\frac{b-\alpha}{\omega}\sin(\omega t)-\cos(\omega t)\right)\right]\right.$$
$$\left.-\frac{1}{(\alpha-k_0)^2+\omega^2}\left[e^{-tk_0}+e^{-\alpha t}\left(\frac{k_0-\alpha}{\omega}\sin(\omega t)-\cos(\omega t)\right)\right]\right]$$
$$+A\frac{(Q_1k_1-Q_0k_0)k_1}{(k_1-k_0)(1-b/k_1)}\left[\frac{1}{(\alpha-b)^2+\omega^2}\left[e^{-bt}+e^{-\alpha t}\left(\frac{b-\alpha}{\omega}\sin(\omega t)-\cos(\omega t)\right)\right]\right.$$
$$\left.-\frac{1}{(\alpha-k_1)^2+\omega^2}\left[e^{-tk_1}+e^{-\alpha t}\left(\frac{k_1-\alpha}{\omega}\sin(\omega t)-\cos(\omega t)\right)\right]\right]$$
$$+A\frac{Q_Sk_{0S}k_1}{(k_1-k_0)(1-b/k_{0S})}\left[\frac{1}{(\alpha-b)^2+\omega^2}\left[e^{-bt}+e^{-\alpha t}\left(\frac{b-\alpha}{\omega}\sin(\omega t)-\cos(\omega t)\right)\right]\right.$$
$$\left.-\frac{1}{(\alpha-k_{0S})^2+\omega^2}\left[e^{-tk_{0S}}+e^{-\alpha t}\left(\frac{k_{0S}-\alpha}{\omega}\sin(\omega t)-\cos(\omega t)\right)\right]\right]$$
$$-A\frac{Q_Sk_{1S}k_1}{(k_1-k_0)(1-b/k_{1S})}\left[\frac{1}{(\alpha-b)^2+\omega^2}\left[e^{-bt}+e^{-\alpha t}\left(\frac{b-\alpha}{\omega}\sin(\omega t)-\cos(\omega t)\right)\right]\right.$$
$$\left.-\frac{1}{(\alpha-k_{1S})^2+\omega^2}\left[e^{-tk_{1S}}+e^{-\alpha t}\left(\frac{k_{1S}-\alpha}{\omega}\sin(\omega t)-\cos(\omega t)\right)\right]\right] \quad \textbf{(III - 34)}$$

Figure III-10: Equation III-34 is the modulation of the index of refraction, for a simple dynamic solvation model of heat release. The strain yields the change in the index of refraction, as determined by Equations III-14 III-15 & III-31. The symbols are defined in the text, just as for the two-level model (III-23 and III-24).

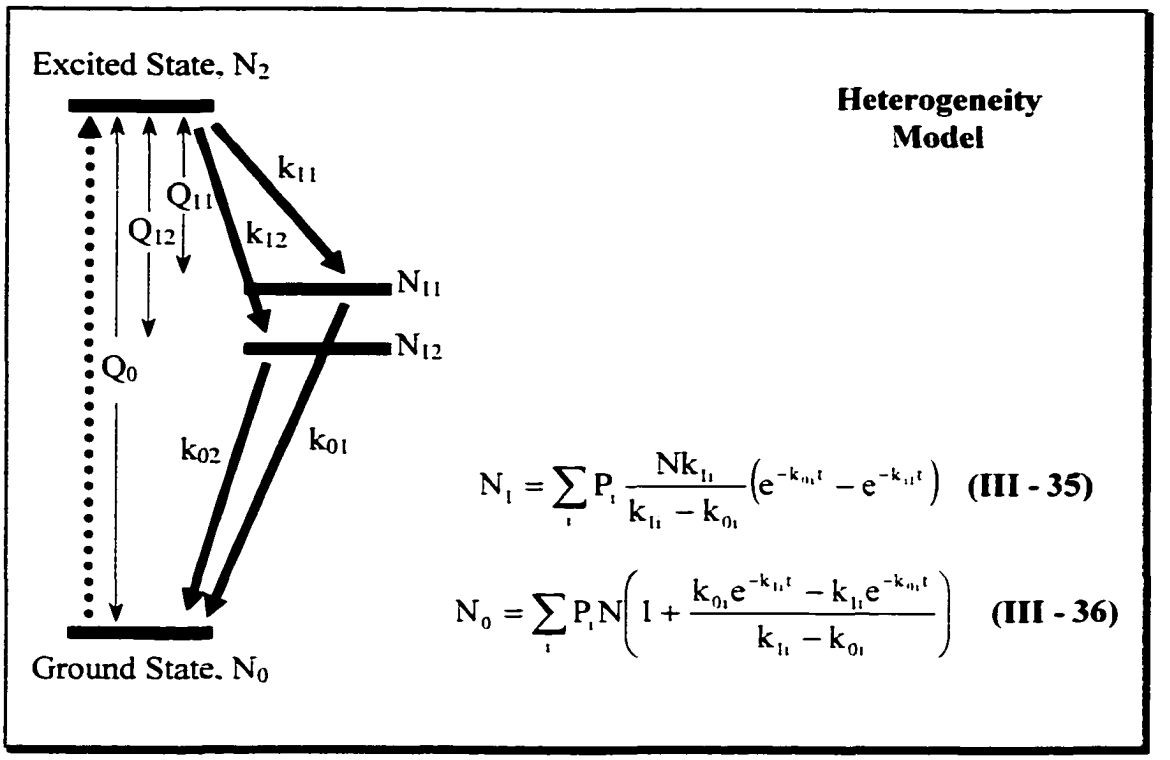

Figure III-11: After a fast initial excitation, the sample relaxes through several allowed intermediate levels, N_{1i}. Any number of levels may be allowed in principle, though it is practical to allow only a few, each weighted by some probability. The solution to the individual first order rate equations for this system is shown to the right. Neither reverse reactions nor intermediate level coupling are included, under the assumption that these effects upon the enthalpy are relatively small.

them), a few levels (five, for example) should reveal the approximate character of this

$$N_1 = \sum_i P_i \frac{N k_{1i}}{k_{1i} - k_{0i}} \left(e^{-k_{0i}t} - e^{-k_{1i}t} \right) \qquad \textbf{(III - 35)}$$

$$N_0 = \sum_i P_i N \left(1 + \frac{k_{0i} e^{-k_{1i}t} - k_{1i} e^{-k_{0i}t}}{k_{1i} - k_{0i}} \right) \qquad \textbf{(III - 36)}$$

model. Unfortunately, this approach demands a very strong signal to noise level, to allow so many parameters to be extracted from the fit.

III.D.4. *Numerical Solutions:* Clearly the analytical approach becomes difficult even for somewhat complicated dynamics. Solutions may also be obtained numerically. By assuming separability of the solutions, the coupled partial differential equations (III-14 and III-15) may be reduced to a series of coupled, first order, ordinary differential equations. These can be solved with fifth order Runge-Kutta (Press, Teukolsky et al. 1992) (Arfken and Weber 1995) methods.

In the first step of this method, a system of energy levels and rate coefficients relating the state populations is prepared. Populations are solved numerically as a function of time. A heat release may then be found (in a form similar to Equation III-18). This serves as the driving term in the heat conduction equation. The solution for the temperature may then be used in the solving the displacement equations. The numerical answer for the displacement is finally inserted into the grating efficiency. This was accomplished using MATLAB for Windows (version 4.2) and the Numerical Algorithms Group (NAG) software.

This approach has been successful in reproducing the features of the grating, and

comparing the expected results for the competing models of charge separation. The parameters of the models of charge separation (obtained from published results and shown in Chapter II) may be placed into the grating formulae (Woodbury, Peloquin et al. 1994) (Peloquin, Williams et al. 1994) (Ogrodnik, Keupp et al. 1994). A strong difference between the models of dynamic solvation and heterogeneity develops. The model of heterogeneity allows some rapid (picoseconds time scale) recombination to the ground state. This releases a significant amount of impulsive energy into the solvent. Thus a much higher signal is observed near zero time for this model than for the dynamic solvation model, which builds much more slowly. However, these results are certainly contingent upon the values of the variables used. Nonetheless, these simulations could indicate the relative importance of heterogeneity versus dynamic solvation.

Finally, these routines may be inserted into a least squares routine, to either confirm the fits of the exact solutions above, or to examine more complicated models. Such an approach is very flexible in principle, as non-exponential decays may be explicitly used, for example, or the strengths of specific transitions altered. Unfortunately, these routines place great demands upon processor time, as well as the signal to noise of the data. In practice (and in the analysis that follows) it is far more practical to utilize the exact solutions from above, as the fits are obtained far more rapidly, are more stable and more robust. However, they are quite useful for Monte Carlo simulations of parameter variance estimations.

III.E. Literature Cited

Arata, H. and W. Parson (1981). "Enthalpy and volume changes accompanying electron transfer from P-870 to quinones in *Rhodopseudomonas sphaeroides* reaction centers." Biochimica et Biophysica Acta **636**: 70-81.

Arfken, G. B. and H. J. Weber (1995). Mathematical Methods for Physicists. San Diego, Academic Press.

Bass, M., E. W. Stryland, et al., Eds. (1995). Handbook of Optics. New York, McGraw-Hill.

Cao, Y. N., H. X. Chen, et al. (1997). "Generation of the Photoacoustic Effect through Heat Diffusion: Transient Grating Measaurements on Reverse Miscelle Solutions." Journal of Physical Chemistry **101**: 3005-3011.

Deak, J., L. Richard, et al. (1994). Picosecond phase grating spectroscopy: Applications to bioenergetics and protein dynamics. Methods in Enzymology. New York, Academic Press: 322-360.

Desai, C. R., M. D. Levenson, et al. (1983). "Forced Rayleigh scattering: Thermal and acoustic effects on phase-conjugate wave-front generation." Physical Review A **27**(4): 1968.

Edens, G. J., M. R. Gunner, et al. (2000). "The enthalpy and entropy of reaction for formation of P+QA- from excited reaction centers of *Rhodobacter sphaeroides*." Journal of the American Chemical Society **122**(7): 1479-1485.

Eichler, H. J., ed., P. Gunter, ed., et al. (1986). Laser-Induced Dynamic Gratings. Berlin, Springer-Verlag.

Fayer, M. D. (1982). "Dynamics of molecules in condensed phases: picosecond holographic grating experiments." Annual Reviews in Physical Chemistry **33**: 63-87.

Fayer, M. D. (1986). "Picosecond holographic generation of ultrasonic waves." IEEE Journal of Quantum Mechanics **QE-22**(8): 1437-1452.

Fetter, A. L. and J. D. Walecka (1980). Theoretical Mechanics of Particles and Continua. New York, McGraw-Hill.

Genberg, L., Q. Bao, et al. (1989). "Picosecond transient thermal phase grating spectroscopy: A new approach to the study of vibrational energy relaxation processes in proteins." Journal of Chemical Physics **131**: 81-97.

Gray, D. E., ed. (1972). American Institue of Physics Handbook. New York, McGraw-Hill.

Kinsler, L. E., A. R. Frey, et al. (1982). Fundamentals of Acoustics. New York, John Wiley & Sons.

Kirkwood, J. G. (1934). Journal of Chemical Physics **2**: 351.

Kleppe, J. A. (1989). Engineering Applications of Acoustics. Norwood, Artech House, Inc.

Kogelnik, H. (1969). "Coupled wave theory for thick hologram gratings." **48**(9): 2909.

Landau, L. D. and E. M. Lifshitz (1997). Fluid Mechanics. Oxford, Butterworth-Heinemann.

Malkin, S., M. S. Churio, et al. (1994). "Photochemical energy storage and volume changes in the microsecond time range in bacterial photosynthesis--a laser induced optoacoustic study." **23**: 79-85.

Mauzerall, D., J. Feitelson, et al. (1995). "Wide band, time-resolved photoacoustic study of electron transfer reactions: Difference between measured enthalpies and redox free energies." Journal of Physical Chemistry **99**(4): 1090-1093.

Mauzerall, D. C., M. R. Gunner, et al. (1995). "Volume contraction on photoexcitation of the reaction center from *Rhodobacter sphaeroides* R-26: Internal probe of dielectrics." Biophysical Journal **68**(1): 275-280.

Miller, R. J. D. (1989). Picosecond transient thermal phase grating spectroscopy: Applications to the study of non-radiative energy relaxation. Time Resolved Spectroscopy. R. J. H. Clark and R. E. Hester, John Wiley and Sons Ltd.: 1.

Miller, R. J. D. (1994). "Energetics and dynamics of deterministic protein motion." Accounts of Chemical Research **27**: 145-150.

Miller, R. J. D., R. Casalengo, et al. (1982). "Laser induced ultrasonics: A dynamic holographic approach to the measurement of weak absorptions, optoelastic constants and acoustic attenuation." Journal of Chemical Physics **72**: 371-379.

Morais, J. and M. B. Zimmt (1995). "Thermodynamics of intramolecular electron transfer in alkane solvents." Journal of Physical Chemistry **99**(21): 8863-8871.

Nelson, K. A. (1982). "Stimulated Brillouin scattering and optical excitation of coherent shear waves." Journal of Applied Physics **53**: 6060-6063.

Nelson, K. A., R. Casalengo, et al. (1982). "Laser-induced excited state and ultrasonic wave gratings: Amplitude and phase grating contributions to diffraction." Journal of Chemical Physics **77**(3): 1144-1152.

Nelson, K. A., D. R. Lutz, et al. (1981). "Laser induced phonon spectroscopy. Optical generation of ultrasonic waves and investiagtion of electronic excited-state interations in solids." Physics Reviews B **24**: 3261-3275.

Nelson, K. A., R. J. D. Miller, et al. (1981). "Optical generation of tunable ultrasonic

waves." Journal of Applied Physics **53**(2): 1144-1149.

Ogrodnik, A., W. Keupp, et al. (1994). "Inhomogeneity of radical pair energies in photosynthetic reaction centers revealed by differences in recombination dynamics of P+HA- when detected in delayed emission and in absorption." Journal of Physical Chemistry **98**(13): 3432-3439.

Peloquin, J. M., J. C. Williams, et al. (1994). "Time-dependent thermodynamics during early electron transfer in reaction centers from *Rhodobacter sphaeroides*." Biochemistry **33**(26): 8089-8100.

Press, W. H., S. A. Teukolsky, et al. (1992). Numerical Recipies in C: The Art of Scientific Computing, Cambridge University Press.

Robinson, M. M., Y.-X. Yan, et al. (1984). "Picosecond impulsive stimulated Brillouin scattering: Optical excitation of coherent transverse acoustic waves and application to time domain investigations of structural phase transitions." Chemical Physics Letters **112**: 491-496.

Shen, Y. R. (1984). The Principles of Nonlinear Optics. New York. John Wiley & Sons.

Sun, T., J. Morais, et al. (1992). "Investigation of viscosity and heat conduction effects on the evolution of a transient picosecond photoacoustic grating." Journal of Chemical Physics **97**(12): 9324-9334.

Vauthey, E. and A. Henseler (1995). "Picosecond transient thermal phase grating study of a photoinduced electron transfer reaction in solution." Journal of Physical Chemistry **99**(21): 8652-8660.

Whalley, E. J. (1963). "Some comments on electrostatic volumes and entropies of solvation." Journal of Chemical Physics **38**(6): 1400-1405.

Woodbury, N. W., J. M. Peloquin, et al. (1994). "Relationship between thermodynamics and mechanism during photoinduced charge separation in reaction centers from *Rhodobacter sphaeroides*." Biochemistry **33**(26): 8101-8112.

IV. TECHNICAL DETAILS

The transient grating experiments of this work are three beam, time domain experiments that are resolved to roughly one picosecond. The laser system necessary for such experiments must generate pulses tunable in the far red of the visible to match the excitation energies of photosynthesis. These short, yet powerful pulses, less than a picosecond long and roughly a milliJoule each, exhibit nonlinear effects in many materials. Two of these effects, white light generation and parametric amplification, are used to generate a nearly non-resonant probe beam tunable in the near to mid infrared. The procedures for light harvesting and reaction center growth and purification allow the concentrated and pure amounts preferable for stronger signals and simpler, uncoupled dynamics. Light harvesting centers, wild type reaction centers and mutant (M)214H reaction centers are grown, characterized and stored for use. Finally, the procedures of the experiments control the protein environment, allow the data to be collected and accurately describes a stable system for correct data analysis.

IV.A. Photons

IV.A.1. *Oscillator and Stretcher:* The full layout of the optical table follows in block form (Figure IV-1), while the individual elements are detailed below. A Coherent *Innova400* argon-ion laser pumps 8 Watts (multi-line) into a *Mira900*. The remaining 14 Watts is directed to a Coherent regenerative amplifier not used in this experiment. The *Mira900*, a titanium:sapphire oscillator, emits approximately one watt of pulsed power, at a repetition rate of 76MHz. These pulses, typically 200fs and 15nm wide, are tuned to approximately 864nm. Pulsewidth and bandwidth are monitored respectively by a fast-scan autocorrelator (Femtochrome Research, Inc.) and a home - built Optical Mode

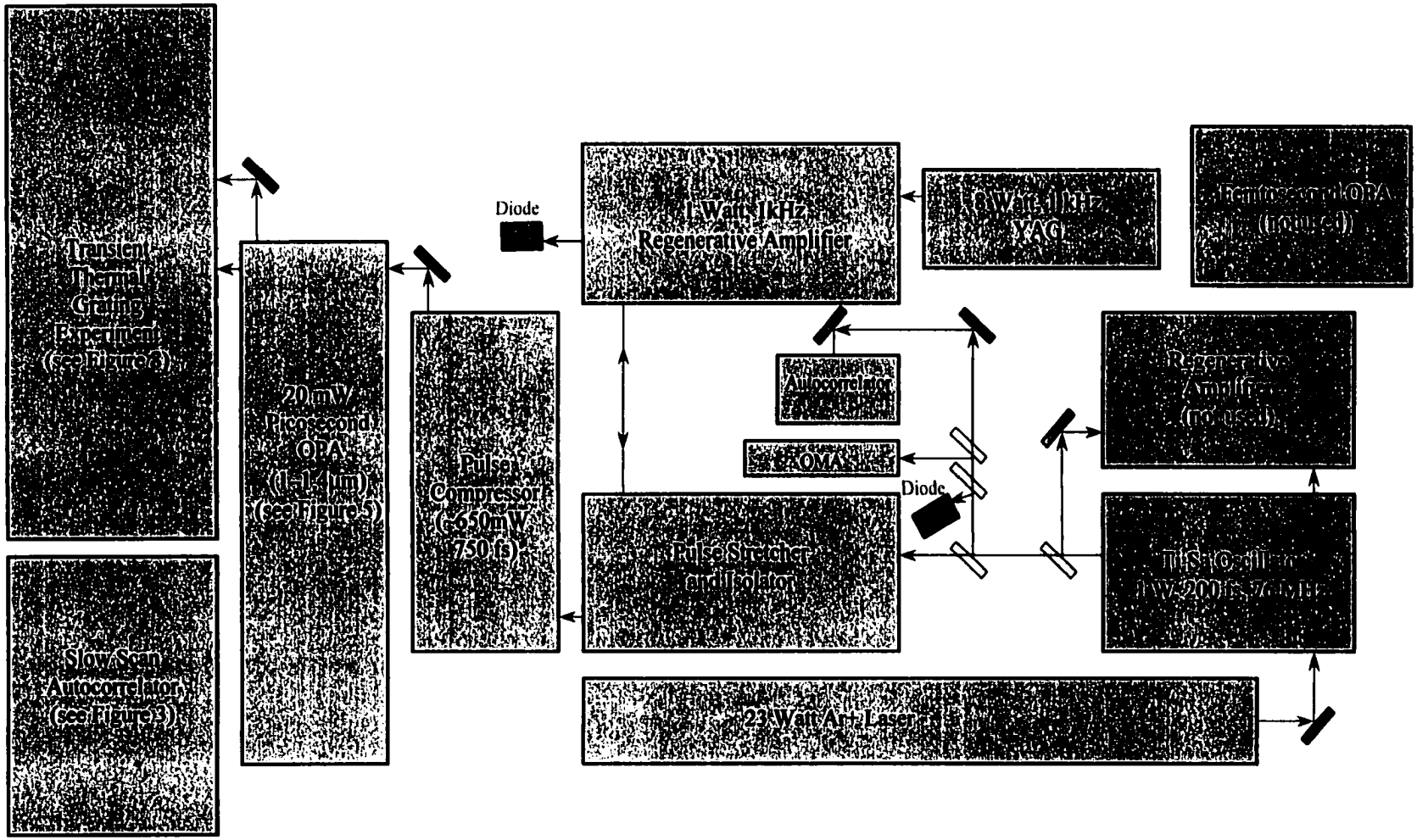

Figure IV-1: Laser system for picosecond spectroscopy. The diode just after the Ti:sa oscillator provides a timing reference for the YAG. The second diode monitors pulse amplification in the regenerative amplifier.

Analyzer (OMA). Monitoring the bandwidth is especially crucial, as the laser will occasionally drift into a continuous wave (cw) mode. The uncertainty-limited bandwidth of this mode is considerably smaller, and potentially damaging to subsequent lasers (see below). A slit near the output coupler is used (in conjunction with the optical Kerr effect in the titanium:sapphire crystal) to attenuate the cw mode, and keep the oscillator mode-locked in the pulsed mode.

To achieve the energies necessary for non-linear effects (required for optical parametric amplification), these pulses must be amplified. Simply seeding these pulses into another excited titanium:sapphire lattice will allow the necessary amplification. However, the resulting instantaneous power will damage the crystal. The pulse stretcher (a Clark-MXR *PS-1000*) then serves to draw out these pulses in time (to roughly 1 nanosecond), preventing the instantaneous power from crossing the damage threshold. Multiple passes onto a grating accomplish this through simple dispersion. A Faraday isolator now allows these pulses to leave the stretcher along a path that is distinct from the incoming beam.

IV.A.2. *Pulse Amplifier:* A Pockels cell (timed from a diode monitoring the oscillator power) allows an individual pulse into the amplifier. Once inside, the pulse traverses the cavity, acquiring energy from a titanium:sapphire crystal that has been pumped by a Nd:YAG laser (Clark-MXR *ORC-1000*). After six round trips (this number can vary with the pumping intensity and pulse wavelength), the crystal has been depleted and absorptive losses begin to outweigh amplification. At this point the pulse is saturated in power, and therefore more stable (fluctuations in the YAG are strong and will otherwise disturb the output). Another high voltage wave is sent to the Pockles cell and

the pulse is ejected, which is now approaching 1mJ after the buildup. An end mirror in the cavity leaks a small amount of light, which is picked up by a diode (1ns, Thorlabs, *DET1-Si* and *DET210*) (Figures IV-1 and IV-2). The ejection timing is monitored to ensure clean pulses (see below). A subsequent pulse will enter the amplifier again 1ms later. This timing corresponds to the repetition rate for the YAG (which is quite variable and will also affect the buildup of the pulse power).

The entire pulse is not successfully expelled, nor is it fully retained in the cavity during amplification. This energy may be amplified after another round trip of 10ns. These pre-pulses, post-pulses and other laser modes (the Ti:sapphire crystal with long wavelength mirrors prefers to lase at 850nm at varying time delays) will attempt to 'leak out' through the Pockels cell. Expanding the time and voltage scales for Figure IV-2 reveals their existence, as pulses 6ns and 10ns after the main pulse appear to be most problematic. Alignment of the Pockels cell, as well as the timing and adjustment of the high voltage pulse is critical to reject these 'ghost pulses.' Typical rejection ratios for the pre- and post-pulses are 10:1000 and < 1:1000 (respectively) with reference to the main pulse. Allowing a slightly inferior ratio for the pre-pulses ensures that the post-pulses are very sharply attenuated. Other modes are also sharply attenuated by ensuring that the Ti:sa rod is not seriously over-pumped by the YAG (a condition checked by observing the spatial mode). Overall power is sacrificed somewhat, however.

IV.A.3. *Compressor and Autocorrelator:* Another pass though the Faraday isolator directs the pulse into the compressor (Clark-MXR *PC-1000*). A second grating, optically paired with the one in the stretcher, employs dispersion to squeeze the pulses back down to approximately 700ps. Alignment is composed of tedious readjustments of

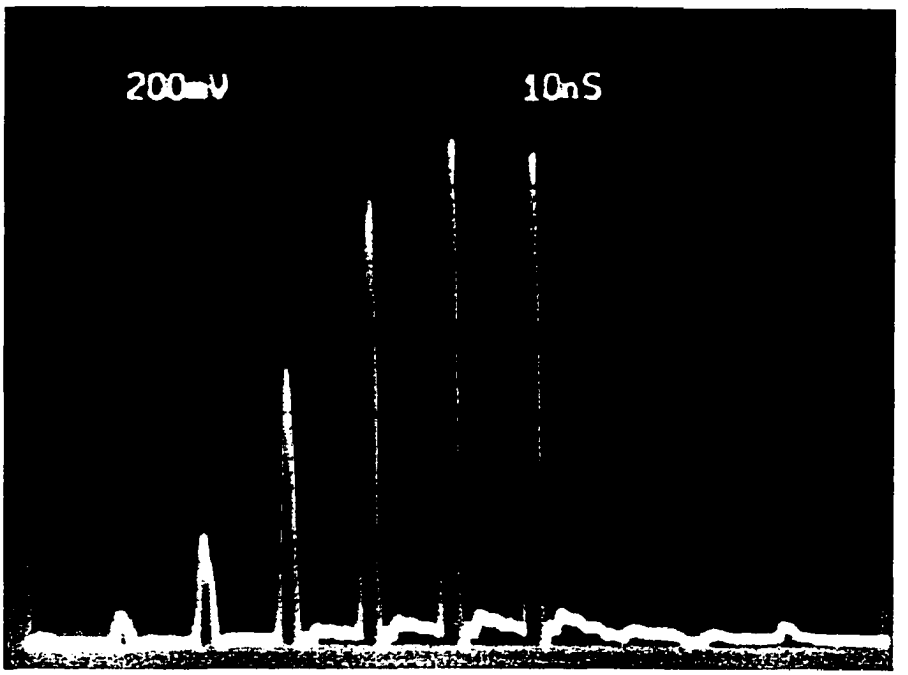

Figure IV-2: This oscilloscope trace has the units of 10ns per division horizontally and 200mV per division vertically. The amplification of the oscillator pulse is apparent, as is the 10ns round trip time of the cavity. Noise between the main peaks is mainly electrical, but also due to other modes attempting to lase within the cavity. The abrupt end of the trace indicates that the pulse has left the cavity.

the beam as it criss-crosses the compressor. Good compression ensures not just the minimum pulse length, but a reasonable (Gaussian) spatial mode as well. This pulse length is measured with the home-built slow scan autocorrelator shown in Figure IV-3. Typical autocorrelation scans are shown (Figure IV-4), including the assumption of pulses that are shaped as hyperbolic secants.

A pair or birefringent crystals in the amplifier cavity may be rotated to select a specific wavelength and bandwidth. As these pulses are compressed nearly to the transform limit, a trade-off between short pulses, and reasonably narrow bandwidth must be accepted. This time–resolved experiment and the white light continuum generation demand short pulses. A length of ~700fs was selected at the expense of the bandwidth. This was measured to roughly 4nm full width on an Instruments SA, Inc *H20* monochromater. Shot-to-shot noise of these pulses is less than 1%.

IV.A.4. *Optical Parametric Amplifier:* Roughly 600μJ leave the compressor every 1ms. Two-thirds of that power are used to drive a home-built optical parametric amplifier (OPA), shown in Figure IV-5. Based on a design by Richmond (Gragson, Alavi et al. 1995), this device delivers up to 30mJ of tunable infrared.

About 1/3 of the compressor output is split off and focused (to about 5μm) into a quartz cell of flowing ethylene glycol. Reed et al., noted that for pulses 170fs long and 1μJ, strong, single filament white-light continuum generation is observable (Reed, Steiner-Shepard et al. 1994). Our pulse-width is considerably longer, necessitating the significantly higher power. Though white light continuum is generated, it is multi-filament, and fairly unstable. The beam heats the ethylene glycol, causing light scattering bubbles to form. Other media, including Li:NbO_3, sapphire, water, and Nd:YAG were

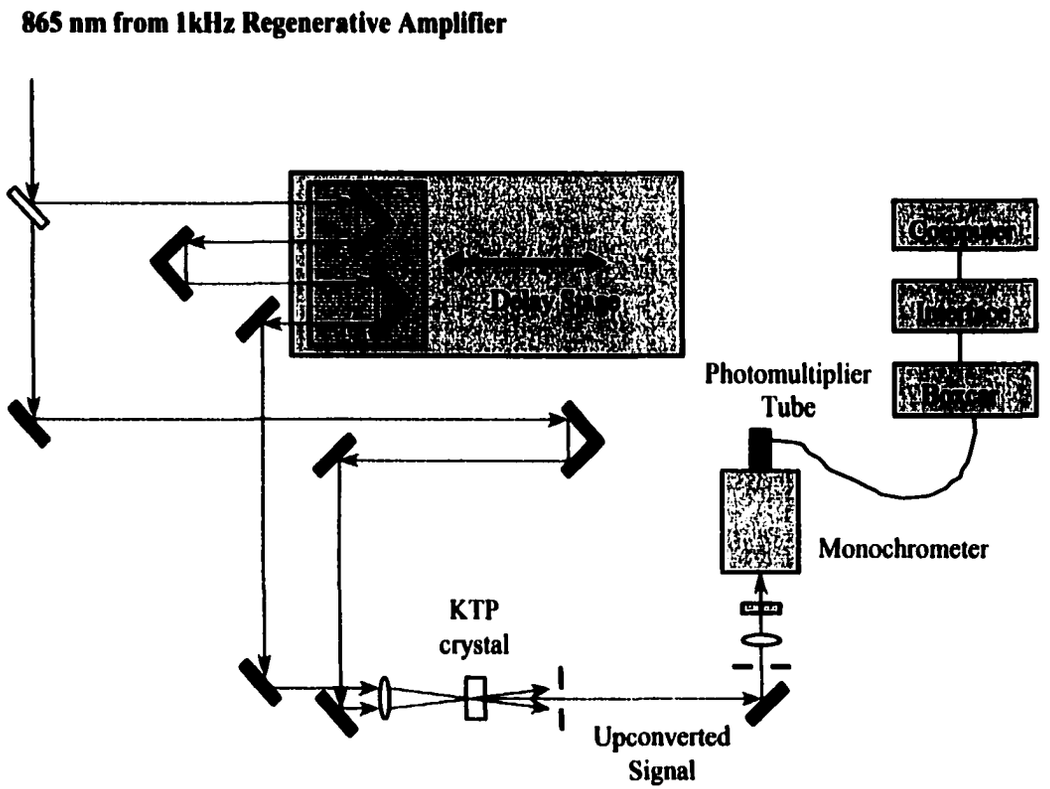

Figure IV-3: Autocorrelator schematic. The pulses are split and recombined with a variable time delay. The upconverted signal (432 nm) is the sum of a photon from each red beam.

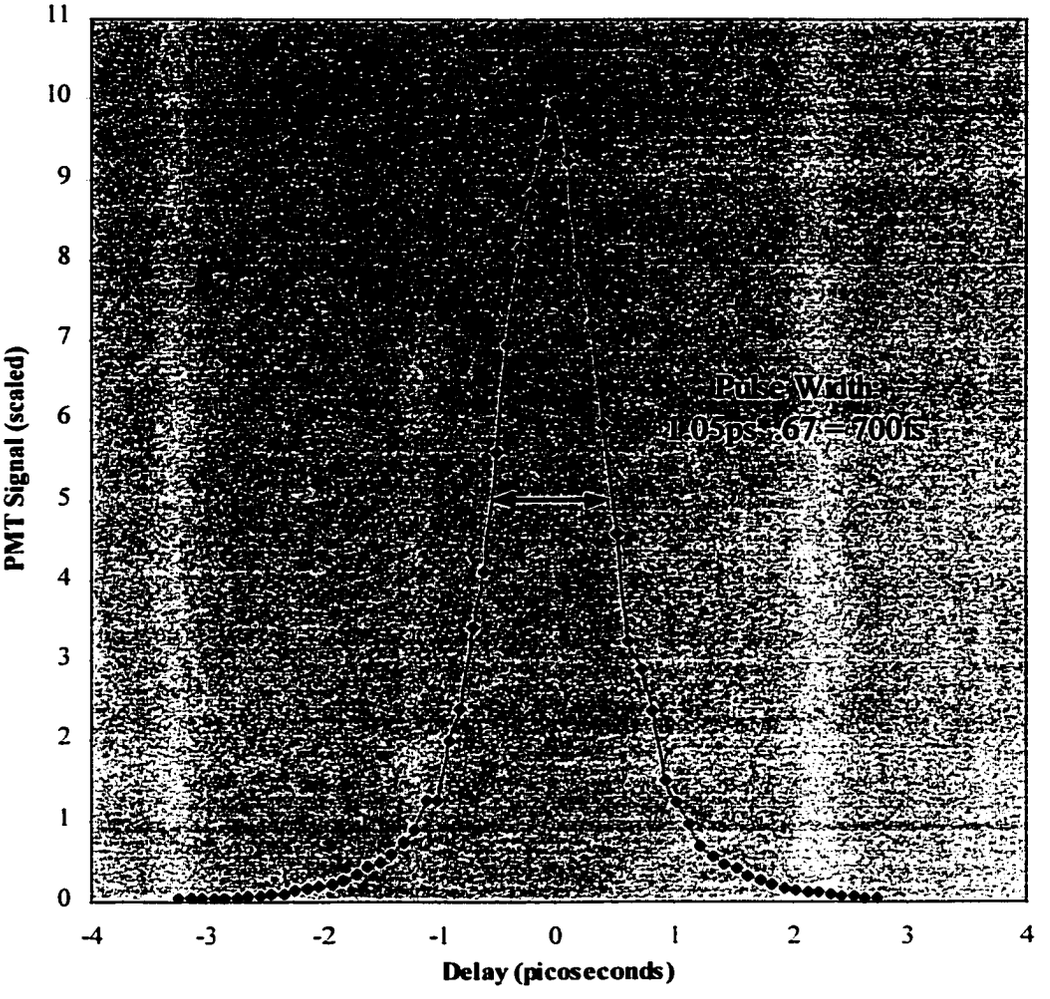

Figure IV-4: Typical pulses exhibited autocorrelation widths of roughly 700fs. Each of the four scans averaged here includes 1000 shots per point. Pulse shapes of hyperbolic secant are assumed.

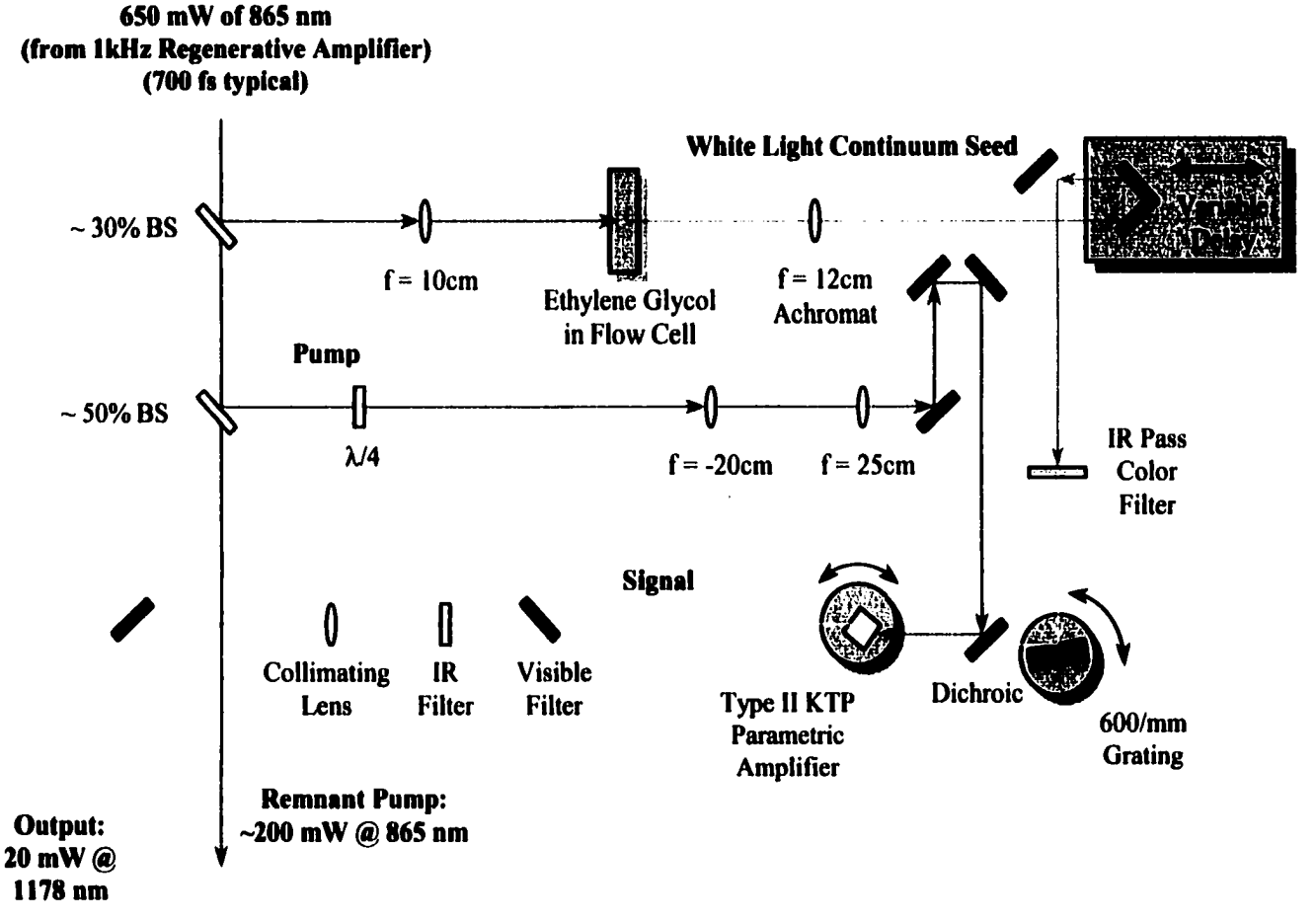

Figure IV-5: Optical parametric amplifier (OPA) layout. A color filter and a diffraction grating select a small portion of the infrared spectrum. This is collinearly phase-matched with the pump in a type II KTP crystal. The system is aligned using the zeroth-order light from the grating. The final alignment step sees the grating rotated to first-order.

also tried, with some success (30mW was the output power for the OPA with Nd:YAG crystal). However, all of the solids suffered from severe power and spatial mode instabilities, and the vapor pressure of water was too low to prevent bubbling. Though unstable, ethylene glycol delivers a beam of light with useful ranges from 400nm to 750nm and 950nm to 1400nm, with a strong peak above this pedestal at the original wavelength of 865nm. A range of spot sizes and input powers have also been attempted, but with no improvement. A filter removes most of the visible light and the remaining infrared beam is sent off of a grating into a Lithium Niobate ($Li:NbO_3$) crystal. If the zeroth order of the grating is directed into the crystal, the entire IR continuum seeds the beam, while the first order diffraction may be used to send only a portion of the continuum.

A second window of the OPA extracts one-half of the remaining compressed light, and is focused directly into the $Li:NbO_3$ crystal. This amplifying pulse, known as the pump pulse, is collinear and phase-matched with the IR seed. Inside the crystal, several nonlinear effects occur, of which the most useful is the parametric amplification of the seed, according to the proper matching angle with the $Li:NbO_3$ crystal (Reed, Steiner-Shepard et al. 1994; Gragson, Alavi et al. 1995). The resulting beam passes through a series of filters to remove the idler, remnants of the seed, and any other nonlinear leftovers, leaving a near-infrared pulse. Up to 30mW (25mW typical) is produced with the full continuum seed. However, if the full IR (900 – 1400nm) is used to seed the pulse, the bandwidth of the final pulse is a full 60nm. Rotating the grating to diffract the continuum allows a final pulse of 5nm bandwidth. Unfortunately, typical power declines to roughly 20mW while the shot-to-shot noise increases from ±20% to

±30% of the average power. This shot-to-shot noise is the direct result of the white light generation's instability. The narrower bandwidth, however, means more photons will satisfy the Bragg condition.

IV.B. Matter

IV.B.1. *Rhodobacter sphaeroides Growth:* Mutant reaction centers were expressed from plasmids transformed into a *Rhodobacter sphaeroides* deletion strain lacking LH_2 and reaction centers on the genome (SK102). Growth was carried out using a protocol descended from the earliest work in this field (Griffiths and Stanier 1956; Sistrom 1960), modified to maximize yields (Krueger-Koplin 1998). All cultures are grown in the dark at 34°C. A single bacterial colony is transferred into 5 ml of M22 (Sistrom 1960) media with 3 μg/ml of tetracycline and grown with shaking for two days. The 5ml culture is used to inoculate 200 ml of M22 media with no antibiotic and allowed to grow for two more days. Finally, the 200ml culture is used to inoculate 3.5 L of M22 media in a 4 L shaker flask and grown semi-aerobically for five days on a shaker (200 rpm). The cultures were harvested by concentration in an Amicon® recirculating hollow-fiber filter followed by centrifugation (30 minutes at ~ 8,000g's). The supernatant is poured off, and the pellets re-suspended in a solution of 10 mM TRIS, 1mM EDTA, and 100 mM NaCl (pH = 8.0, known as BUG buffer). The cells are ruptured by passing them though a French Press® (~18,000 psi) twice, yielding approximately 150 grams (wet cell weight) from 28 liters.

IV.B.2. *Reaction Center Purification:* Now the reaction centers must be separated from the cell debris (Reed and Clayton 1968). The broken, centrifuged cells are diluted with BUG buffer until the optical absorbance at 870nm is 50. Then, 0.25%

LDAO, 3% PEG (which facilitates aggregation) and 50mM CaCl are added. Spinning this mixture for 1 hour at 40,000g's yields several pellets containing reaction centers. The pellets are diluted back to an optical absorbance at 870nm of 50. A second detergent treatment with .5% LDAO liberates the reaction centers from the membranes. After centrifuging for 70 minutes at ~200,000 g's (Heller and Loach 1990), the supernatant is mixed with 333mL of aqueous ammonium sulfate (500g per L, pH = 7.0) and spun again at 40,000 g's for 15 minutes. Another 666 ml of the ammonium sulfate is added per liter of supernatant, and a 20 minute, 40,000g centrifuge run performed. The reaction center rich levitate is resuspended in 0 M NaCl buffer. This buffer consists of 10mM TRIS, 1mM EDTA and .1% LDAO, pH = 8.0. The protein is dialyzed in 4L of 0 M buffer overnight (12,000 – 14,000 cutoff).

IV.B.3. *HIS Tag Purification:* Sometimes wild-type RC's were purified using a poly-histidine tag added to the reaction center (Goldsmith and Boxer 1996). The broken cells were centrifuged and BUG buffer added just as above, without the presence of EDTA, however. 0.5% LDAO was then added to the supernatant to suspend the chromataphores. The supernatant was mixed with Ni-NTA chromatography resin and then rinsed with a solution of 10mM TRIS and 0.1% LDAO. Finally, the His tagged RC's were eluted off the resin with 10mM TRIS, 0.1% LDAO with 50mM imidazole.

IV.B.4. *Chromatography, Concentration and Detergent Environment:* The purification described in sections IV.B.2. and IV.B.3. results in a mixture of free pheophytin, reaction centers, light harvesting complexes and some other unidentified proteins. A large Toyopearls DEAE ion exchange column (10cm by 40cm length) is used to separate these components. After loading the sample, a wash of 100mM NaCl

buffer elutes the pheophytins. The reaction centers elute near the middle of a gradient from 100mM to 350mM NaCl.

The progress of the chromatography can easily be monitored visually. The yellow-orange band of the pheophytin is followed by the purple of the reaction center, and finally the bright red of the LH_2 complex. The quality of the reaction centers is discerned by comparing the optical absorbance at 280nm to the optical absorbance at 800nm. The absorbance at 280nm is diagnostic for various amino acids (particularly tryptophan, recall Chapter I), so the ratio provides a measure of total protein to photosynthetic reaction centers (Pace, Vajdos et al. 1995). A ratio of 1.2 is preferred for wild type and 1.4 for the (M)214H mutant (Kirmaier, Gaul et al. 1991) (the differences are due variations in the extinction coefficient at 800nm introduced by the histandine substitution. Typically two or three passes through the column were required to achieve the necessary purity.

The reaction centers are finally dialyzed to remove the salt in a 0 M NaCl buffer solution, concentrated to ~5 ml (*8200 concentrator*, Amicon) (*YM10 filter*, Diaflo), and frozen until use. Just prior to an experiment, the 0 Molar buffer which contains the detergent LDAO is exchanged for a .8% (weight by volume) βOG detergent (by dialysis and concentration), including 10mM Tris and 1mM EDTA (pH = 8.0). This provides a more stable chemical environment for the reaction centers. This is the same buffer used for the light harvesting complexes so that the bulk properties of both solutions should be reasonably similar.

IV.B.5. *Light Harvesting Center Purification:* Small amounts of LH_2 complexes are purified as byproducts in the reaction center protocol above. However, a simpler

method that takes advantage of a strain of *R. sphaeroides (Ya*)* lacking reaction centers (Krueger-Koplin 1998), was used to obtain the large amounts of LH_2 used in these studies. First the chromataphores are purified as above (following the procedure of section IV.B.2. until the ultra-centrifugation). Approximately one gram of these are added to 10ml of 1.6% βOG (with 10mM TRIS and 1mM EDTA). The mixture is centrifuged (200,000g, 4°C, 1 hour), and the supernatant is passed through a small Toyopearls column (1cm by 10cm length). A gradient of 0M to 1M NaCl is applied in the detergent solution described above. The pure LH_2 is collected, and dialyzed to remove the salt.

IV.B.6. *Sample Storage:* Both the reaction center and the light harvesting proteins will dissociate in the presence of heat, light or oxygen. To reduce this rate until the experiment, concentrations of each protein are kept in small (~ 5mL) tubes. The tubes are held at four degrees Celsius in a light tight box. Since the concentrator uses nitrogen gas to push solvent though the membrane, the remaining solution should have little dissolved oxygen left in it. A head of nitrogen gas is blown into the tubes containing the protein. After each experiment, the sample is diluted into buffer, and re-concentrated for storage, to remove any oxygen.

IV.C. Interaction

IV.C.1. *Quinone Reduction:* To prevent the slow recombination of the electron from the quinone (several 100ms, recall Chapter I), the quinone may be chemically reduced. The electron then recombines directly to the P* state at a lifetime of tens of nanoseconds. A solution of .5 Molar TRIS (recall Chapter I) is titrated to a pH of 8, then .25 Molar Sodium Dithionite and .25 Molar L-Ascorbic Acid is added. This mixture is

added in a maximum volume ratio of 1 to 100 of sample. As this solution has a lifetime of only several hours, it must be made and added just before running the experiment. The effectiveness of this technique has been verified in a grating/absorption experiment. Without reduction, the lifetime of the charge-separated state is clearly longer than 10ns, while the reduced sample shows a lifetime of tens of nanoseconds. One unfortunate consequence of this reduction is the eventual dissociation of the reaction centers. Keeping the sample under a head of nitrogen gas and occasionally running the sample though the concentrator minimizes this effect. Any dissolution of the protein may be monitored by performing a spectral scan before and after each experiment.

IV.C.2. *Sample Optical Density:* The absorption of the samples must be found to calibrate the absolute heat release. Samples placed in a spectrophotometer may have the absorption as a function of wavelength measured (as in Chapter I). This data not only reveals the optical density, but the general quality of the sample. Typical scans are reprinted from Chapter II, as Figure IV-6. Once the absorption at 865nm is measured, the sample concentration may be deduced utilizing a modified form Beer's law (Equation IV-1). T represents the transmission, ε the absorption cross section, c is the sample concentration, and b stands for the sample thickness. Typical spectrophotometers, however, usually report absorbance in units of optical density (OD). Equation IV-2 relates transmission to optical density. To produce the necessary signal-to-noise (and sample-to-photon) ratio, samples generally require an optical density of 10 (at the pump

$$T = e^{-bc\varepsilon} \qquad \textbf{(IV - 1)}$$

$$T = 10^{-OD} \qquad \textbf{(IV - 2)}$$

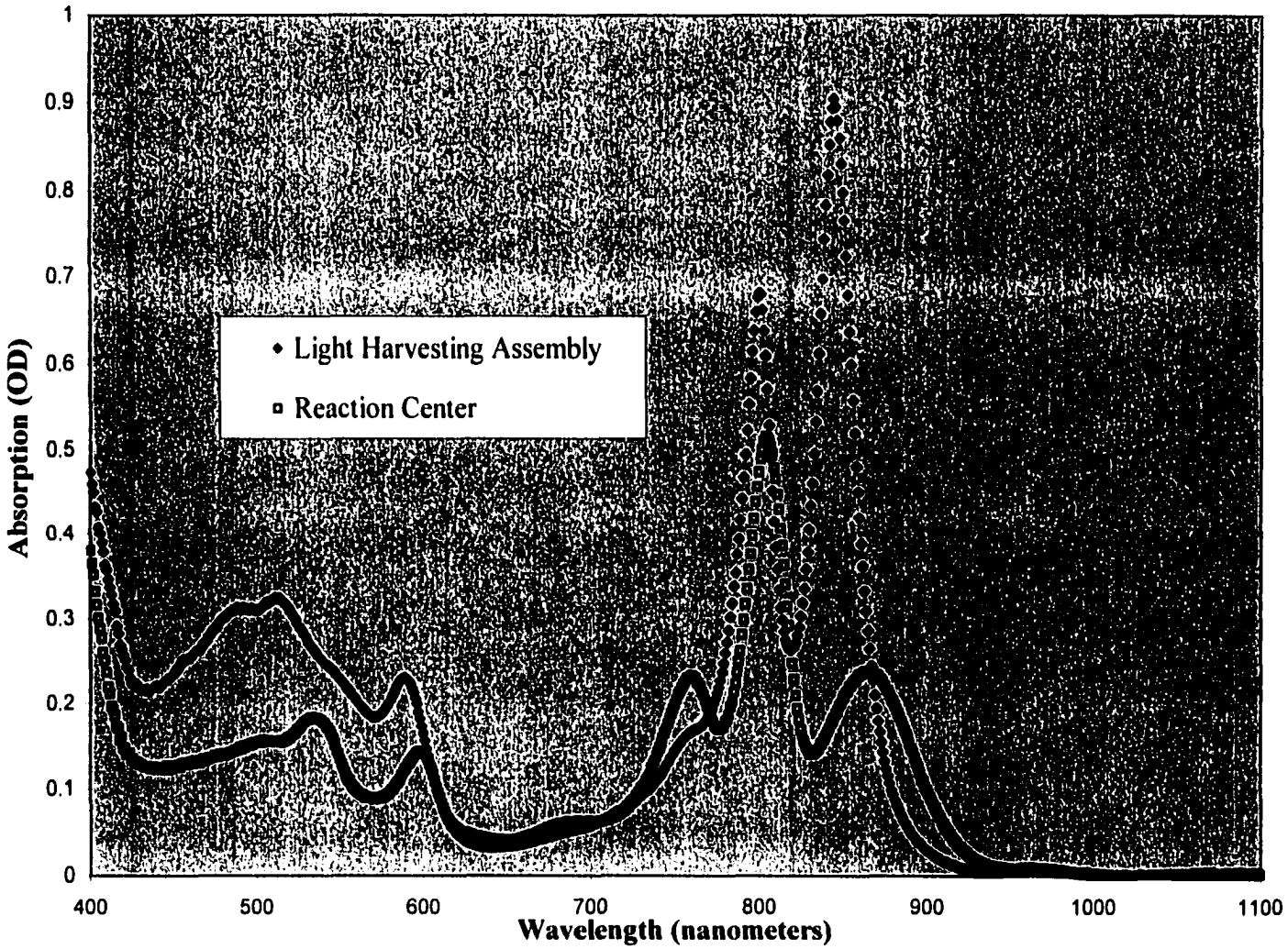

Figure IV-6: Spectra for photosynthetic reaction center and light harvesting assembly. Absorption at 865nm as well as general sample quality may be assessed from this data. Note the low absorption at the longest wavelengths. The absorption is measured in units of optical density, as described in the text, in 1cm cell. Each scan is typically diluted in buffer in a ratio of 100 to 1.

wavelength) in a 1cm cell. The sample occupies a total volume of about 4mL. As this measurement and the experiment itself is performed, great care must be taken to avoid exposing the samples to room light, which will disassociate the protein.

Some gradual sample degradation, however, is inevitable. However, the typical optical density for these experiments is quite high (at least 10). This allows the sample to suffer fairly significant degradation, while the overall heat deposited into the experiment remains roughly constant. Furthermore, when the protein deteriorates, the products have absorption far into the blue and the ultraviolet. Neither the pump nor the probe will interact with this matter.

IV.C.3. *Flow Cell:* To prevent oxidation and degradation of the reaction centers, a closed, refrigerated sample flow system was created, pictured in Figure IV-7. A 1mm path length, UV quartz flow cell (*48-UV-1* NSG, Inc.) is surrounded by an aluminum holder. This holder is drilled out to allow a one to one mixture of ethylene glycol and water to flow through it. This fluid is temperature controlled from a large chiller (*Model 1178*, VWR Scientific). The sample's temperature monitored with a small volume thermocouple (Omega, Inc.) inserted near the quartz cell. To prevent condensation on the glass surface, a cooled nitrogen purge is released onto the glass.

Sample travels from the cell through a closed system, including a bent glass tube where heat exchange takes place with another small reservoir of the glycol/water mixture. This glass tube and the flow cell are connected by Nalgene tubing, a section of which is inserted though a peristaltic pump (MasterFlex, *L/S Series*). A syringe is used to inject the sample into the flow tubing, and the plunger is depressed and taped in place to provide a positive pressure that deters bubbling. Furthermore, the positive pressure

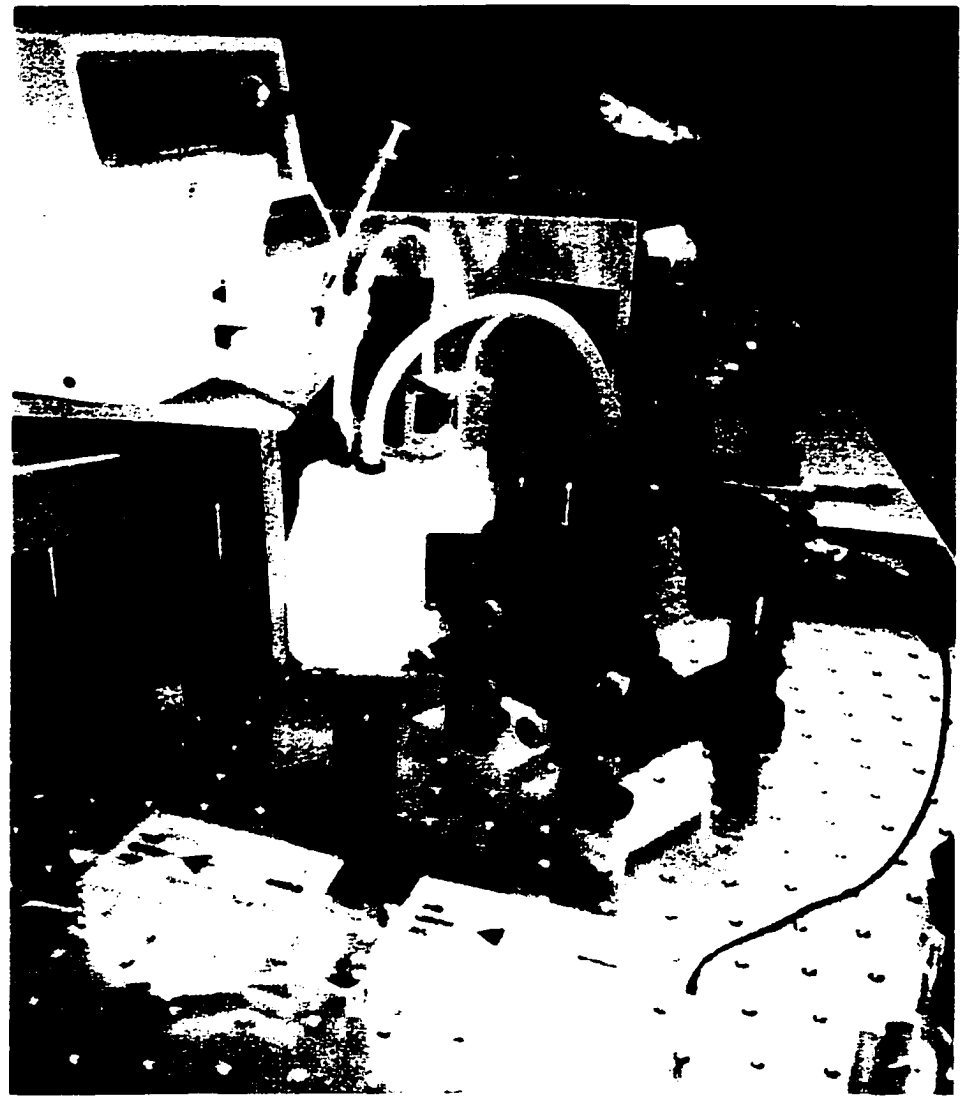

Figure IV-7: The back of the flow cell is visible in the center of this figure, as the glass piece in the aluminum holder. The sample is injected into this system using the syringe at the top of the picture, near the peristaltic pump. The yellow tube marks the sample's path. Both the aluminum holder and the plastic reservoir are connected through the white tubing to a temperature bath below the optical table. The thermocouple is visible as the thin wire on the upper (outgoing) tube. Behind the cell, on the right, is the signal detector, while the reference is on the left. The two mounts in the foreground (beyond the pre-amps) contain a pinhole and a doubling crystal, used for alignment as described in the text. The nitrogen purge is omitted from this figure.

prevents oxygenation of the sample. A vacuum system draws the used sample out of the flow tubing and into a reservoir. The cell must be kept rigorously clean to minimize scattered light from its surface. Though filtered water is flushed through the system between runs, the cell must be translated after each experiment and fully replaced after five or six experiments.

One drawback to the detergents is that the sample will foam if the flow rate is too high (scattering light that dwarfs the signal). Preferably, the rate should still be high enough that the sample should clear the laser beams' path between shots. However, the recombination time is very short compared to the time between shots. Since the sample is allowed to return to the ground state, the rate need only be fast enough to prevent thermal degradation. Our specimens are able to clear the beam path after two shots, and have shown no measurable thermal degradation.

IV.C.4. *Transient Grating Layout:* The schematic for the transient thermal grating experiment follows (Figure IV-8 – see also Figure IV-7). The pump beam (865nm) traverses a delay stage (Aerotech, Inc.), then is split and focused to 530μm. Due to the beam divergence, this diameter increases when the stage is fully forward, but up to no more than about 550μm. The pair crosses through the sample at 60°, with approximately 10mW in each line. Using the absorption detailed above, the concentrations of the protein samples are typically 100 mM. These concentrations and power densities (ranging from 1 to 10 mJ/cm^2) compare well with other work (Deak, Richard et al. 1994) (Cao, Chen et al. 1997) (Lim, Jackson et al. 1996) (Richard, Genberg et al. 1992). Another rough calculation estimates that any given pulse excites approximately 10% of the proteins (or dye molecules). This is a necessary condition to

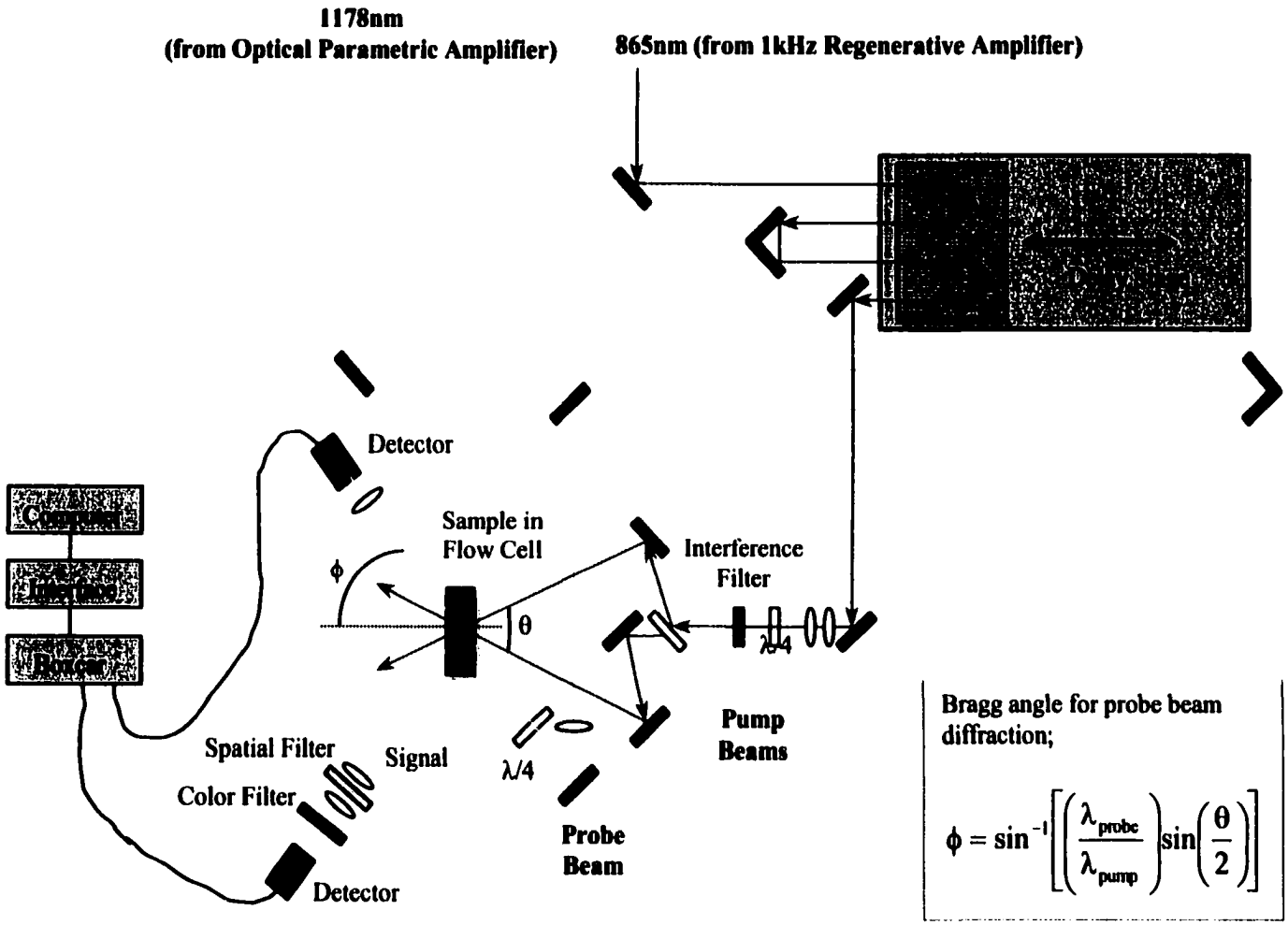

Figure IV-8: Transient grating experimental layout. The far red (865 nm) pulses are split, crossing again in the sample at θ. The near infrared probe is brought in at the Bragg angle, defined above. The flow cell actually sits at a small angle (~1°) to minimize reflections and scattered light. The flow cell and detector are also shown in the photograph of Figure 7.

ensure that there is a minimum of two photon excitations. A better way to verify the linearity of the experiment is to vary both the pump and probe power and measure the amplitude of the response. These power dependence experiments should show the signal to be a linear function of the excitation (these results are shown in the next chapter).

Recalling the grating equations of the previous chapter (shown as Equation IV-3 and Equation IV-4), a 60° crossing angle yields a grating wavelength of 865nm. The

$$\Lambda = \frac{\lambda_{ex}}{2\sin\theta/2} \qquad \textbf{(IV-3)}$$

$$\phi = \sin^{-1}\left[\left(\frac{\lambda_{probe}}{\lambda_{pump}}\right)\sin\left(\frac{\theta}{2}\right)\right] \qquad \textbf{(IV-4)}$$

probe line, approximately non-resonant at 1178nm, crosses the sample approximately 350μm in diameter, and roughly 10mW in power. The probe is typically set to a diameter of $1/\sqrt{2}$ of the pump, to allow some drift of the beams while minimizing the effect on the signal (Miller 1989). The diffraction angle (the incident and transmitted probe angle) may be found from equation IV-4 to be 43.0°. The properties of gratings in methanol and in water are summarized in Table IV-1, where v is the wave speed of sound and τ is the acoustic period. Finally, the polarization of both the pump and probe beams must be rotated to the vertical to improve grating efficiency. A pinhole is used to ensure rough beam alignment.

As even the pump beams are difficult to see, a doubling crystal is inserted at the crossing point. At equal time delays, the two pump beams will cross and a third beam will appear between the two. This blue beam (425nm), consists of photons that are each created by a photon from each red beam. This beam (the same as the autocorrelation

Solvent	ϕ (°)	Λ (nm)	v (m/s)	τ (ps)
Methanol	43.0 ± .1	865 ± 1	1120 ± 6	772 ± 5
Water	43.0 ± .1	865 ± 1	1497 ± 2	578 ± 2

Table IV-1: Summary of theoretical grating and acoustic properties in methanol and water (at roughly 25 °C). The diffraction angle (ϕ) and the grating wavelength (Λ), are the same, while the speed of sound (c) and the period (τ) vary. The protein and detergent solution of the experiments are assumed to have roughly similar properties as water.

beam), verifies the timing and overlap of the pumps. Next, the probe is unblocked. If the probe timing is correct, a bright green dot will appear between the pump and upconverted probe. When the Bragg condition is satisfied, a faint green dot will appear directly over the blue beam created by the pump beams. Finally, small red spots will appear just inside of each pump beam. Interestingly, these dots are due to parametric addition of a pump and probe photon.

Finally, the quartz cell is placed at the beam crossing, IR140 in methanol is injected into the flow and the signal from the photodiode (see below) is observed on an oscilloscope. Methanol has a large coefficient of thermal expansion, allowing relatively easy adjustments. The stage is generally moved to check the signal (the grating signal is zero at time zero). Without disturbing the system, the flow cell is flushed out and another sample may be inserted. Any residual trace of laser dye is insoluble in the buffer solution, and may be ignored. For the last protein experiments, this step was performed using LH_2 in βOG (which was also used as a reference compound – see the next chapter).

IV.C.5. *Detection and Collection:* Referring again to Figures IV-7 and IV-8, the diffracted beam is run through a spatial filter to remove background scatter (which is otherwise considerably larger than the signal). Any scattered 865nm is removed with an IR filter while a fast (3ns) germanium diode (Thorlabs, Inc., *DET3-GE*) detects the probe signal. Two 20dB high-speed video amplifiers (*CLC100*, Comlinear Corp.) intensify the grating signal. The undiffracted probe is monitored by a large area germanium diode (100ns, JG&G *J16 Series*). Both the signal and the reference are sent to a boxcar-gated integrator (Stanford Research Systems *Model 250*).

These outputs are interfaced to a Pentium computer (via an SRS *245* interface), and collected using LabVIEW 5.1 acquisition software. This program divides the signal by the reference, typically collects 1000 laser shots, and then advances the stepper motor (on the delay stage – Aerotech *E2100*) 10ps (typically) and repeats. After a total of 4 to 10ns have been traversed, the stage rewinds (while the laser is blocked), and the system is ready for another scan. Collecting a full scan (9ns) requires approximately 30 minutes. Each data point in a scan is retained and preserved using the datalog feature in LabVIEW. For further analysis, individual scans are averaged and transferred to a text file, where they may be subjugated to nonlinear fit routines.

IV.D. Literature Cited

Cao, Y. N., H. X. Chen, et al. (1997). "Generation of the Photoacoustic Effect through Heat Diffusion: Transient Grating Measaurements on Reverse Micelle Solutions." Journal of Physical Chemistry **101**: 3005-3011.

Deak, J., L. Richard, et al. (1994). Picosecond phase grating spectroscopy: Applications to bioenergetics and protein dynamics. Methods in Enzymology. New York, Academic Press: 322-360.

Goldsmith, J. O. and S. G. Boxer (1996). "Rapid isolation of bacterial photosynthetic reaction centers with an engineered poly-histidine tag." BBA-Bioenergetics **1276**(3): 171-175.

Gragson, D. E., D. S. Alavi, et al. (1995). "Tunable Picosecond infrared laser system based on parametric amplification in KTP with a Ti:sapphire Amplifier." Optics Letters **20**(19): 1991-1993.

Griffiths, M. and R. Y. Stanier (1956). "Some Mutational Changes in the Photosynthetic Pigment System of *Rhodopseudomonas spheroides*." Journal of General Microbiology **14**: 698-715.

Heller, B. A. and P. A. Loach (1990). "Isolation and characterization of a subunit form of the B875 light-harvesting complex from *Rhodobacter capsulatus*." Photochemistry and Photobiology **51**: 621-627.

Kirmaier, C., D. Gaul, et al. (1991). "Charge Separation in a Reaction Center Incorporating Bacteriochlorophyll for Photoactive Bacteriopheophytin." Science **251**: 922-927.

Krueger-Koplin, R. D. (1998). Structural Constraints and Assembly of Subunits from the Proximal Light-Harvesting Antenna of *Rhodobacter sphaeroides*. Department of Biochemistry and Molecular Biology. Fort Collins, Colorado State University: 198.

Krueger-Koplin, S. (1998). .

Lim, M. H., T. A. Jackson, et al. (1996). "Femtosecond Near-Ir Absorbance Study of Photoexcited Myoglobin: Dynamics of electronic and Thermal Relaxation." Journal of Physical Chemistry **100**(29): 12043-12051.

Miller, R. J. D. (1989). Picosecond transient thermal phase grating spectroscopy: Applications to the study of non-radiative energy relaxation. Time Resolved Spectroscopy. R. J. H. Clark and R. E. Hester, John Wiley and Sons Ltd.: 1.

Pace, C. N., F. Vajdos, et al. (1995). "How to Measure and Predict the Molar Coefficient of a Protein." Protein Science **4**: 2411-2423.

Reed, D. W. and R. K. Clayton (1968). "Isolation of a Reaction Center Fraction from Rhodopseudomonas spheroides." Biochemical and Biophysical Research Communications **30**(5): 471-475.

Reed, M. K., M. K. Steiner-Shepard, et al. (1994). "Widely tunable femtosecond optical parametric amplifier at 250 kHz with a Ti:sapphire regenerative amplifier." Optics Letters **19**(22): 1855.

Richard, L., L. Genberg, et al. (1992). "Picosecond Phase Grating Spectroscopy of Hemoglobin and Myoglobin: Energetics and Dynamics of Global Protein Motion." Biochemistry **31**: 10703-10715.

Sistrom, W. R. (1960). "A Requirement for Sodium in the Growth of *Rhodopseudomonas spheroides*." Journal of General Microbiology **22**: 778-785.

V. DATA AND ANALYSIS

To obtain the bulk properties and thermodynamic parameters the fits of Chapter III must be applied to the to the data of the experiments from Chapter IV. The first step in this process is to understand how the data is stored and manipulated, and to realize the limitations of the data. A consistent process for data reduction must then be determined, as the choice of fitting functions must be based upon not only upon the quality of the fit but upon reasonable physical models. Next, the data of the dye, light harvesting and reaction center data are reviewed. Power dependencies ensure that the experiment is in the linear response regime. Temperature dependence experiments on the proteins allow the volume and enthalpy changes to be separated. Finally, rates and relative signals are determined and compared to data from other experiments.

V.A. Data Reduction and Analysis

V.A.1. *Description and Averaging:* Individual data points consist of the diffracted laser pulse signal divided by the reference signal, which is then averaged over 1000 laser pulses (which is over one second for a 1kHz system). A full scan consists of 200 to 600 data points each separated in time by 20ps. Though an individual scan may be fairly noisy, it is possible to distinguish the rough amplitude and the presence of experimental artifacts.

These artifacts include the presence of 'ghost pulses' mentioned in the previous chapter, as well as a noticeable drifts in the amplitude. Though these pulses may be quite small (amplitudes of 1/1000 the main pulses), the excited state absorption of these biological samples may be unfortunately high (Hochstrasser 1998). These pulses surface in the scan as a narrow absorption peak at the time the pulse has leaked out of the Pockles

cell (which may occur at approximately 3.3, 6.6, and 9.9ns). This is often followed by an abrupt decrease in the signal, as these doubly excited states, often triplet excited states, are long lived and do not contribute substantially to the grating (Hochstrasser 1998). However, these pulses appear to consist of multiple wavelengths (800nm in addition to 864nm). Some pulses do contribute to the grating amplitude. Careful alignment of the amplifier cavity and the Pockels cell minimizes this problem, though the 9.9ns pulse never completely disappears.

The amplitude may drift further during a scan due to temperature fluctuations, laser drift and contamination of the flow cell surface. Contamination is due to the cell debris adhering to the inner surface of the glass, increasing the light scattering of the probe. If this effect is not noticeable (it may be larger than the signal) and consistent, then it will only affect the estimation of the thermal diffusion (see below). When the effect becomes large, the quartz flow cell may be replaced between runs (but not between scans).

Drift of the laser is another difficult problem. The laser shows shot-to-shot drift (in position) that the signal averaging should remedy. The sheer length of the delay stage affects the beam in two ways. Any deviation of the beam from the axis of the retro-reflectors will cause the pump beam to shift slightly as the stage moves. Furthermore, the changing distance traveled by the beam as the stage inches forward can become considerable for long scans. The stage moves approximately a meter, and the beam traverses this distance four times (see Figure IV-6). The divergence of the beam changes, making it difficult to preserve the focusing condition at the sample. Though the alignment may be finessed, the divergence change and a substantial 'ghost' pulse just

after 9ns impose an upper limit on the timing of the experiment at about 9ns. For this delay, the difference between the focus at the sample is only around 5%, as mentioned in Chapter IV.

Finally, temperature fluctuations in the room over the course of a day limit data collection. Although the Clark-MXR system components are provided with a temperature stabilization system, the stretcher, amplifier and compressor are mounted on large base plates that lie flat on the optical table. As the Argon ion and YAG laser heads and power supplies generate significant heat, some thermal expansion is unavoidable, though it can be mitigated by increasing the cold airflow into the room. However, a fluctuation in the room environment of a few degrees will cause a further expansion in the system that deviates the beam path and compromises the signal.

Nonetheless, if the condition of the beam is rigorously monitored, it is possible to get good signal-to-noise ratios. Figure V-1 documents the results of continuous improvements upon the system over a two-year period. The signal collected upon wild type reaction centers of *Rhodobacter sphaeroides* improves over the four slides by roughly 100, while the signal to noise improves by a similar amount. In addition to the corrections mentioned above, improvements in the system mentioned in the previous chapter were also carried out. Increases in sample concentration, careful compression of the pulses (to minimize filament instability in the OPA), over-pressuring the sample (to minimize bubbling) and changing the beam polarizations to vertical improved the data as well. The uncertainty in the data is still dominated by shot-to-shot noise, however.

V.A.2. *M-L Nonlinear Fits and Reduced* χ^2: Data sets with acceptable signal to noise are averaged together, and stored in text files. Averaged sets are fit using a

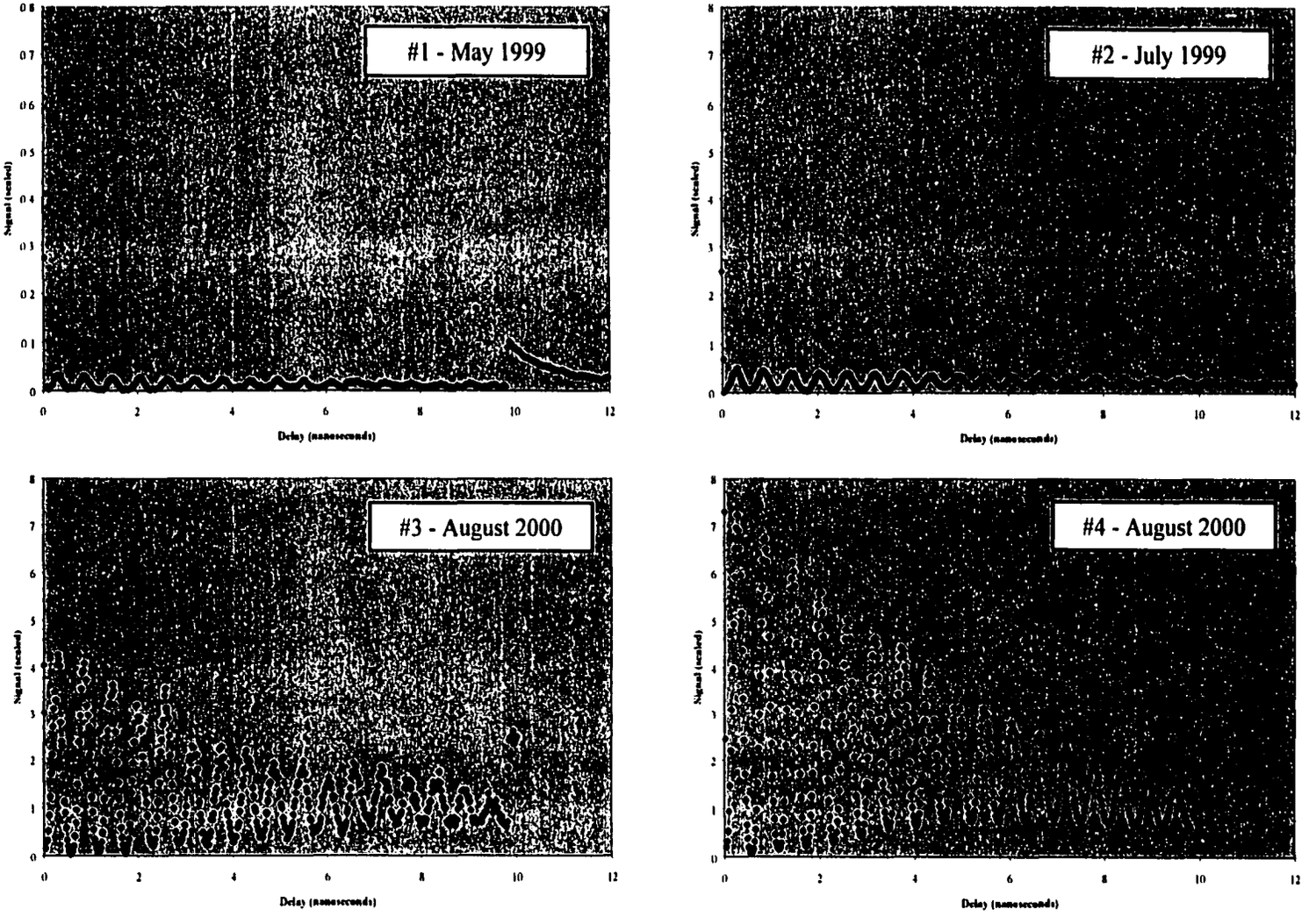

Figure V-1: Improvements in the signal to noise for transient grating data upon wild type reaction centers for *Rhodobacter sphaeroides*. All experiments were taken using the scheme depicted in Figure IV-8, though the laser's polarization for the first two experiemnts was horizontal, not vertical (the Pockels cell was replaced after that time). The scale on the first graph is 1/10 of the scale on the others. Note the effects of the 'ghost' pulses, appearing prominently near 10ns. All data was collected at approximately 15°C.

Marquardt-Levinson (Press, Teukolsky et al. 1992) (BEVINGTON) routine, fit to the functions derived in Chapter III. A variation on non-linear routines, the Marquardt-Levinson technique nonetheless varies a set of parameters in a fitting function, until the reduced mean squared deviation (known as the chi-squared, χ^2) is minimized. Giving the parameters new starting values, and verifying that fit ends up with the same final parameters and χ^2 checks the robustness of the fit. Realistically, the signal to noise of the data is never high enough to permit fitting using all of the parameters of the equations of Chapter III. Consequently, several parameters are held constant, while only a few key variables are allowed. The choice of these variables depends upon the experiment.

One parameter that is never allowed to vary is the baseline, or the zero of the vertical axis. This zero-signal line is very difficult to ascertain during an experiment, due to an extreme amount of light scattering. To determine its exact location would require placing a parameter in the fitting routine that is allowed to vary. Unfortunately this causes the fitting routine to lose its robustness. Making slight alterations from fit to fit, and finding the minimum χ^2, uncovers the baseline. This is a reasonable approach that works well for systems with a rapid (delta function) heat release and a relatively slow thermal diffusion, so the first minimum of the acoustic wave is essentially at the baseline. This baseline was also observed by collecting data upon pigment-less solvents just prior to or after an experiment. Baselines were also observed before the zero time delay, when the probe beam arrived before the pump beams. These observed baselines compare well with the values obtained though the fitted data.

V.A.3. *Excited State Absorption:* Though the probe beam is non resonant, some probe absorption occurs. It is important to consider the effect of the excited state upon the

amplitude and the phase (dispersive) gratings as a function of the wavelength (Morais and Zimmt 1995) (Nelson, Casalengo et al. 1982) (Deak, Richard et al. 1994). Equations V-1, V-2 and V-3 are borrowed from Chapter III. Recall that these equations are found by assuming a damped harmonic oscillator model for excited state dispersion. The

$$\Delta n_{ex} = -\frac{N_1}{N_o}\frac{2(\omega_o - \omega)}{\gamma_o}k_o(\omega) \qquad \textbf{(V - 1)}$$

$$\Delta k_{ex} = -\frac{N_1}{N_o}k_o(\omega) \qquad \textbf{(V - 2)}$$

$$k_o(\omega) = \frac{N_o f_o \gamma_o}{2n_o\omega_o}\frac{1}{4(\omega_o - \omega)^2 + \gamma_o^2} \qquad \textbf{(V - 3)}$$

resonance is centered about the frequency ω_0, N_1 is the number density of excited molecules and N_o and n_o are the unperturbed density and index of refraction, respectively. Finally, γ_o is FWHM transition linewidth and f_o is the absorption strength (the absorption cross section summed over the various oscillators) (Nelson, Casalengo et al. 1982). Note that the absorption change maximizes at resonance while the dispersion change maximizes on either side (recall that the efficiency follows the change squared in III-3). Furthermore, the change in the absorption may generate an acoustic wave, though the amplitude appears small relative to the exponential decay, especially near resonance (Fayer 1986).

Additionally, given the high peak powers, some additional three-wave mixing is inevitable at zero delay (which was visible in Chapter IV). This absorption is then re-radiated at the probe wavelength and shows up at early times in the grating signal. Rather than fit these events with the complicated models above, they are fit directly with the phenomenological model of Equations V–4 and V–5 (Deak, Richard et al. 1994; Cao,

$$\Delta k_{ex} = X_k e^{-K_k t} \qquad \text{(V - 4)}$$

$$\Delta n_{ex} = X_n e^{-K_n t} \qquad \text{(V - 5)}$$

Chen et al. 1997). These excited state terms affect the absorption (Δk_{ex}) and the index of refraction (Δn_{ex}). Different coefficients and rate constants are necessary as the dominant effect due to pump/probe overlap is shown in Δn_{ex}, while the subsequent absorption and decay of the excited state is evident in Δk_{ex}. Due to the limited number of data points in this early part of the scan and the superposition of the larger grating signal, these parameters are not determined precisely. Furthermore, this approach does not address possible simultaneous combinations of excited state terms. However, these equations do allow the fit to account approximately for these effects, allowing the acoustic oscillations to be determined. Finally, due to the size of the coherence spike, reasonable minimum χ^2 may only be found with these terms.

V.A.4. *Error Budgets:* The detector noise (around 5mV for a typical 1000 shot data point) and the integrator's maximum linear voltage (around a few volts) determine the best practical signal to noise (S/N) possible. Averaging scans together may improve this number, but only as the square root of the number of scans (Press, Teukolsky et al. 1992), (Bevington 1969). The limitations described above usually demand that only a few (three or four) scans may be averaged for the results that follow. The detector noise, OPA fluctuations, sample fluctuations, and A/D noise (and its lowest resolution of 2mV) conspire to keep the noise at a minimum of around 2mV, though this minimum varies sinusoidally with the acoustic wave. Amplifying the signal electronically also amplifies the noise. Using smoothing techniques will inevitably destroy the higher frequency elements of the data (Press, Teukolsky et al. 1992). The signal may still be amplified by

increasing the laser power, but only as long as the signal remains linear. This maximum signal to noise (around 100) determines how many parameters may be extracted from the fits, as well as defining a reasonable standard error in the data.

As the data is fit, the routines yield standard errors in the parameters as well as the reduced χ^2. The fit usually assumes that the standard errors in the individual parameters are linearly independent. Likewise, the assumption that the individual standard deviations in the data are equal is only an approximation. To compensate, the first derivative (of each parameter) is examined and the standard deviation is adjusted accordingly. This is accomplished by examining the effect of variations in individual parameters upon the reduced χ^2, through the fitting routines and Monte Carlo simulations (Press, Teukolsky et al. 1992) (Bevington 1969).

V.B. Laser Dyes and Power Dependence

V.B.1. *Properties and Preparation of IR125 & IR140:* The expense and difficulty of preparing considerable amounts of protein prohibit its everyday use. To diagnose the experiment and perfect alignment, laser dyes dissolved in methanol were substituted for biological samples. The symmetric structure of the indocyanine dyes IR125 (also known as indocyanine green) and IR140 are shown in Figure V-2. Both dyes have been used extensively as fluorescence sources in biological tissues (Fox, Brookes et al. 1957), laser dyes, and as saturable absorbers. Chosen for their fast, non-radiative decay, the fluorescence yields are typically around 5% (Soper and Mattingly 1994). With an absorption maximum a bit further into the near infra-red, it seemed that IR140 would make a stronger non-radiative source than IR125 for testing the grating apparatus.

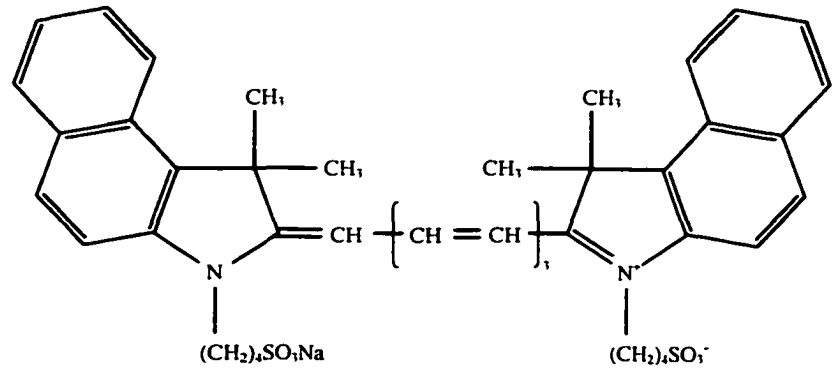

IR 125 – Indocyanine Green

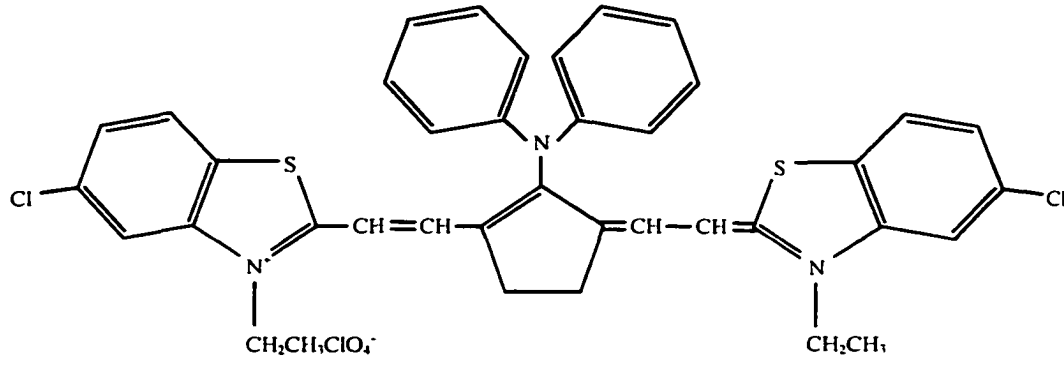

IR 140

Figure V-2: Tricarbocyanine laser dyes used in grating experiments. IR125 (MW = 774.97), also known as indocynaine green, is deep green when dissolved in methanol, while IR140 (MW = 779.20) is clear blue. Both structures exhibit a high degree of symmetry. π stacking between the benzene rings contributes to the strong tendency to aggregate.

Both dyes are mesophilic, and experiments have been performed on them in water as well as βOG. However, the results are complicated by their strong tendency to aggregate, especially in high concentrations (> 1mM). Ultimately, methanol was chosen as a solvent to avoid the formation of aggregates. This had the additional effect of moving the absorption peaks further into the red. The peak of IR125 was observed at 782nm while IR140 maximized at 800nm. Both dyes were prepared to approximately 1mM concentrations, and stored in darkened containers for at least a day, to allow the solution to fully mix. Both dyes have a long shelf life if kept out of the light, though some decreases in optical absorption seem apparent after a few months. While carrying out the grating experiments, the room was kept dark.

V.B.2. *Grating Experiments for IR125 & IR140 in Methanol:* Figures V-3 and V-4 detail the results of full grating experiments (and appropriate spectral scans) for IR125 and IR140, respectively. In these experiments, the electrostrictive change is assumed small compared to the thermal component. As mentioned in the previous section, it is not possible to fit all of the desired parameters to the data.

The amplitude and rates of the excited state contribution in particular are held fixed, and other parameters allowed to vary. These fixed parameters may be slightly adjusted by hand, and the fit performed again. Once χ^2 is reasonably minimized (and the fitted parameters are only weakly affected by changes in the fixed terms), this routine stops. These transient absorption terms are due a variety of solvent and solute contributions (Gumy, Nicolet et al. 1999). Interestingly, data collected upon methanol only show no grating signal, yet still reveal these excited state terms. Thus these very

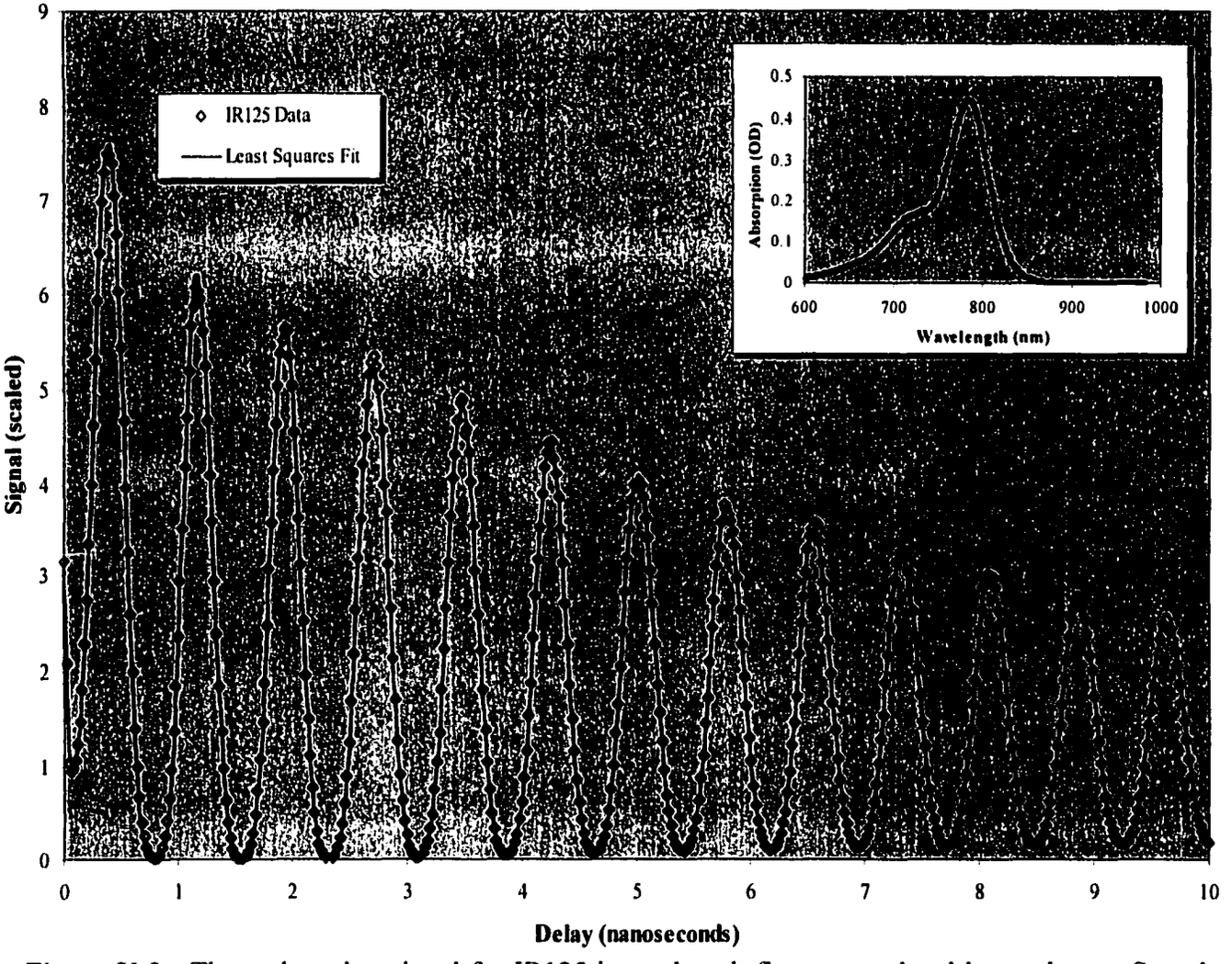

Figure V-3: Thermal grating signal for IR125 in methanol, fit to a two level heat release. Sample temperature was approximately 21°C. Inset shows wavelength scan on a sample diluted 1000 to 1 in a 1 cm cell. Fitted parameters obtained from this set are shown in Table V-1.

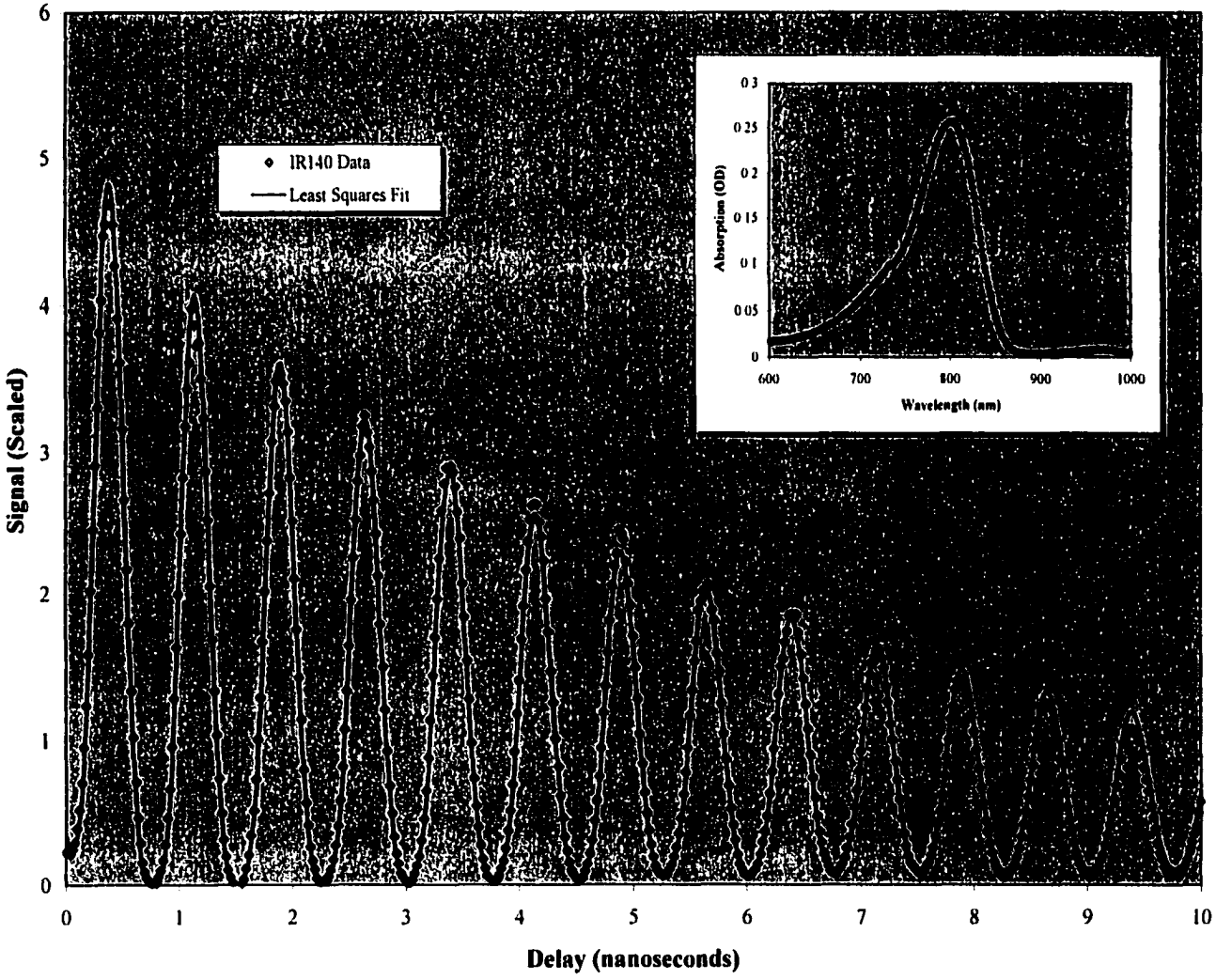

Figure V-4: Transient grating signal for IR140 in methanol, fit to a two level heat release. Sample temperature was approximately 21°C. Inset displays a section of a wavelength scan on the sample, diluted 1000 to 1, in a 1cm cell. Parameters obtained from this fit are displayed in Table V-1.

early events (tens of picoseconds) appear to be dominated by coherence effects between the pump beams and the probe.

Analyzed data on these compounds yields the properties shown in Table V-1. All parameters were found directly from the fit, with the exception of the speed of sound, which was calculated using the grating wavelength of 864nm. Non-radiative lifetimes are compared with previous experiments (Soper and Mattingly 1994) (Mohanty, Palit et al. 2000). While the signal amplitude and decay rate is determined by the dye, the other parameters are functions of the grating angle and the solvent. The bulk parameters are compared to a variety of other references (Gray 1972) (Kaye and Laby 1995) (Grigoriev and Meilikhov 1997). The references used for methanol's properties were the most recent that could be found, while the uncertainties, if not explicitly defined, were inferred by comparing across sources. These uncertainties are typically in the last significant digit, with the exception of the acoustic attenuation, which is typically only accurate to 20-30% (GREY). The thermal decay rate for IR125 (as measured at 750nm) varies over different solvents (Soper and Mattingly 1994) and appears dependent upon concentration (Philip, Penzkofer et al. 1996). Less is known about IR140, though some femtosecond transient grating experiments have been performed, up to 830nm (Gumy, Nicolet et al. 1999). The dominant exponential is shown in both cases. The fitted parameters show a curious deviation from both theory and the previous experiment.

V.B.3. *Concentration Dependence:* The discrepancy between theory and experiment appears especially great for the thermal diffusivity, though the uncertainty may be higher than it seems. Yet the speed of sound data for IR140 is also unexpected, as the uncertainty of this parameter should be low. The high concentrations would seem

Sample	OD (@ 864nm)	A (–)	τ (ps)	f (GHz)	v_0 (m/s)	h (10^{-9} m^2/s)	α (10^{-15} s^2/m)
IR125 (MeOH)	4.5 ± .5	89.2 ± 1.5	19 ± 5	1.300 ± .002	1123 ± 3	509 ± 10	45 ± 5
ref	-	-	200 ± 20	-	1123	100	33
IR140 (MeOH)	12.3 ± .5	77.7 ± 1.5	18 ± 5	1.333 ± .002	1151 ± 3	894 ± 10	55 ± 5
ref	-	-	.26 ± .01	-	1123	100	33

Table V-1: Parameters resulting from least squares fit to data for laser dyes in methanol. The experiments were performed at 21 degrees Celsius. The optical density was measured separately, in a standard 1 cm cell, with varying dilutions that are corrected here. Both samples were prepared to concentrations of less than 1mM. As mentioned in the text, the fit directly determines the angular frequency (ω) and thermal diffusivity (h) and acoustic attenuation (α) coefficients. The thermal diffusivity and the acoustic attenuation are converted to the conventional units above (α is divided by the acoustic frequency squared). The speed of sound was calculated using the grating wavelength, which was found from Chapter IV to be 864nm. The references were found as described in the text.

to be the cause. Figure V-5 and Table V-2 give the results for an experiment where the concentration of IR140 was varied. At the lower dye concentrations, the correct value for the speed of sound is recovered and the thermal diffusivity approaches the value for IR125. However, a discrepancy still remains with the theoretical value. It is possible that even the low concentrations are high enough to affect this rate, although a presence of even a small amount of dye may be necessary to affect this parameter.

Additionally, the amplitude of the IR140 signal increases with the concentration. As the dye concentration increases from .3 to 1mM, the absorption strengthens by the same ratio. The signal amplitude increases as well, though not quite as much as expected. However, the efficiency expression of Equation III-3 includes the effect of absorption outside the grating volume. The increased absorption of a more concentrated sample yields a smaller observed thermal signal. Recall that the measured optical densities of Table V-2 are for a standard 1cm cell, and that the sample region is less than 500μm.

V.B.4. *Power Dependence:* Verifying the dependence of the signal versus the input power is an important experiment that determines the linearity of the system. The amplitude of the signal may be fit as a function of either the probe or pump intensity. The signal height should be linear with the probe power. However, the pump should affects the intensity in quadrature (linear with amplitude), as the intensity is affected by the square of the heat deposited in the sample. As power dependence these scans are short, only the amplitude and the decay rates were fit. The other parameters were borrowed from the long scan fits above. The relatively high values of the reduced χ^2 indicate that this is only an approximate approach (though the choice of function may in

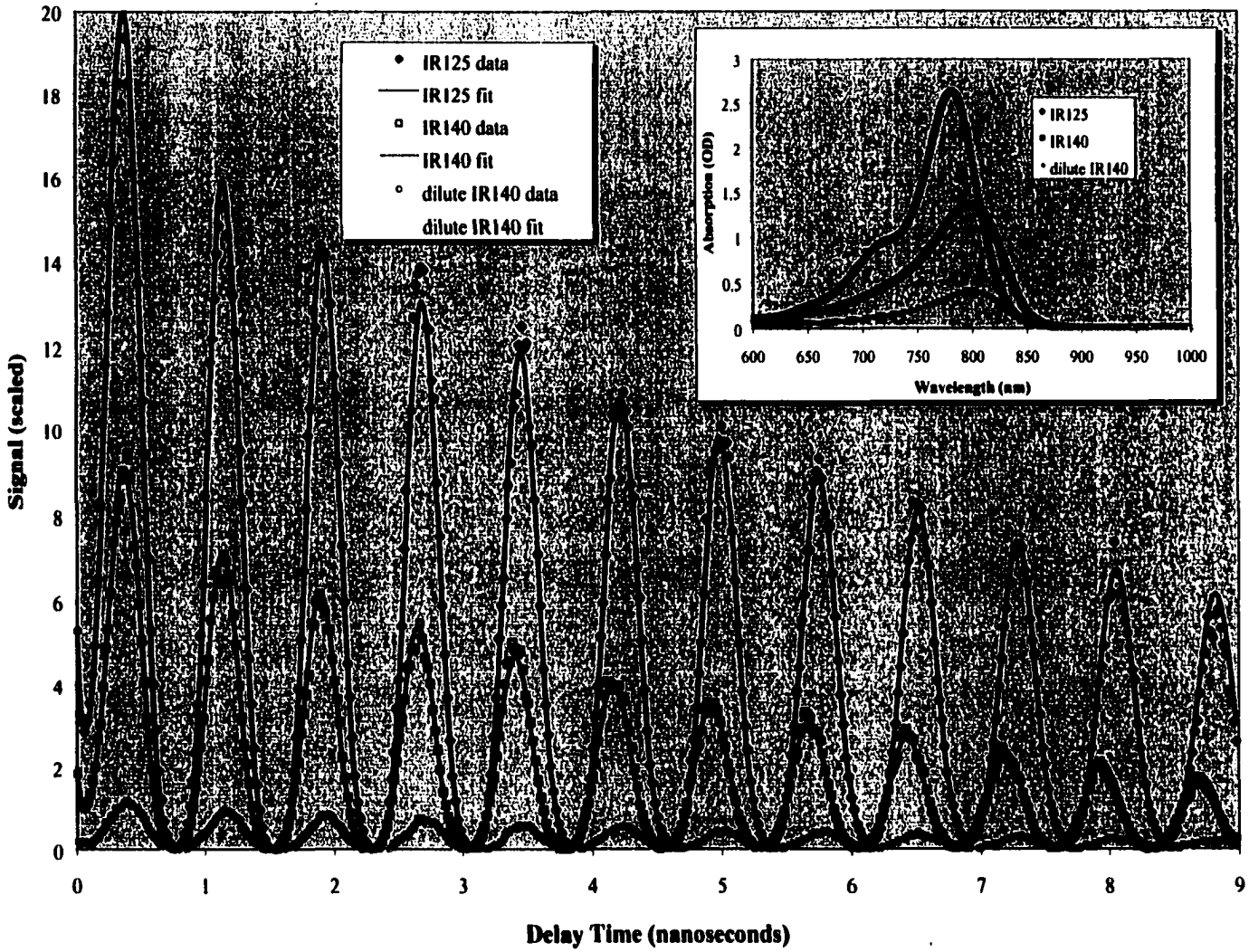

Figure V-5: Thermal grating signals for IR125 and IR140 in methanol, fit to a two level heat release. The IR125 was prepared to a concentration of 1mM, while the IR140 was prepared to 1mM and .3mM. Sample temperature was fixed at 15°C. Inset shows wavelength scan on a sample, diluted 100 to 1 in a 1 cm cell. Fitted parameters obtained from this set are shown in Table V-2.

Sample	OD (@ 864nm)	A ( )	τ (ps)	f (GHz)	v_0 (m/s)	h (10^{-6} m^2/s)	α (10^{-15} s^2/m)
IR125 (1mM MeOH)	2.4 ± .1	144.0 ± 1.5	< 5	1.304 ± .002	1126 ± 3	.741 ± .010	47 ± 5
ref	-	-	200	-	1123 ± 1	.100 ± .001	33 ± 10
IR140 (1mM MeOH)	5.6 ± .1	102.7 ± 1.5	22 ± 8	1.323 ± .002	1143 ± 3	1.301 ± .010	58 ± 5
IR140 (.3mM MeOH)	1.7 ± .1	36.0 ± 1.0	< 5	1.302 ± .002	1125 ± 3	.847 ± .010	77 ± 5
ref	-	-	.26	-	1123 ± 1	.100 ± .001	33 ± 10

Table V-2: Concentration effects for parameters resulting from least squares fit to data for laser dyes in methanol. The experiments were performed at 15 degrees Celsius. The optical density was measured separately, in a standard 1 cm cell, with varying dilutions that are corrected here. As mentioned in the text, the fit directly determines the angular frequency (ω) and thermal diffusivity (h) and acoustic attenuation (α) coefficients. The thermal diffusivity and the acoustic attenuation are converted to the conventional units above. The speed of sound was calculated using the grating wavelength, which was found from Chapter IV to be 864nm. The references were found as described in the text.

fact be in error). However, as long as these parameters are used consistently, their exact values do not affect the results significantly.

For IR125, the results appear to conform to theory, as the signal intensity appears linear with the probe. The amplitude appears linear with the pump power, as expected. The results are shown in Figure V-6. The signal is normalized with respect to the largest signal. The power dependence experiment for IR140, the results of which follow in Figure V-7, yields an unexpected result. While the intensity dependence due to the probe is linear, the dependence due to the pump is to the fourth power, and not quadratic. So the dependence upon the amplitude, and thus the heat release is quadratic. This appears to occur for relatively high and low concentrations of the dye. The reason for this dependence is unclear, though perhaps exciting the molecule is a two-photon process (Mukamel 1995).

V.B.5. *Three Level Models and Fits:* Typical kinetic experiments generally reveal multiple exponential decays. Some of the incident energy is fluoresced, while much is lost though non-radiative channels. The ratio of magnitude of these two, the quantum yield, is generally small for these dyes (about 5%) (Soper and Mattingly 1994). Yet another source of energy dissipation is through solvation. Picosecond measurements generally detect fluorescence rates and yields, while femtosecond measurements aim for solvation rates. While limited fluorescence data is known for both IR125 (Soper and Mattingly 1994) and IR140 (Mohanty, Palit et al. 2000), solvation data is also known for IR140 (Gumy, Nicolet et al. 1999).

The transient grating data for IR125 and IR140 from above may be fit to a three-level model of Chapter III. The results are shown in Figures V-8 and V-9. In this

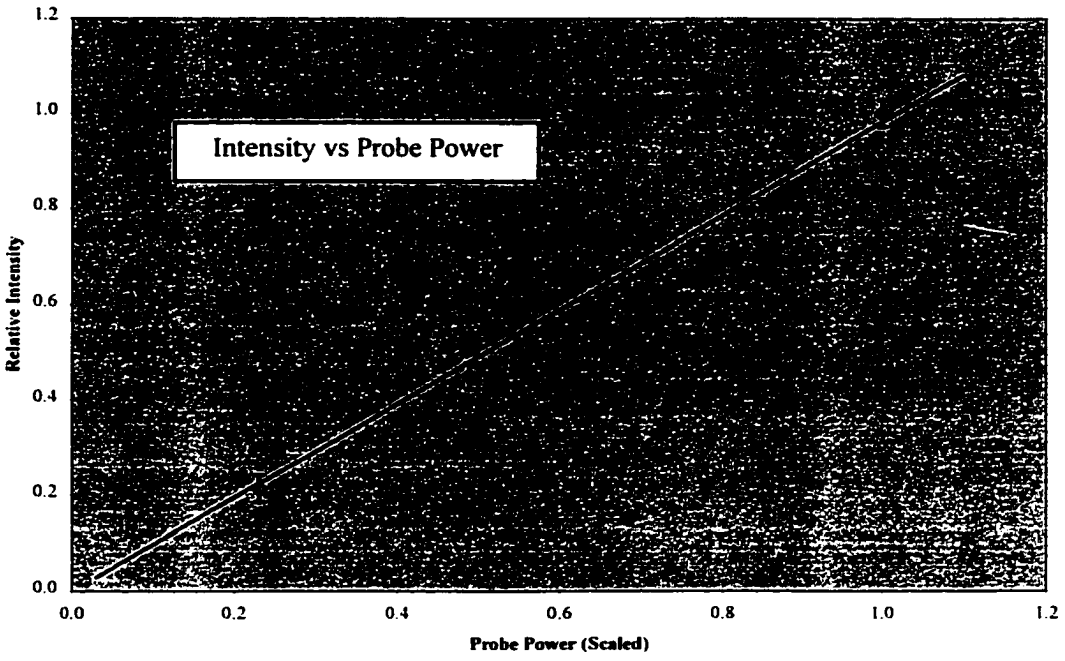

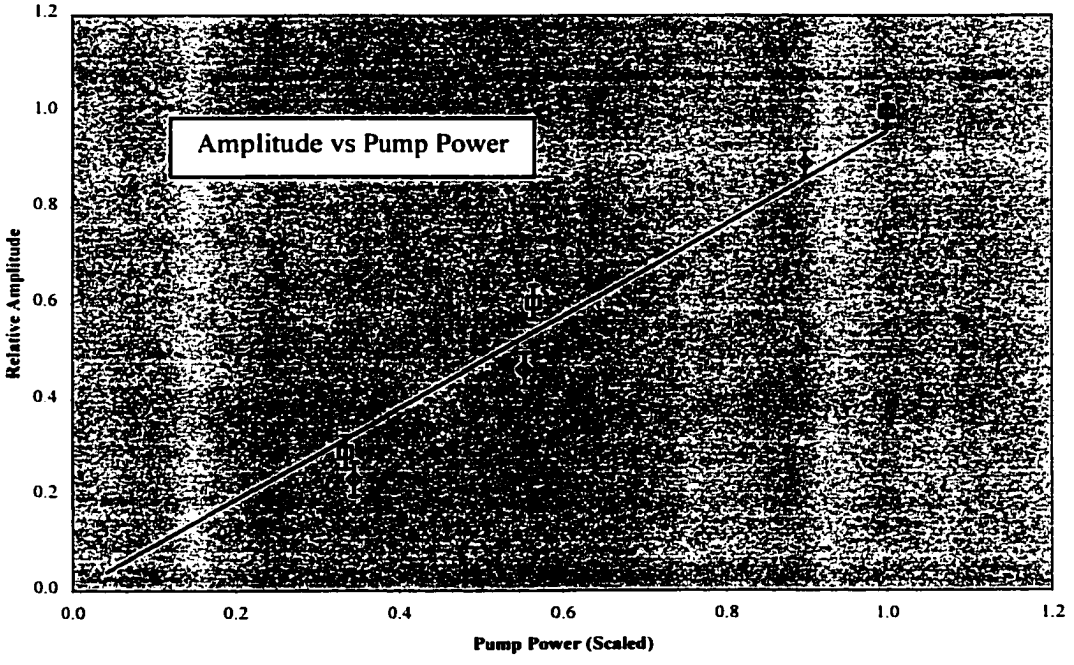

Figure V-6: Signal dependence upon the pump and probe beam power for IR125 in methanol. Linear regression confirms that the intensity and the probe power are linearly related, with a slope of 1.03 ± .04. The pump and the amplitude are linear as well, with a slope of 1.11 ± .07.

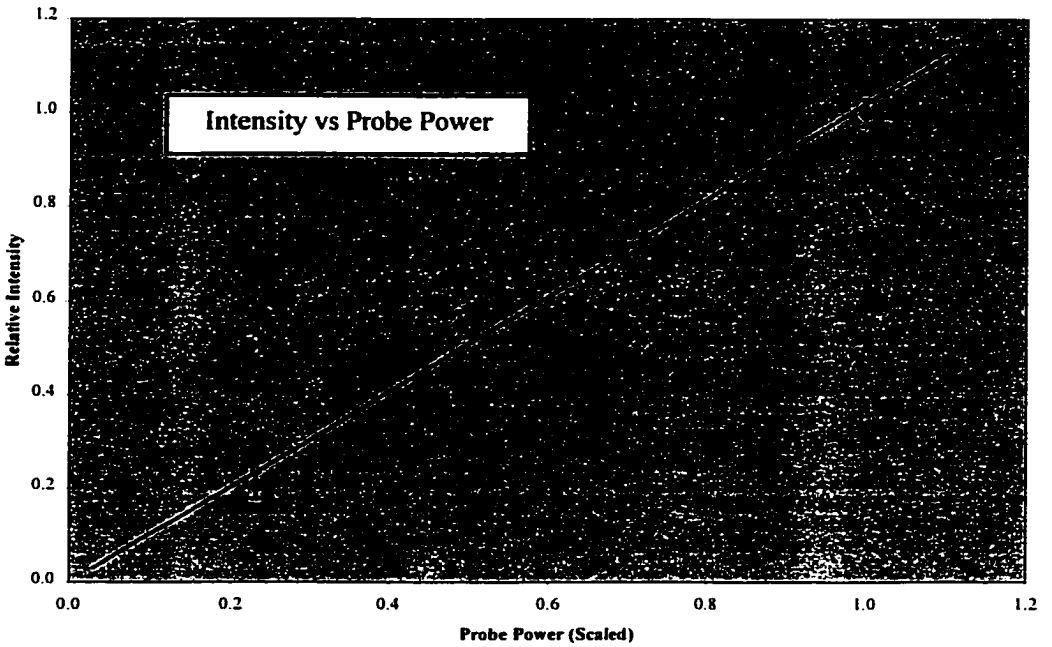

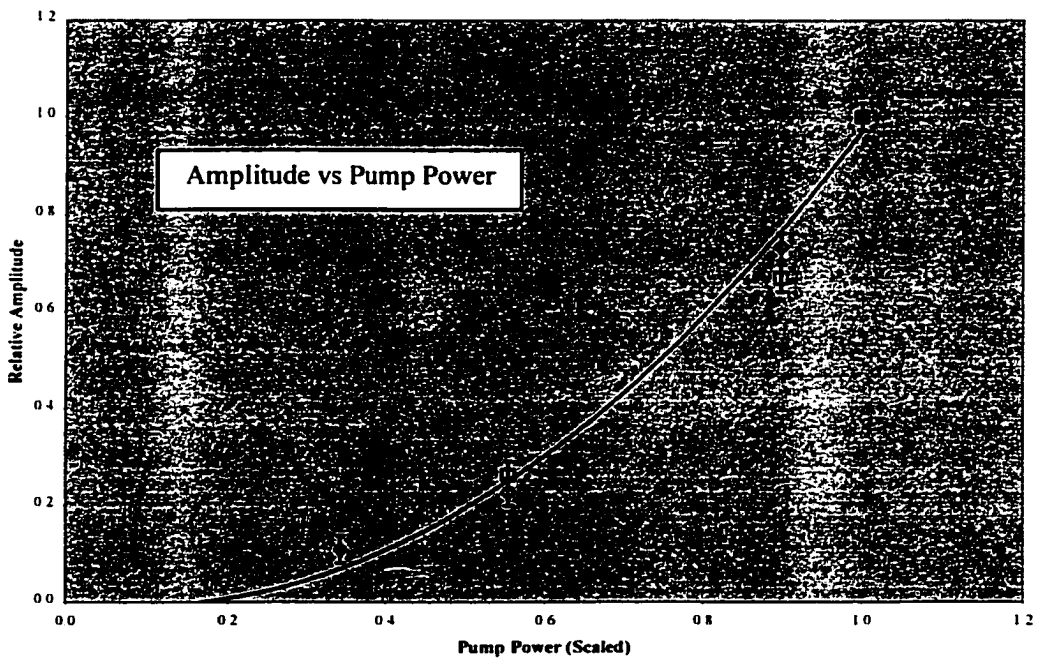

Figure V-7: Signal dependence upon the pump and probe beam power for IR140 in methanol. Regression analysis determines the signal intensity to be linear with probe power, with a slope of 1.01 ± .11. However, the pump power affects the amplitude very nearly quadratically, to a power of 2.08 ± .11.

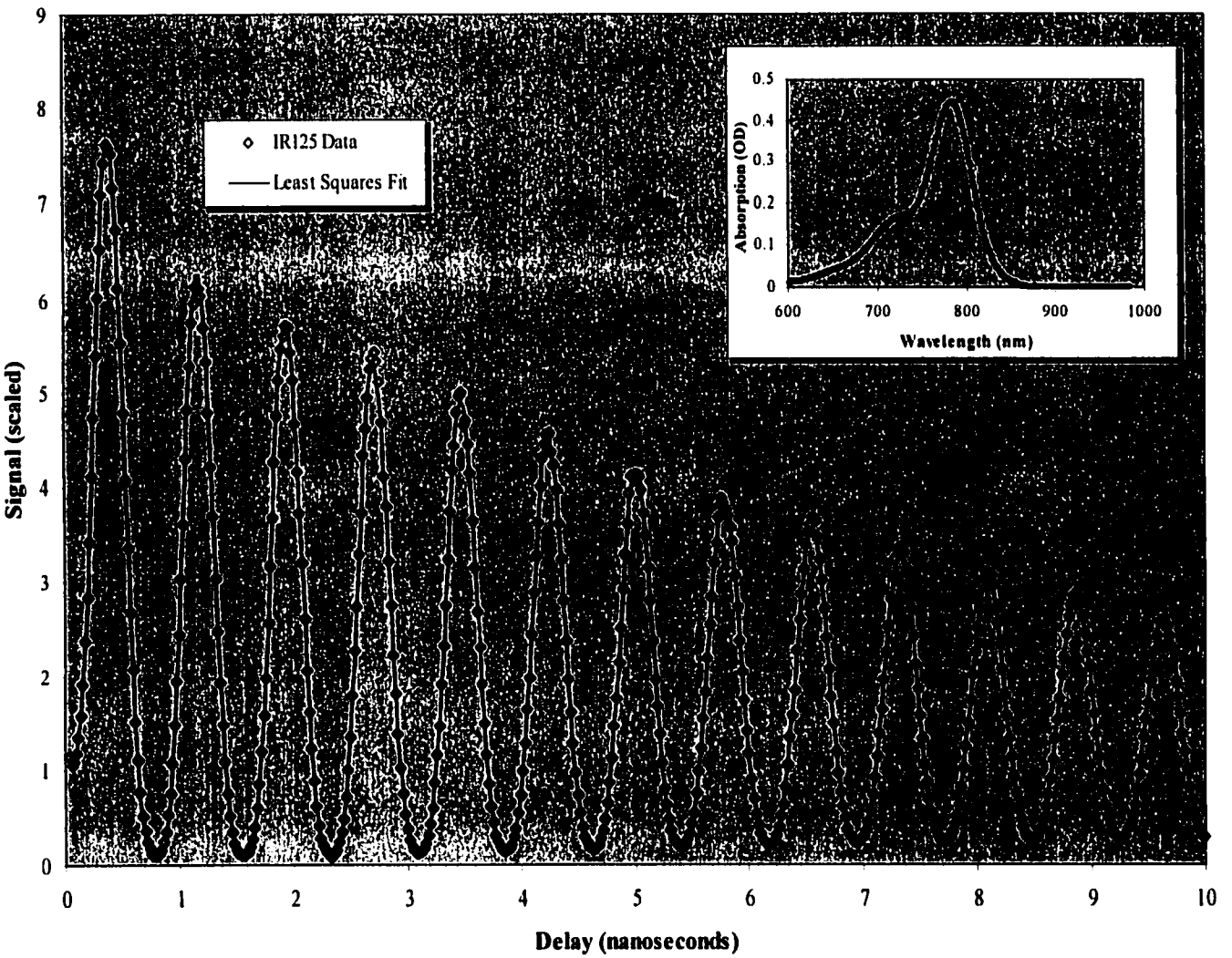

Figure V-8: Thermal grating signal for IR125 in methanol, fit to a three level heat release. Sample temperature was approximately 15°C. Inset shows wavelength scan on a sample diluted 1000 to 1 in a 1 cm cell. Fitted parameters obtained from this set are shown in Table V-3.

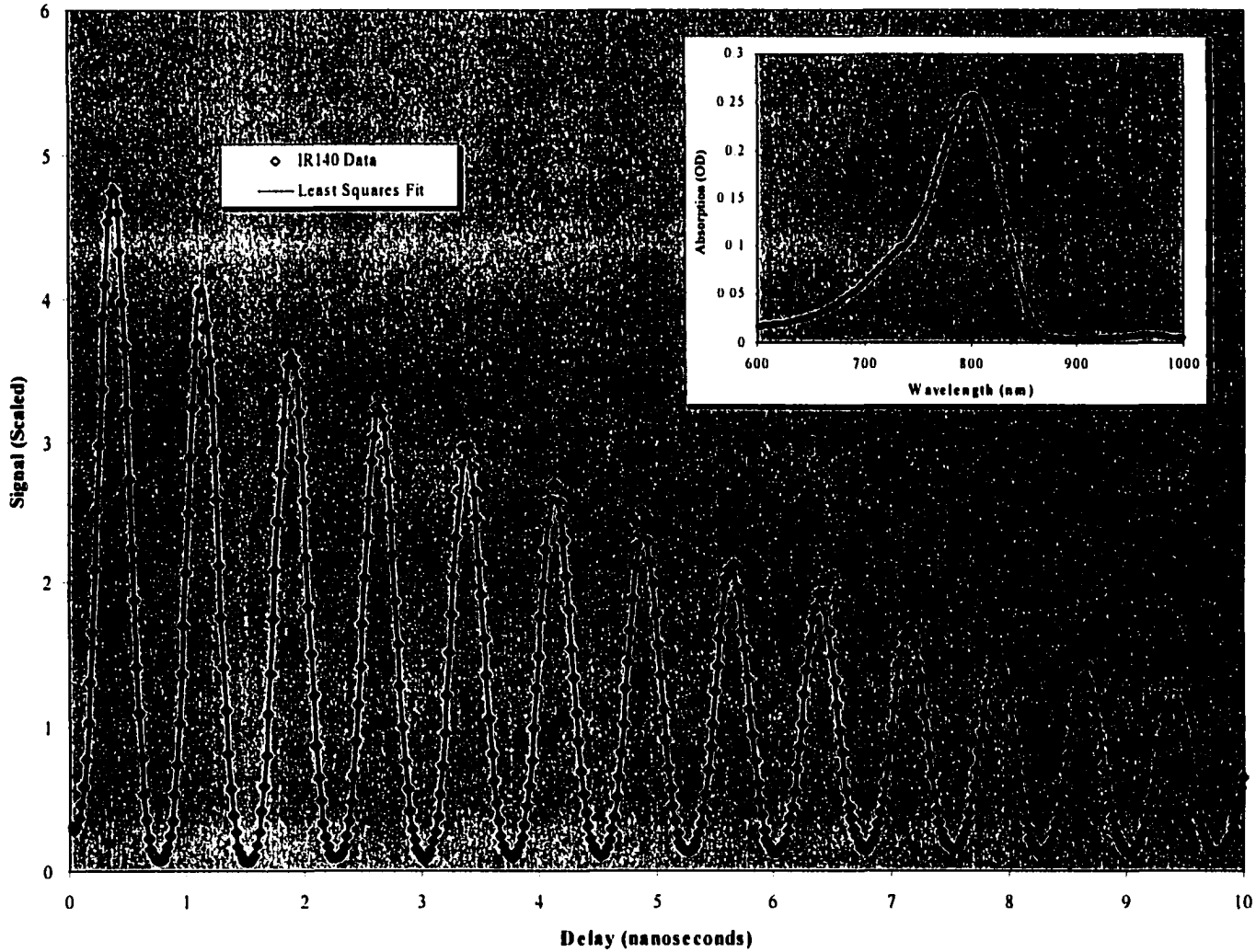

Firgure V-9: Transient grating signal for IR140 in methanol, fit to a three level heat release. Sample temperature was approximately 15°C. Inset displays a section of a wavelength scan on the sample, diluted 1000 to 1, in a 1cm cell. Parameters obtained from this fit are displayed in Table V-3.

Sample	OD (@ 864nm)	A_1 ( )	τ_1 (ps)	A_0 ( )	τ_0 (ps)
IR125 (MeOH)	4.5 ± .5	74 ± 5	3 ± 1	94 ± 2	130 ± 20
ref	-	-	-	-	500
IR140 (MeOH)	12.3 ± .5	62 ± 2	< 1	83 ± 2	143 ± 20
ref	-	-	.26	-	330

Table V-3: Parameters resulting from three level (two parameter) least squares fit to data for laser dyes in methanol. The experiments were performed at 15 degrees Celsius. The optical density was measured separately, in a standard 1 cm cell, with a dilution of 1000 to 1, which is corrected here. The bulk properties were lifted from Table V-1, as described in the text. The references were found as described in the text.

instance, the exponentials are not independent. The times shown in Table V-3 are sequential. The first time (τ_1) should correspond to a fast, thermal release of energy, due to some vibrational relaxation. The second (τ_0) should correspond to some fraction of energy that exists in a longer-lived state. The amplitude of the second rate is in fact the overall amplitude of thermal energy release. The amount of relative energy released from the intermediate upon its return to the ground state should be simply $A_0 - A_1$. Note that this does not determine the quantum yield, as we can not detect the light lost as fluorescence.

V.C. Light Harvesting Center

V.C.1. *Characteristics of LH_2 in βOG:* The characteristics of energy delocalization and transfer in the peripheral light harvesting center and βOG were discussed in Chapter I. Light harvesting proteins in βOG was prepared according to IV.B.5., allocated in 200 ODV samples and chilled for use at 4 degrees. Grating experiments upon LH2 were expected to show a single, rapid thermal release minus only a small fluorescence yield. Typical grating signals versus temperature are shown in Figure V-10. Recall that the amplitude of the thermal signal is directly proportional to the volume expansion coefficient of water. Interestingly, this signal, which was believed to be purely thermal, does not vanish at the zero expansion point of water.

V.C.2. *Simple Two Level Fits:* Nonlinear fits were made as with the laser dyes, by keeping the excited state terms fixed and allowing the thermal grating parameters to vary. The excited state terms are fit phenomenologically, using the equations mentioned earlier (V-4 and V-5) and are not presented. Simple two level nonlinear fits were made and are shown explicitly on the same sample at 15°C and 4°C in Figure V-11. While the

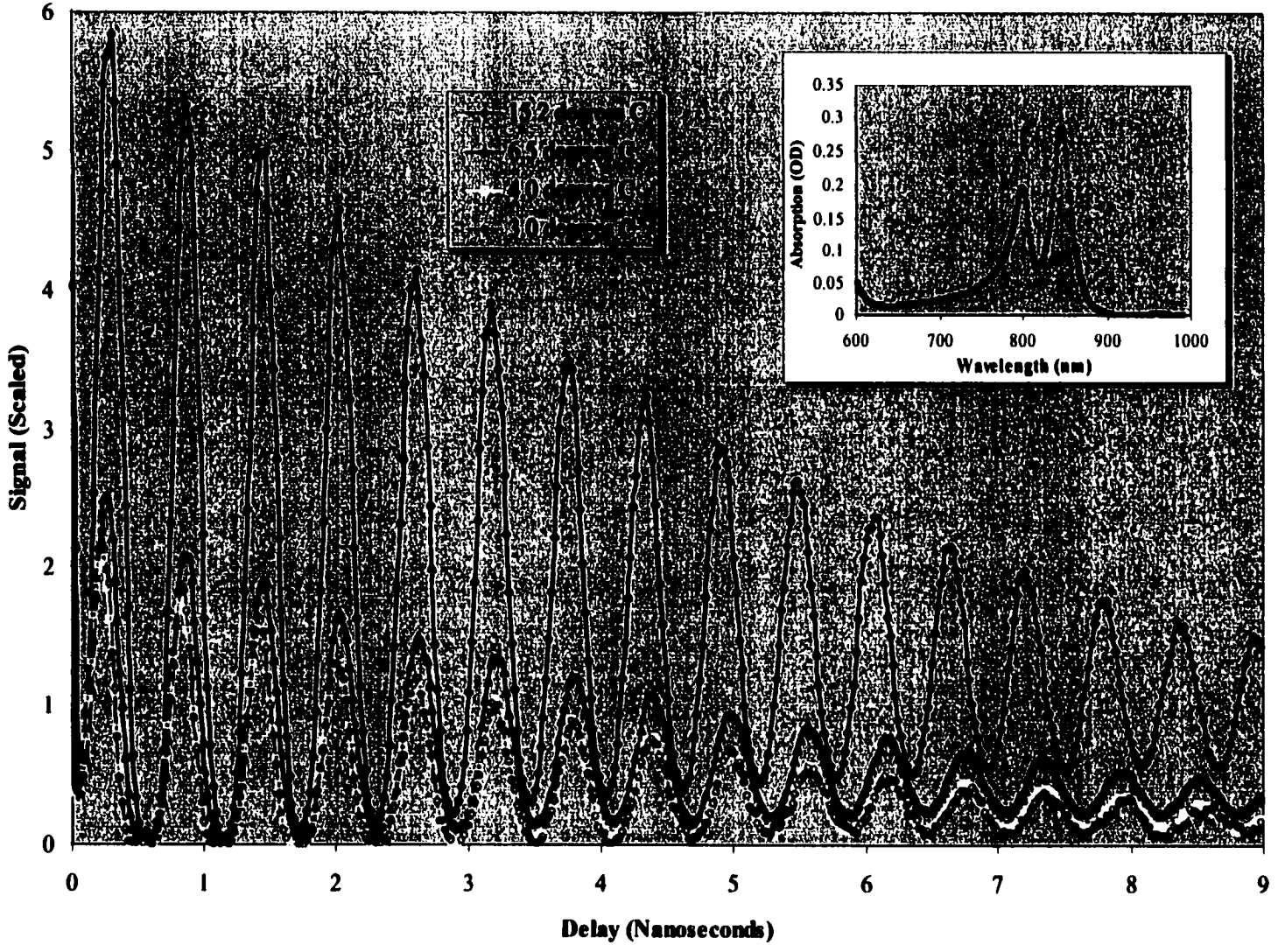

Figure V-10: Raw tremperature dependence of the transient grating signal for the peripheral light harvesting center in βOG. The thermal signal vanished at the zero expansion point of water, leaving a conformational volume change. Inset displays a section of a wavelength scan on the sample, diluted 200 to 1, in a 1cm cell. Parameters obtained from this fit are displayed in Table V-4.

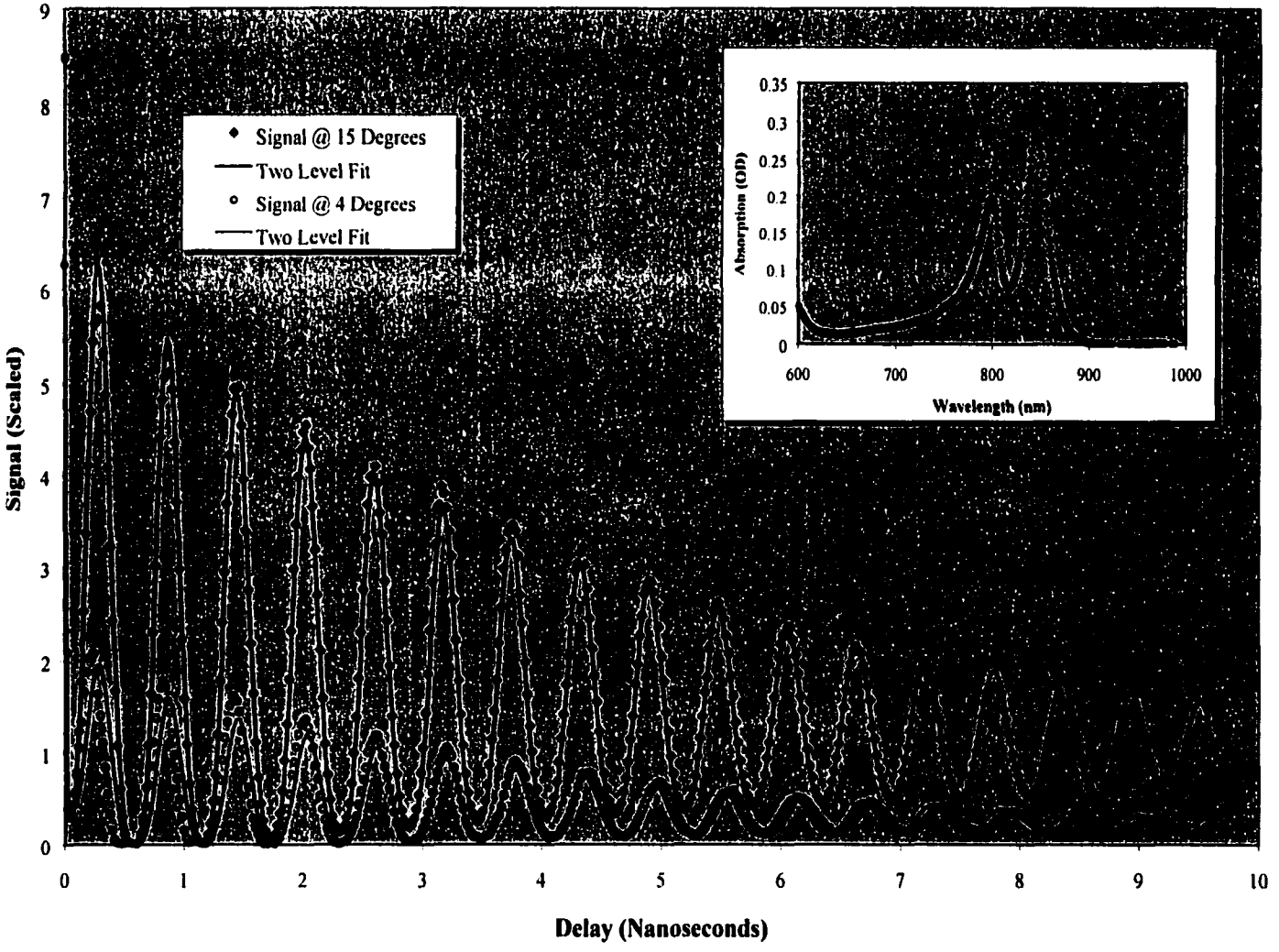

Figure V-11: Transient grating signal for LH2, fit to a two level heat release. Only the data at 15 and 4 degrees are shown for clarity. While the data at 15 degrees is well fit, the low temperature data shows a strong shift in time that cannot be fit to the simple model. Parameters obtained from these fits, as well as for those at 6 and 3 degrees, are displayed in Table V-4.

Temperature (°C)	**A** ( )	**τ** (ps)	**f** (GHz)	**v_o** (m/s)	**h** (10^{-9} m^2/s)	**α** (10^{-15} s^2/m)
15.2 ± .2	1.00 ±.07	<.5	1.735 ± .002	1499 ± 2	473 ± 100	39 ± 2
ref (water)	-	-	-	1467	140	28
6.5 ± .2	.62 ± .05	< .5	1.713 ± .012	1480 ± 12	575 ± 100	52 ± 5
ref (water)	-	-	-	1433	136	42
4.0 ± .2	.54 ± .05	< .5	1.721 ± .012	1487 ± 12	813 ± 100	48 ± 5
ref (water)	-		-	1422	134	45
2.8 ± .2	.56 ± .05	< .5	1.723 ± .012	1488 ± 12	940 ± 100	51 ± 10
ref (water)	-	-	-	1416	131	48

Table V-4: Temperature variation for LH_2 in βOG, fit to a two level model of decay. The samples were prepared to an optical density of approximately 18 at 864nm in a standard 1cm cell. Signal amplitude was normalized to the signal at 15 degrees. The parameters are determined directly by the fit are the amplitude (A), the relaxation time (t) and the acoustic frequency (f). The speed of sound (v_o), the thermal diffusivity (h) and the acoustic attenuation (a) are represented in conventional units, using the grating wavelength of 864nm. References were found as mentioned in the text and are considered to the last digit, unless otherwise noted.

fit to the higher temperature is acceptable, a clear discrepancy appears at the lower temperature. Parameters from the fits for all four temperatures are summarized in Table V-4. These numbers do not appear to conform to expected values, or to trend in the right direction with temperature.

V.C.3. *Electrostrictive Gratings:* A signal was captured on a sample of only βOG, yielding no apparent thermal grating, but the coherence signal at early times. This signal is shown on Figure V-12, alongside a sample with LH2 in the buffer. Within uncertainty, the protein-less signal appears to be zero, while the LH2 signal appears to fit normally. However, adding an electrostricitive term (also known as a stimulated Brillouin grating from Chapter III as III-9 and III-10) improves the reduced χ^2 of *both* fits by a full order of magnitude. Both fits show the same amplitude of electrostrictive signal. It is important to remember that these terms sum and square in the overall efficiency expression (Equation III-3). Even when the electrostricive term is small relative to the thermal signal, the cross terms between the two may be somewhat large.

V.C.4. *Temperature Dependence:* Figure V-13 shows the dramatic correction this term has upon the fits at low temperature. The two level thermal fit shows an improvement of a factor of at least ten in the reduced χ^2. Note the shift of the first peak to earlier time relative to the fit without electrostriction. Only a term proportional to the sine function, as in the stimulated Brillouin expression, may simultaneously shift the peak and produce the small intermediate peaks. This was also demonstrated in Figure III-2.

Now the data of Figure V-10 may be reconsidered. The resulting parameters are shown on TableV-5. Comparisons to other experiments are made (Sundstrom, Pullerits et al. 1999), while the bulk properties of water are noted (Gray 1972) (Grigoriev and

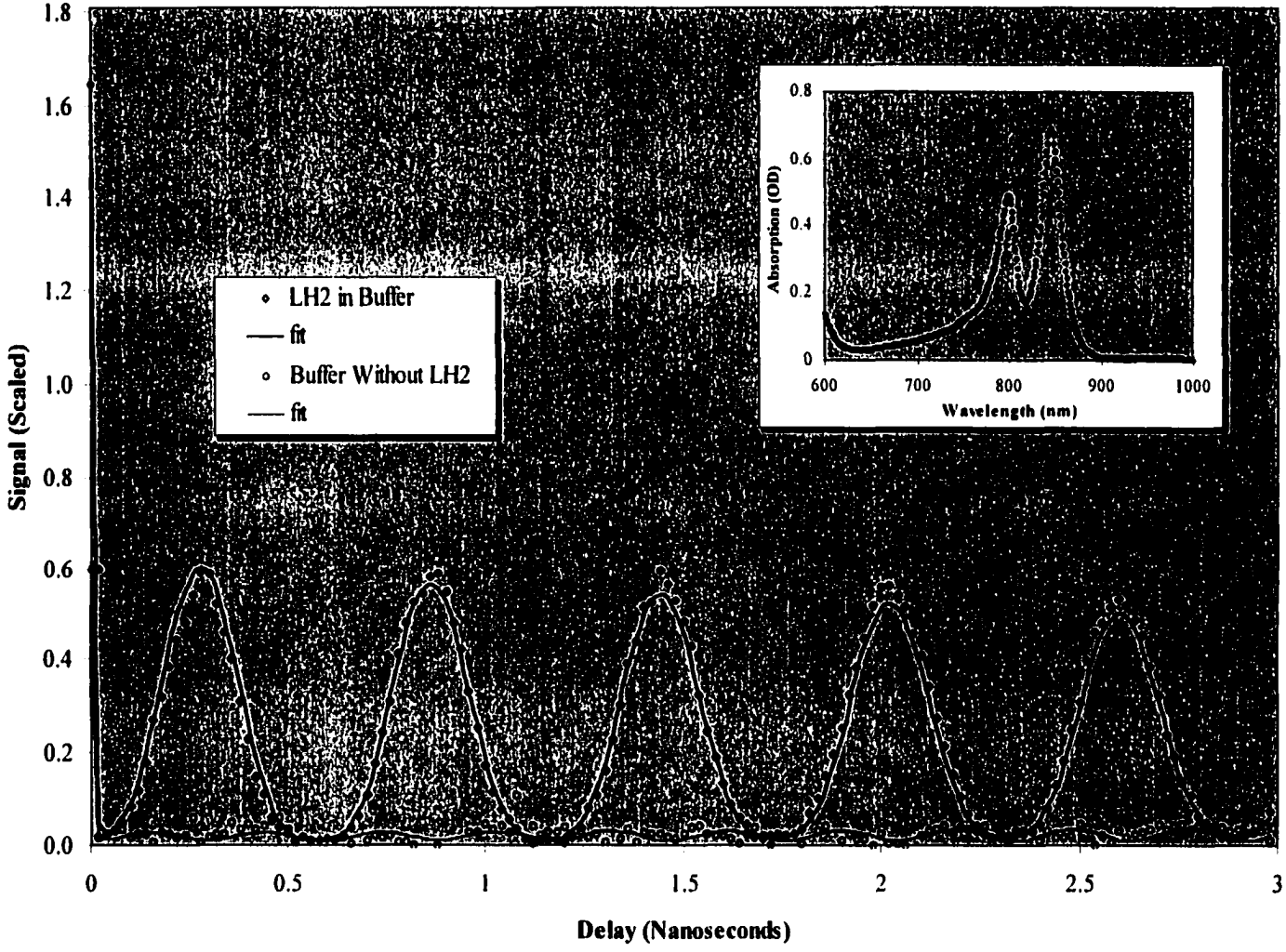

Figure V-12: Transient grating signal for IR140 in methanol, fit to a two level heat release, including the effect of a stimulated Brillouin grating. While the signal appears to vanish without the protein, as small purely electrostrictive signal does remain. Sample temperature was approximately 15°C. Inset displays a section of a wavelength scan on the sample, diluted 400 to 1, in a 1cm cell. The apparent offset in the graphs is actually an artifact due to Excel.

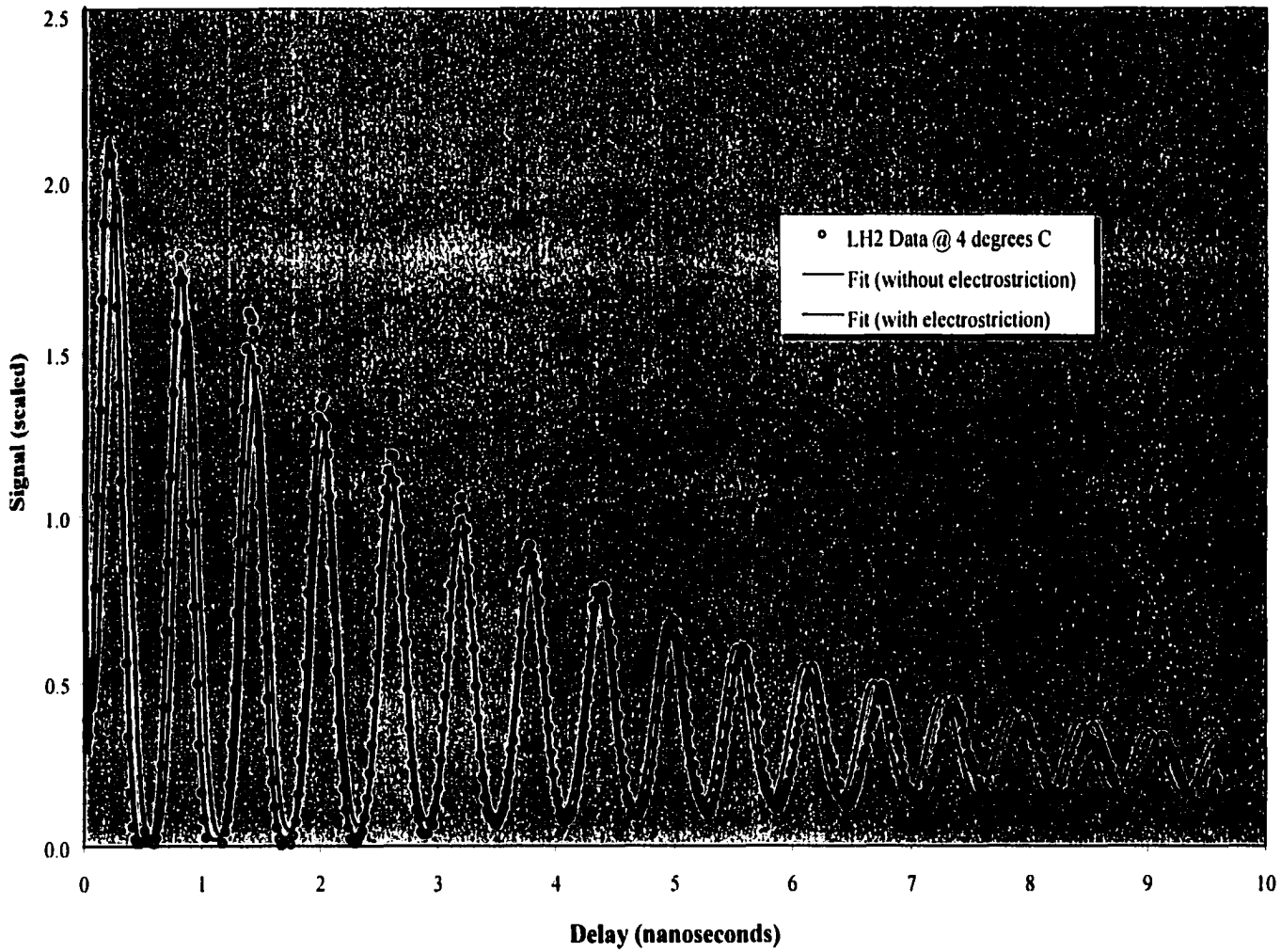

Figure V-13: The grating signal for LH2 at 4°C, fit to a two level heat release. The addition of an electrostrictive term (also referred to as a stimulated Brillouin term) described in the text corrects the discrepancy in the acoustic frequency. Note the shift toward forward time in the data and the correct fit for the first few nanoseconds.

Temperature (°C)	**A** ( )	**E** ( )	**τ** (ps)	**f** (GHz)	**v_0** (m/s)	**h** (10^{-9} m^2/s)	**α** (10^{-15} s^2/m)
15.2 ± .2	1.00 ± .01	.54 ± .02	34 ± 3	1.732 ± .005	1496 ± 5	592 ± 100	36 ± 2
ref (water)	-	-	-	-	1467	140	28
6.5 ± .2	.57 ± .01	.54 ± .02	30 ± 3	1.695 ± .005	1464 ± 5	637 ± 100	51 ± 5
ref (water)	-	-	-	-	1433	136	42
4.0 ± .2	.45 ± .01	.55 ± .02	29 ± 3	1.685 ± .005	1456 ± 5	783 ± 100	51 ± 5
ref (water)	-	-	-	-	1422	134	45
3.2 ± .2	.45 ± .01	.69 ± .02	16 ± 3	1.683 ± .005	1454 ± 5	852 ± 100	53 ± 5
ref (water)	-	-	-	-	1416	131	48

Table V-5: Temperature variation for LH_2 in βOG, fit to a two level model of decay which includes stimulated Brillouin grating. The sample is the same as displayed in Figure V-10 and analyzed in Table V-4. Signal amplitude was normalized to the signal at 15 degrees. The thermal component of the signal vanishes at the zero expansion point, revealing only the volume grating. The Brillouin amplitude (E) persists and appears to increase with decreasing temperature.

Meilikhov 1997). Though a signal still appears at the zero expansion point, the other parameters appear reasonable and trend in the appropriate direction with temperature. The rate of thermal diffusion appears unusually large, and increases through the zero expansion point of water. This effect is dealt with below. Interestingly, the electrostrictive amplitude appears to increase slightly with decreasing temperature.

To verify the amplitude dependence with temperature, several data sets were collected, fitting the full scans at various temperatures, as detailed above. The temperature dependence of the grating amplitude is displayed graphically in Figure V-14. The solid dots represent the starting temperatures and the open dots subsequent data sets. Despite the difficulty of maintaining a steady temperature near zero degrees, and the variability due to electrostriction (which varies with the laser power and alignment from day to day), the data seems repeatable. Though the change appears quadratic and seems to minimize at four degrees, the amplitude does not decay to zero, as almost 1/2 of the amplitude remains. This is attributed to a volume change within the sample, due to conformational changes and electrostriction. Such a change should be constant over the range of temperatures of these experiments, and must offset the thermal signal.

V.C.5. *Power Dependence:* Given the large sample concentrations and the relatively large laser intensities, it is important to directly determine the linearity of the system for these proteins. The data was analyzed as with the laser dyes, with the short (3ns) scans being fit with signal amplitude and a decay constant, according to the two level thermal models. Fits were performed with and without electrostricive contributions. The bulk properties of water were carried over from the long scans of the previous section. Figure V-15 details those results, ignoring electrostrictive components, which

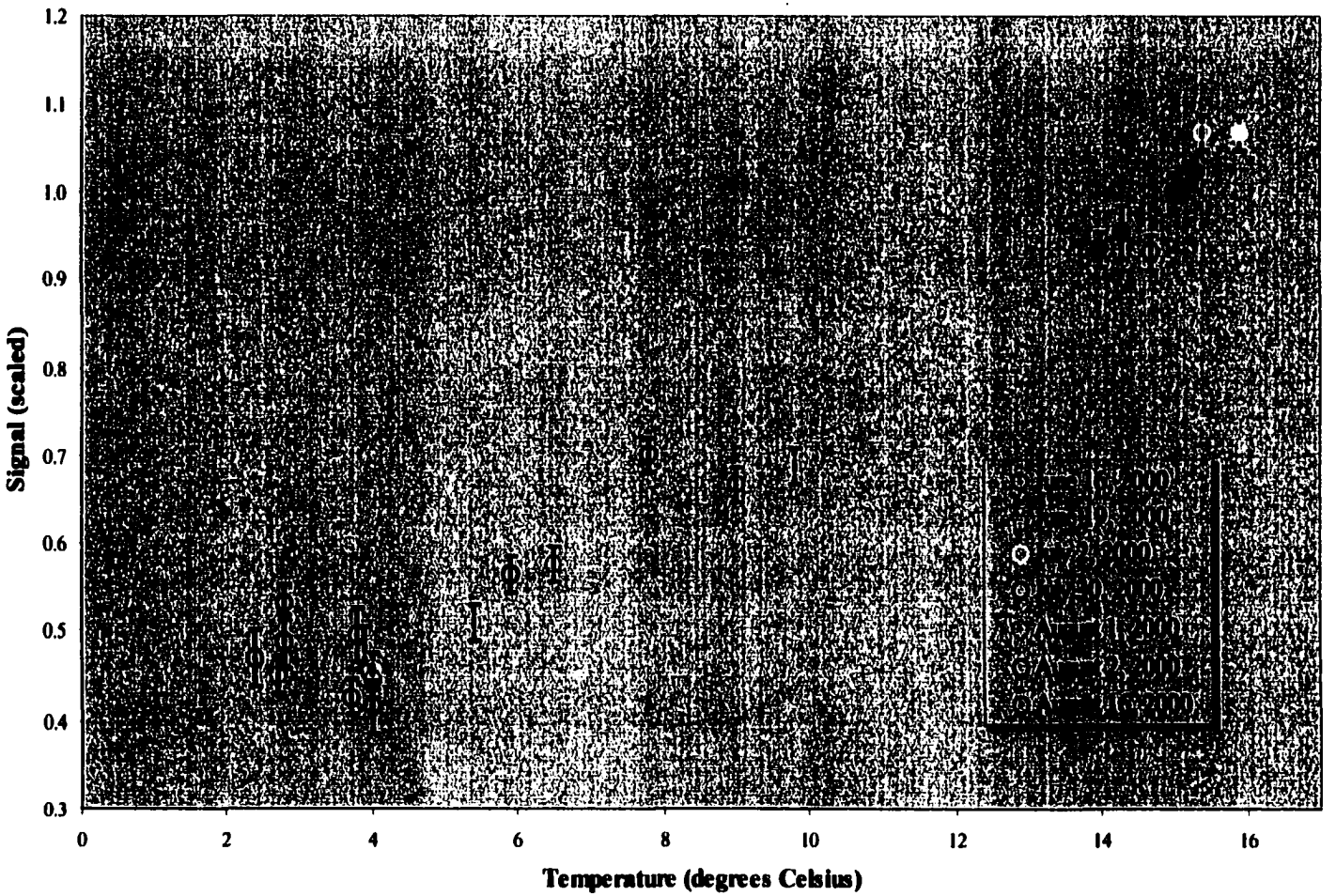

Figure V-14: The amplitude (A) of the transient grating signal decreases with the coefficient of thermal expansion (β), according to the familiar, if rough, parabolic shape. However, the overall signal does not vanish at the zero expansion point of water, indicating a conformational volume change that offsets the curve. All temperatures are normalized to the signal at 15°C.

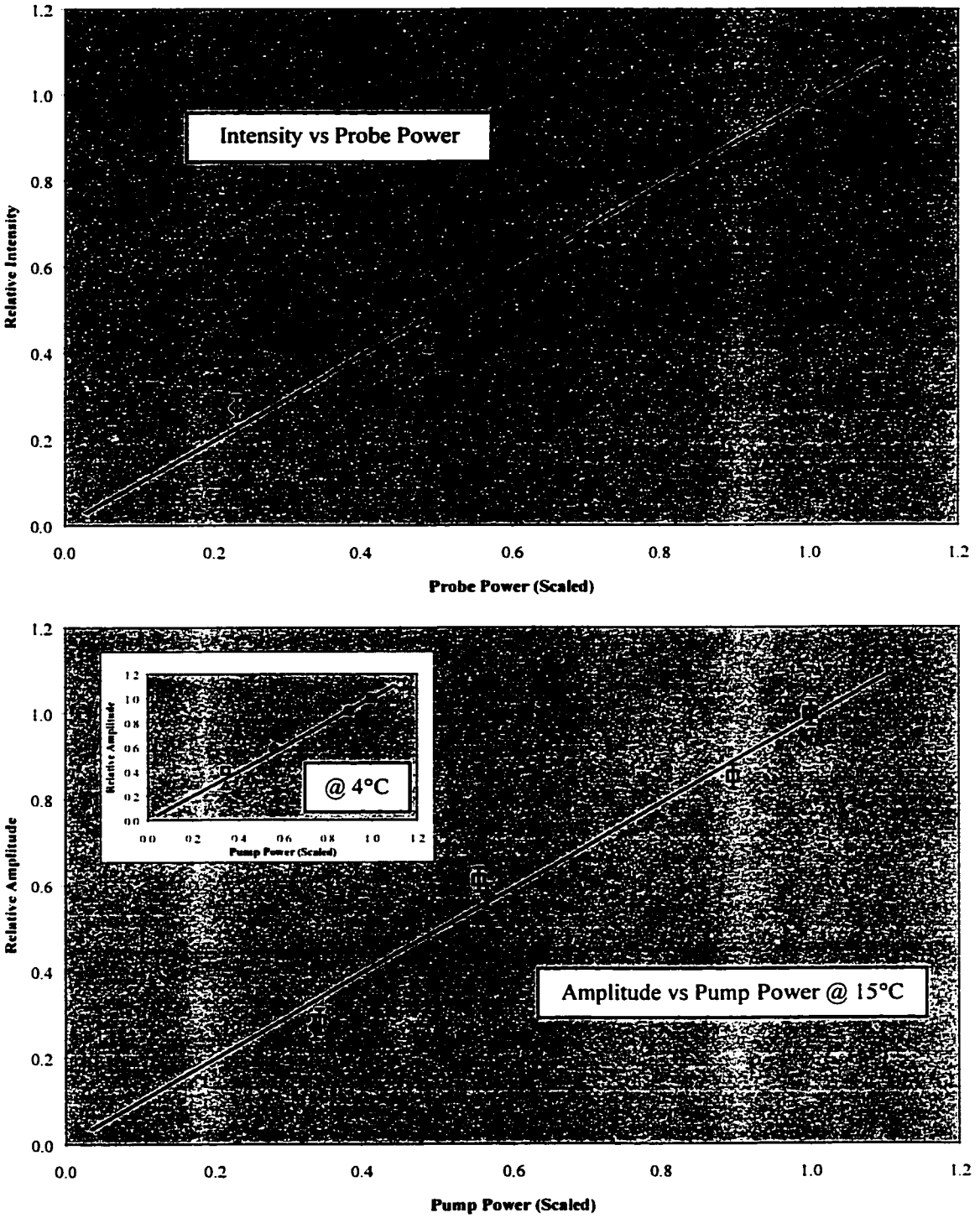

Figure V-15: Signal dependence upon the pump and probe power for the peripheral light harvesting complex in βOG. Probe power exerts a linear influence on the amplitude intensity, with a slope of .97 ± .12 (found using linear regression). Likewise, the amplitude of the signal varies with the normalized pump power as 1.04 ± .06 at 15 degrees Celsius and .98 ± .06 at 4 degrees (inset).

proved small for these timescales. The intensity appears to be linear with the probe power, while the amplitude appears linear with the pump power. Furthermore, the signal is linear within uncertainties for both the thermal and the non-thermal parts of the signal. These concentrations (mM) are typical of all of the following protein experiments.

V.C.6. *Thermal Analysis of the Light Harvesting Center:* Grating formation for the light-harvesting complex is impulsive (fast), while the relaxation is dominantly thermal. The experiments of section V.C.4. demonstrate reasonable results for both the amplitudes of the heat release versus temperature and the bulk properties of water. However, though much of the remaining discrepancies in the bulk parameters may be attributed to the presence of the large concentrations of the proteins, the presence of a signal at the zero expansion point requires further attention. In particular, a two level thermal grating is an inappropriate model for such a signal. The three level volume grating of section III.C.4. must be used instead. Furthermore, to consistently fit the full scans at 15° requires that the three level model of thermal decay (III.C.3) be supplemented by subtracting the appropriate volume correction.

The analysis begins with two level thermal fits to the 15° data. Next, the three level volume grating is applied to the zero expansion point data, yielding a signal amplitude and time scales for intermediate formation and decay. The next iteration in the analysis returns to the signal at 15°, fitting it to a full three level thermal decay. The parameters from the volume grating and the bulk properties from the two level fit are included as fixed parameters in this routine. These parameters may be adjusted slightly to ensure that the fit is robust and reasonably minimized. The improvement upon the data

reduction is shown graphically for the 15° scans in Figure V-16. Scans between 15° and 4° are generally not analyzed this way, as the thermal signal is relatively too small.

Three sets of the data above were judged to have sufficient signal to noise for further analysis. These sets and their final fits follow as Figures V-17, V-18 and V-19. The final fitted curves produce a typical reduced χ^2 of roughly .5 for the upper temperatures and .2 for the lower temperatures. Though somewhat small, these values are not unreasonably so (Press, Teukolsky et al. 1992) (Bevington 1969). The results of the volume analysis are summarized in Table V-6, while the bulk parameter results follow in Table V-7. Comparisons are made for pure water and a mixture of water and salt. Finally, the three level thermal analysis of Table V-8 includes comparisons to previous work, which is discussed further in the next chapter {BOPP} (Joo, Jia et al. 1996) (Nagarajan and Parson 1997). Though much of the energy is released impulsively, a considerable fraction of typically 20% persists in the protein for a few nanoseconds.

The fast and largely impulsive character of the heat release in LH2 allows this protein to be used calibration compound for the amplitude of the signal. Subsequent experiments on the reaction centers each consist of first collecting data on a known sample of LH2. This amplitude of the signal, when corrected for the long-term heat release, the fluorescence yield and differences in optical density, may be set to the energy of the exciting pump beam. Thus the instrument response of the system may be known.

V.D. Wild-Type & (M)214H Reaction Center

V.D.1. *Characteristics of the Reaction Center Data:* Samples of the light harvesting complex, the wild-type and (M)214H reaction center were prepared according to the methods of Chapter IV.B. Grating data was collected on wild-type reaction centers

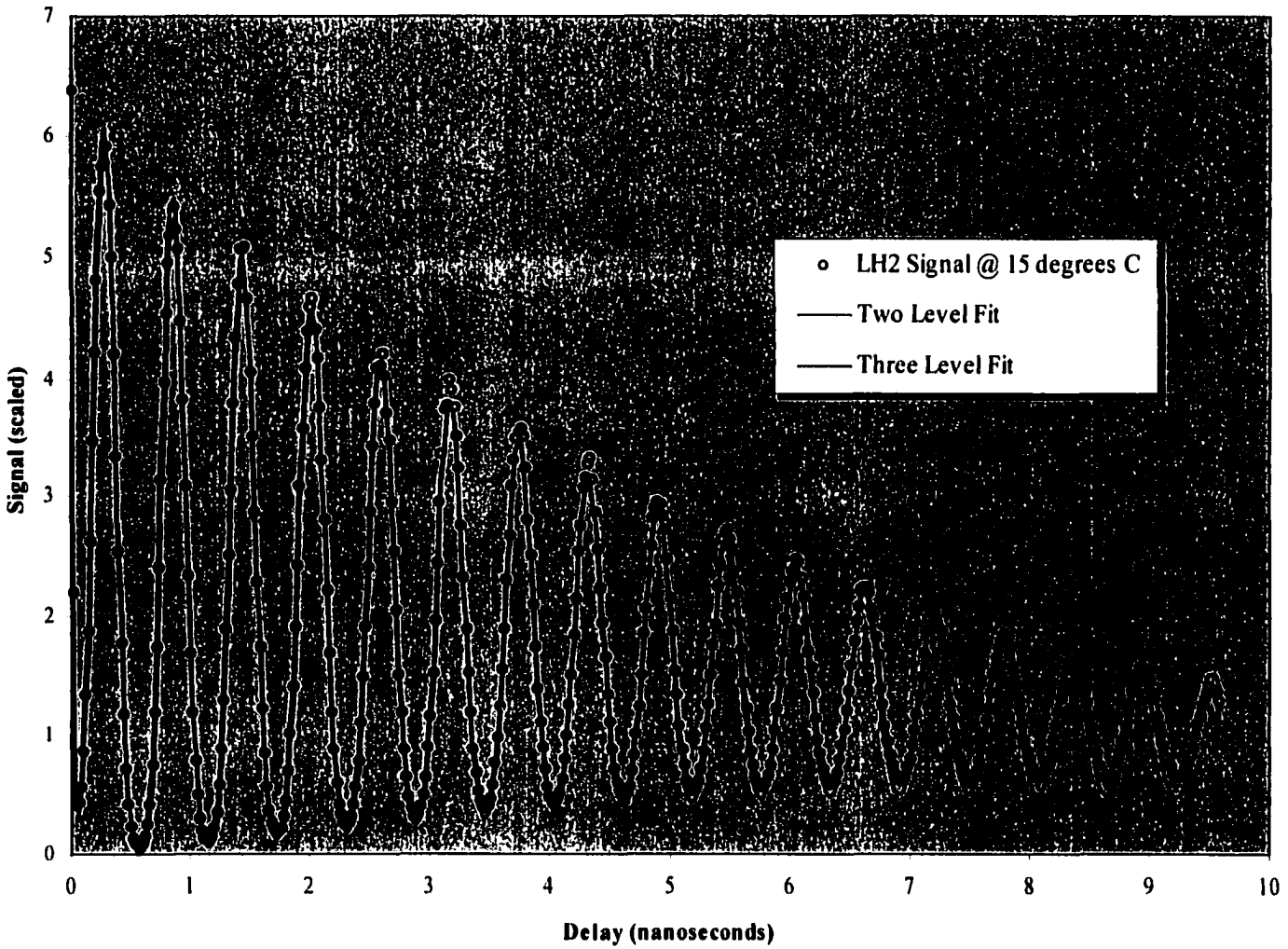

Figure V-16: Data on the peripheral light harvesting center and a comparison of grating fits. The two level fits are used to determine the bulk parameters of the fluid. These constants are then held constant in a three level fit described in the text. This fit includes the volume expansion grating, determined by the data at 4°C, and assumed to be constant over this narrow temperature range.

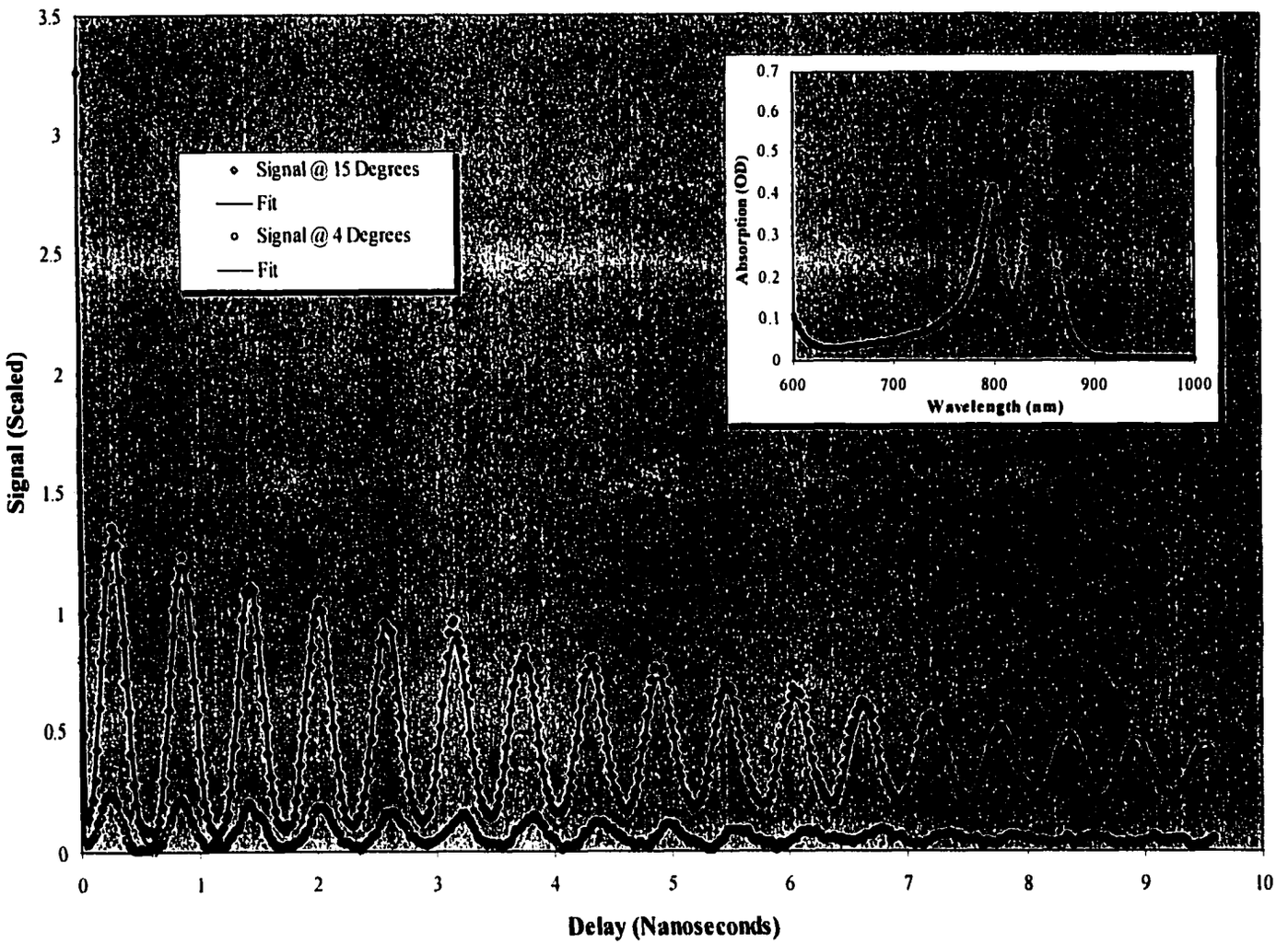

Figure V-17: Transient grating signal for the peripheral light harvesting complex in βOG, at 15°C and 4°C. The fits are to the three level heat release and three level volume changes, respectively, as described in the text. Inset displays a section of the wavelength scan on the sample, diluted 100 to 1, in a 1cm cell. Parameters obtained from this fit are displayed in Tables V-6, V-7 and V-8, as set #1.

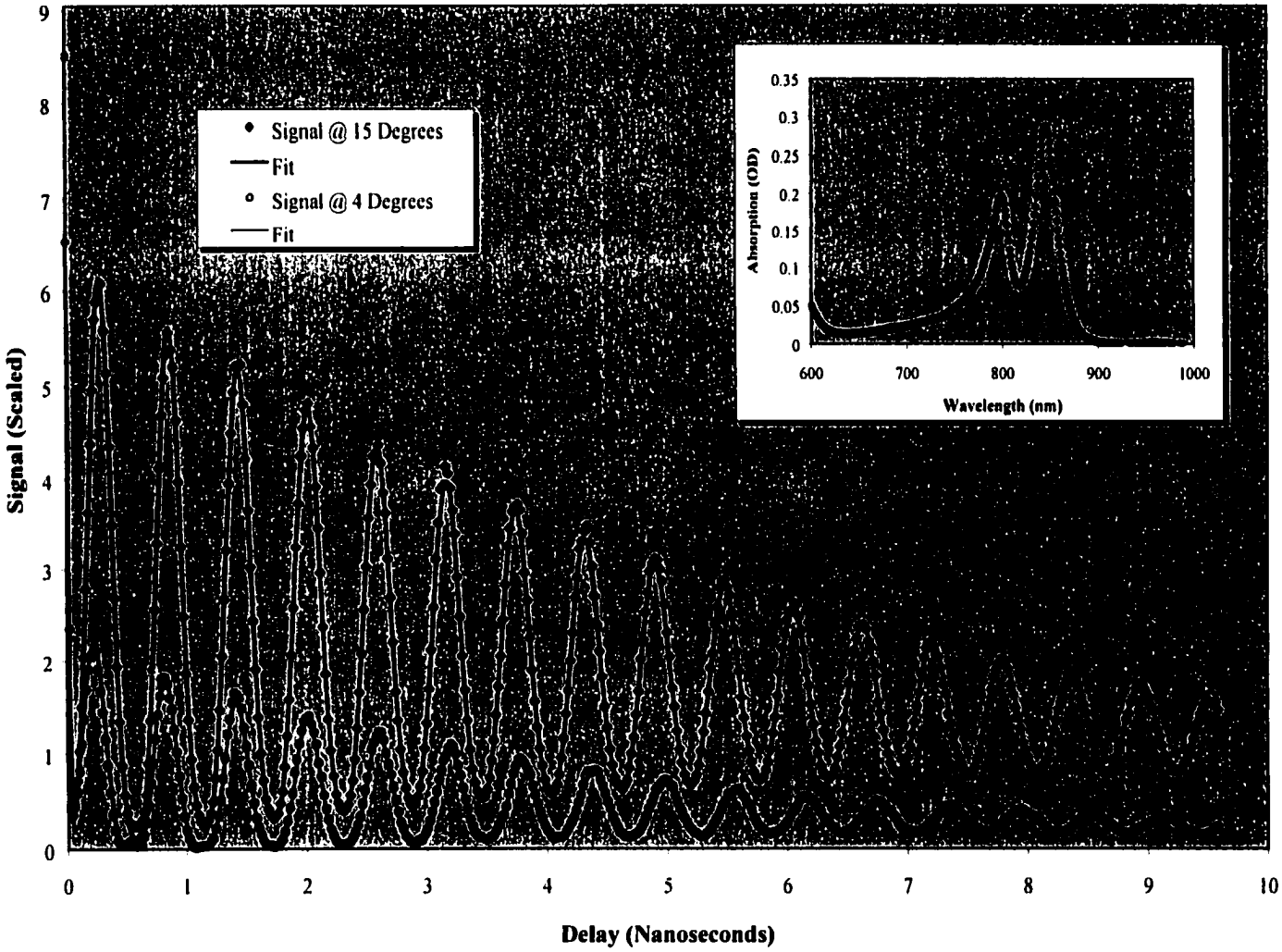

Figure V-18: Transient grating signal for the peripheral light harvesting complex in βOG, at 15°C and 4°C. The fits are to the three level heat release and three level volume changes, respectively, as described in the text. Inset displays a section of the wavelength scan on the sample, diluted 200 to 1, in a 1cm cell. Parameters obtained from this fit are displayed in Tables V-6, V-7 and V-8, as set #2.

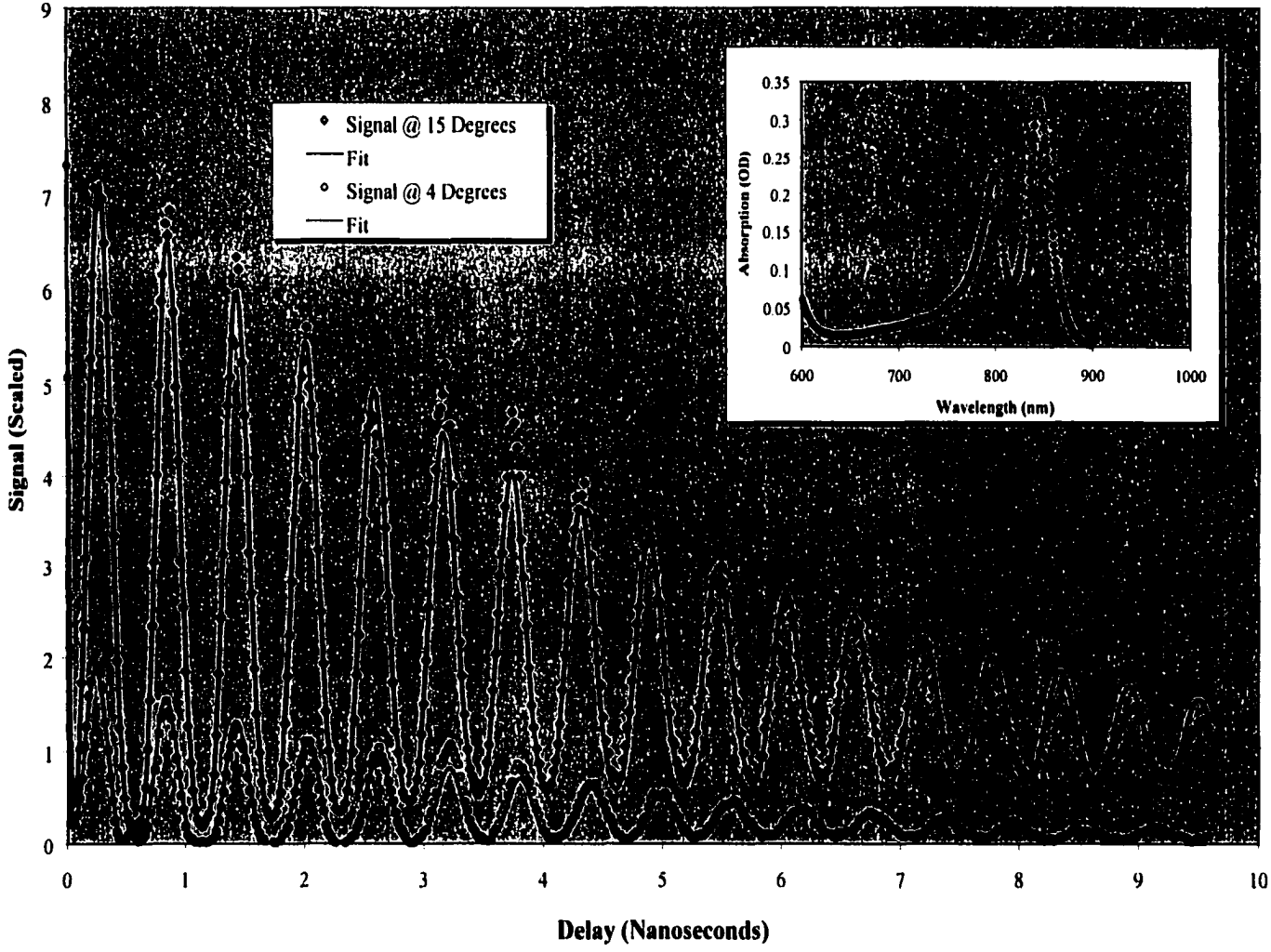

Figure V-19: Transient grating signal for the peripheral light harvesting complex in βOG, at 15°C and 4°C. The fits are to the three level heat release and three level volume changes, respectively, as described in the text. Inset displays a section of the wavelength scan on the sample, diluted 200 to 1, in a 1cm cell. Parameters obtained from this fit are displayed in Tables V-6, V-7 and V-8, as set #3. Note the noise in both scans after 3ns, due probably to a post pulse. Nonetheless, the fits seem to yield good data.

Sample	T (°C)	B ( )	τ_1 (ps)	τ_0 (ns)	E ( )	f (GHz)	v_0 (m/s)	α (10^{-15} s^2/m)
LH2 (βOG) #1	4.0 ± .2	32.3 ± .3	67 ± 5	32 ± 3	.25 ±.02	1.684 ± .005	1455 ± 5	47 ± 2
LH2 (βOG) #2	4.0 ± .2	80.3 ± .3	29 ± 1	24 ± 3	.72 ±.02	1.685 ± .005	1456 ± 5	51 ± 2
LH2 (βOG) #3	3.7 ± .2	76.6 ± .3	15 ± 1	15 ± 3	.50 ±.02	1.686 ± .005	1457 ± 5	52 ± 2
Average	3.9 ± .1	-	26 ± 1	32 ± 2	-	-	1456 ± 3	50 ± 5
ref (water)	4.0	-	-	-	-	-	1418 (1461)	60 (60)

Table V-6: LH2 in βOG near the zero expansion point of water, fit to a three level model of conformational change and decay. The signals and fits are shown in Figures V-17, V-18 and V-19. The parameters are determined directly by the fit are the volume amplitude (B), Brillouin amplitude (E), the relaxation time (t) and the acoustic frequency (f). The speed of sound (v_0), the thermal diffusivity (h) and the acoustic attenuation (a) are represented in conventional units, using the grating wavelength of 864nm. References were found as mentioned in the text and are considered to the last digit, unless otherwise noted. The references in parenthesis are for a salt and water mixture.

Sample	T (°C)	OD (@ 864nm)	A ( )	E ( )	f (GHz)	v_0 (m/s)	h (10^{-9} m^2/s)	α (10^{-15} s^2/m)
LH2 (βOG) #1	15.9 ± .2	19.6 ± .1	43.1 ± .1	.27 ± .03	1.733 ± .003	1497 ± 5	363 ± 100	39 ± 2
LH2 (βOG) #2	15.2 ± .2	18.2 ± .1	70.4 ± .1	.42 ± .02	1.732 ± .002	1496 ± 4	586 ± 100	42 ± 2
LH2 (βOG) #3	15.3 ± .2	20.3 ± .1	86.6 ± .2	.43 ± .03	1.735 ± .002	1499 ± 4	843 ± 100	42 ± 2
Average	15.5 ± .1	-	-	-	-	1497 ± 2	597 ± 60	41 ± 1
ref (water)	15.0	-	-	-	-	1467 (1506)	140	45 (45)

Table V-7: Temperature variation for LH_2 in βOG, fit to a three level model of decay which includes stimulated Brillouin grating and a conformational volume change. The signals and fits are shown in Figures V-17, V-18 and V-19. The parameters are determined directly by the fit are the thermal amplitude (A), Brillouin amplitude (E), the relaxation time (t) and the acoustic frequency (f). The speed of sound (v_0), the thermal diffusivity (h) and the acoustic attenuation (a) are represented in conventional units, using the grating wavelength of 864nm. References were found as mentioned in the text and are considered to the last digit, unless otherwise noted. References in parenthesis are for a water and salt mixture.

Sample	T (°C)	OD (@ 846nm)	A_1 ( )	τ_1 (ps)	A_0 ( )	τ_o (ns)
LH2 (βOG) #1	15.9 ± .2	19.6 ± .1	43.1 ± .1	24.2 ± 1.5	51.1 ± .5	1.69 ± .20
LH2 (βOG) #2	15.2 ± .2	18.2 ± .1	70.4 ± .1	16.8 ± 1.5	96.2 ± .5	1.25 ± .20
LH2 (βOG) #3	15.3 ± .2	20.3 ± .1	86.6 ± .2	24.5 ± 1.5	122.1 ± .5	1.43 ± .20
Average	15.5 ± .1	-	-	19.8 ± .6	-	1.41 ± .12
ref	~ 20	-	-	26.3 ± 1.0	-	1.0 ± .2

Table V-8: Thermal signal for LH_2 in βOG, fit to a three level model of decay which includes the bulk terms of the previous table and the volume terms of Table V-6 as constants. The signals and fits are shown in Figures V-17, V-18 and V-19. References were found as mentioned in the text and are considered to the last digit, unless otherwise noted.

stabilized in both LDAO and βOG, while (M)214H reaction centers were in βOG only. Figures V-20 and V-21 show the data collected upon wild-type and (M)214H centers respectively. All experiments were compared to the impulsive thermal signal of the peripheral light-harvesting complex, to calibrate the heat release. Scans of both the light harvesting and the reaction center were collected before and after each grating experiment. Note the differences in the wavelength scans for the wild-type and (M)214H reaction centers, due to the replacement of the pheophytin with a chlorophyll.

V.D.2. *Thermal Analysis:* This data follows the same iterative procedure as for the light harvesting procedure above. The low temperature scans are analyzed using the three level volume grating, while the two level model obtains the rough bulk properties from the upper temperature data. As above, these parameters were held fixed as the three level model was applied to the upper temperature data. The thermal diffusivity, however, is not held fixed. The light harvesting protein and laser dye data showed a strong increase in this bulk parameter. The increase is even stronger for reaction centers. Figure V-22 reveals the trend. The poorest fit utilizes the theoretical value for water, while a better fit stems from the value determined by the two level fit. Yet, a continual improvement in the fit may be realized by adjusting the thermal diffusion parameter further. This typically decreases the reduced χ^2 by a factor of two from the 'measured' value, and a factor of five overall from the theoretical value. The other bulk parameters do not show this behavior, which is also not as apparent in light harvesting centers, especially after the three level fits are applied. Similar to the light harvesting centers, the final fitted curves produce a typical reduced χ^2 just under unity. However, there is more variability in the signal to noise, due to the larger ranges of the signal. The thermal

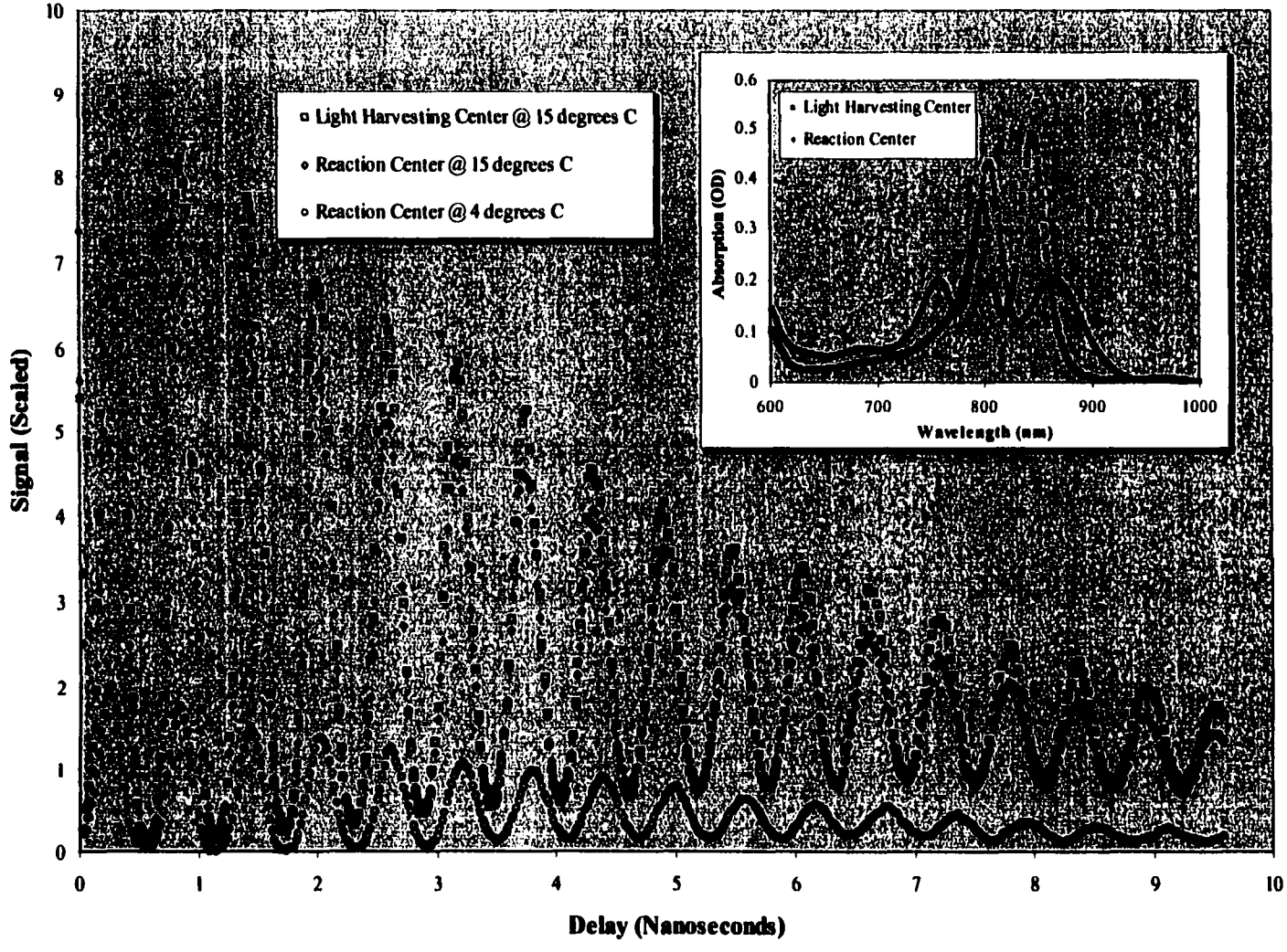

Figure V-20: Raw transient grating signal for the reduced reaction center at 15°C and at 4°C. Signal from LH2 was collected as well, as a reference. Inset displays a section of a wavelength scan on the sample, diluted 100 to 1, in a 1cm cell. Once again, the signal does not vanish at the zero expansion point of water, indicating a non-thermal volume change that offsets the signal.

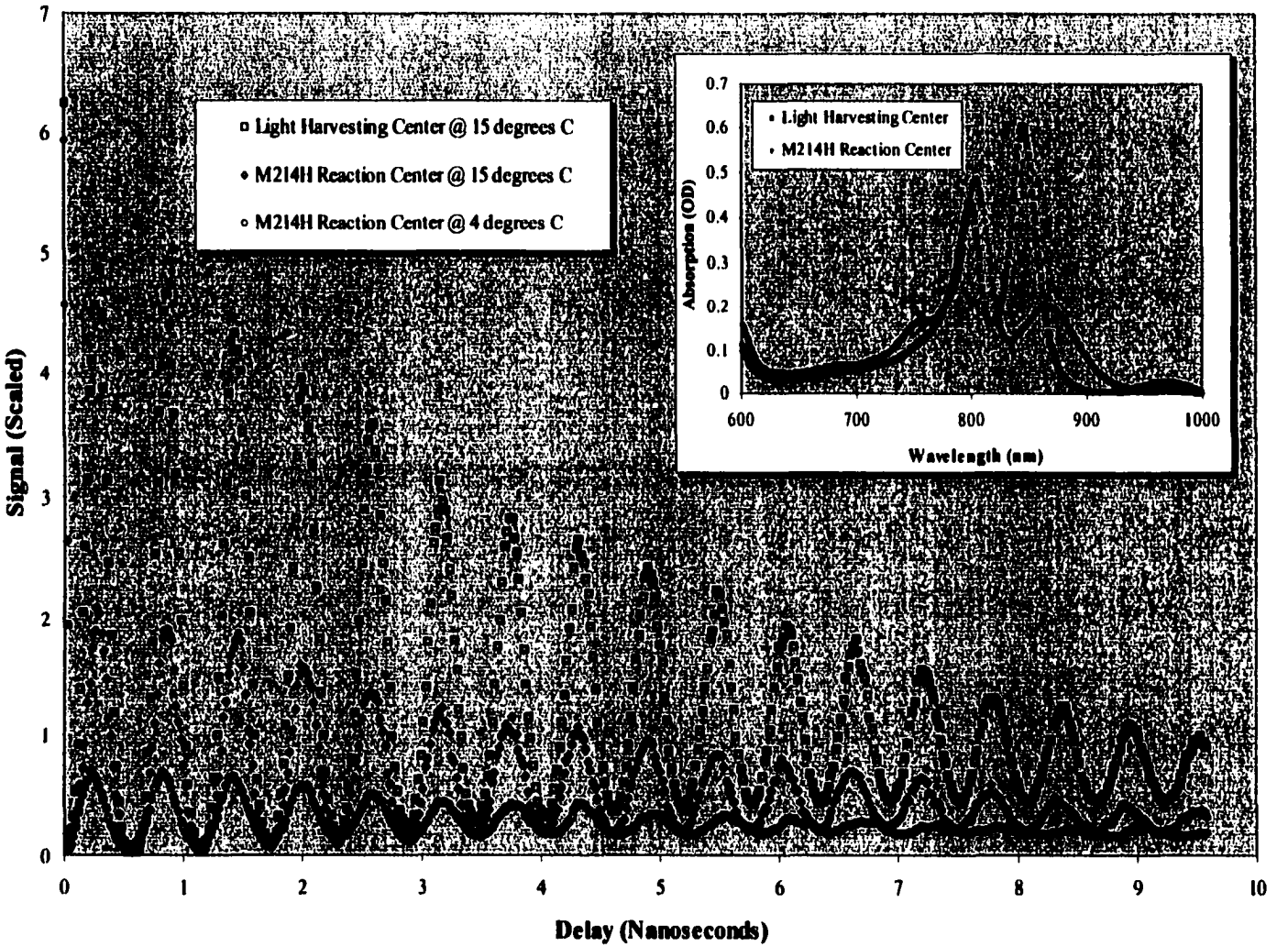

Figure V-21: Raw transient grating signal for the (M)214H reaction center at 15°C and 4°C. Signal was collected from LH2 as well, as a reference. Inset displays a section of a wavelength scan on the sample, diluted 100 to 1, in a 1cm cell. Once again there is a non-zero signal at 4 degrees, though the thermal signal is considerably smaller than the comparable signal for the light harvesting protein.

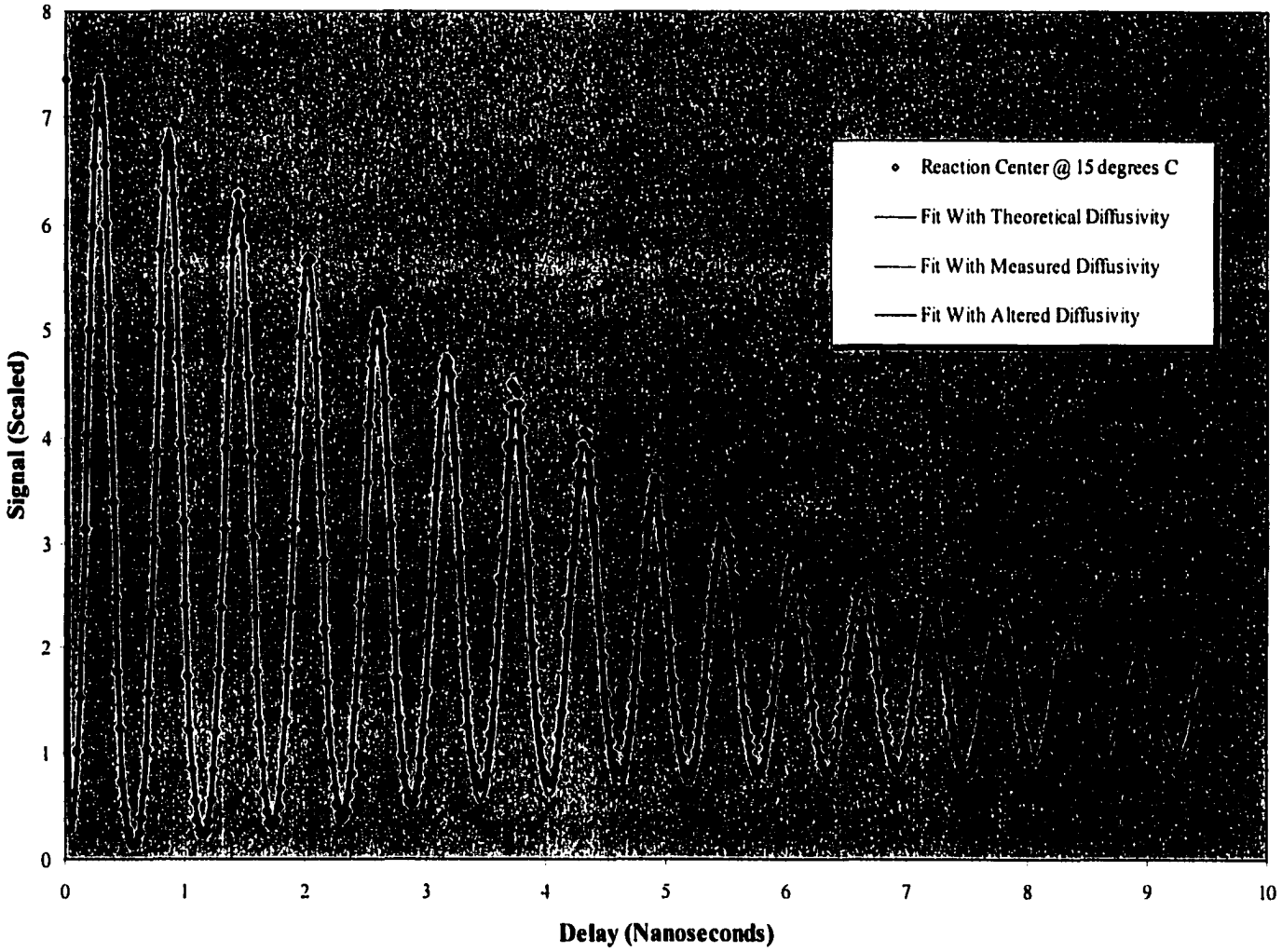

Figure V-22: Reaction center data, fit to a three level model including the volume change at the zero expansion point. Two level fits yield the bulk parameters that are used as constants in the three level fits shown here. Though this 'measured' thermal diffusivity allows better fits to the data than using the theoretical diffusivity for pure water, the value must be altered further to adequately fit the data. The reduced χ^2 decreases by a factor 5 across the three fits.

grating generates values from 1 to .6, while the volume grating produces values near .3. As mentioned above, an ideal result should be near unity (especially for a system with a high number of degrees of freedom), though values just short are acceptable (Bevington 1969) (Press, Teukolsky et al. 1992).

V.D.3. *Wild-Type Reaction Center Data and Analysis:* Reaction center data was collected upon pre-reduced and unreduced centers. Figure V-23 shows data and the final fits for pre-reduced reaction centers at 15° only. Since no low temperature signal is present, only a two level analysis is performed. Note the low impulsive amplitude, due to the low energy gap of charge separation. The excited state terms also appear to be small, a characteristic common among all of the reaction center data. The data of Figure V-24 is for reaction centers in βOG. The reduced data shows a higher signal due to higher concentration, while the unreduced data shows a much higher signal from the larger energy gap of charge separation to the quinone. The zero expansion point signal is not unexpected for a system involving a moving charge. Unfortunately, this set lacks the time resolution of the previous data. Finally, the reduced centers of Figure V-25 show the strongest signal to noise. Low temperature results are summarized in Table V-9, bulk properties in V-10 and the three level thermal analysis is detailed in V-11. These values are compared to other values for reaction centers in bulk (Fleming, Breton et al. 1988) (Arata and Parson 1981) (Kirmaier, Gaul et al. 1991). The pre-reduced reaction centers are analyzed further utilizing the triplet and dynamic solvation models of Chapter III. These results are pursued further in the next chapter.

V.D.4. *Mutant (M)214H Reaction Center Data and Analysis:* Reaction centers may undergo site - directed mutagenesis that substitutes an M subunit Leu^{214} by His,

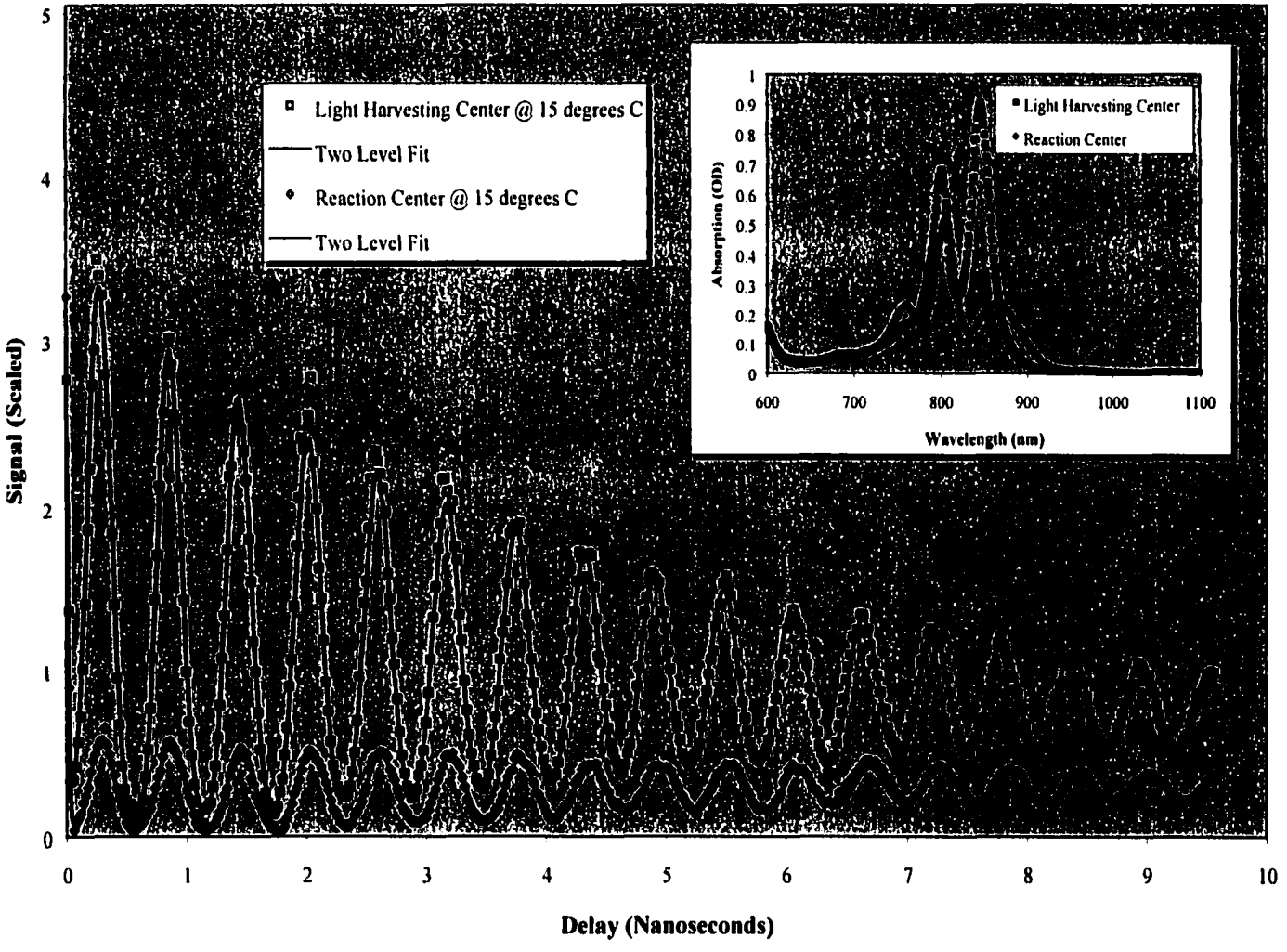

Figure V-23: Transient grating signal on reduced reaction centers and peripheral light harvesting centers in LDAO, at 15°C. Absent a zero expansion point signal, the fits here are to a two level thermal system. Nonetheless, parameters from this fit are shown in Tables V-10 and V-11, as set #1. The scan inset was performed in a 1cm cell, at a 40 to 1 dilution.

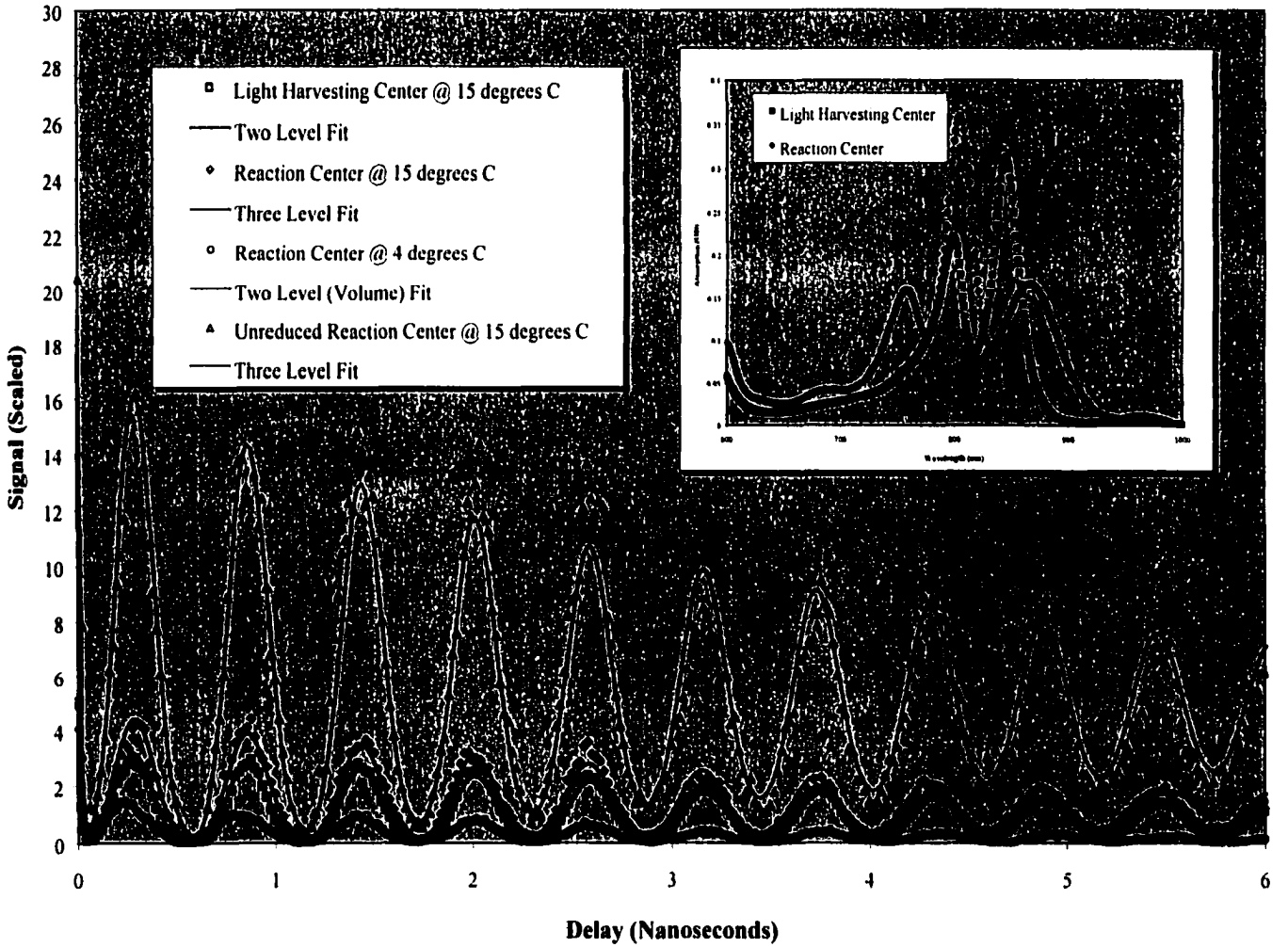

Figure V-24: Transient grating signal for the reduced and unreduced reaction center at 15°C and 4°C. Results for LH2 are also shown as a reference. Note the strong signal from the unreduced reaction center, due to the relatively large energy gap between the excited state and the quinone. Inset displays a section of a wavelength scan on the sample, diluted 200 to 1, in a 1cm cell. Parameters obtained from this fit are displayed in Tables V-9, V-10 and V-11, as set #2.

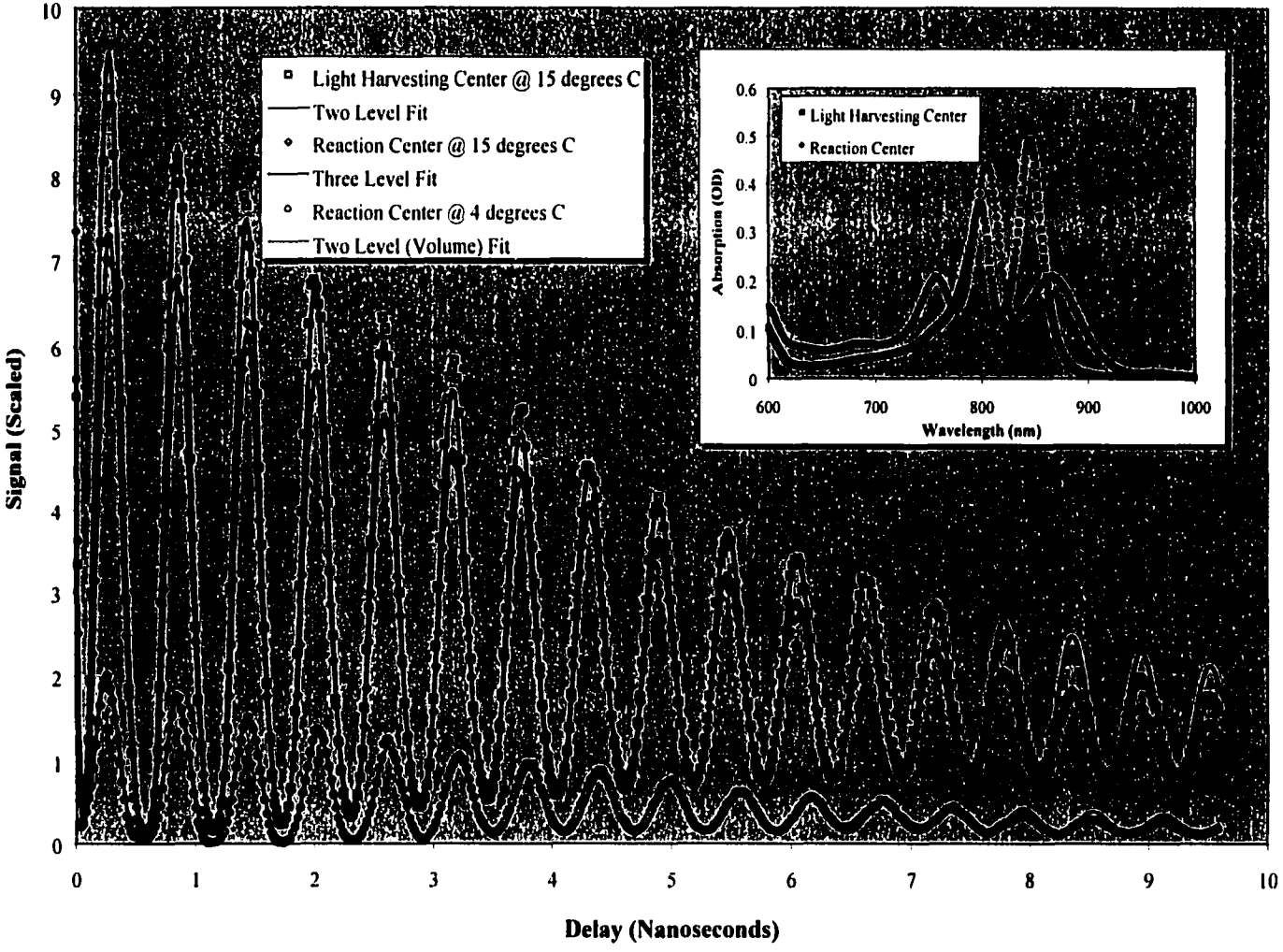

Figure V-25: Transient grating signal on reduced reaction centers and peripheral light harvesting system in βOG. Sample temperature ranges as shown. Inset displays a section of a wavelength scan on the sample, diluted 100 to 1, in a 1cm cell. Parameters obtained from this fit are displayed as set #3 in Tables V-9, V-10 and V-11.

Sample	T (°C)	B ( )	τ_1 (ps)	τ_0 (ns)	E ( )	f (GHz)	v_o (m/s)	α (10^{-15} s^2/m)
Wild-Type (βOG) #2	3.7 ± .2	79.8 ± .3	80 ± 5	9 ± 2	.56 ±.02	1.706 ± .004	1474 ± 6	51 ± 2
Wild-Type (βOG) #3	3.7 ± .2	88.0 ± .3	50 ± 5	20 ± 1	.62 ±.02	1.691 ± .002	1461 ± 3	47 ± 2
Average	3.7 ± .1	-	65 ± 3	16 ± 1	-	-	1465 ± 3	49 ± 1
ref (water)	4.0	-	-	-	-	-	1418 (1461)	60 (60)

Table V-9: Reduced reaction centers in βOG near the zero expansion point of water, fit to a three level model of conformational change and decay. The signals and fits are shown in V-23, V-24 and V-25. The parameters determined directly by the fit are the volume change (B), Brillouin amplitude (E), the relaxation time (t) and the acoustic frequency (f). The speed of sound (v_o), the thermal diffusivity (h) and the acoustic attenuation (a) are represented in conventional units, using the grating wavelength of 864nm. References were found as mentioned in the text and are considered to the last digit, unless otherwise noted. The references in parenthesis are for a salt and water mixture.

Sample	T (°C)	OD (@864nm)	A ( )	E ( )	f (GHz)	v_o (m/s)	h (10^{-9} m^2/s)	α (10^{-15} s^2/m)
Wild-Type (LDAO) #1	18 ± 1	9.5 ± .1	48.2 ± .1	.15 ± .02	1.718 ± .003	1484 ± 5	331 ± 100	37 ± 4
Wild-Type (βOG) #2	14.7 ± .2	33.2 ± .1	57.8 ± .3	.30 ± .02	1.742 ± .006	1505 ± 8	166 ± 80	43 ± 4
Wild-Type (βOG) #2 ◊	14.7 ± .2	33.2 ± .1	185.1 ± .3	.40 ± .02	1.742 ± .006	1505 ± 8	38 ± 20	47 ± 4
Wild-Type (βOG) #3	14.4 ± .2	20.8 ± .1	84.7 ± .1	.41 ± .02	1.734 ± .002	1498 ± 4	2600 ± 200	43 ± 2
Average	14.9 ± .1	-	-	-	-	1501 ± 4	248 ± 20	43 ± 2
ref (water)	15.0	-	-	-	-	1467 (1487)	140	45 (45)

Table V-10: Temperature variation for reaction centers in βOG and LDAO, fit to a three level model of decay which includes stimulated Brillouin grating. An unreduced sample is shown by '◊'. The signals and fits are shown in Figures V-23, V-24 and V-25. The parameters determined directly by the fit are the thermal amplitude (A), Brillouin amplitude (E), the relaxation time (t) and the acoustic frequency (f). The speed of sound (v_o), the thermal diffusivity (h) and the acoustic attenuation (a) are represented in conventional units, using the grating wavelength of 864nm. References were found as mentioned in the text and are considered to the last digit, unless otherwise noted. References in parenthesis are for salt and water mixture.

Sample	T (°C)	OD (@ 864nm)	A_1 ( )	τ_1 (ps)	A_0 ( )	τ_o (ns)
Wild-Type (βOG) #2	14.7 ± .2	33.2 ± .1	57.8 ± .3	2.4 ± 1.0	273 ± 2	17 ± 2
Wild-Type (βOG) #2 ◊	14.7 ± .2	33.2 ± .1	185.1 ± .3	-	313 ± 2	19 ± 2
Wild-Type (βOG) #3	14.4 ± .2	20.8 ± .1	84.7 ± .1	3.7 ± .2	453 ± 2	8 ± 2
Average	14.6 ± .1	-	-	3.5 ± .2	-	12 ± 1
ref	14.0	-	-	3.7	-	20

Table V-11: Thermal signal for reaction centers in βOG, including an unreduced sample marked by '◊'. The bulk terms of Table V-10 and the volume grating terms of V-9 were utilized in these three level fits. The signals and fits are shown on Figures V-23, V-24 and V-25. The averages are over the two pre-reduced samples only, and are weighted where appropriate. References were found as mentioned in the text and are considered to the last digit, unless otherwise noted.

which ultimately replaces the photoactive pheophytin by a chlorophyll. Clearly even the rates as well as the energetics of charge transfer are affected. All of the (M)214H data is stabilized in βOG and has been pre-reduced. The first set of Figure V-26 has no low temperature data, but may be analyzed for bulk parameters. The data of Figures V-27 and V-28 show continual improvement in signal to noise, with data at the zero expansion point. All sets show a much-reduced impulsive signal, due to a much smaller energy gap of charge separation. However, the low temperature data still reveals a significant volume change, due to charge motion. The low temperature analysis follows in Table V-12 and the bulk results follow with Table V-13. The three level thermal parameters in Table V-14 are compared to other known values (Laporte, Mcdowell et al. 1995) (Kirmaier, Gaul et al. 1991) and are discussed more fully in Chapter VI.

V.E. Literature Cited

Arata, H. and W. Parson (1981). "Delayed Fluorescence from *Rhodopseudomonas sphaeroides* reaction centers: Enthalpy and free energy changes accompanying electron transfer from P-870 to quinones." Biochimical et Biophysica Acta **638**: 201-209.

Bevington, P. R. (1969). Data Reduction and Error Analysis for the Physical Sciences. New York, McGraw-Hill.

Cao, Y. N., H. X. Chen, et al. (1997). "Generation of the Photoacoustic Effect through Heat Diffusion: Transient Grating Measaurements on Reverse Miscelle Solutions." Journal of Physical Chemistry **101**: 3005-3011.

Deak, J., L. Richard, et al. (1994). Picosecond phase grating spectroscopy: Applications to bioenergetics and protein dynamics. Methods in Enzymology. New York, Academic Press: 322-360.

Fayer, M. D. (1986). "Picosecond holographic generation of ultrasonic waves." IEEE Journal of Quantum Mechanics **QE-22**(8): 1437-1452.

Fleming, G. R., J. Breton, et al. (1988). "Rates of Primary Electron Transfer in Photosynthetic Reaction Centers and Their Mechanistic Implications." Nature **333**: 190-192.

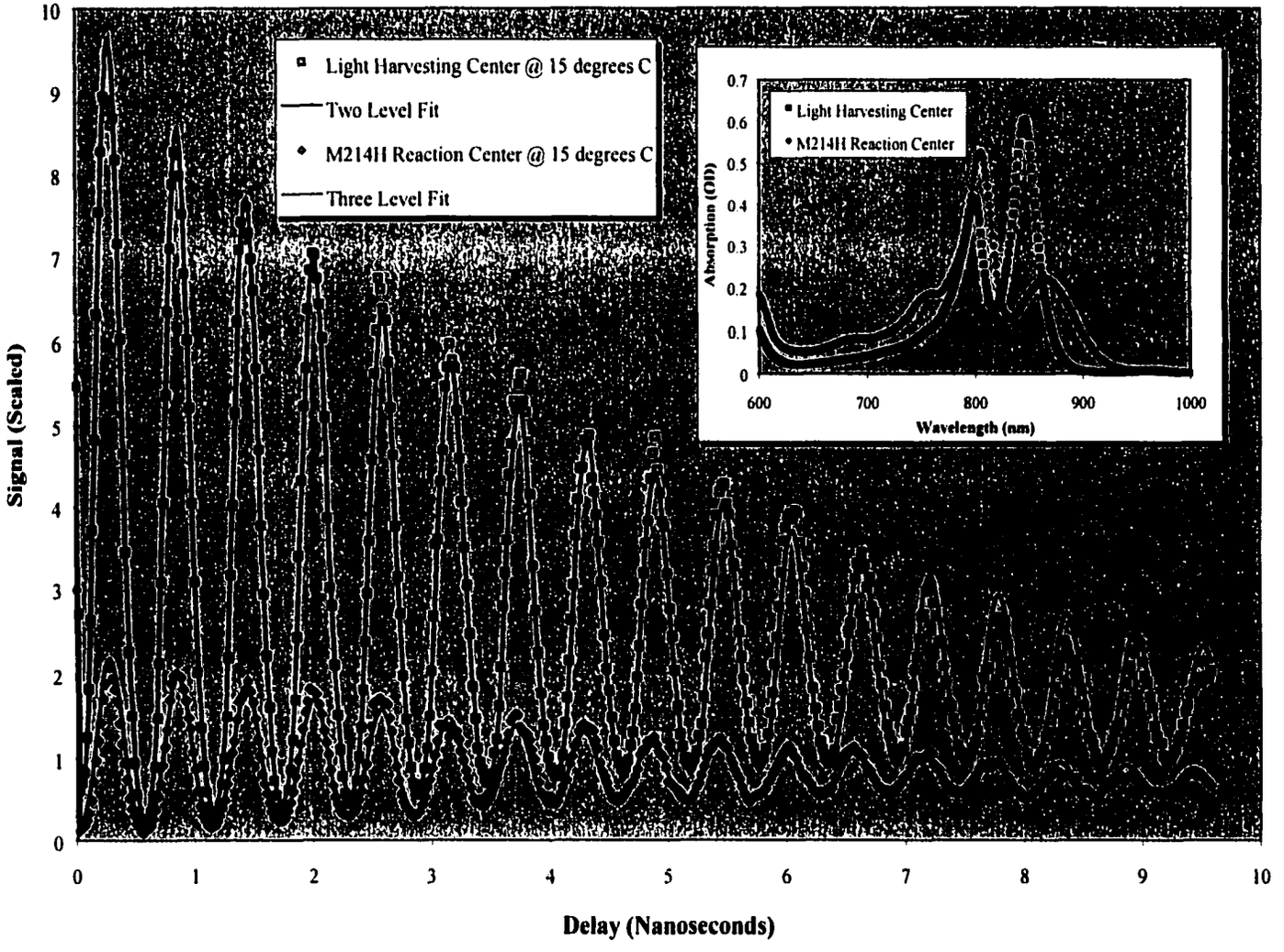

Figure V-26: Transient grating signal on (M)214H reaction centers and peripheral light harvesting centers in βOG, at 15°C. Absent a zero point expansion signal, the fits here are to a two level system. Inset displays a section of a wavelength scan on the sample, diluted 100 to 1, in a 1cm cell. Parameters obtained from this fit are displayed as set #1 in Tables V-13 and V-14.

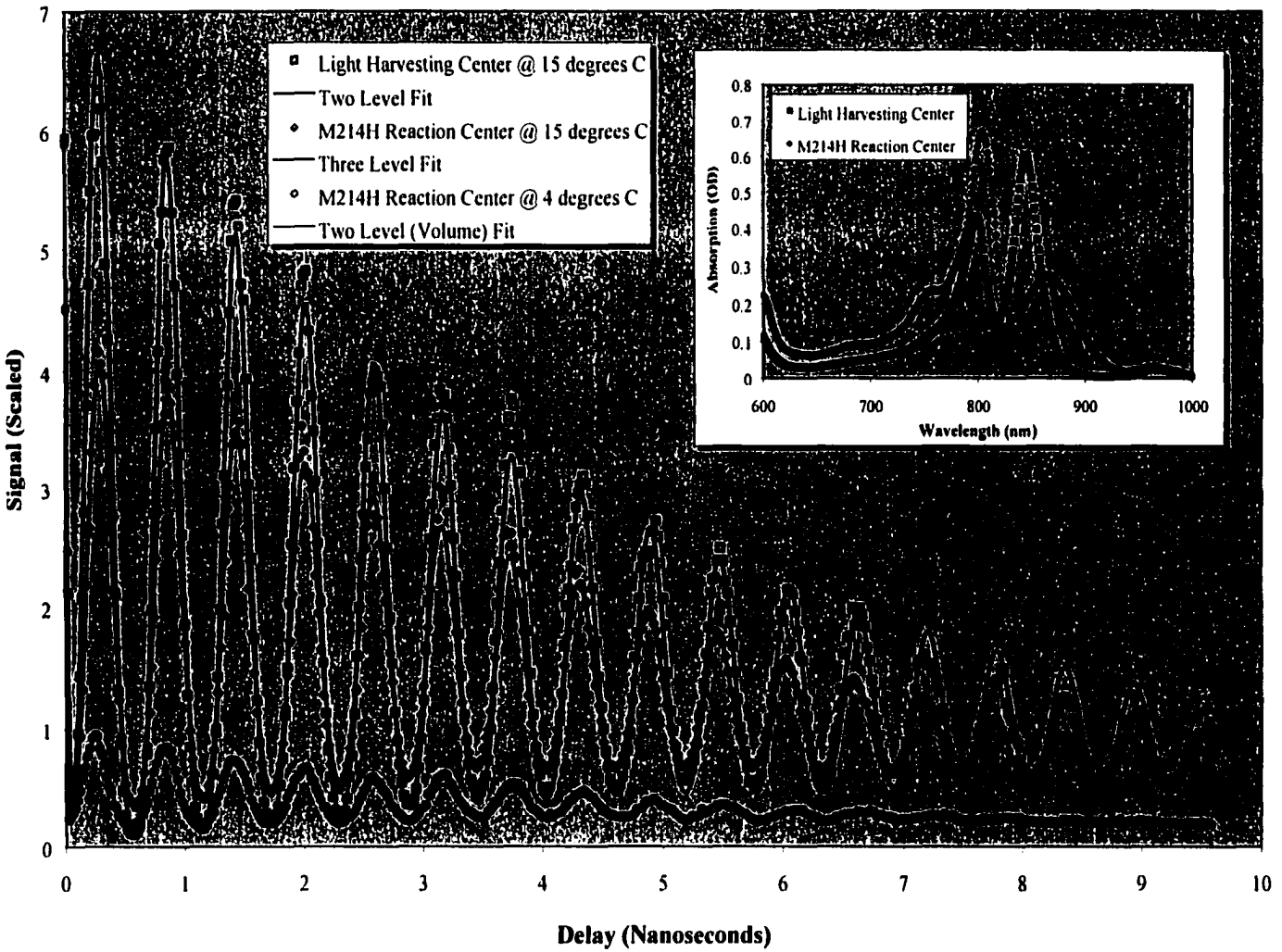

Figure V-27: Transient grating signal on (M)214H reaction centers and LH2 in βOG including a zero expansion signal. Inset displays a section of a wavelength scan on the sample, diluted 200 to 1, in a 1cm cell. Parameters obtained from this fit are displayed in Tables V-12, V-13 and V-14, as set #2.

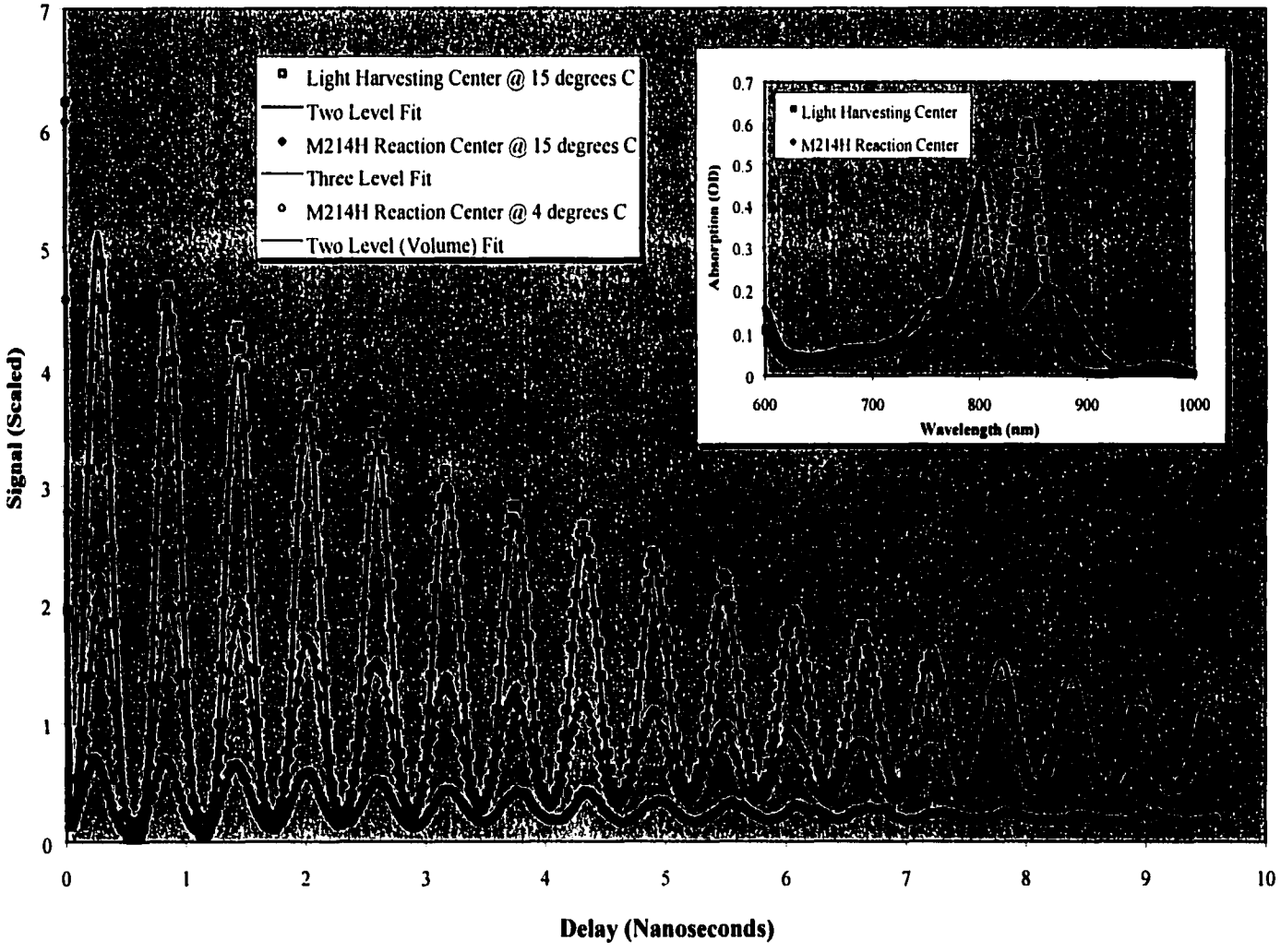

Figure V-28: Transient grating signal on (M)214H reaction centers and LH2 in βOG including a zero expansion signal. Inset displays a section of a wavelength scan on the sample, diluted 100 to 1, in a 1cm cell. Parameters obtained from this fit are displayed in Tables V-12, V-13 and V-14, as set #3.

Sample	T (°C)	B ( )	τ_1 (ps)	τ_0 (ns)	E ( )	f (GHz)	v_o (m/s)	α (10^{-15} s^2/m)
M214H (βOG) #2	3.9 ± .2	78.8 ± .3	111 ± 5	22 ± 2	.51 ±.02	1.708 ± .002	1476 ± 3	67 ± 2
M214H (βOG) #3	3.7 ± .2	65.2 ± .3	98 ± 5	33 ± 2	.48 ±.02	1.696 ± .002	1466 ± 3	59 ± 2
Average	3.8 ± .1	-	105 ± 3	28 ± 1	-	-	1471 ± 2	63 ± 1
ref (water)	4.0	-	-	-	-	-	1418 (1461)	60

Table V-12: (M)214H reaction centers in βOG near the zero expansion point of water, fit to a three level model of conformational change and decay. The signals and fits are shown in V-26, V-27 and V-28. The parameters determined directly by the fit are the volume change (B), Brillouin amplitude (E), the relaxation time (t) and the acoustic frequency (f). The speed of sound (v_o), the thermal diffusivity (h) and the acoustic attenuation (a) are represented in conventional units, using the grating wavelength of 864nm. References were found as mentioned in the text and are considered to the last digit, unless otherwise noted.

Sample	T (°C)	OD (@ 864nm)	A ( )	E ( )	f (GHz)	v_0 (m/s)	h (10^{-9} m^2/s)	α (10^{-15} s^2/m)
M214H (βOG) #1	14 ± 1	22.1 ± .1	114± 2	.52 ± .04	1.748 ± .006	1510 ± 8	217 ± 80	42 ± 2
M214H (βOG) #2	14.9 ± .2	27.6 ± .1	62.3 ± .2	.41 ± .02	1.743 ± .002	1506 ± 4	2700 ± 200	45 ± 2
M214H (βOG) #3	14.1 ± .2	20.2 ± .1	41.2 ± .2	.31 ± .02	1.737 ± .002	1501 ± 4	2080 ± 200	43 ± 2
Average	14.5 ± .1	-	-	-	-	1504 ± 3	2390 ± 140	44 ± 1
ref (water)	15.0	-	-	-	-	1467 (1487)	140	45 (45)

Table V-13: Fitted parameters for (M)214H in βOG, fit to a three level model of decay which includes stimulated Brillouin grating. The signals and fits are shown in V-26, V-27 and V-28. The parameters are determined directly by the fit are the thermal amplitude (A), Brillouin amplitude (E), the relaxation time (t) and the acoustic frequency (f). The speed of sound (v_0), the thermal diffusivity (h) and the acoustic attenuation (a) are represented in conventional units, using the grating wavelength of 864nm. References were found as mentioned in the text and are considered to the last digit, unless otherwise noted.

Sample	T (°C)	OD (@ 864nm)	A_1 ( )	τ_1 (ps)	A_0 ( )	τ_0 (ns)
M214H (βOG) #2	14.9 ± .2	27.6 ± .1	62.3 ± .1	5.8 ± .2	123.3 ± .5	3.4 ± .5
M214H (βOG) #3	14.1 ± .2	20.2 ± .1	41.2 ± .1	5.6 ± .2	67.3 ± .5	2.8 ± .5
Average	14.5 ± .1	-	-	5.7 ± .1	-	3.1 ± .4
ref	14.0	-	-	5.8	-	1.0

Table V-14: Thermal signal for (M)214H in βOG, fit to a three level model of decay. The bulk terms of Table V-13 and the volume grating terms of Table V-12 were utilized in these three level fits. The signals and fits are shown on Figures V-26, V-27 and V-28. References were found as mentioned in the text and are considered to the last digit, unless otherwise noted.

Fox, I. J., L. G. S. Brookes, et al. (1957). "A tricarbocyanine dye for the continuous recording of dilution curves in whole blood independent of variations in blood oxygen saturation." Proceedings of Staff Meetings Mayo Clinic **32**: 478-484.

Gray, D. E., ed. (1972). American Institue of Physics Handbook. New York, McGraw-Hill.

Grigoriev, I., .S. and E. Z. Meilikhov, Eds. (1997). Handbook of Physical Quantities. Moscow, CRC Press.

Gumy, J.-C., O. Nicolet, et al. (1999). "Investigation of the solvation dynamics of an organic dye in polar solvents using the femtosecond grating technique." Journal of Physical Chemistry A **103**(50): 10737-10743.

Hochstrasser, R. M. (1998). "Ultrafast Spectroscopy of Protein Dynamics." Journal of Chemical Education: Waters Symposium **75**(5): 559-564.

Joo, T. H., Y. W. Jia, et al. (1996). "Dynamics in isolated bacterial light harvesting antenna (LH2) of *Rhodobacter sphaeroides* at room temperature." Journal of Physical Chemistry **100**(6): 2399-2409.

Kaye, G. W. C. and T. H. Laby (1995). Tables of physical and chemical constants. Essex, Harlow.

Kirmaier, C., D. Gaul, et al. (1991). "Charge Separation in a Reaction Center Incorporating Bacteriochlorophyll for Photoactive Bacteriopheophytin." Science **251**: 922-927.

Laporte, L., L. Mcdowell, et al. (1995). "Free-energy dependence of the rate of electron transfer to the primary quinone in beta-type reaction centers." Journal of Chemical Physics **197**: 225.

Mohanty, J., D. K. Palit, et al. (2000). "Photophysical properties of two infrared laser dyes - IR-144 and IR-140: a picosecond laser photolysis study." Proceeding of the Indian National Science Academy **66**(2): 303-315.

Morais, J. and M. B. Zimmt (1995). "Thermodynamics of intramolecular electron transfer in alkane solvents." Journal of Physical Chemistry **99**(21): 8863-8871.

Mukamel, S. (1995). Principles of Nonlinear Optical Spectroscopy. New York, Oxford University Press.

Nagarajan, V. and W. W. Parson (1997). "Excitation energy transfer between the B850 and B875 antenna complexes of *Rhodobacter sphaeroides*." Biochemistry **36**: 2300-2306.

Nelson, K. A., R. Casalengo, et al. (1982). "Laser-induced excited state and ultrasonic wave gratings: Amplitude and phase grating contributions to diffraction." Journal of Chemical Physics **77**(3): 1144-1152.

Philip, R., A. Penzkofer, et al. (1996). "Absorption and fluorescence spectroscopic investigation of indocyanine green." Journal of Photochemistry and Photobiology A:Chemistry **96**: 137-148.

Press, W. H., S. A. Teukolsky, et al. (1992). Numerical Recipies in C: The Art of Scientific Computing, Cambridge University Press.

Soper, S. A. and Q. L. Mattingly (1994). "Steady-state and picosecond laser fluorescence studies of non-radiative pathways in tricarbocyanine dyes: Implications to the design of near-ir fluorochromes with high fluorescence efficiencies." Journal of the American Chemical Society **116**(9): 3744-3752.

Sundstrom, V., T. Pullerits, et al. (1999). "Photosynthetic light harvesting: Reconciling dynamics and structure of purple bacterial LH2 reveals function of photosynthetic unit." Journal of Physical Chemistry B **103**(13): 2327-2346.

VI. DISCUSSION

Overall, the grating analysis leads to good agreement with previous data. The laser dye results suggest molecules that undergo a fast initial relaxation followed by a slower release of heat, and this appears to conform to previous results. However, the precise values of the bulk parameters, especially the thermal diffusion coefficient for methanol, are not clear. The peripheral light harvesting protein shows a similar pattern of fast relaxation coupled with a slower process. Furthermore, LH2 appears to have a strong signal at the zero expansion point of water. This unexpected result possibly indicates some solvation as the energy delocalizes upon the ring. Similarly, the data for the wild-type and the mutant (M)214H reaction centers fixes the rates and energy levels for the charge separated state. While the complicated grating expressions of Chapter III yield improved fits to the thermal data, the volume change gives some insight into the progress of solvation effects upon the charge separated state.

VI.A. Laser Dyes IR125 & IR140

VI.A.1. *IR125 & IR140 in Methanol:* The chief purpose of the IR125 and IR140 experiments was to calibrate the grating solution by measuring the properties of the dyes, as well as the bulk properties of methanol. The dye structures were given in Figure V-2. The absorption peak of IR125 was measured at 782 nm while IR140 peaked at 800 nm. Both grating signals were initially believed to be impulsive, due to thermal relaxation in fast, two level systems. Since the excitation pulse wavelengths are far to the red of the absorption maxima, fairly simple transitions are expected. The results of the fits, as shown in Figures V-1 and V-2 and Table V-1, showed that this worked well. However,

there were surprises in the results, as longer lifetimes appeared upon closer analysis and concentration and power dependence experiments yielded unexpected results.

VI.A.2. *Sample Concentration and Solvent Reorganization:* An important concern is the bulk parameters offered by the two level fit. The results of Table V-1 show discrepancies in the values for the speed of sound, as well as the acoustic attenuation, though there is much error in both the current and previous data (Gray 1972) (Grigoriev and Meilikhov 1997) (Kaye and Laby 1995) (Pastor, Junquera et al. 1998). The results for the thermal diffusivity seem especially high.

Thus the concentration experiment of Figure V-5 (also VI-1) and Table V-2 was performed. It is important to bear in mind that the optical densities therein are relative and that the actual path length in the sample is of the order of the spot size. The IR140 data seems to reveal consistent thermal amplitudes across the two concentrations, when corrected for absorption. Curiously, the enthalpies are less than that of IR125, which has a higher concentration. This could indicate the presence of another channel for energy relaxation, possibly a long-lived triplet or even an isomeric state (Dietz and Rentsch 1985) (Soper and Mattingly 1994) (Mohanty, Palit et al. 2000). The dye should have a very low tendency to aggregate in methanol. Furthermore, such aggregation would result in the appearance of fast energy channels to the ground state, which is not the observed effect, as the corresponding time constant is still on the order of nanoseconds.

Finally, the data also shows that the increasing concentration affects the parameters of the bulk solvent. Most importantly, the value for the speed of sound returns to the expected value at lower concentrations, while the thermal diffusivity lessens, but does not agree with that of bulk methanol. The reason for this is unclear,

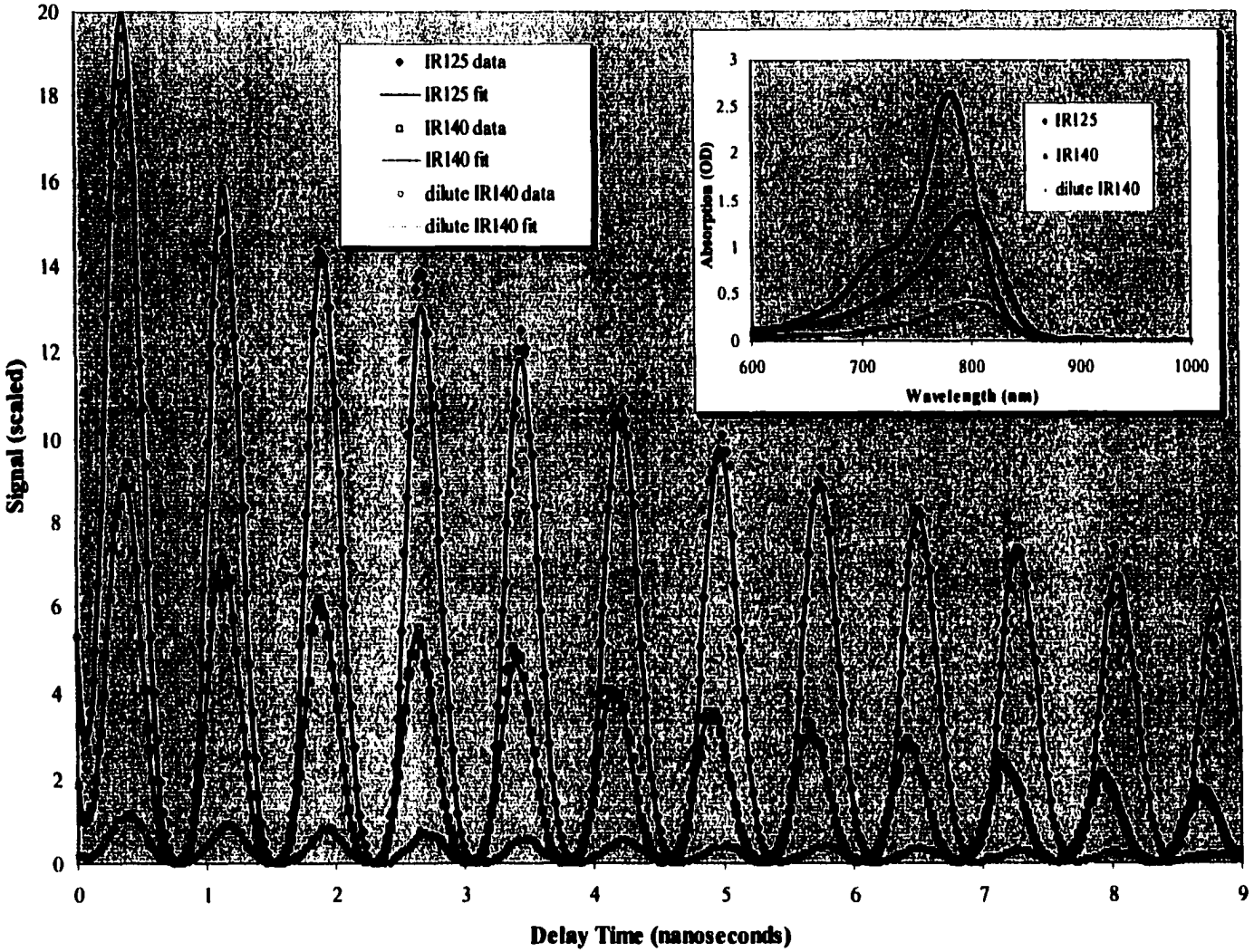

Figure VI-1: Thermal grating signals for IR125 and IR140 in methanol, fit to a two level heat release. The IR125 was prepared to a concentration of 1mM, while the IR140 was prepared to 1mM and .3mM. Sample temperature was fixed at 15°C. Clearly the bulk parameters change with concentration, though considerable offset persists for many constants at lower concentrations.

though previous measurements were performed on pure solvents (Gray 1972) (Grigoriev and Meilikhov 1997). Molecules of the solvent will organize about a solute, rearranging the solvent – solvent interactions in the vicinity. It is possible that some of the bulk properties of methanol are strongly affected by the presence of the dyes, especially in the high concentrations (mM) of these experiments. A decrease in the heat capacity would be reasonable, which would increase the thermal conductivity. Other results suggest that the changes are due to the sum of effects from salts, the buffer and the dyes themselves (Pastor, Junquera et al. 1998) (Gray, Wachtveitl et al. 1992) (Grigoriev and Meilikhov 1997). Another possibility is that the 3–D model of thermal diffusion mentioned in Chapter III is more appropriate for the description of this data (Cao, Chen et al. 1997) (Sun, Morais et al. 1992).

Yet another likely cause lies in the assumption that there is no non-thermal component to the signal. Though the fluorescence yield is small, some of the energy may show up as a volume change due to electrostrictive or conformational changes. Though such effects should be small, a series of experiments should be run versus temperature. As the coefficient of thermal expansion changes with temperature, the non-thermal component may be deduced. Subtracting this part from the signal and refitting the data should yield a better value of the thermal diffusivity. Finally, using a photo-multiplier tube would enhance the detection sensitivity and allow a more detailed series of concentration experiments to be run. This would give further insight into any solvation effects.

VI.A.3. *Power Dependence Experiments:* Another useful insight to the experiment may be provided by varying the laser power to insure that the sample is not

saturated with photons. Varying the probe power should produce linear variations in the diffracted intensity, while changing the pump power should exert a linear influence upon the signal amplitude, which is proportional to the heat release, as described in Chapter III. Such experiments upon the dye solutions were performed to characterize the system. These experiments were performed over relatively shorter time scales (a few ns) than the full scan shown in other figures, to determine amplitudes, not relaxation times.

Interpreting the probe experiments is straightforward, as the intensity should be linear with the probe power. The pump data is necessary to determine whether the sample is undergoing a one – photon process, or whether the dye is saturated. The data for IR125 in methanol in Figure V-6 is linear on both counts, as expected. Figure V-7, for IR140 in methanol shows a quadratic dependence of the amplitude upon the pump power. The unexpected result for IR140 may to be due to the strong two-photon absorption of the dye (possibly due to photo-isomerization) (Dietz and Rentsch 1985). Thus the amplitude of the signal, which is proportional to the enthalpy of the reaction, depends quadratically upon the pump power, as the probability of a single dye molecule's excitation varies as the photon concentration squared.

VI.A.4. *Thermal Relaxation:* Improvements in the signal to noise on subsequent data allowed the scans of Figures V-8 and V-9 to be collected, and analyzed using the three level model. These scans and fits are repeated as Figure VI-2. Given the available data, the lifetime of the excited states seems to match what is known. Typically the rate of fluorescence and the competing non-radiative rate may be summed to obtain the overall lifetime of the excited state of a system. The quantum yield of the fluorescence should provide the relative ratio between the fluorescence and the non - radiative rate.

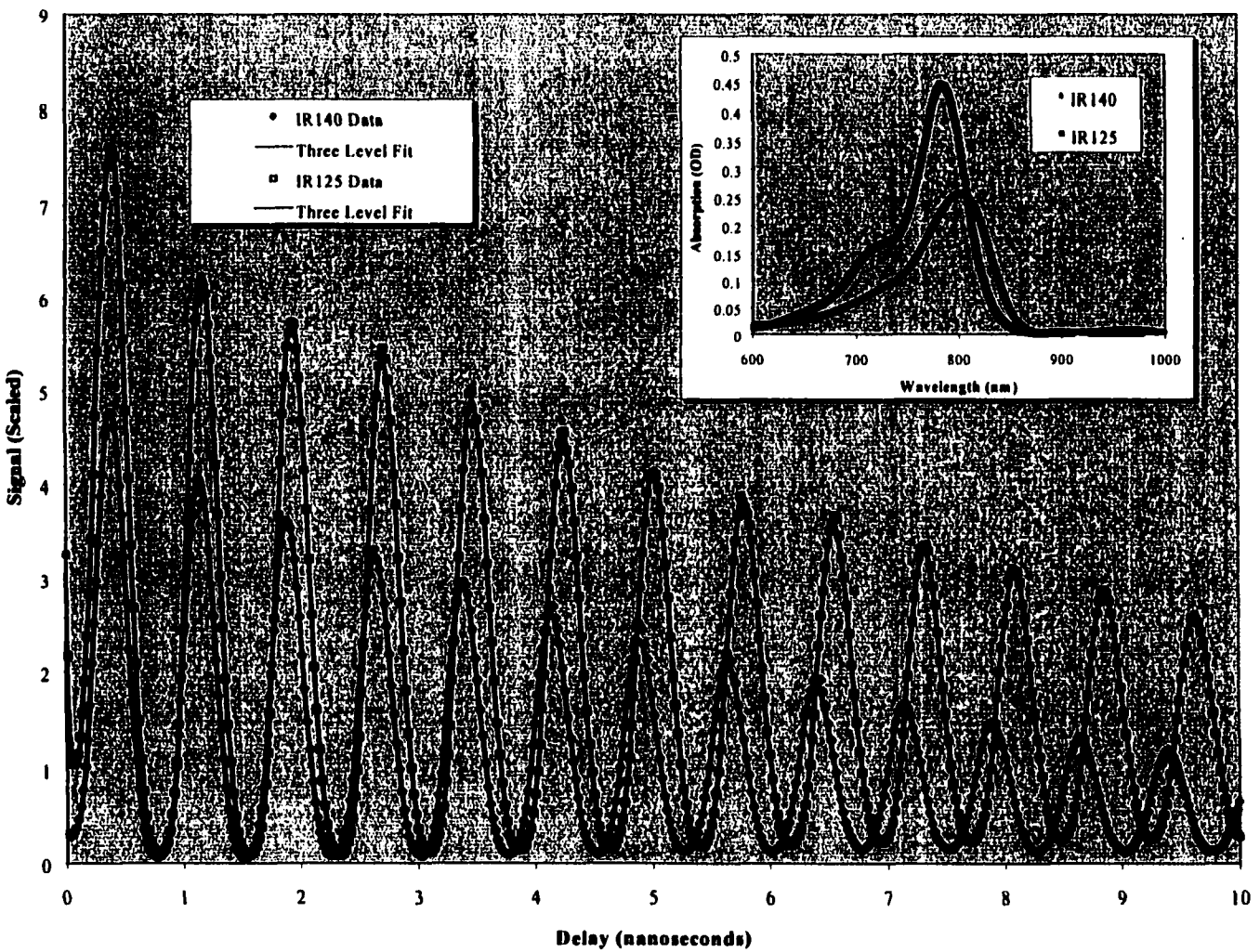

Figure VI-2: Transient grating signal for IR 125 and IR140 in methanol, fit to a three level heat release. Sample temperature was approximately 15°C. This fit produced the data found in Table VI-1. The peak of absorption for IR125 is at 782nm, while it is at 800nm for IR140. Note that the concentration of IR140 is lower, though it clearly affects the solvent more than IR125, as evidenced by the acoustic shift.

Thus the rates for IR125 and IR140 in a range of solvents have been seen previously, if indirectly. These numbers are compared in Table V-3 to the values measured in the thermal grating experiment, and are also in Table VI-1, along with enthalpies of reaction. The fast rates measured here are reasonable and essentially impulsive, with an upper limit of a few picoseconds, followed by a much longer lifetime (Mohanty, Palit et al. 2000) (Soper and Mattingly 1994) (Gumy, Nicolet et al. 1999).

The energy release of the short time scale should be linked to a combination of solvation and vibrational relaxation. The longer times should be associated with the fluorescence times. This is illustrated schematically in Figure VI-4. The amplitudes of the grating data indicate that only about 25% of the enthalpy release is associated with the longer lifetime. The absorption spectra indicate that there should be only a small energy loss prior to subsequent fluorescence (Soper and Mattingly 1994; Mohanty, Palit et al. 2000). Consequently, most of the fast enthalpy release must be associated with rapid internal energy conversion directly to the ground state. Finally, the spectra of the figures seem to indicate that aggregation is not happening, though it seems possible in methanol at these concentrations (Philip, Penzkofer et al. 1996). Though more experiments at reduced concentration would certainly be desirable, the transient grating technique offers promising insights into the non-radiative rates of energy transfer.

VI.B. Peripheral Light Harvesting Centers

VI.B.1. *Protein Spectrum and Concentration:* Spectra from a standard optical absorbance scan show the expected maxima at 850 nm and 800 nm. The typical optical density of LH2 in a 1cm cell found at 850 nm was 50, and 15 at 865 nm. Using the approximate molar absorption (at 850 nm) of 200 $(mM*cm)^{-1}$, the concentration may be

Sample	ΔH_1 (eV)	τ_1 (ps)	ΔH_0 (eV)	τ_0 (ps)
IR125 (MeOH)	-1.12 ± .09	3 ± 1	-1.43 ± .01	130 ± 20
ref	-	-	-	500
IR140 (MeOH)	-1.07 ± .06	< 1	-1.43 ± .01	143 ± 20
ref	-	.26	-	330

Table VI-1: Parameters resulting from three level (two parameter) least squares fit to data for laser dyes in methanol. The first time constant for the IR140 data was less than the resolution of the experiment. Errors propagate from previous measurements and stem from assumptions described in the text. The references were found as described in the text.

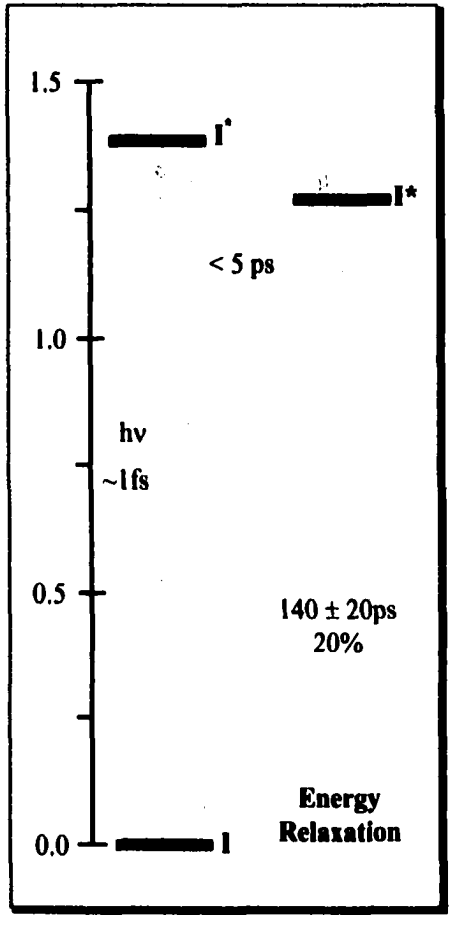

IR 125 – Indocyanine Green

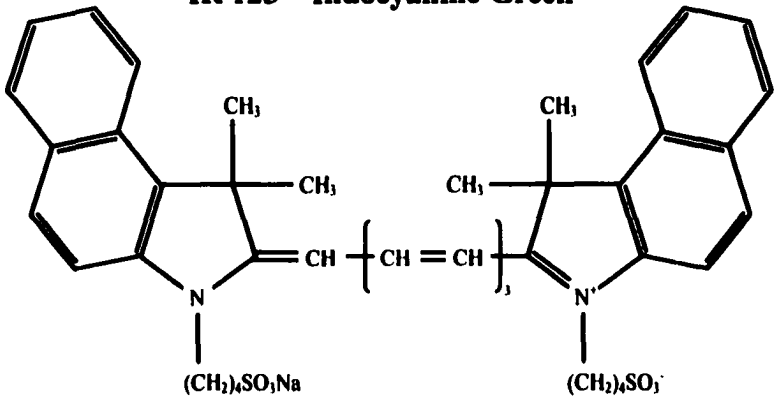

IR 140

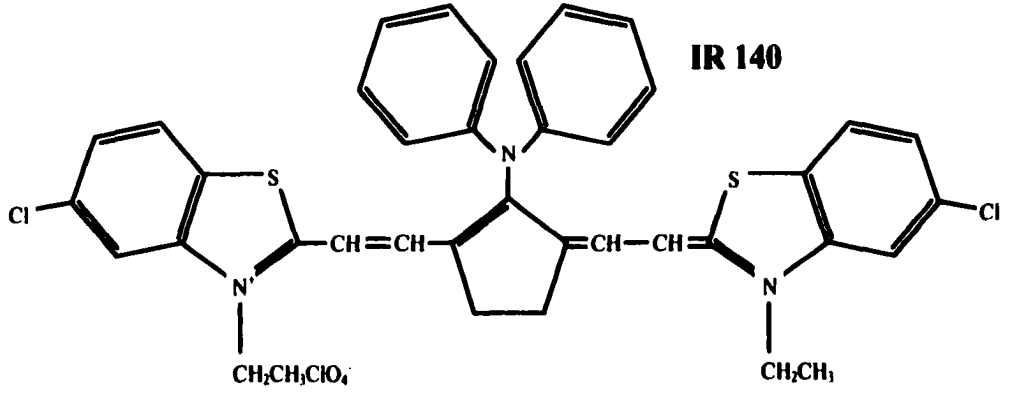

Figure VI-3: Energetics of the laser dyes IR 140 and IR125. Following rapid excitation, most of the energy is internally converted. Some fraction of the excited molecules relax vibrationally by some small amount, ultimately releasing their energy over a timescale of 140ps. See the text for differences between the two dyes.

deduced to be roughly 250μM, though less concentrated samples were used as well. Pump pulse energies of 1μJ were focused to a diameter of about 600μm. This should yield average photon concentrations near 60μM. Alternatively, the molar absorption may be rewritten as a cross-section (at 850 nm) of 10^{-16} cm^2. The photons will be focused to 10^{15} cm^{-2}. These estimates provide only one photon for every eight or ten light harvesting protein, keeping multiple absorption events to a minimum. Similar absorption coefficients and concentrations applied to the reaction center samples as well (Parson and Cogdell 1975).

However, these calculations assume that photons are not absorbed before they reach the crossing volume, which is certainly untrue. The optical density of the sample in the 1cm quartz spectrophotometer cell was 15 at 865 nm. The flow cell of the grating experiment was only 1mm in path length. Yet significant absorption of the laser light (>95%) would be expected during this experiment. However, this was not observed, as significant power passed through the sample. Perhaps the cross-sections are only approximately known. It seems more likely that the heavy dilutions of the spectrophotometer scans lead to measurements that may not be absolute, though comparisons may still be made between samples.

VI.B.2. *Power Dependence Experiments:* To ensure the linearity of the protein samples in these experiments, the laser intensity may be varied. Power dependence experiments for the peripheral light harvesting centers showed the expected linearity for the pump and probe signal upon the signal amplitude and intensity, respectively. Figure V-15 details the linear regression on the samples, including two series at the zero expansion point of water. As none of the results appear saturated, there should be

relatively little absorption per protein, presumably at or less than one photon per ten light harvesting centers. Furthermore, this should indicate that the probe is only diffracted and not significantly absorbed by the grating (where the intensity would run as the square of the probe power).

VI.B.3. *Temperature Dependence:* That there is any significant signal at the zero expansion point is a surprise. As discussed in Chapter I, the light harvesting protein consists of two rings of chlorophyll, named after their absorbance maxima. A photon's energy is absorbed and delocalized upon several chlorophyll in the ring. Photons that excite the 800 nm ring ultimately transfer that energy to the 850 nm ring, then unto another light harvesting protein. As these proteins are isolated by the buffer and are not in contact, this energy should either fluoresce or be internally converted. Thus the signal is dominantly thermal and there should be no signal when the experiment is performed at the zero-expansion point of water. Surprisingly, the data of Figure V-14 reveals a much stronger amplitude than expected. A possible mechanism for this signal is due to increased absorption of the probe beam by the excited state of LH2 (Nelson, Casalengo et al. 1982). However, changes in the excited state absorption should be small and any grating signal generated should be small as well. Alternatively, a volume change associated with the excitation could drive an acoustic wave. Distortions in the light harvesting ring have recently been reported upon proteins bound to mica surfaces (Bopp, Stynik et al. 1999).

VI.B.4. *Free Enthalpies of the Light Harvesting Center in βOG:* Whatever the source of the signal at the zero expansion point, the three level fit to the data at the zero expansion point may be subtracted from the thermal signal at 15 degrees. The zero

expansion point signal should be constant over the short temperature range between 15 and 4 degrees Celsius, though there is a change in the compressibility. The full three level fits of Figures V-17, V-18 and V-19 are the result of the three step process detailed in Chapter V. After fitting the zero expansion point signal, this information subtracted from the two-level equation used to obtain the bulk parameters. Finally the three level fits are obtained. One set of these results is shown as Figure VI-4. Though heat releases are obtained from the nonlinear fits, they may be generalized to changes in free enthalpies (ΔH), as the two differ only by kT.

Averaging the data sets together reveals that after the protein absorbs a photon, heat is released with a time constant of 26ps. As the incident wavelength is 864 nm, only the 850 nm (B850) ring is excited. The kinetics of this enthalpy change have been observed before, as part of the process of energy transfer from B850 to B875 (the LH1 ring) (Nagarajan and Parson 1997). This rate was interpreted as energy migration along through LH2 before transfer. However, this does not appear to be due to exciton formation, which occurs on a much faster timescale in the membrane as well as in bulk (Nagarajan, Johnson et al. 1999). This formation appears to delocalize the energy over some three to four pigments (Monshouwer, Abrahamsson et al. 1997). Furthermore, the rate of transfer between pigments is believed to be only around 1ps or less (Novoderezhkin, Monshouwer et al. 2000) (Jimenez, Dikshit et al. 1996). Since our proteins are isolated, we may suggest that this migration and energy decay occur along an individual ring.

A significant fraction of the energy remains trapped in the ring until the subsequent relaxation takes place with a characteristic time constant of roughly 1.4 ns.

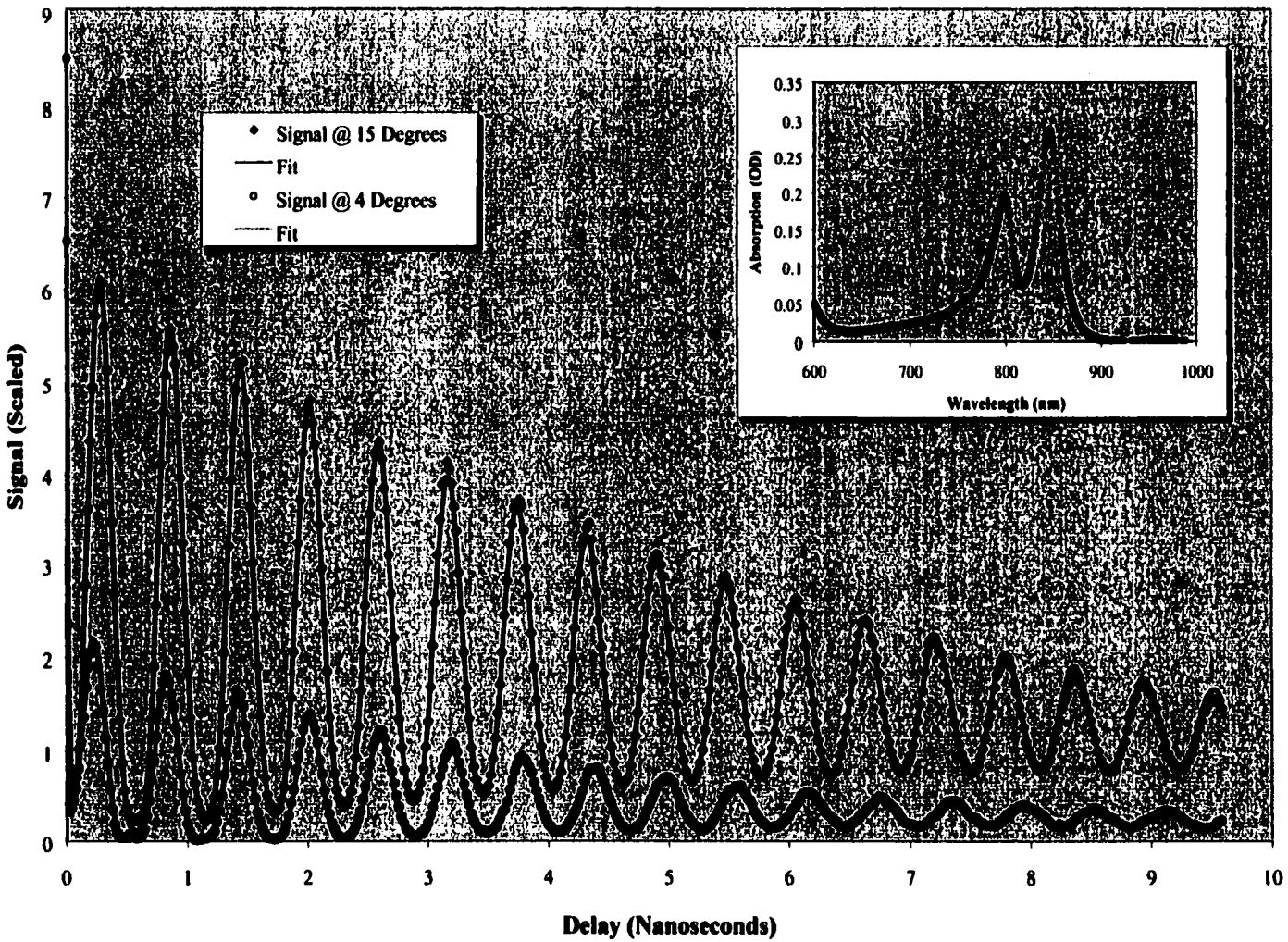

Figure VI-4: Samples of the transient grating signal for the peripheral light harvesting complex in βOG, at 15°C and 4°C. The fits are to the three level heat release and three level volume changes, respectively, as described in the text. Rates and free energies from this and other fits are averaged in Table V-2.

This appears reasonably close to the time obtained from fluorescence lifetimes from bulk reaction centers (986ps) and from the immobilized proteins (1.0ns) (Bopp, Jia et al. 1997) (Van Amerongen, Valkunas et al. 2000) (Monshouwer, Abrahamsson et al. 1997).

VI.B.5. *Free Energies of LH2:* Though a volume change implies some entropy difference, we may assume that such a change is small, especially at room temperature. Accordingly, we may assign free energy changes for the transition discussed above. Since one of the parameters of the fit is the overall heat release, this may be normalized to that of the incoming photon (865 nm or 1428 meV). The heat release sees only a small correction for the fluorescence yield of ~10% (Monshouwer, Abrahamsson et al. 1997), assuming that this applies only to the energy of the subsequent recombination. These results are summarized in Table VI-2 and are interpreted in Figure VI-5. Roughly three-fourths of the initial energy is released with the time constant of 21 ps, though some small fraction undoubtedly arises from exciton formation and ultrafast vibrational relaxation. The remaining energy is emitted according to the 1.5 ns timescale.

VI.B.6. *Volume Changes in LH2:* The amplitude of the volume grating may give us insight into the relative volume change in the sample. If we take the ratio of the thermal and the volume coefficients from the grating expressions of Chapter III (Equations III-21 and III-29), the volume change may be ascertained. Unfortunately, the bulk parameters of these samples, especially the heat capacity, are not well known, as remarked earlier. However, we may make an estimate of the volume change, by first noting that the rough coefficients of the volume and thermal expansion appear similar. This leads us to an estimate of the volume change of only about -2Å^3 per protein. This change appears to be due largely to a contraction of the solvent. However, a change in

Sample	T (°C)	ΔG_1 (meV)	τ_1 (ps)	ΔG_0 (meV)	τ_0 (ns)
LH2 (βOG) #1	15.9 ± .2	-1204 ± 20	24.2 ± 1.5	-1428 ± 14	1.69 ± .20
LH2 (βOG) #2	15.2 ± .2	-1045 ± 12	16.8 ± .5	-1428 ± 7	1.25 ± .10
LH2 (βOG) #3	15.3 ± .2	-1012 ± 12	24.5 ± 1.5	-1428 ± 6	1.43 ± .20
Average	15.5 ± .1	-1087 ± 8	19.8 ± .6	-1428 ± 6	1.41 ± .12
ref	~ 20	-	26.3 ± 1.0	1428	1.0 ± .2

Table VI-2: Rates and free energies for the thermal signal for LH_2 in βOG, fit to a three level model of decay. Roughly 75% of the excitation energy is converted to thermal energy within 25ps. The remainder fluoresces or is lost after a few nanoseconds. The three fits are in agreement with each other, though the times of the second fit are more precise, due to better signal to noise. The times are weighted toward this set. References were found as mentioned in the text and are considered to the last digit, unless otherwise noted.

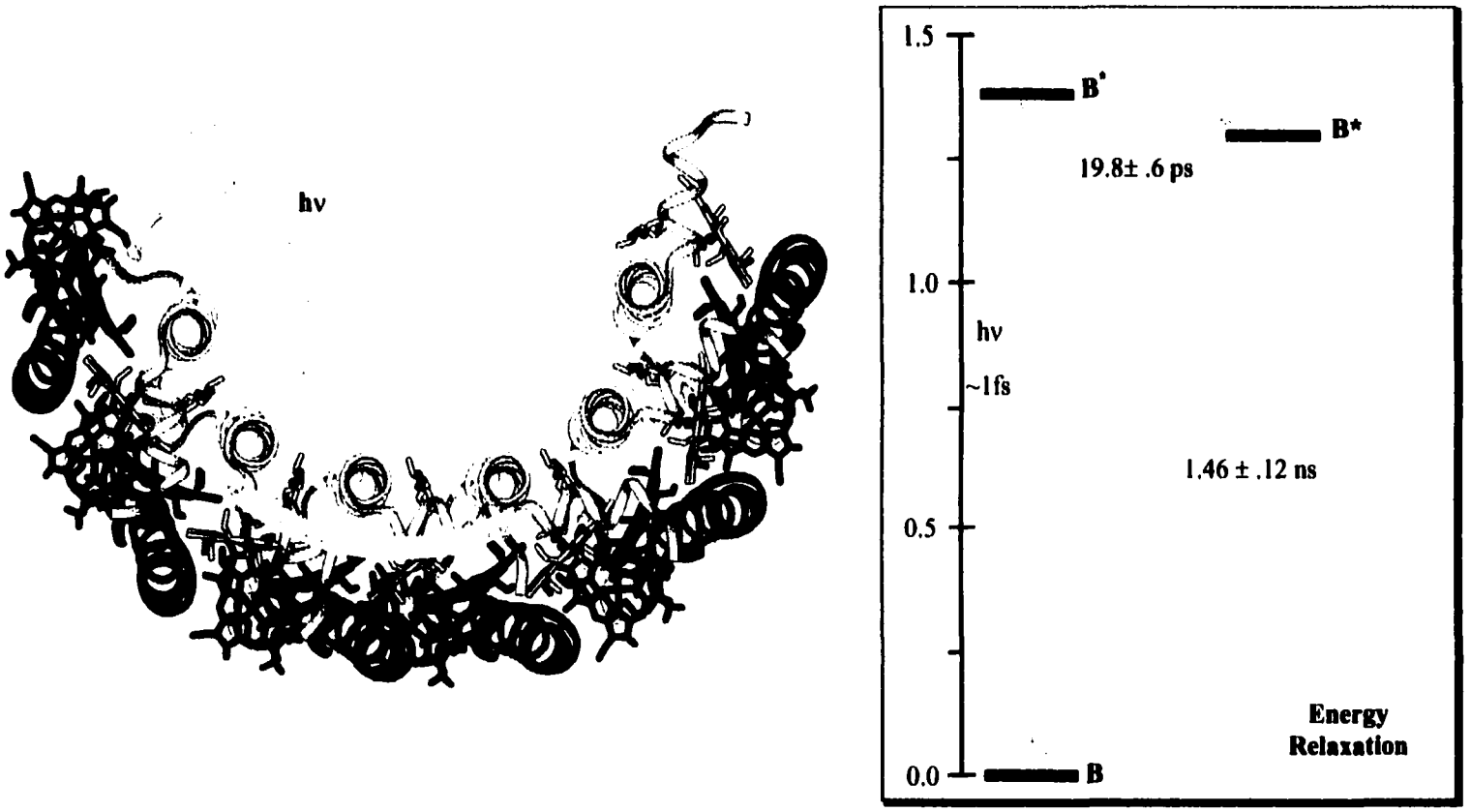

Figure VI-5: Measured energetics of the photosynthetic peripheral light harvesting center. The photon excites the B850 ring (composed of pairs of bacteriochlorophyll seen edge on in green and yellow), which rapidly relaxes vibrationally. A fraction of the energy does appear to remain in the ring. With no proximal LH ring to trap the excitation, is remains delocalized upon several chlorophyll (roughly four) for a little over a nanosecond. Then energy is then lost as fluorescence or as thermal energy. Free energies are in electronvolts.

the protein's volume may be part of this effect. Few have seen this structural change directly, though others have reported evidence of a 'mobile deformation' in isolated LH2, presumably linked with exciton transfer around the ring (Bopp, Stynik et al. 1999).

The rates of formation and decay of this state were found in Table V-6. The volume change appears in roughly 26ps and decays in ~30ns. The first rate appears consistent with the release of thermal energy from the previous section. The second rate seems quite long, though if we multiply the long thermal decay time of 1.5 ns by the fluorescence yield, a time of 15ns should correspond to the non-thermal time constant of energy release. This release would seem to correspond with the final volume relaxation of the sample.

VI.C. Wild-Type Reaction Centers

VI.C.1. *Free Enthalpies of the Wild-Type Reaction Center in βOG:* The data sets of Figures V-23, V-24 and V-25 and Tables V-9, V-10 and V-11 were fit using the techniques mentioned above. The zero expansion signal was fit to the three level volume grating and this was used as a baseline. Three level thermal fits were applied to the 15 degree signal. Figure VI-6 reprints a typical set. Recall that the LH2 data was taken as a reference. Again the parameters of the fit are normalized to the overall energy release, which is 1428 meV. On the wavelength scan in figure VI-6, this corresponds to the 865 nm energy peak. As discussed in Chapter I, this has been shown to correspond to direct excitation of the special pair (P*).

The first event that data of Table V-11 indicates is a relatively small, fast heat release with a time constant of only 3.5 ps. This event is assigned to the first step in electron transfer. Here, the electron has left the special pair and has localized upon the

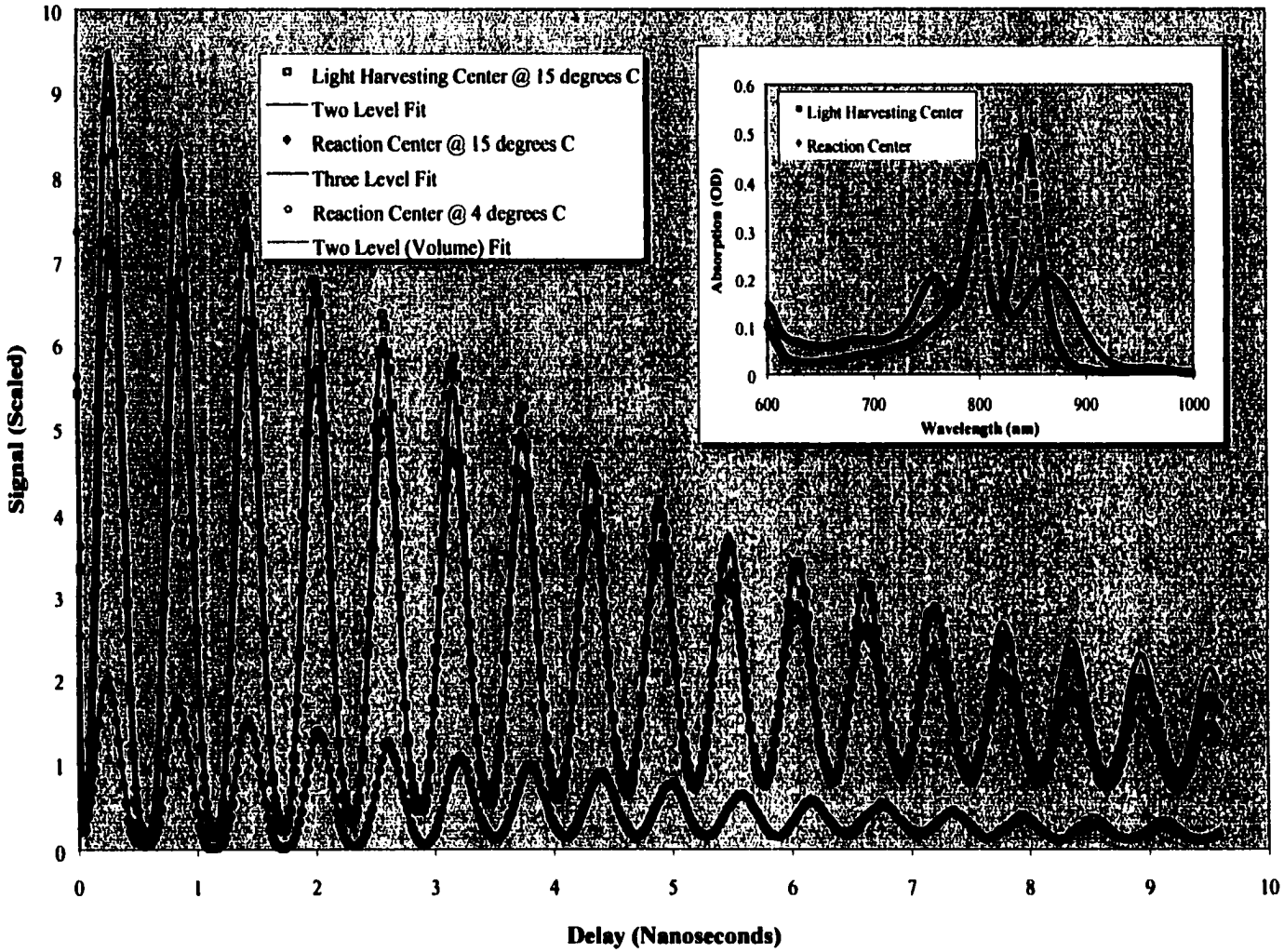

Figure VI-6: Transient grating signal on reduced reaction centers and peripheral light harvesting system in βOG. Sample temperature ranges as shown. The low temperature signal leads to the electrostrictive volume changes, while the thermal signal produces the thermodynamic data. Rates and free energies from this fit are found in Table VI-3.

active pheophytin (P^+H^-). This rate agrees well with the rates reported by other methods (Parson and Cogdell 1975) (Parson, Schenck et al. 1978) (Vos, Lambry et al. 1991; Vos, Lambry et al. 1992) (Du, Rosenthal et al. 1992). The experiment's time resolution is too coarse to determine whether the electron has even temporarily localized upon the accessory chlorophyll (P^+B^-).

Unlike the light harvesting center data, the second heat release carries most of the free enthalpy change of the sample. As these quinones of these samples were pre-reduced, the electron is expected to return directly to the special pair, and the system to its ground state in energy. The time constant of this release is 12 ns. which compares fairly well with the rate known for charge recombination (Woodbury and Parson 1984).

VI.C.2. *Triplet Yield and the Free Enthalpy:* The normalization of the signal assumes that all of the energy in non-fluorescent samples is lost thermally during the timescale of the experiment. However, there is a substantial and long lived (10-100μs) triplet yield of 30% in the reaction centers that is not present in the antennae, effectively removing a source of fast heat release for the reaction centers (Schenck, Blankenship et al. 1982) (Parson and Cogdell 1975) (Boxer, Lockhart et al. 1990) (Chidsey, Kirmaier et al. 1984).

Implementing these corrections may be done in two ways. The first and most formal is to incorporate this mechanism directly into the grating solution, as derived in Chapter III. However, the yield and rate constant of triplet formation may not be directly obtained from the fits. Instead, these parameters must be assumed from previous data and set as constants into the fits. Other work has established the yield at a time constant of 10ns, though this is only approximately known (Chidsey, Kirmaier et al. 1984).

Furthermore, these corrections provide no improvement to the reduced χ^2, while they do reduce the stability of the fit. An easier method simply applies the correction to the energy. There is a small change in the recombination rate between these two methods, but it is well within the uncertainty.

VI.C.3. *Free Energies of the Initial Step in Charge Transfer:* To obtain the free energy, the fluorescence yield and the entropy change must be estimated. As with the light harvesting center, the fluorescence from the excited state only affects the overall efficiency, not the relative free energies. The fluorescence from the charge transfer state is assumed to be small.

Similarly, the entropic change for charge separation is assumed to be small. This conclusion is also consistent with small entropy changes observed for photochemical electron transfer between donor/acceptor molecules in solution (Morais and Zimmt 1995). In the case of the photosynthetic reaction center, we anticipate a small, positive entropic contribution for the formation of the charge-separated state, due to ordering of dipoles around the photogenerated charges. This idea is consistent with recent theoretical work as well (Tachiya and Seki 1995). However, others have suggested that the entropic change due to electrostriction (probably the dominant contribution) can be quite large (Edens, Gunner et al. 2000) or at least fairly significant (Arata and Parson 1981) (Arata and Parson 1981). A way to assess the entropy change is to determine the temperature dependence of the free energy change. Unfortunately the entropy is needed to determine the free energy change, though it is possible to iterate to a solution.

To obtain some estimate of the free energy, we will ignore the change in the free energy. This produces the free energies of Table VI-3, which are shown in Figure VI-7.

Sample	T (°C)	ΔG_1 (meV)	τ_1 (ps)	ΔG_0 (meV)	τ_0 (ns)
Wild-Type (βOG) #2	14.7 ± .2	-302 ± 20	2.4 ± 1.0	-1428 ± 5	17 ± 2
Wild-Type (βOG) #3	14.4 ± .2	-267 ± 10	3.7 ± .2	-1428 ± 5	8 ± 2
Average	14.6 ± .1	-279 ± 11	3.5 ± .2	-1428 ± 5	12 ± 1
ref	~ 20	-260 ± 10	3.7	-1428	12
Wild-Type (βOG) #2 ◊	14.7 ± .2	-910 ± 20	-	-	-
ref	~ 20	-.86 ±	-	-	-

Table V-3: Thermal signal for reaction centers in βOG, including an unreduced sample marked by '◊'. While times and energies are reported for the pre-reduced sample, only energies are available for the unreduced sample. Corrections produced by triplet yields are discussed in the text. Uncertainties reflect possible systematic errors in assumptions described in text. Sample #3 possessed the best signal to noise and the time and energies of charge separation are weighted toward that sample. References were found as mentioned in the text and are considered to the last digit, unless otherwise noted.

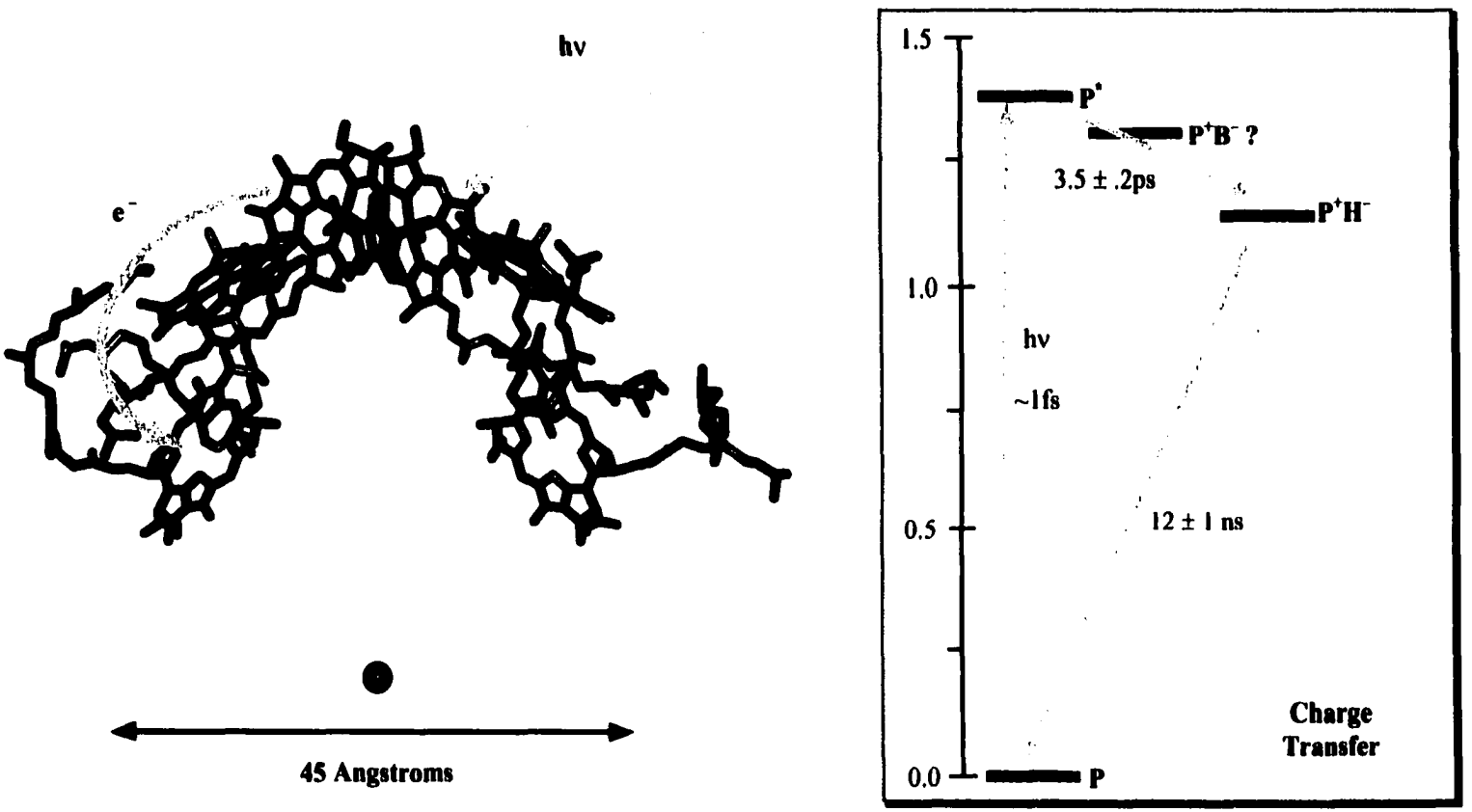

Figure VI-7: Measured energetics of the reduced reaction center. A rapid heat release, of roughly 279 ± 10 meV., signals the first step in charge separation. A subsequent release over a longer time scale appears to be due to recombination. Free energies are in electronvolts. Apparent agreement of these free enthalpies with the free energies (ΔG) of the Figure II-7 confirm a small change in the entropy (small $T\Delta S$).

The free energy of the charge separated state is shown to be –302 meV and –267 meV over two separate experiments. The second result is due to an experiment with better signal to noise, and the average is weighted, to produce a free energy change of –279 meV. Apparently in good agreement with previous experiments (Arata and Parson 1981) (Arata and Parson 1981), this value is nonetheless contingent upon the assumption of small entropic changes.

VI.C.4. *Time Dependent Free Energies:* In Chapter II, the discrepancy of multiple fluorescence components was discussed. An explanation of this phenomenon was termed dynamic solvation. In this model, the free energy of the charge separated state (P^+H^-) decreases with time, due to solvation effects (Peloquin, Williams et al. 1994) (Woodbury, Peloquin et al. 1994). A schematic is pictured in Figure VI-8. This signal that this model should produce was developed in Chapter III. This grating equation was applied to the pre-reduced data above. These fits were very unstable, and never produced any reasonable estimate of a solvation rate. Moreover, the solvation energy change was never more than 10 meV, which is below the uncertainty of the energy level's position.

The failure of the dynamic solvation model to generate significantly improved fits may simply indicate that the data does not have the requisite signal to noise. It would seem that an increase of another order of magnitude would be necessary to produce the data that would resolve this dispute. However, this result most likely suggests that there is no compelling reason to adopt a model of dynamic solvation to explain the kinetics seen. However, it is not clear what would explain the discrepancies in the kinetic rates, though they may simply be caused by a time-dependence in the reorganization energy, as discussed in Chapter II. Such a change in the reorganization energy may also imply a

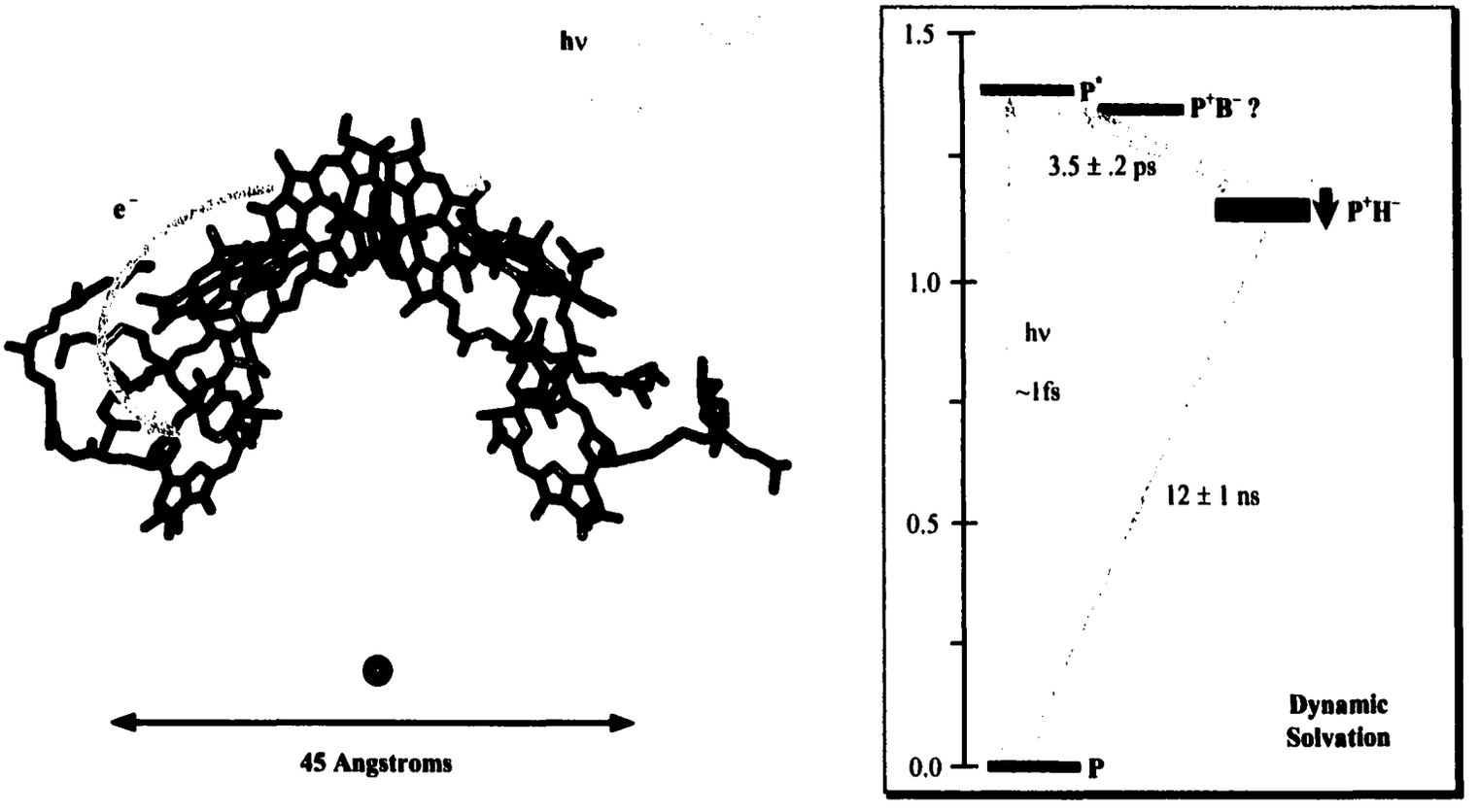

Figure VI-8: The dynamic solvation picture of charge transfer as studied by transient gratings. Excitation of the special pair initiates the release of a free electron, which localizes upon a nearly isoenergetic pheophytin after a few picoseconds. The times appear from the previous figure. No reliable solvation time could be fixed, while the solvation energy was found to be less than 10 meV. Entropy changes may be more significant. Recombination may be present, though it is not explicitly found in the grating equations. Approximate free energies are in electronvolts.

change in the free energy. Furthermore the free energy may be time dependent due to enthalpy or entropy changes. The thermal grating analysis fails to detect any enthalpy change, while the volume change appears well fit to a three level model. This implies no entropy change of the intermediate level (see below), though further analysis may be necessary.

VI.C.5. *Unreduced Reaction Centers and the Quinone Free Energy:* Thermal grating data was collected for unreduced reaction centers, to determine the free energy of subsequent charge separation. Typical data appears in Figure VI-9. Here the three thermal levels correspond to the excited state of the dimer (P*), the charge separated state (P^+H^-) and the reduced menaquinone state ($P^+Q_A^-$). The reduced ubiquinone state and the ground state are too long to observe on the experimental time scale. Unfortunately, the signal to noise was quite high for these scans (compare to the pre-reduced set). Furthermore, no volume grating was collected for the unreduced sample. The volume change for this charge separated step is assumed to be quite high (see below). Without this information, only a two level fit may be performed, with only the approximate time resolution of a few hundred picoseonds. This enthalpy change is associated with the charge transfer from P* to the menaquinone $P^+Q_A^-$.

This enthalpy may scale against the enthalpy change of the initial step of charge transfer, as the sample was subsequently pre-reduced, and the scan taken again. This leads to a free energy change of –.58 eV. This value may be somewhat high, as the reference that the signal was scaled to is believed to be high. Furthermore, the sample did not fully clear the reaction volume between shots. Since the recovery time should be 100 ms, and the repetition rate of the laser is 1 kHz, some multiple excitations will occur.

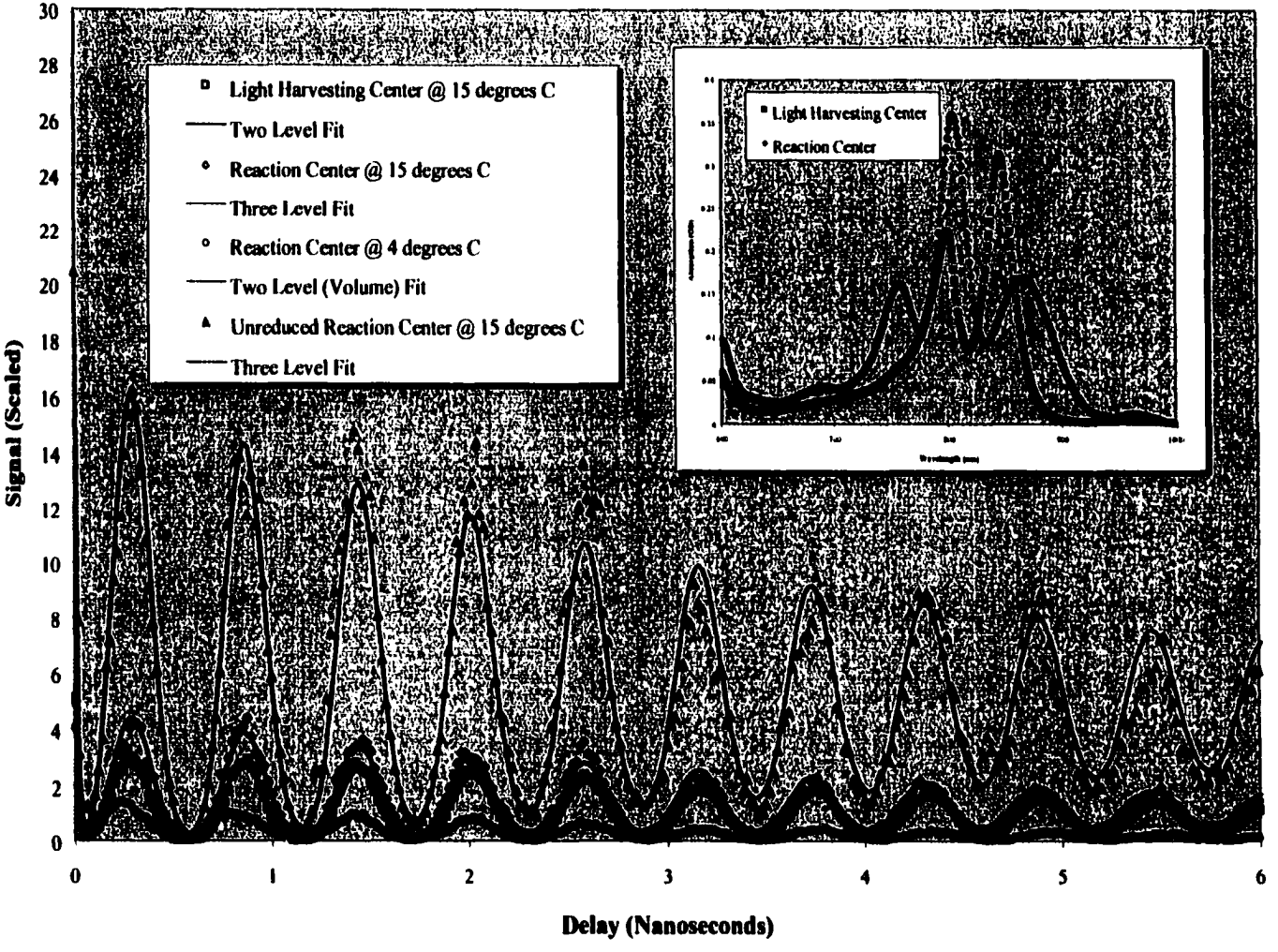

Figure VI-9: Transient grating signal for the reduced and unreduced reaction center at 15°C and 4°C. Results for LH2 are also shown as a reference. Note the strong, though noisy signal from the unreduced reaction center, due to the relatively large energy gap between the excited state and the quinone. Rates and free energies from this fit are found in Table VI-3.

These excitations will lead to excessive heat release. Assuming 10% of the reaction centers are excited with each pulse, and that our sample clears the flow cell after 2 shots, roughly a 16% correction is required. A conservative correction for this effect yields an enthalpy change of –.49 eV. There is a considerable spread in the previous data for this parameter, though this value seems to be in reasonable agreement with other direct calorimetric techniques (Edens, Gunner et al. 2000).

Assigning a free energy is difficult due to the presence of large entropy changes. A fairly wide range of data exists here, as well. As shown below, our efforts to determine the entropy directly were frustrated by a lack of data on the bulk properties on these protein mixtures. We will use a value of .42 eV inferred from previous calorimetric results, though this assumed a known free energy (Edens, Gunner et al. 2000). This produces a free energy difference of .91 eV, which compares well against previous values (Arata and Parson 1981) (Arata and Parson 1981) (Edens, Gunner et al. 2000). This data is superposed upon the results from above in Figure VI-10, and on table VI-3

VI.C.6. *Volume Changes in Wild-Type Reaction Centers:* Unlike the LH2 data, some signal at the zero expansion point was expected in reaction centers, due to reorganization of the protein and the solvent after the charge transfer. Similar signals have been seen in myoglobin (Miller 1994). The relative size of this change indicates the importance of solvation in the motion of the charge.

In the same manner as the LH2 data, an approximate volume estimate may be made of -5Å^3 per protein. This is probably largely due to electrostriction in the solvent. Scaling this with the overall amplitude of the thermal plus the volume change offers a full, or photoacoustic volume change of roughly - 30Å^3. This compares well with

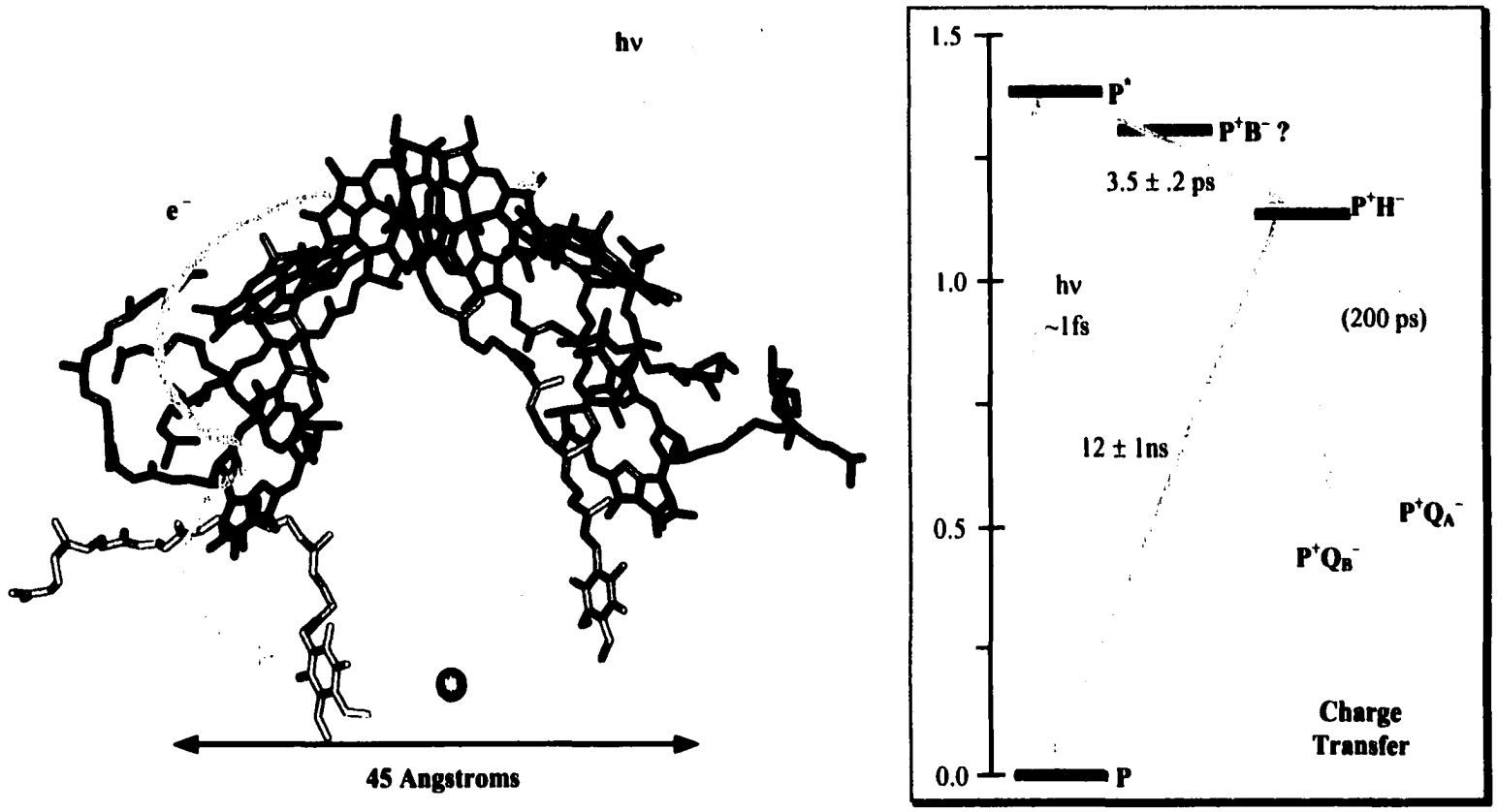

Figure VI-10: Charge separation and the measured energetics of pre-reduced and unreduced photosynthetic reaction centers. The data from Figure VI-7 is combined with the unreduced data of Table VI-3. The electron appears to transfer to the menaquinone after a few hundred picoseconds (the exact time constant was not determined), with a free energy change of -.91 eV. The subsequent transfer to the ubiquinone and recombination are not apparent on the timescale of these experiments. Free energies are in electronvolts.

directly measured values (Puchenkov, Kopf et al. 1995) (Edens, Gunner et al. 2000). This volume requires only 65ps to establish and 16ns to dissipate. It is not clear why the volume change occurs in 65ps, when charge transfer is complete after only a few ps.

The calorimetric work mentioned in Chapter II detects volume changes associated with charge transfer (Edens, Gunner et al. 2000) (Hara, Hirota et al. 1996) (Feitelson and Mauzerall 1996). The volume change is believed to be due to the heat release accompanying the reaction (as with these experiments) plus a volume change usually associated with electrostriction. The volume change may provide an indirect measure of the entropy. Using the Drude-Nerst equation and a relation for entropy reveals Equations VI-1 and VI-2, where ΔV_{el} and ΔS_{el} are the volume and entropy changes of

$$\Delta V_{el} = \frac{\partial \Delta G_{el}}{\partial P} = \left(\frac{e^2}{2r\varepsilon}\right)\frac{\partial \ln \varepsilon}{\partial P} \qquad \textbf{(VI - 1)}$$

$$\Delta S_{el} = -\frac{\partial \Delta G_{el}}{\partial T} = \left(\frac{e^2}{2r\varepsilon}\right)\frac{\partial \ln \varepsilon}{\partial T} \qquad \textbf{(VI - 2)}$$

electrostrcition, e is the charge on a sphere of radius r, and ε is the dielectric coefficient (Drude and Nernst 1894). In principle, then if ΔV_{el} is measured (at the zero expansion point of water, for instance), and the behavior of ε may be looked up in a table, then the entropy (or at least its relative magnitude) may be determined. Unfortunately, the dielectric coefficient is not well known as a function of temperature and pressure. Consequently, those who have measured the enthalpy have simply found the difference between it and a known free energy (Edens, Gunner et al. 2000).

VI.D. (M)214H Reaction Centers

VI.D.1. *Free Enthalpies of the (M)214H Reaction Center in βOG:* As mentioned before, site-directed mutagenesis allows the replacement of the photo-active pheophytin with a chlorophyll. The data of Figures V-26, V-27 and V-28 revealed the parameters in Tables V-12, V-13 and V-14. A typical set is reproduced as Figure VI-11. Again, the first heat release would appear to correspond to charge separation to the chlorophyll, requiring a time constant of 5.7ps, which compares well with previous values (Kirmaier, Laporte et al. 1995) (Kirmaier, Gaul et al. 1991) (Laporte, Mcdowell et al. 1995). The recombination requires around 3.1ns, somewhat longer than the prior reported values. The reason for this discrepancy is unclear.

VI.D.2. *Free Energies of the Initial Step in Charge Transfer for (M)214H:* The free energies of charge separation were assumed to be largely unaffected by triplet formation, fluorescence relaxation and any entropy change. Table VI-4 and Figure VI-12 summarize the results. Since most of the enthalpy change is in the impulsive part of the signal, there would appear to be only a small efficiency of charge separation. While previous work did not see this, it may be due to failure to reduce the quinone. To resolve the scale of the signal, it may be compared to the wild-type signal of Figure VI-6, including the LH2 reference. In this instance, corrections for the concentrations must also be made. These results reveal a free energy change of –.12 eV from P* to the charge separated state. This compares well with previous values, though borrowing the values of the free enthalpy change to the quinone produces an efficiency of this transfer to be only 13% (Kirmaier, Laporte et al. 1995) (Kirmaier, Gaul et al. 1991). It is possible that the entropy difference is not .42 eV, as assumed. Furthermore, it is possible that probe is

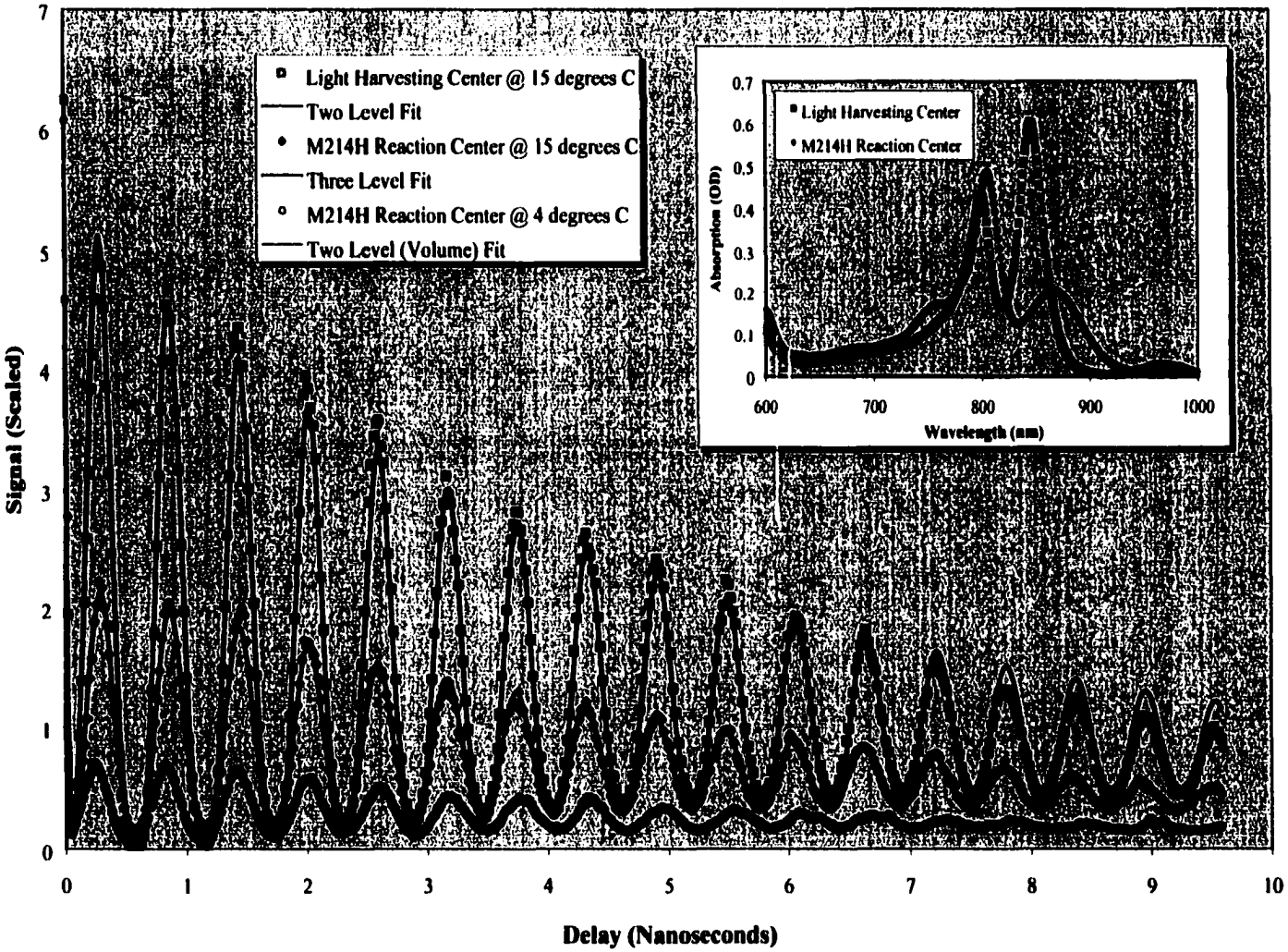

Figure VI-11: Transient grating signal on reduced M214H reaction centers and LH2 in βOG including a zero expansion signal. Note the overall weakness of the signal relative to the light harvesting centers, implying a small free energy gap of charge separation. Rates and free energies from this fit and others may be found in Table VI-4.

Sample	T (°C)	ΔG_1 (meV)	τ_1 (ps)	ΔG_0 (meV)	ε ($P^+Q_A^-$)	τ_0 (ns)
M214H (βOG) #2	14.9 ± .2	- 140 ± 20	5.8 ± .2	- 559 ± 20	16 %	3.4 ± .5
M214H (βOG) #3	14.1 ± .2	- 94± 20	5.6 ± .2	- 559 ± 20	10 %	2.8 ± .5
Average	14.5 ± .1	- 117 ± 14	5.7 ± .1	- 559 ± 14	13 %	3.1 ± .4
ref	~ 20	~ 100	5.8	- 559	60 %	1.0

Table VI-4: Thermal signal for M214H in βOG, fit to a three level model of decay. To correct these signals for the scale of the free energy change, the LH2 reference was used against the reference for the reaction center. These amplitudes were further corrected for differences in optical density. The energy of the quinone was assumed to be unchanged from the wild-type samples. The considerable uncertainties in this process are reflected in the error bars. The efficiency column represents the efficiency of transfer to the quinone. References were found as mentioned in the text and are considered to the last digit, unless otherwise noted. The free energies and rates are summarized on Figure VI-12.

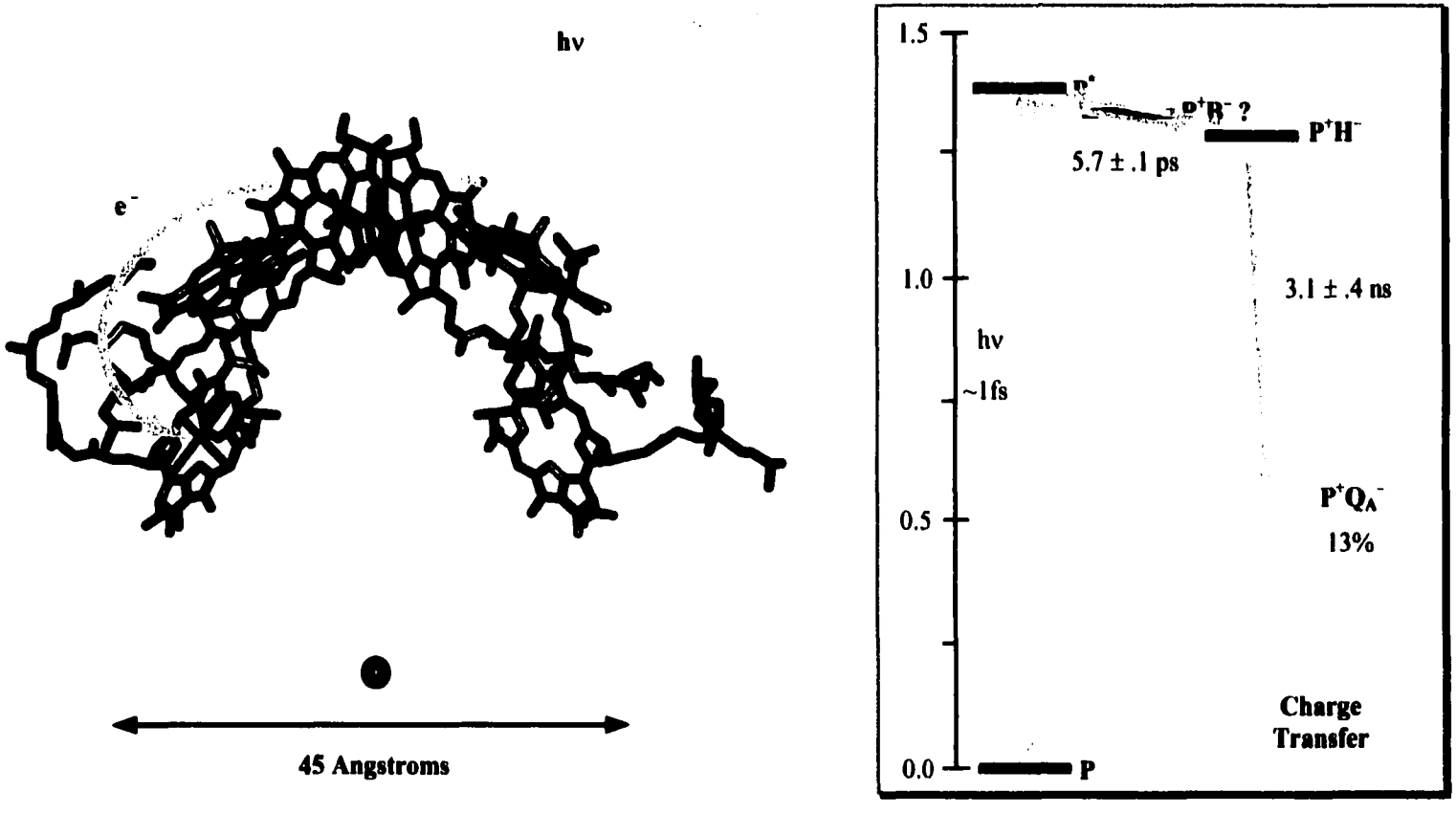

Figure VI-12: Measured energetics of the pre-reduced M214H reaction center. Electron transfer begins with a rapid heat release with a time constant of 5.7ps, with a free energy difference of -.11 eV. The subsequent recombination indicates that the efficiency of transfer is surprisingly low, and occurs with a longer time constant than expected. The quinone energy may only be approximately known, however. Free energies are in electronvolts.

exciting the charge separated state into a trip-doublet excited state, though this isn't observed in the wild-type reaction centers (Hochstrasser 1998).

VI.D.3. *Volume Changes in (M)214H Reaction Centers:* The approximate volume change may be deduced from the ration of the thermal signal and the volume signal, and should be roughly –6 $Å^3$ per protein (plus or minus 1 $Å^3$). This signal develops over a longer time of 105 ps, compared to the wild-type reaction center. As with the wild-type center, it is not clear why this rate is so much slower than that of charge separation. The rate of recombination is similarly lengthened, to a time constant of 28 ns. Though there may be considerable error in this rate, it and the results for light harvesting centers and wild-type centers suggest that solvation effects appear to be the limiting factor in recombination.

VI.D. Literature Cited

Arata, H. and W. Parson (1981). "Delayed Fluorescence from *Rhodopseudomonas sphaeroides* reaction centers: Enthalpy and free energy changes accompanying electron transfer from P-870 to quinones." Biochimical et Biophysica Acta **638**: 201-209.

Arata, H. and W. Parson (1981). "Enthalpy and volume changes accompanying electron transfer from P-870 to quinones in *Rhodopseudomonas sphaeroides* reaction centers." Biochimica et Biophysica Acta **636**: 70-81.

Bopp, M. A., J. Jia, et al. (1997). "Fluorescence and photobleaching dynamics of single light harvesting complexes." Proceedins of the National Academy of Science USA **94**: 10630-10635.

Bopp, M. A., A. Stynik, et al. (1999). "The dynamics of structural deformations of immobilized single light-harvesting complexes." Proceedings of the National Academy of Sciences USA **96**: 11271-11276.

Boxer, S. G., D. J. Lockhart, et al. (1990). . Current Research in Photosynthesis. M. Baltscheffsky. Boston, Kluwer Academic Publishers: 113-116.

Cao, Y. N., H. X. Chen, et al. (1997). "Generation of the Photoacoustic Effect through Heat Diffusion: Transient Grating Measaurements on Reverse Miscelle Solutions." Journal of Physical Chemistry **101**: 3005-3011.

Chidsey, C. E. D., C. Kirmaier, et al. (1984). "Magnetic field dependence of radical-pair decay kinetics and molecular triplet quantum yield in quinone-depleted reaction centers." Biochimica et Biophysica Acta **766**: 424-437.

Dietz, F. and S. K. Rentsch (1985). "On the mechanism of photoisomerization and the structure of the photoisoners of cyanine dyes." Chemical Physics **96**: 145-151.

Drude, P. and W. Nernst (1894). "Uber elektrostriktion durch freie ionen." **15**: 79-85.

Du, M., S. J. Rosenthal, et al. (1992). "Femtosecond Spontaneous Emission Studies of Reaction Centers from Photosynthetic Bacteria." **89**: 8517-8521.

Edens, G. J., M. R. Gunner, et al. (2000). "The enthalpy and entropy of reaction for formation of P+QA- from excited reaction centers of *Rhodobacter sphaeroides*." Journal of the American Chemical Society **122**(7): 1479-1485.

Feitelson, J. and D. Mauzerall (1996). "Photoacoustic evaluation of volume and entropy changes in energy and electron transfer. Triplet state porphyrin with oxygen and naphthoquinone-2-sulfonate." Journal of Physical Chemistry **100**(18): 7698-7703.

Gray, D. E., ed. (1972). American Institue of Physics Handbook. New York, McGraw-Hill.

Gray, K. A., J. Wachtveitl, et al. (1992). "Photochemical Trapping of a Bacteriopheophytin Anion in Site Specific Reaction Center Mutants from the Photosynthetic Bacterium Rhodobacter Sphaeroides." European Journal of Biochemistry **207**: 723-731.

Grigoriev, I., .S. and E. Z. Meilikhov, Eds. (1997). Handbook of Physical Quantities. Moscow, CRC Press.

Gumy, J.-C., O. Nicolet, et al. (1999). "Investigation of the solvation dynamics of an organic dye in polar solvents using the femtosecond grating technique." Journal of Physical Chemistry A **103**(50): 10737-10743.

Hara, T., N. Hirota, et al. (1996). "New application of the transient grating method to a photochemical reaction: The enthalpy, reaction volume, and partial molar volume measurements." Journal of Physical Chemistry **100**(24): 10194-10200.

Hochstrasser, R. M. (1998). "Ultrafast Spectroscopy of Protein Dynamics." Journal of Chemical Education: Waters Symposium **75**(5): 559-564.

Jimenez, R., S. N. Dikshit, et al. (1996). "Electronic excitation transfer in the LH2 complex of *Rhodobacter sphaeroides*." Journal of Physical Chemistry **100**(16): 6825-6834.

Kaye, G. W. C. and T. H. Laby (1995). Tables of physical and chemical constants. Essex, Harlow.

Kirmaier, C., D. Gaul, et al. (1991). "Charge Separation in a Reaction Center Incorporating Bacteriochlorophyll for Photoactive Bacteriopheophytin." Science **251**: 922-927.

Kirmaier, C., L. Laporte, et al. (1995). "The nature and dynamics of the charge-separated intermediate in reaction centers in which bacteriochlorophyll replaces the photoactive bacteriopheophytin. 1. Spectral characterization of the transient state." Journal of Physical Chemistry **99**: 8903-8909.

Laporte, L., L. Mcdowell, et al. (1995). "Free-energy dependence of the rate of electron transfer to the primary quinone in beta-type reaction centers." Journal of Chemical Physics **197**: 225.

Miller, R. J. D. (1994). "Energetics and dynamics of deterministic protein motion." Accounts of Chemical Research **27**: 145-150.

Mohanty, J., D. K. Palit, et al. (2000). "Photophysical properties of two infrared laser dyes - IR-144 and IR-140: a picosecond laser photolysis study." Proceeding of the Indian National Science Academy **66**(2): 303-315.

Monshouwer, R., M. Abrahamsson, et al. (1997). "Superradiance and exciton delocalization in bacterial photosynthetic light-harvesting systems." Journal of Physical Chemistry B **101**(37): 7241-7248.

Morais, J. and M. B. Zimmt (1995). "Thermodynamics of intramolecular electron transfer in alkane solvents." Journal of Physical Chemistry **99**(21): 8863-8871.

Nagarajan, V., E. T. Johnson, et al. (1999). "Femtosecond pump-probe spectroscopy of the B850 antenna complex of *Rhodobacter sphaeroides* at room temperature." Journal of Physical Chemistry B **103**: 2297-2309.

Nagarajan, V. and W. W. Parson (1997). "Excitation energy transfer between the B850 and B875 antenna complexes of *Rhodobacter sphaeroides*." Biochemistry **36**: 2300-2306.

Nelson, K. A., R. Casalengo, et al. (1982). "Laser-induced excited state and ultrasonic wave gratings: Amplitude and phase grating contributions to diffraction." Journal of Chemical Physics **77**(3): 1144-1152.

Novoderezhkin, V., R. Monshouwer, et al. (2000). "Electronic and vibrational coherence in the core light-harvesting antenna of rhodopseumonas viridis." Journal of Physical Chemistry B **104**(50): 12056-12071.

Parson, W. W. and R. J. Cogdell (1975). "The primary photchemical reaction of bacterial photosynthesis." Biochimica et Biophysica Acta **415**: 105-149.

Parson, W. W., C. C. Schenck, et al. (1978). Kinetics of Photochemical Electron Transfer Reactions *in vivo* and *in vitro*. Frontiers of Biological Energetics. New York, Academic Press.

Pastor, O., E. Junquera, et al. (1998). "Hydration and micellization processes of n-Octyl β-D-Glucopyranoside in aqueous solution. A thermodynaimc and fluorimetric study in the absenece and presence of salts." Langmuir **14**: 2950-2957.

Peloquin, J. M., J. C. Williams, et al. (1994). "Time-dependent thermodynamics during early electron transfer in reaction centers from *Rhodobacter sphaeroides*." Biochemistry **33**(26): 8089-8100.

Philip, R., A. Penzkofer, et al. (1996). "Absorption and fluorescence spectroscopic investigation of indocyanine green." Journal of Photochemistry and Photobiology A:Chemistry **96**: 137-148.

Puchenkov, O. V., Z. Kopf, et al. (1995). "Photoacoustic diagnostics of laser-induced processes in reaction centers of *Rhodobacter sphaeroides*." Biochimica et Biophysica Acta: Bio-Energetics **1231**(2): 197-212.

Schenck, C. C., R. E. Blankenship, et al. (1982). "Radical-pair decay kinetics, triplet yield and delayed fluorescence from bacterial reaction centers." Biochimica et Biophysica Acta **680**: 44-59.

Soper, S. A. and Q. L. Mattingly (1994). "Steady-state and picosecond laser fluorescence studies of non-radiative pathways in tricarbocyanine dyes: Implications to the design of near-ir fluorochromes with high fluorescence efficiencies." Journal of the American Chemical Society **116**(9): 3744-3752.

Sun, T., J. Morais, et al. (1992). "Investigation of viscosity and heat conduction effects on the evolution of a transient picosecond photoacoustic grating." Journal of Chemical Physics **97**(12): 9324-9334.

Tachiya, M. and K. Seki (1995). "Microscopic reversibility of the rate constants given by the generalized Marcus equation." Chemical Physics Letters **243**: 330-333.

Van Amerongen, H., L. Valkunas, et al. (2000). Photosynthetic Excitons. Singapore, World Scientific.

Vos, M. H., J. C. Lambry, et al. (1991). "Direct Observation of Vibrational Coherence in Bacterial Reaction Centers Using Femtosecond Absorption Spectroscopy." **88**: 8885-8889.

Vos, M. H., J. C. Lambry, et al. (1992). "Femtosecond Spectral Evolution of the Excited State of Bacterial Reaction Centers at 10 K." **89**: 613-617.

Woodbury, N. and W. Parson (1984). "Nanosecond fluorescence from isolated photosynthetic reaction centers of *Rhodopseudomonas sphaeroides*." **767**(2): 345-361.

Woodbury, N. W., J. M. Peloquin, et al. (1994). "Relationship between thermodynamics and mechanism during photoinduced charge separation in reaction centers from *Rhodobacter sphaeroides*." Biochemistry **33**(26): 8101-8112.

VII. CONCLUSION

VII.A. Progress

VII.A.1. *Laser Dyes IR125 & IR140:* The experiment was teethed on two well known dyes in methanol (to prevent aggregating). The signal to noise of the experiment was improved considerably using the thermal signal of these dyes as a guide. Three level fits successfully described the data from these compounds. The lifetimes, however, appeared shorter than the times that have appeared in the literature, suggesting aggregation by the dye, though this wasn't readily apparent from the spectra.

VII.A.2. *Peripheral Light Harvesting Centers:* Considerable data collected upon purified peripheral light harvesting complexes (in βOG) reveal a three level heat decay. The first, faster transition appears to be due to relaxation as delocalized energy propagates around the ring. A significant fraction of the energy (25%) remains trapped for longer times. Curiously, what was expected to be a thermal signal does not disappear at the zero expansion point of water. Though this may partially be due an excited state grating, the low absorption of the protein at the probe wavelength suggests that there may be some protein motion during resonance energy transfer, as well as some rearrangement of the solvent.

VII.A.3. *Wild-Type and (M)214H Reaction Centers:* High signal to noise data has been collected on both the wild type and the mutant (M)214H reaction centers. As with the light harvesting data, the signal appears strongly impulsive and largely thermal. However, as with the light harvesting center, the signal is actually best fit to a three level model. The early heat release corresponds to charge separation, while recombination causes the larger subsequent release. For the wild-type data, the enthalpies match the free

energies of previous data, suggesting a very small entropic contribution to the reaction. The unreduced wild-type data, by contrast, shows a significant entropy change for charge migration to the menaquinone. While the energy of initial charge separation in the (M)214H mutant verifies previous data, the rate and free energy of the menaquinone deviate. The reason for this is unclear. Both wild-type and (M)214H data show a strong non-thermal component to the signal due to reorganization of the solvent.

Time dependence of the free energy of the charge separated state was not detected. Rates and energies of relaxation for all proteins appeared well described by exponential rates of decay (within the grating model). This may only indicate that the signal to noise was not high enough.

VII.B. Directions

VII.B.1. *Experiment:* Though much information may be obtained from the transient grating experiment, the difficulty of interpretation clouds the results. Furthermore, such a difficult experiment (overlapping three infrared beams in space and time) makes data tough to reproduce. While the designs of the pressurized flow cell (to prevent bubbles) and the optical parametric amplifier (to limit bandwidth) eliminate much of the unwanted noise, a few more improvements would make even better signal to noise data possible. Clearly a photomultiplier tube would be desirable in place of the detection diode. Experiments could be performed upon samples with much lower concentrations, simplifying sample preparation and placing the experiment in the low absorption regime. Experiments could even be performed in vivo, rather than upon purified proteins. Furthermore, this would also allow very sensitive absorption measurements to be taken, by simply blocking one of the beams. Finally, dispensing

with the delay stage (at least for the long delay time grating experiments) would eliminate the laser divergence problem. In its place, a fast data acquisition card (10-100 ps response) could collect the data from a continuous probe. The low peak intensity of the probe would further reduce the problem of excited state absorption, as well as reduce the alignment complexity.

VII.B.2. *Properties of Biological Samples:* To help elucidate the entropy, the dielectric response (versus temperature and pressure) of various proteins will need to be measured. This would not only provide information on protein response, but would allow the use of the Drude-Nerst equations of Chapter VI. Though the entropic contribution may be small, determining its magnitude will be key to understanding the reorganization of the electron's environment during charge transfer. Furthermore, even the basic knowledge of the bulk properties of proteins, as well as detergent/water mixtures would allow more certain comparisons between experiments.

VII.B.3. *Photosynthesis & Ultrafast Spectroscopy:* Finally, it seems that while photosynthetic components allow a variety of energy transfers to be studied, the complexity of the systems have often prevented consistent interpretation of the data for even simple experiments (calorimetric studies versus fluorescence decay, for example). Nonetheless, both the light harvesting protein and the reaction center remain uniquely interesting systems to study energy transfer by resonance transfer and charge separation, respectively. As some of the necessary basic information upon membrane proteins is gathered, the overall importance of the key variables will emerge. Among the wave of ultrafast spectroscopy techniques, the transient thermal grating experiment will offer unique insight into vibrational relaxation.